

USER'S GUIDE

Integrated Stable Isotope – Reactive Transport Model
Approach for Assessment of Chlorinated Solvent Degradation

ESTCP Project ER-201029

November 2014

Tomas Kuder
Paul Philp
University of Oklahoma

Boris van Breukelen
Héloïse Thouement
VU University of Amsterdam

Mindy Vanderford
Charles Newell
GSI Environmental Inc.

Distribution Statement A

This document has been cleared for public release



REPORT DOCUMENTATION PAGE

Form Approved
OMB No. 0704-0188

Public reporting burden for this collection of information is estimated to average 1 hour per response, including the time for reviewing instructions, searching existing data sources, gathering and maintaining the data needed, and completing and reviewing this collection of information. Send comments regarding this burden estimate or any other aspect of this collection of information, including suggestions for reducing this burden to Department of Defense, Washington Headquarters Services, Directorate for Information Operations and Reports (0704-0188), 1215 Jefferson Davis Highway, Suite 1204, Arlington, VA 22202-4302. Respondents should be aware that notwithstanding any other provision of law, no person shall be subject to any penalty for failing to comply with a collection of information if it does not display a currently valid OMB control number. **PLEASE DO NOT RETURN YOUR FORM TO THE ABOVE ADDRESS.**

1. REPORT DATE (DD-MM-YYYY) 17-11-2014		2. REPORT TYPE Final Technical User Guidance		3. DATES COVERED (From - To) Jan 2011 - Nov. 2014		
4. TITLE AND SUBTITLE Integrating Stable Isotope Analysis and Reactive Transport Modeling for Assessing Chlorinated Solvent Degradation User Guide				5a. CONTRACT NUMBER W912HQ-10-C-0060		
				5b. GRANT NUMBER ER-201029		
				5c. PROGRAM ELEMENT NUMBER		
6. AUTHOR(S) Kuder, Tomasz; Philp, Richard, P.; vanBreukelen, Boris; Vanderford, Mindy; Newell, Charles, J.				5d. PROJECT NUMBER ER-201029		
				5e. TASK NUMBER		
				5f. WORK UNIT NUMBER		
7. PERFORMING ORGANIZATION NAME(S) AND ADDRESS(ES) University of Oklahoma School of Geology and Geophysics 100 E. Boyd St., SEC 810 Norman, OK 73019-2115				8. PERFORMING ORGANIZATION REPORT NUMBER		
GSI Environmental, Inc. 2211 Norfolk, Suite 1000; Houston, TX 77098 Vrije Univ Amsterdam; Faculty of Earth & Life Science, Dept Hydrology & Geo Environmental Science						
9. SPONSORING / MONITORING AGENCY NAME(S) AND ADDRESS(ES) Environmental Security Certification Program (ESTCP)				10. SPONSOR/MONITOR'S ACRONYM(S) ESTCP		
				11. SPONSOR/MONITOR'S REPORT NUMBER(S) ER-201029		
12. DISTRIBUTION / AVAILABILITY STATEMENT						
13. SUPPLEMENTARY NOTES						
14. ABSTRACT This document presents the results of ESTCP Project ER-201029 Integrated Stable Isotope - Reactive Transport Model Approach for Assessment of Chlorinated Solvent Degradation. The objective of this guidance is to help site managers apply a Reactive Transport Modeling (RTM) approach for improved Compound-Specific Isotope Analysis (CSIA) data interpretation and to use models to estimate more accurate attenuation processes for chlorinated solvents. The quantification of various destructive and transport processes and how they contribute to plume size and longevity may help extend Monitored Natural Attenuation (MNA) remedies to sites that have, heretofore, not been able to apply this important technology. The Guidance includes a description of standard CSIA laboratory methods, simple data interpretation and a step-by-step guide to downloading and using software developed as part of this project. In comparison with traditional data interpretation, the approach presented has several important benefits: (1) improvement of a conceptual site models by identification and quantification of prevalent attenuation pathways and identification of secondary inputs from DNAPL dissolution or non-degradative sinks such as sorption or volatilization, diffusion or dispersion. (2) a more accurate assessment of degradation of the parent contaminant; (3) quantitative assessment of the net degradation/accumulation of the dechlorination intermediates.						
15. SUBJECT TERMS Compound-specific isotope analysis, reactive transport modeling, groundwater, chlorinated solvents						
16. SECURITY CLASSIFICATION OF:			17. LIMITATION OF ABSTRACT UU	18. NUMBER OF PAGES 244	19a. NAME OF RESPONSIBLE PERSON Mindy Vanderford	
a. REPORT	b. ABSTRACT	c. THIS PAGE			19b. TELEPHONE NUMBER (include area code) 713 522 6300	



This document is a product of the Department of Defense Environmental Security

Technology Certification Program (ESTCP)

The following User Guide provides an overview of the use of Compound-Specific Isotope Analysis (CSIA) combined with simple to complex Reactive Transport Models (RTMs) for characterizing groundwater solvent plumes. The CSIA-RTM approach discussed herein has a particular focus on conceptual site model (CSM) development for monitored natural attenuation (MNA) remedies. The envisioned audience includes state and federal regulators, industry, consultants, Department of Defense staff, and members of the local community involved in selecting and evaluating remedies for contaminated sites. The intended value of the document is to provide current knowledge in support of sound remedial decisions for groundwater affected by chlorinated solvents. In the interest of brevity, the document assumes that the reader has a general understanding of hydrogeology, basic isotope chemistry, the movement of chemicals in porous media, remediation technologies, and the remedy selection process.

The CSIA with RTM Guidance was inspired by advances in chemical characterization supporting MNA since publication by the EPA of the 1998 *Technical Protocol for Evaluating Natural Attenuation of Chlorinated Solvents in Ground Water* and *A Guide for Assessing Biodegradation and Source Identification of Organic Ground Water Contaminants using Compound Specific Isotope Analysis (CSIA)* in 2008. While still useful for many topics, by 2014 these guidance documents were missing several important advances in data interpretation, and regulatory thinking that are now mainstays of CSIA for CSMs supporting MNA.

The authors of this document wish to acknowledge the financial support of ESTCP for this project and the important contributions of researchers, scientists, and engineers that have built the knowledge base upon which this document stands. The authors also wish to acknowledge the invaluable contribution of reviewers from government, industry, academia, and the public at large who have supported this project.

How to Cite: ESTCP Project ER-201029. Environmental Security and Technology Certification Program, Arlington, Virginia

This page left intentionally blank.

QUICK START

Monitored Natural Attenuation (MNA) is an important groundwater remediation technology based on a carefully controlled and monitored demonstration of contaminant attenuation from natural subsurface processes (USEPA 1998).

MNA remedies have several advantages over active remedies in terms of cost, effort, carbon footprint, and energy savings. However, demonstrating the strength of attenuation processes, particularly *contaminant mass destruction* can be challenging in heterogeneous environments. For this reason, recent research efforts have focused on improving methods for demonstrating intrinsic mass destruction processes in the subsurface.

Conventional MNA analyses rely on developing “*lines of evidence*” such as concentration vs. distance or concentration vs. time plots and other simple data visualization techniques to demonstrate contaminant destruction. We call this a “**Generation 1 MNA Analysis.**”

Compound-specific isotope analysis (CSIA) is a specialized laboratory method that can provide a more direct signal of biological degradation and support assessment of the strength of physical attenuation processes. The popularity of CSIA has risen rapidly among project managers as one line of evidence supporting MNA remedies. We call this a “**Generation 2 MNA Analysis.**” The following report describes the technique and summarizes simple methods for collecting and interpreting CSIA data including carbon isotope mass balances, dual isotope plots and isotope ratio vs. fraction of contaminant remaining plots.

While CSIA results can address some gaps in conceptual site models, CSIA data alone can be difficult to interpret, especially at sites with complex hydrogeology or release histories. This report introduces a “**Generation 3 MNA Analysis**” where CSIA data and simple reactive transport models (RTMs) are combined in a new and novel way to strengthen interpretation of both CSIA and conventional analytical data. Generation 3 MNA analyses provide stronger, clearer evidence of the strength of attenuation processes for chlorinated solvent plumes.

The goal of the following document is to present methods for quantitative assessment of natural attenuation processes, including mass destruction, for chlorinated solvents using a combined compound-specific isotope analysis (CSIA) and numerical reactive transport modeling (RTM) approach.

Quick Start to this Guidance

I want to find out....	Go to...
If CSIA with Reactive Transport Models is for me?	Quick Start
Why CSIA? Why CSIA with Reactive Transport Modeling?	Section 1
What are conventional MNA lines of evidence and when to consider CSIA	Section 2
More about CSIA data interpretation for site characterization	Section 3
A quick overview of how CSIA with Reactive Transport Models works	Section 4
The overall technical modeling approach for CSIA with RTM	Section 5
More about the models – where to get them, what data inputs are required	Section 6
In-depth technical use of Reactive Transport “Template models”	Section 7

Summary of Generations of Evidence for MNA

	Generation 1 MNA	Generation 2 MNA	Generation 3 MNA
Key Goals	Demonstrate contaminant degradation	Demonstrate contaminant degradation	Quantitative demonstration of contaminant degradation as well as the strength of other natural attenuation processes
Historical Timeframe	Late 1990s – Early 2000s	Early 2000s - Now	Now
Key Lines of Evidence	<ul style="list-style-type: none"> • Concentration vs. time or distance plots • Statistical Trends • Change in plume mass over time • Daughter products • Rate calculations • Simple concentration modeling 	<ul style="list-style-type: none"> • Generation 1 MNA • Collect and analyze carbon, hydrogen or chlorine isotope data • Evaluate isotope fractionation vs. distance from source • Evaluate concentration vs isotope fractionation, compare with laboratory results • Evaluate carbon mass balance 	<ul style="list-style-type: none"> • Generations 1 and 2 MNA • Collect and analyze carbon, hydrogen, and chlorine isotope data • Use reactive transport models to evaluate strength of all attenuation processes
Key References	<ul style="list-style-type: none"> • USEPA MNA Directive (1999) • USEPA Chlorinated Solvent MNA Protocol (1998) • Natural Attenuation of Fuels, Solvents (1999) 	<ul style="list-style-type: none"> • USEPA <i>Guide for Assessing Biodegradation and Source Identification of Organic Ground Water Contaminants using Compound Specific Isotope Analysis</i> (2008) 	<ul style="list-style-type: none"> • This document
Key Results	<ul style="list-style-type: none"> • Trend of mass over time • Trend of mass over distance • Reaction rates k and λ 	<ul style="list-style-type: none"> • Extent of parent compound mass destruction 	<ul style="list-style-type: none"> • Simulation of attenuation mechanisms for parent and daughter compounds to compare with site data • Reaction rates for different reaction mechanisms (reductive dechlorination, oxidation)
Key Issues	<ul style="list-style-type: none"> • Is it degradation or dispersion? • Molar mass never balances • Rough estimates of degradation rate • Difficult to demonstrate aerobic degradation processes 	<ul style="list-style-type: none"> • Daughter product CSIA confusing • Is vinyl chloride being destroyed? 	<ul style="list-style-type: none"> • More complex • Requires isotope data from multiple sampling locations • Requires some modeling expertise
What Happened...?	<ul style="list-style-type: none"> • Not always clear if mass destruction is occurring... 	<ul style="list-style-type: none"> • Better resolution, but still confounding factors including influence of physical transport, dilution and dispersion at some sites 	<ul style="list-style-type: none"> • Higher resolution, clear proof of degradation. • Refined conceptual site model.

CSIA-RTM GUIDANCE AT A GLANCE

This document presents the results of ESTCP Project ER-201029 *Integrated Stable Isotope – Reactive Transport Model Approach for Assessment of Chlorinated Solvent Degradation*. The objective of this guidance is to help site managers apply a RTM approach for improved CSIA data interpretation and to use models to estimate more accurate attenuation processes. The quantification of various destructive and transport processes and how they contribute to plume size and longevity may help extend MNA remedies to sites that have, heretofore, not been able to apply this important technology.

In comparison with traditional interpretation of the field, analytical and, even, isotope data, the approach presented below has several important benefits: (1) improvement of a CSM by identification and quantification of prevalent attenuation pathways (i.e., reductive biotic dechlorination vs. abiotic dechlorination vs. aerobic degradation) and identification of secondary inputs from DNAPL dissolution or non-degradative sinks such as sorption or volatilization, diffusion or dispersion. (2) a more accurate assessment of degradation of the parent contaminant; (3) quantitative assessment of the net degradation/accumulation of the dechlorination intermediates.

The following ‘Quick Start’ summary identifies several key questions and resources addressed in each section of the Guidance. **Sections 1 – 4** constitute the Overview Manual, presenting the basic concepts of MNA, CSIA and RTM. The Technical Manual found in **Sections 5-7** describes the RTM software tools developed for this project and how to apply them using CSIA data. Appendix A provides a Case Study demonstrating how high density CSIA sampling and RTM can be applied to a complex chlorinated solvent plume. **Appendices B through D** provide additional resources for interpreting CSIA data, including training course notes and a resource list of CSIA service providers.

OVERVIEW MANUAL

SECTION 1 includes background information on CSMs for chlorinated ethene contamination, MNA remedies and the basic application of CSIA to solvent sites.

Key Questions Addressed in Section 1:

- What is the typical CSM for applying MNA to groundwater plumes containing chlorinated solvents (**Section 1.1**)?
- What are the challenges to applying MNA at chlorinated solvent sites (**Section 1.2**)?
- What is CSIA (**Section 1.3**)?
- How does CSIA help distinguish between contaminant destruction and dilution processes (**Section 1.3**)?
- What is the benefit of combining CSIA with RTM? (**Section 1.4**)?

SECTION 2 discusses conventional approaches to MNA remedy evaluations. Topics include contaminant attenuation processes and common lines of evidence supporting MNA remedies.

Key Questions Addressed in Section 2:

- What are the key features of Generation 1 MNA? What attenuation mechanisms are used to support selection of MNA remedies (**Section 2.1**)?

- How does Generation 1 MNA evaluate each of the main attenuation processes (**Section 2.1**)?
- What are the main biodegradation pathways for chlorinated solvents (**Section 2.1.7**)?
- What are the conventional ‘lines of evidence’ to evaluate MNA remedies (**Section 2.2**)?
- How are attenuation rates calculated for Generation 1 MNA evaluations (**Section 2.2.3**)?
- When should I use CSIA to support MNA implementation decisions (**Section 2.3**)?

SECTION 3 provides a more in-depth discussion of CSIA laboratory methods, data interpretation, sampling strategies, and data management.

Key Questions Addressed in Section 3:

- What are isotopes and isotope ratios? Why do we want to analyze them (**Section 3.0**)?
- How are isotope ratios determined in the lab (**Section 3.1**)?
- What level of quality assurance and data management is needed to ensure good CSIA data (**Sections 3.1.2 – 3.1.4**)?
- How are conventional CSIA data interpreted (**Section 3.2**)?
 - What is isotope fractionation (**Section 3.2.1**)?
 - What is the Rayleigh fractionation model (**Section 3.2.2**)?
 - Do physical processes cause isotope fractionation (**Section 3.2.4**)?
 - How do I estimate the rate and extent of biodegradation with CSIA data (**Section 3.2.5**)?
 - How do I estimate the isotope signature of the original release (**Section 3.2.6**)?
 - Is the observed isotope ratio shift significant (**Section 3.3.1**)?
 - How do I visualize CSIA data? (**Section 3.3.3**)?
 - What are dual isotope plots and how are they constructed (**Section 3.3.4**)?
 - What is the Carbon Isotope Mass Balance (C-IMB) analysis (**Section 3.3.5**)?
- What is a typical CSIA sample plan design? How many samples and where (**Section 3.4**)?
- Which elements should I evaluate (**Section 3.4.4**)?
- When and why do I need to apply RTM for CSIA interpretation (**Section 3.5**)?

SECTION 4 introduces RTM with a discussion of available models, input data, and examples of their application for various geochemical settings.

Key Questions Addressed in Section 4:

- What are Reactive Transport Models (**Section 4.1**)?
- What type of input data do I need (**Section 4.1.2**)?
- How do I calibrate RTM with CSIA data (**Section 4.1.3**)?
- What kind of output can I expect from combining CSIA with RTM (**Section 4.1.4**)?

- Can you give me some examples of the types of attenuation scenarios I can expect?
 - Reductive dechlorination under anaerobic conditions (**Section 4.2.1**)
 - Stall of DCE/VC: Detection of potential oxidation (**Section 4.2.2**)
 - Simulation of reductive dechlorination in plume core and oxidation at fringe (**Section 4.2.3**)
 - Hydrogen isotope fractionation during reductive dechlorination of PCE/TCE (**Section 4.2.4**)

TECHNICAL MANUAL

Sections 5 through **7** constitute the RTM Technical Manual and describe how to download software, develop input files, and run models developed for the current ESTCP project to interpret CSIA data. A case study using RTM for CSIA data is included as **Appendix A**.

Section 5 introduces the key RTM software and programs, including those developed for ESTCP Project ER-201029. The overall CSIA-RTM approach is presented.

Key Questions Addressed in Section 5:

- What software applications and platforms are required for CSIA-RTM (**Section 5.1**)?
- What is the model reaction network and kinetics (**Section 5.4**)?
- How is isotope fractionation simulated in the models (**Section 5.4**)?

Section 6 explains where to access the software tools required to perform various levels of RTM modeling for CSIA and how to run the models

Key Questions Addressed in Section 6:

- Where do I download the software for RTM (**Section 6**)?
- How do I install the software (**Section 6**)?

Section 7 provides a step-by-step manual on how to run the template and visualization models developed for this project to site-specific CSIA data.

Key Question Addressed in Section 7:

- How does this software work (**Section 7**)?

Appendix A presents the results of the Case Study for Hill Air Force Base Operable Unit 10 chlorinated solvent plume using the CSIA/RTM tools developed for this project.

Appendix B provides an up-to-date list and chart of literature sources for carbon and chlorine enrichment factors (ϵ)

Appendix C includes the training manual and slides for the RTM-CSIA-MNA Training Course prepared as a part of this project.

Appendix D is a list of laboratories providing CSIA services.

TABLE OF CONTENTS

Quick Start

Acronyms and Equation Parameters

Overview Manual

1.0	The Basics: CSMs, MNA, and CSIA.....	1-1
1.1	Conceptual Model for Chlorinated Ethene Degradation.....	1-2
1.2	Challenges to Applying MNA at Chlorinated Solvent Sites.....	1-4
1.3	Overview of Compound-Specific Isotope Analysis for MNA Remedies.....	1-6
1.4	Why CSIA with Reactive Transport Modeling?.....	1-8
2.0	Background: Conventional MNA (Generation 1 MNA).....	2-1
2.1	Key Attenuation Processes.....	2-1
2.2	Key Methods for Demonstrating Generation 1 MNA Studies.....	2-10
2.3	When to Use CSIA to support MNA Decisions.....	2-12
3.0	Background: CSIA for CSM Development and MNA (Generation 2 MNA).....	3-1
3.1	CSIA Methodology: How are Isotope Ratios Determined?.....	3-3
3.2	Interpretation of CSIA Results.....	3-11
3.3	Conventional Data Interpretation for CSIA.....	3-18
3.4	Practical Aspects of CSIA Implementation.....	3-25
3.5	When to Move to CSIA with Reactive Transport Models.....	3-31
4.0	CSIA with Reactive Transport Models (Generation 3 MNA).....	4-1
4.1	Introduction to Reactive Transport Models.....	4-1
4.2	Example Scenarios.....	4-7
5.0	CSIA with RTM: Overall Modeling Approach.....	5-1
5.1	Software and System Requirements.....	5-1
5.2	User Qualification and Training Recommendation.....	5-2
5.3	Aims and Overview of Models Developed.....	5-2
5.4	Model Reaction Network and Equations.....	5-3
5.5	Model Limitations.....	5-13
5.6	Additional Information.....	5-14
6.0	Downloading and Installing of Software.....	6-1
6.1	PHREEQC Batch or Flow path Reaction Model.....	6-1
6.2	Two Dimensional/Three Dimensional Simulations - PHAST.....	6-2
6.3	Two Dimensional/Three Dimensional Simulations - PHT3D.....	6-3
6.4	Python for Visualization of PHREEQC/PHAST Results.....	6-3

7.0	Step-By-Step Explanation of Template Models	7-1
7.1	Template Model Case 1: Full Dechlorination.....	7-1
7.2	Template Model Case 2: Stall of VC: Detection of potential oxidation (C&Cl-CSIA).....	7-11
7.3	Template Model Case 3: Core Reductive Dechlorination and Fringe Oxidation (C&Cl-CSIA).....	7-15
7.4	Template Model Case 4: Hydrogen Isotope Fractionation During Reductive Dechlorination of PCE/TCE	7-17
	References	R-1

APPENDICES

Appendix A: Case Study

**Appendix B. Literature Sources for Carbon and Chlorine Enrichment
Factors**

Appendix C. RTM CSIA MNA Training Course

Appendix D. CSIA Service Providers

ACRONYMS AND EQUATION PARAMETERS

AFB	Air Force Base
ARD	Advection – Reaction –Dispersion
BTEX	Benzene, Toluene, Ethylbenzene and Xylenes
DCE	Dichloroethene
C	Carbon
CE	Chlorinated Ethenes
C-IMB	Carbon Isotope Mass Balance
Cl	Chlorine
COCs	Constituents of Concern
CR	Chemical Reduction
CSIA	Compound-Specific Isotope Analysis
CSM	Conceptual Site Model
cVOC	Chlorinated Volatile Organic Contaminant
DED	Dual Equilibrium Desorption
DIF	Diffusion Induced Isotope Fractionation
DNAPL	Dense Non-aqueous Phase Liquid
DO	Dissolved Oxygen
EMD	Environmental Molecular Diagnostics
ETH	Ethene
EPA	U.S. Environmental Protection Agency
GC	Gas Chromatography
GC-IRMS	Gas Chromatography Isotope Ratio Mass Spectroscopy
GIS	Geographic Information System
GUI	Graphical User Interface
H	Hydrogen
IF	Isotope Fractionation
IMB	Isotope Mass Balance
IRMS	Isotope Ratio Mass Spectrometry
KIE	Kinetic Isotope Effect
MBT	Molecular Biological Tools
MCL	Maximum Contaminant Level
MNA	Monitored Natural Attenuation
MTBE	tert-Methyl Butyl Ether
NA	Natural Attenuation
OU	Operable Unit
OX	Aerobic Oxidation
PAH	Polyaromatic Hydrocarbons
PCE	Tetrachloroethene (Perchloroethene)
P&T	Purge and Trap
QAQC	Quality Assurance Quality Control
RD	Reductive Dechlorination
RTM	Reactive Transport Modeling
SIRTM	Stable Isotope Reactive Transport Model
SKIE	Secondary Kinetic Isotope Effect
SMOC	Standard Mean Ocean Chloride

SPME	Solid Phase Micro-Extraction
TCE	Trichloroethene
TEA	Terminal Electron Acceptor
USGS	U.S. Geological Survey
VC	Vinyl Chloride
VPDB	Vienna Pee Dee Belemnite
VSMOW	Vienna Standard Mean Ocean Water

EQUATION PARAMETERS

$\alpha =$	stable isotope fractionation factor, ratio of the rate of reaction of the heavy versus the light isotope.
$R =$	ratio of heavy or less common stable isotope to lighter or more common isotope (e.g. $^{13}\text{C}/^{12}\text{C}$)
$\delta =$	the difference between the measured abundance of the heavy isotope in a sample versus the reference material (e.g., $\delta^{13}\text{C} = R_{\text{sample}} - R_{\text{standard}}/R_{\text{standard}}$) – measured in per mil (‰) – Higher δ values are ‘enriched’ in heavy isotope. Lower δ values are ‘depleted’
$\Delta =$	the difference between the δ signal of downgradient versus upgradient (or in time).
$f =$	ratio of concentration of CE at a certain time to the concentration at time 0.
$\varepsilon =$	enrichment factor, related to α by the equation $\varepsilon = (\alpha - 1) * 1000$
$K =$	hydraulic conductivity
$i =$	gradient
$\eta_e =$	effective porosity
$v_s =$	seepage velocity
$\rho_b =$	soil bulk density
$R_c =$	retardation factor
$k_d =$	partition coefficient
$v_c =$	apparent solute velocity
$k =$	reaction rate constant

ACKNOWLEDGMENTS

This report presents the results and conclusions from a collaborative project between researchers at University of Oklahoma (UO), VU University Amsterdam (Vrije Universiteit Amsterdam in Dutch), the Netherlands, and GSI Environmental, Inc. (GSI). This demonstration project was funded by the Environmental Security Technology Certification Program (ESTCP), with the main goal of demonstrating the utility of combining Compound-Specific Isotope Analysis (CSIA) and Reactive Transport Modeling (RTM) to quantify and strengthen support for Monitored Natural Attenuation (MNA) remedies for groundwater contaminated with chlorinated ethene constituents (CEs).

Investigators for this project included Dr. Tomasz Kuder (Principal Investigator, UO), Dr. Paul Philp (Co-Principal Investigator, UO), Dr. Boris van Breukelen (VU), and Dr. Mindy Vanderford and Dr. Charles Newell (GSI). The modeling tool that was generated as part of this project was developed by Boris van Breukelen, Philip Stack and H elo ise Thouement. The microcosm experiment was modeled as part of a research project of Philip Stack. The Hill AFB OU10 site case study was evaluated as part of the dissertation of H elo ise Thouement.

We gratefully acknowledge Kyle Gorder (US Air Force) for his help in identifying potential demonstration sites and coordinating the field work at Hill Air Force Base (AFB), Operable Unit (OU) 10. We also acknowledge the support of AEEC in conducting the field sampling at Hill OU10.

Finally, the project team wishes to thank Dr. Andrea Leeson, Dr. Jeff Marqusee, and the support staff from the ESTCP program office for their help and guidance throughout the demonstration.

This page left intentionally blank.

OVERVIEW MANUAL

1.0 THE BASICS: CSMS, MNA, AND CSIA

Active remediation of contaminated groundwater has been on-going in the United States for over 30 years at a cost of billions of dollars. However, for many sites, remediation technologies have failed to achieve restoration goals. One of the reasons cited for the disparity in remedial performance relative to expectations is the difficulty in characterizing the nature, extent and fate of contamination in heterogeneous environments (NRC 2012).

Increasing attention is being focused on developing detailed, functional Conceptual Site Models (CSMs) that describe the fundamental chemical, geological, and biological processes that control distribution and persistence of contaminants. Site CSMs unite all aspects of the site into a coherent, integrated and actionable set of relationships and are essential in designing effective remedial strategies.

Monitored Natural Attenuation (MNA) is a remedial approach for affected groundwater based on a carefully controlled and monitored demonstration of contaminant attenuation from intrinsic, natural processes (USEPA 1998). Processes such as biodegradation, chemical degradation, dispersion, dilution, sorption, and volatilization can achieve goals related to contaminant mass reduction, plume control and reduction of toxicity. Because active remedies alone rarely attain cleanup goals, MNA is now recognized as a component of almost all remedial strategies.

Much of the success and regulatory acceptance of MNA rests on development of a strong CSM that documents attenuation processes and demonstrates contaminant mass removal using multiple lines of evidence. The 1998 EPA *Technical Protocol for Evaluating Natural Attenuation of Chlorinated Solvents in Groundwater* (USEPA 1998) describes the technical basis for evaluating MNA as a remedy for chlorinated ethenes (CEs) using conventional analyses. The technical protocol articulates an evidence-based approach to application of MNA to chlorinated solvent sites including three lines of evidence:

- Historical groundwater analytical data documenting a clear trend of decreasing contaminant mass over time (e.g. concentration vs. time data).
- Hydrogeologic and geochemical data that indirectly support an active natural attenuation (NA) mechanism.
- Data from field or microcosm studies that directly demonstrate the occurrence of a specific NA process at the site.

MNA remedies are now commonly approved for many sites affected by CEs. Remedies incorporating NA processes have several advantages over active remedies in terms of cost, effort, carbon footprint, and energy savings. While several individual attenuation mechanisms can affect long-term restoration of groundwater plumes, the confirmation that CEs can be destroyed through the action of indigenous microbial communities has provided the strongest support for development of MNA approaches to date.

The best documented method of CE mass destruction by biological processes is through anaerobic biodegradation by a competent microbial community. For many sites, decreasing mass, the presence of intermediate degradation products, low oxygen concentrations, and favorable geochemical indicators (e.g., nitrate, sulfate, alkalinity etc.) are sufficient to support selection of a full or partial MNA remedy. However, in the absence of some or all of these lines of evidence, MNA remedies can be difficult to implement.

Consequently, improved tools to both document and quantify natural attenuation (NA) processes are of vital importance. Since publication of the 1998 guidance, a number of advanced technical methods and tools have been developed to characterize attenuation processes in the subsurface (Adamson and Newell 2014). Molecular biological tools (MBTs) demonstrate the presence and abundance of key organisms and enzymes capable of degrading contaminants in situ (ITRC 2013). Advances in geotechnical characterization methods have identified the importance of geologic heterogeneity to quantify matrix or ‘back’ diffusion (Farhat, Newell et al. 2012). Investigations into groundwater sampling methods have identified sources of sampling variability and demonstrated the utility of high-density sampling for site characterization.

Compound-specific isotope analysis (CSIA) has emerged as a promising new tool to document biological destruction of CEs in the subsurface over the past 15 years (Hunkeler, Meckenstock et al. 2008). Several studies have used CSIA results to demonstrate biodegradation of a variety of organic contaminants including hydrocarbons and MTBE (Kelley, Hammer et al. 1997; Lollar, Slater et al. 2001; Mancini, Ulrich et al. 2003; Kuder, Wilson et al. 2005). However, for CEs, sequential transformation of daughter products and complex sequestration or physical transport processes can make interpretation of CSIA results difficult at many sites. Because of these complexities, implementation of CSIA to strengthen CSMs and support MNA assessments requires new modeling tools.

The following document describes the application of CSIA with Reactive Transport Modeling (RTM) for characterizing subsurface contamination with the goal of strengthening CSMs supporting MNA remedies. CSIA data combined with RTM will improve site data interpretation by accounting for both chemical and physical processes affecting the fate of CEs.

Section 1 includes background information on CE degradation, MNA remedies and the basic application of CSIA to solvent sites. **Section 2** discusses key contaminant attenuation processes and conventional lines of evidence supporting MNA remedies. **Section 3** provides a more in-depth discussion of CSIA data interpretation, sampling strategies, and data management. **Section 4** introduces RTM with a discussion of available models, input data, and examples of their application for various geochemical settings. **Sections 5** through **7** constitute the RTM Technical Manual and describe how to download software, develop input files, and run models developed for the current ESTCP project to interpret CSIA data. A case study using RTM for CSIA data is included as **Appendix A**.

The goal of the guidance is to help site managers determine if CSIA is appropriate for their site, and how CSIA data along with RTM can be used most efficiently to support MNA remedies or optimize combined MNA/active remediation systems.

1.1 Conceptual Model for Chlorinated Ethene Degradation

Microbial degradation of groundwater contaminants can occur by aerobic and anaerobic microbial metabolism. Chlorinated solvents have been known to degrade under anaerobic conditions for several decades, and methods for documenting NA of chlorinated solvent plumes have been published by several authors (Vogel and McCarty 1985; Freedman and Gossett 1989; DeBruin, Kotterman et al. 1992; Hartmans and DeBont 1992; Chang and Alvarez-Cohen 1996; McCarty 1996; USEPA 1998).

Figure 1-1 presents a simplified conceptual model of the degradation of chlorinated ethenes in the subsurface. Releases of CEs to the environment primarily occur as tetrachloroethene

(perchloroethene) (PCE) and/or trichloroethene (TCE) leaking from industrial processes or storage and transport systems. While other solvents (e.g. 1,1,1-trichloroethane, 1,2-dichloroethane, carbon tetrachloride) are frequently encountered, PCE and TCE represent the majority of persistent chlorinated groundwater contaminants and are the primary topic of this guidance.

Secondary release CEs may occur via spread of Dense Non-Aqueous Phase Liquids (DNAPL) towards the hydrogeological base (aquitard) of the aquifer where liquid may accumulate as DNAPL pools or as dissolved PCE/TCE in the water column. As PCE/TCE are typically stable in the short term under aerobic conditions, they need to either spread to anaerobic parts of the aquifer or co-occur with organic rich media such as hydrocarbons to degrade via either reductive dechlorination (RD) and/or chemical reduction (CR).

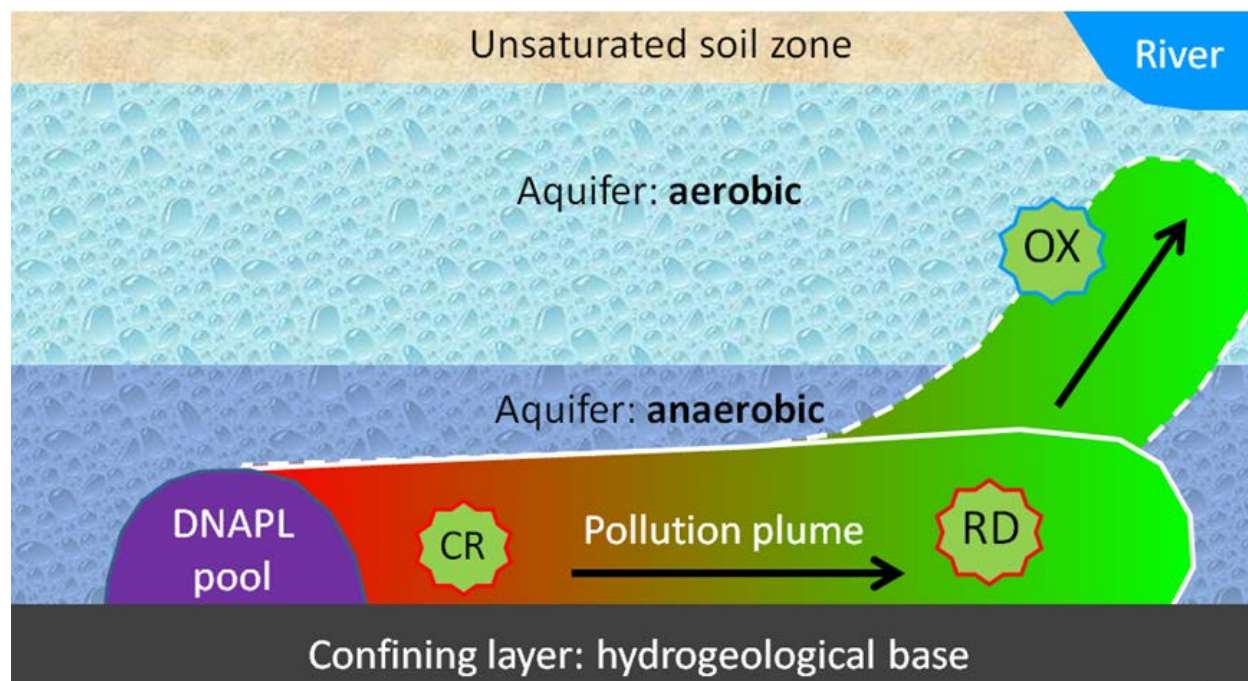


Figure 1-1. Conceptual model for degradation of chlorinated ethenes. RD = reductive dechlorination; CR = chemical reduction; OX = aerobic oxidation.

RD is commonly observed to occur under anaerobic conditions when the availability of organic matter to support bacterial growth is sufficient. **Figure 1-2** shows the full sequence of RD from PCE to ethene (ETH) via TCE, dichloroethene (DCE), and vinyl chloride (VC). DCE and/or VC often accumulate in groundwater due to various factors including insufficiently reducing conditions and the absence of specific microorganisms involved in the final dechlorination steps or because the rate of conversion of parent compounds to DCE is much faster than steps resulting in further degradation. Accumulation of intermediate products is often referred to as ‘stalling’ or a ‘DCE stall’. Fortunately, DCE and VC may also degrade via oxidation under aerobic and anaerobic conditions. However, the oxidative transformation can be hard to confirm as end products are unstable and rapidly converted to carbon dioxide.

While RD is the best documented (conventional) biodegradation process for chlorinated solvents, several studies have found evidence of alternative processes that may be responsible for biodegradation of CEs (Arp, Yeager et al. 2001; Verce, Gunsch et al. 2002; Chapelle, Widdowson et al. 2003). These processes include aerobic and anaerobic oxidation, particularly of anaerobic

daughter products, and aerobic cometabolism. Aerobic degradation processes for CE destruction have been documented under laboratory conditions for many years. Aerobic cometabolism of chlorinated solvents is an evolving field of research (Alvarez-Cohen and Speitel 2001; Chu, Mahendra et al. 2004).

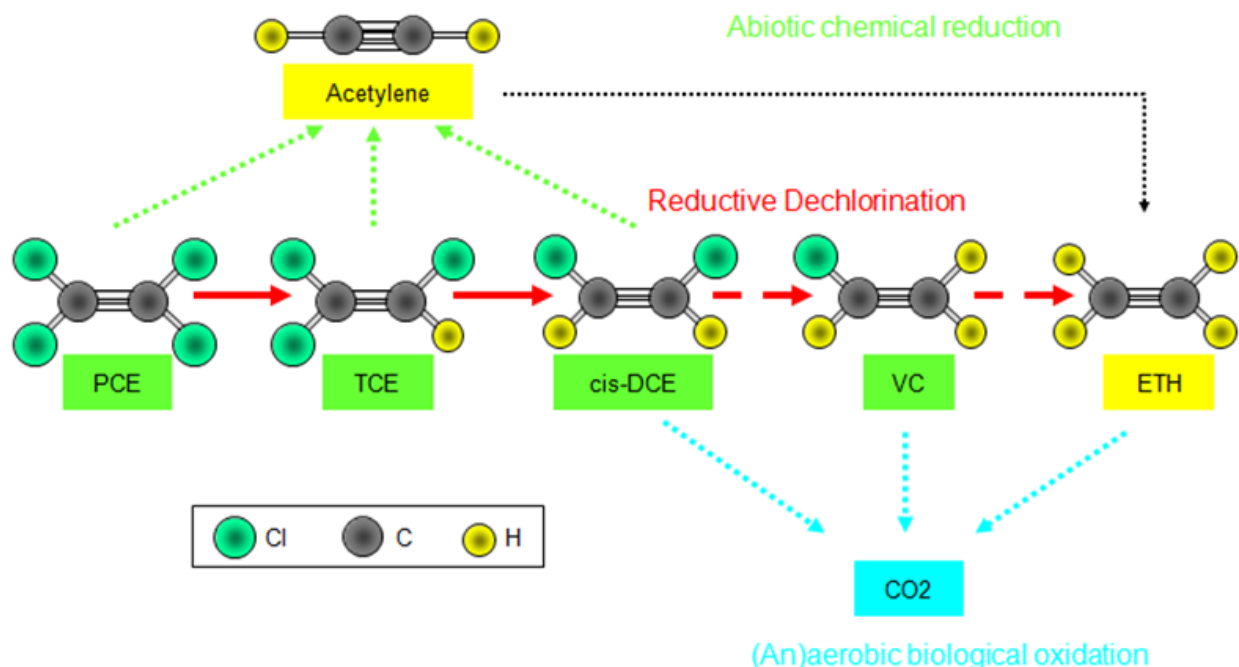


Figure 1-2. Reaction pathways for degradation of chlorinated ethenes. Figure 1-2 summarizes the primary degradation processes in a reaction network for chlorinated ethene degradation (see more detailed reaction networks see Section 2). While the anaerobic degradation pathway is dominant for most sites with MNA remedies, quantifying each pathway is the specific topic of the following guidance.

Cometabolism or fortuitous metabolism occurs when an organism transforms a molecule but does not gain carbon or energy from the process. *Cometabolic degradation of CEs and their daughter products do not leave characteristic intermediate products, so the presence and strength of these pathways is difficult to quantify.* Also, cometabolic pathways may result in very long half-lives, and plume concentrations may not show strongly decreasing trends solely as a result of cometabolic processes. However, aerobic biotransformation of CEs may be a significant attenuation process for certain plumes over long periods of time.

Higher chlorinated CEs like PCE, TCE and even DCE may also degrade via naturally occurring chemical reduction (CR). In lieu of organic matter, reduced minerals such as pyrite can act as electron-donors for the biological reduction process for CEs. Evidence for the strength of this process in most environments is limited and the reaction will not be further considered in the following guidance (Elsner, Chartrand et al. 2008). **Section 2** of this document discusses chemical and biological degradation mechanisms in more detail.

1.2 Challenges to Applying MNA at Chlorinated Solvent Sites

One challenge to applying the 1998 EPA MNA Protocol to chlorinated solvent sites is the indirect nature of the lines of evidence supporting contaminant destruction. Decreasing concentration

trends may be caused either by mass destruction or by other, non-destructive, attenuation mechanisms such as advection and dilution (see **Section 2.1**). In some cases, apparent mass loss may be an artifact of poor sampling design.

It is often difficult to prove that a contaminant is being transformed to benign end-products in sufficient quantity to control the spread of the plume or to reduce toxicity. Estimating the rate of mass decrease from concentration versus time data may not provide a reliable biodegradation rate. Geochemical indicators can demonstrate favorable conditions for anaerobic decay, but can be difficult to interpret due to data variability and do not directly show mass destruction. Conversely, the absence of geochemical indicators may not mean that biodegradation is not occurring.

As stated above, RD is the best documented biodegradation process for CEs. Demonstrating that processes such as aerobic and anaerobic oxidation, and aerobic cometabolism are contributing to plume attenuation is extremely difficult as these processes do not produce stable daughter products. In the absence of pathway-specific daughter products, a critical line of evidence is unavailable in the MNA assessment for more aerobic parts of the plume.

Anaerobic degradation may be significant in historical source zones, where organic co-contaminants such as benzene help sustain dechlorination reactions; however, plume-wide anaerobic biodegradation may not be well supported. The absence of VC over much of the plume may indicate that complete dechlorination is not occurring. Alternately, the absence of VC may indicate daughter products are rapidly degrading by aerobic mechanisms.

Figure 1-2 illustrates the problem in closing C mass balances for chlorinated solvent degradation (that is the sum of all parent CEs and degradation products) when there are so many possible daughter products and mineralization is a potential sink. The molar mass balance approach (summing the molar quantities of all CEs –see **Section 3**) will work if RD is the only transforming process and produced ETH remains stable and measurable. Studies have shown, however, that ETH degrades rapidly under both aerobic and anaerobic conditions (Mundle, Johnson et al. 2012). This situation may lead to underestimating the extent of biodegradation when using a mass balance approach based on CE concentrations alone.

Figure 1-2 also illustrates that the alternative degradation pathways of aerobic oxidation (OX) and CR may confound the molar mass balance approach as the reaction products of these two pathways are commonly not determined (acetylene for CR) or not directly indicative of CE degradation due to high background concentrations (CO₂/HCO₃ for OX). Therefore, the occurrence of OX, CR and ETH degradation may lead to a pessimistic evaluation of CE degradation as decay of parent compounds cannot be linked to reaction products.

For sites that do not conform to the standard conceptualization of anaerobic microbial decay, approval of MNA remedies can be hard to negotiate among site stakeholders, even given decreasing mass concentrations over time. Even in the presence of conventional proof of NA processes, determining degradation rates and quantifying the strength of processes to estimate plume control is a technical challenge.

In addition to geochemical and biological heterogeneity, complexity of subsurface geology and hydrogeology contributes to uncertainty about the strength and location of biodegradation processes. Increasingly, conceptualizing the distribution of mass among phases (including sorbed, DNAPL and dissolved phases) and media (such as fine-grained versus coarse-grained material) is seen as essential to designing and evaluating remedies. Uncertainty on the distribution of

contaminant mass combined with uncertainty on dominant biogeochemical processes acting on different phases and media create technical challenges in demonstrating the efficacy of MNA.

For these reasons, new analytical tools are being developed to document the effect of alternative degradation scenarios and complex environments. CSIA and RTM tools may help overcome some challenges to demonstrating the strength and location of NA processes.

1.3 Overview of Compound-Specific Isotope Analysis for MNA Remedies

The technique of CSIA was developed as a biogeochemical tool in the 1970's and 1980's (Galimov 1985; Hedges, Clark et al. 1988) and has been applied to questions of groundwater contamination since the 1990's. Stable isotope ratio analysis has been used extensively in investigations of environmental releases to characterize the source and fate of several environmentally significant contaminants. Carbon isotope signatures have been used to identify sources of polyaromatic hydrocarbons (PAH) (McRae, Sun et al. 1999), benzene, toluene, ethylbenzene and xylene (BTEX compounds) (Kelley, Hammer et al. 1997) and CE's (Hunkeler et al. 2004; Wiegert, Aeppli et al. 2012; Lutz and Van Breukelen 2014; Lutz and Van Breukelen 2014). The majority of CSIA applications concern the assessment of biodegradation and chemical degradation of several volatile organic-class contaminants (VOCs) in groundwater including MTBE (Kuder, Wilson et al. 2005), benzene (Mancini, Ulrich et al. 2003), and CEs (Van Breukelen, Hunkeler et al. 2005; Pooley, Blessing et al. 2009; Aeppli, Hofstetter et al. 2010; Hunkeler, Abe et al. 2011)

CSIA measures the ratio of stable isotopes of common elements within a contaminant molecule relative to a standard. The method relies on the comparing the abundance of the most common isotopes (e.g., ^{12}C , ^1H , ^{35}Cl , ^{16}O or ^{14}N) with the significantly less abundant heavy isotope of the same element (^{13}C , ^2H , ^{37}Cl , ^{18}O or ^{15}N). Isotope ratios can be used to distinguish between manufactured sources of chemical compounds and identify contaminants that have undergone significant chemical transformation.

The benefit of CSIA applied to groundwater contamination lies in its ability to distinguish microbial mass destruction from other types of mass attenuation. The principle of the analytical approach is that stable isotope ratios (for example $^{13}\text{C}/^{12}\text{C}$) of a contaminant remain constant as the groundwater is diluted. However, the ratio of the heavy isotope increases as degradation proceeds, as microbes 'prefer' to transform molecules composed of lighter elements (**Figure 1-3**) Microbial enzymes react optimally with molecules composed of lighter elements, resulting in an enrichment of heavy isotopes in the remaining parent molecules (Galimov 1985).

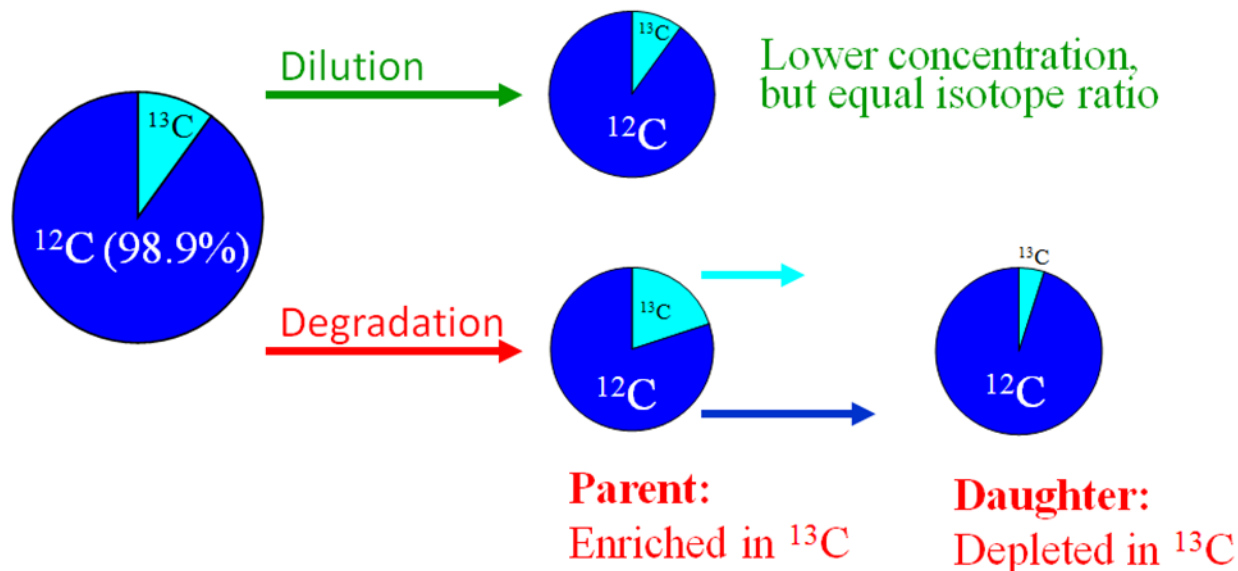


Figure 1-3. CSIA results for a CE subjected to dilution versus biodegradation processes. Dilution results in no change in isotope ratios while biodegradation results in an increase in the proportion of the heavy isotope of the parent compound. A daughter product will have a depleted isotope ratio compared to the parent compound.

A growing number of studies utilizing CSIA to detect and quantify degradation at contaminated sites highlight the potential of CSIA to become a key component of implementing and testing MNA remedies (Hunkeler, Meckenstock et al. 2008). A detailed discussion of CSIA theory and application is provided in **Section 3.0**.

Application of CSIA for supporting remediation management decisions is often hampered by the difficulty in quantitative interpretation of results. A number of reasons have been cited to account for these difficulties:

- Isotope effects differ between biotic and abiotic processes, as well as among different microbial consortia.
- For compounds that are reaction intermediates, (e.g., DCE formed in the reductive dechlorination pathway), the observed isotope effect is a function of simultaneous generation and degradation of the compound, not simply of degradation, creating problems in applying conventional interpretation models directly.
- The Rayleigh equation (the conventional interpretation approach for CSIA data) was written for a closed system, and it does not translate well to complex, flow-through hydrogeological settings.
- Commingling of inputs from multiple sources of the contaminant as well as dissolution from DNAPL and low-porosity matrices complicate interpretation of CSIA results.
- Degradation of CEs usually occurs via reductive dechlorination. However, in addition abiotic reduction (Liang, Dong et al. 2007) and biological oxidation (Abe, Aravena et al. 2009) may occur. Quantifying the latter two degradation processes is difficult as reaction

products are either transient (chemical reduction) or lost in high natural background levels (e.g., CO₂).

The 2008 EPA *Guide for Assessing Biodegradation and Source Identification of Organic Ground Water Contaminants using Compound Specific Isotope Analysis* is a comprehensive discussion of CSIA principals including the theory and protocols for sampling and chemical analysis. The following guidance is intended to supplement the 2008 guide with information on when and how to use CSIA, particularly in combination with RTM to develop CSMs to support MNA remedies or remedial components. A summary of the CSIA method and recommendations for developing a sampling protocol is provided in **Section 3.0** of this guidance;

1.4 Why CSIA with Reactive Transport Modeling?

CSIA applied to CE degradation in laboratory microcosms clearly indicates isotope enrichment of parent compounds undergoing microbial degradation (Bloom, Aravena et al. 2000; Hunkeler, Aravena et al. 2002; Kuder, van Breukelen et al. 2013). Simple microcosm data can be interpreted using the conventional Rayleigh equation approach. However, the conventional application of the Rayleigh equation is insufficient to describe the sequential degradation of CEs involving various intermediates that are controlled by simultaneous degradation and production. Additionally, subsurface environments are highly heterogeneous with multiple processes (transport, degradation and mixing of solutes in groundwater) that can affect transport, the fate of the parent CEs and the daughter products. Application of CSIA to complex environments, therefore, requires new tools to interpret results in the context of fate and transport processes. Numerical reactive transport modeling of isotope effects can potentially combine the benefits of traditional CSIA (robust compound-specific signal of in-situ degradation) with improved quantitative assessment of the data (Van Breukelen, Hunkeler et al. 2005; Atteia, Franceschi et al. 2008).

In comparison with traditional interpretation of the CSIA field data based on the Rayleigh equation, the RTM approach presented in this document has several important benefits:

1. Improvement of a CSM by direct identification and location of prevalent degradation pathways (i.e., reductive biotic dechlorination vs. abiotic dechlorination vs. aerobic degradation) and identification of secondary inputs from DNAPL dissolution or non-degradative sinks such as dilution, dispersion, sorption, matrix (back) diffusion or volatilization.
2. A more accurate assessment of degradation of the parent contaminant.
3. Quantitative assessment of the net degradation/accumulation of the dechlorination intermediates.

2.0 BACKGROUND: CONVENTIONAL MNA (GENERATION 1 MNA)

Decision rationales for application of MNA at sites affected by petroleum or CEs have been well documented and rely on chemical indicators specific to the degradation of each compound class (USEPA 1998; USEPA 1999). Most MNA protocols rely on a “weight of evidence” approach that documents natural processes at the site and the rate of progress toward remediation goals.

2.1 Key Attenuation Processes

Implementation of MNA as all or part of a groundwater remedial strategy relies on the development of a strong CSM and ‘lines of evidence’ documenting the impact of various attenuation mechanisms (ASTM 2008; USEPA 2011).

NA processes include a variety of physical, chemical, and/or biological processes that act, without human intervention, to reduce the mass or concentration of contaminants. These *in situ* processes include both non-destructive physical processes and destructive chemical and biological processes (USEPA 1999). While these processes alone are not always anticipated to result in reduction of contaminant concentrations below clean-up standards, the attenuation mechanisms may produce a collective and substantive impact on concentrations in the long-term. While the processes of advection, dispersion, dilution, and sorption are non-destructive of contaminants, an understanding of their impact can help optimize remedy design and predict remedy performance. A description of each of these key processes is essential to a complete CSM. Also, understanding the parameters based on each of these processes that go into models of contaminant transport and persistence can support interpretation of conventional and CSIA monitoring data.

The primary attenuation and transport mechanisms for groundwater contaminants are summarized below. Many of these mechanisms are characterized by field data collection including methods such as CSIA as well as modeling efforts. An understanding of the site attenuation and transport mechanisms is essential to interpreting both CSIA and conventional contaminant concentration data in support of MNA remedies.

2.1.1 Advection

Advective transport refers to the transport of solutes by the bulk movement of groundwater. Advection moves contaminants from source areas by infiltration through unsaturated zones under the influence of gravity to groundwater, which transports contaminants in the direction of bulk groundwater flow. The volumetric discharge of water in an aquifer is often represented as by *Darcy velocity* – an equation relating discharge to hydraulic head.

$$v_x = \frac{K_x \frac{\partial h}{\partial x}}{n_e} \quad (2-1)$$

The rate at which contaminants move through porous media from advection alone is estimated by the seepage velocity (v_s). The pore water velocity or seepage velocity is the average speed of water movement through the saturated zone. Seepage velocity can be calculated from the hydraulic conductivity (K), gradient (i) and effective porosity (η_e) of the aquifer using the equation:

$$v_s = Ki/\eta_e \quad (2-2)$$

Seepage velocity can be used to estimate the time of travel of a contaminant front (time of travel = distance/ v_s) (Wiedemeier, Rifai et al. 1999).

Hydraulic conductivity describes the intrinsic permeability of a medium and is expressed as the rate at which water moves through a unit area of aquifer (distance/time) (Charbeneau 2000) The gradient has units of distance per distance and porosity is unitless, so the units of seepage velocity are, like K , distance/time. In the subsurface, geologic materials can have widely variable K and porosity values, even over short distances. This heterogeneity results in variable contaminant transport velocities as well as variations in sorption that must be considered in CSM development.

Advection is often the strongest process in aquifers with high porosity and strong gradients. Contaminant transport due to advection can be influenced by recharge as well as groundwater extraction systems. Parameters to model advective transport in aquifers are obtained through field investigations of K , porosity, and gradient and classification and delineation of aquifer sediments.

Factors that support adoption of MNA include demonstrating that NA processes are sufficient to control the plume migration resulting from advection.

2.1.2 Dispersion

Hydrodynamic dispersion causes a groundwater plume to spread perpendicular to the direction of groundwater flow. On the larger scale, dispersion effects in a plume can be seen as reduced concentrations in the center, but wider plumes overall. Mechanical dispersion is the dominant component of total dispersion. Mechanical dispersion occurs due to local variations in groundwater velocity. These variations arise when water passes through pores and path lengths of various sizes, (i.e., tortuosity) or from variable friction within individual pores (Wiedemeier, Rifai et al. 1999). Molecular dispersion is analogous to diffusion and occurs when concentration gradients exist and molecules travel from areas of high to low concentration. (Diffusion is discussed in more detail in **Section 2.1.4.**)

Dispersion is a lumped parameter that is a proxy for the amount of apparent spreading that occurs at a site due to heterogeneity, the vertical variation of horizontal hydraulic conductivity, and changes in groundwater flow direction over time. It should be emphasized dispersion is not an aquifer property that is directly measureable, but a construct that is used to account for aquifer features that appear to reduce the concentration of groundwater plumes as they migrate away from the source.

The advective (reaction) dispersion equation (ARD) is the primary tool used to model solute transport in aquifers. In the ARD equation, dispersivity is a function of groundwater seepage velocity and dispersivity (D).

$$\frac{\partial C}{\partial t} = -v \frac{\partial C}{\partial x} + D_L \frac{\partial^2 C}{\partial x^2} - \frac{\partial q}{\partial t} \quad (2-3)$$

Dispersion occurs in the longitudinal (“alpha x”), transverse (“alpha y”), and vertical (“alpha z”) directions to flow (Wiedemeier, Rifai et al. 1999). Dispersivity is typically estimated using scale-dependent relationships, such as those compiled by Newell et al., 1996 (Newell, McLeod et al. 1996):

$$\text{Alpha } x = 3.28 \cdot 0.82 \cdot \left[\log_{10} \left(\frac{x}{3.28} \right) \right]^{2.446} \quad (\text{Xu and Eckstein, 1995}) \quad (2-4)$$

Alpha x = 0.1 • x (Pickens and Grisak, 1981)
 Alpha y/alpha x = 0.10
 Alpha z = very small value or Alpha z/alpha y = 0.10

(Xu and Eckstein 1995)

2.1.3 Dilution

Dilution within the aquifer occurs when fresh recharge of uncontaminated water enters the area of the contaminant plume. Dilution may result in reduced toxicity due to reduction in the concentration (mass per volume) of contaminant in the plume, but does not destroy contamination.

Dilution effects can be modeled using estimates of recharge entering the aquifer, dimensions of the mixing zone, Darcy velocity of groundwater and thickness of the aquifer or mixing zone (Wiedemeier, Rifai et al. 1999), obtained from field investigations.

2.1.4 Diffusion

Diffusion, or molecular dispersion, is the process by which individual molecules move as a result of kinetic energy of random motion rather than by bulk transport. Historically, diffusion has not been considered a significant process in groundwater modeling; however, its importance is increasingly recognized particularly as it relates to long-term secondary sources such as matrix or back diffusion. Diffusion is modeled using Fick’s Law for diffusive flux:

$$F_D = D_{mol} \frac{dC}{dx} \quad (2-5)$$

Where F_D is contaminant mass flux and dC/dx is the concentration gradient. The molecular diffusion coefficient (D_{mol}) must be estimated from laboratory data and is often dependent on temperature (Fetter 1993). Contaminants can move into low-permeability (low hydraulic conductivity) layers via diffusion and/or slow advection over time. Once in low-permeability layers, contaminants can desorb or back-diffuse into the aquifer over very long time-frames (Boving and Grathwohl 2001; Liu and Ball 2002; Chapman and Parker 2005; AFCEE 2007). Matrix diffusion has the potential to sustain dissolved contaminant concentrations in groundwater long after the source is removed and may be a significant factor for remediation at many sites contaminated with CEs. Depending on the biogeochemical conditions of the low-porosity zone, contaminants may be more or less susceptible to biodegradation while retained in these layers.

Diffusion is not a strong NA process, but diffusion of contaminants into low-porosity matrices can be significant when evaluating the potential success of active remedies and when calculating the anticipated life-time of the plume. Often, matrix or back diffusion will limit the efficacy of active remedies such as pump and treat, making MNA a more attractive long-term remedial option.

Matrix diffusion may also result in confusing CSIA results if the diffusing contaminants have a different isotope signatures than the bulk of molecules in the transmissive zone.

2.1.5 Sorption/Retardation

Sorption is the process by which dissolved contaminants partition onto solids. Desorption or dissolution is the repartitioning of solutes back into the dissolved phase. Sorption can cause retardation or slowing of plume migration as well as reducing bioavailability of contaminants for microbial degradation.

Retardation factors are calculated to account for two processes: 1) the degree to which a particular constituent moves slower than groundwater seepage velocity, and 2) the ratio of total constituent mass per volume of aquifer matrix to the volume of dissolved constituents. Retardation factors (R_c) are calculated from the soil bulk density (ρ_b) and the effective porosity

(η_e) of the medium and the partition affinity of the specific contaminant (K_d). K_d is calculated from the fraction organic carbon in the soil and the affinity of the compound to sorb to organic matter ($K_d = f_{oc} * K_{oc}$). K_{oc} is determined from laboratory experiments while ρ_b and η_e are characteristics of the aquifer solids. Retardation factors are, therefore, dependent on both the characteristics of the medium and the specific contaminant being evaluated.

$$R_c = 1 + \frac{\rho_b \times K_d}{\eta_e} \quad (2-6)$$

Overall, R_c is lower in sandy, low organic matter sediments and greater in less porous soils with higher organic matter content. Retardation affects transport by reducing the apparent solute velocity (v_c) by the seepage velocity divided by the retardation factor:

$$v_c = v_s / R_c \quad (2-7)$$

Slow desorption from sediments can result in long-term, low-level inputs to a plume – similar to matrix diffusion discussed above. Therefore, sorption mechanisms are of major importance to the eventual size and longevity of a contaminant plume.

Two characteristics of aquifer material have the greatest impact on sorption: grain-size and organic content. CEs and other organic compounds sorb through hydrophobic bonding, so the quantity of organic matter in the solids controls sorption and retardation. Typically, aquifer material is low in organic matter, so hydrophobic bonding is only anticipated to be significant in very limited areas.

Unlike matrix diffusion, where diffusion in and out of matrices follow roughly the same temporal kinetic profile, many aquifer sediments display rapid sorption followed by very slow desorption of hydrophobic organic compounds (Pignatello and Xing 1996; Chen, Lakshmanan et al. 2004). This phenomenon is referred to as dual-equilibrium desorption (DED) or desorption hysteresis. DED can have significant impacts on both the persistence of plumes and the availability and bioavailability of contaminants. Therefore, identification of aquifer materials with low-permeability or high organic matter is essential to evaluating remedial performance in the long term.

2.1.6 Abiotic Degradation

Abiotic chemical degradation involves the spontaneous chemical transformation of a contaminant. Spontaneous transformation is not influenced by most geochemical conditions such as the presence

or absence of oxygen (Vogel and McCarty 1987), but may be influenced by factors such as temperature. Therefore, abiotic degradation occurs in both aerobic and anaerobic environments.

Most poly-chlorinated solvents, such as PCE and TCE, do not undergo significant spontaneous reactions such as hydrolysis. 1,1,1-Trichloroethane (1,1,1-TCA) is the exception, transforming spontaneously to acetic acid and 1,1-dichloroethene (1,1-DCE) (Vogel and McCarty 1987). At 1,1,1-TCA sites, 1,1-DCE in a groundwater plume is an indication that the parent 1,1,1-TCA has undergone spontaneous chemical degradation. 1,1-DCE is extremely resistant to most forms of chemical and biological degradation, and can persist for long periods. Some chlorinated volatile organic contaminants (cVOCs) like 1,1-DCA and carbon tetrachloride hydrolyze, but have very long half-lives on the order of 40 to 60 years (Wiedemeier et al. 1999). The inclusion of 1,4-dioxane in commercial preparations of 1,1,1-TCA solvent was intended to stabilize the compound from spontaneous decay (Zenker, Borden et al. 2003).

As stated in **Section 1**, higher chlorinated CEs like PCE, TCE and even DCE may also degrade via naturally occurring CR, where reduced minerals such as pyrite can act as electron-donors for the biological reduction process for CEs. However, this is not considered to be a major fate process for CEs (Elsner, Chartrand et al. 2008).

2.1.7 Biodegradation

CE biodegradation in the subsurface has been a topic of intensive research for over 20 years with multiple degradation pathways described in the literature (Vogel and McCarty 1987; Freedman and Gossett 1989; DeBruin, Kotterman et al. 1992; Hartmans and DeBont 1992; Chang and Alvarez-Cohen 1996; Bradley and Chapelle 1997; Klier, West et al. 1999; Bradley and Chapelle 2000; Chen, Lakshmanan et al. 2004). Complete decay chains for CEs developed by Truex et al. (2007) (Truex, Newell et al. 2007) for anaerobic, aerobic, and anoxic (in the middle between strongly anaerobic and strongly aerobic) geochemical environments are shown in **Figures 2-1, 2-2, and 2-3**.

Biological degradation can be separated into two basic processes (McCarty 1996): 1) use of an organic compound to provide energy and material for growth (primary growth and carbon substrate) and 2) unintentional microbial metabolism that does not benefit the organism directly (co-metabolism). Use of organic constituents as a primary growth substrate is the most efficient mechanism as it results in both degradation of the compound and supports growth of the degrading community. Because the microbes gain energy for growth and reproduction by transferring electrons from an electron donor to an electron acceptor, a target contaminant filling one of these roles is highly likely to be transformed.

In the case of anaerobic RD, depending on the geochemical characteristics of the groundwater (such as redox conditions) and the type of microorganisms present, organic compounds can either be the electron donors or acceptors. If the redox conditions are favorable, biodegradation is expected, but it can be fast or slow depending on the geochemical and thermodynamic conditions and the specific microbial community as well as bioavailability factors.

CEs are used as terminal electron acceptors by strictly anaerobic organisms. These reactions only occur under anaerobic conditions (i.e., no or very low oxygen conditions). With the CE as an electron acceptor, dissolved hydrogen is the electron donor (generated through other fermentation-based biological reactions under anaerobic conditions). The general form of the reductive dechlorination reaction is:



Hydrogen is generated by fermentation of other non-chlorinated compounds; and when the reaction is completed, the chlorinated solvent has been consumed to form a dechlorinated reaction by-product (daughter product) and a chloride ion. Note that most of the reaction by-products can also be biodegraded via reductive dechlorination. However, dechlorination of parent compounds is more advantageous to the microorganisms, so daughter products can build up in groundwater until parent compounds are degraded (the so-called DCE or VC “stall”).

Co-metabolism of contaminants is typically less important under naturally-occurring conditions (Wiedemeier, Rifai et al. 1999) as the biodegradation rates are much lower. The low co-metabolism rates are explained by the fact that reaction of contaminants does not provide the microorganisms any direct benefit. However, in cases where the compound is extremely resistant to degradation, an initial co-metabolic transformation can form a more labile compound and speed the degradation (Casing and Aitken, 2000). Co-metabolic degradation may have cumulatively large effects over large distances and time frames.

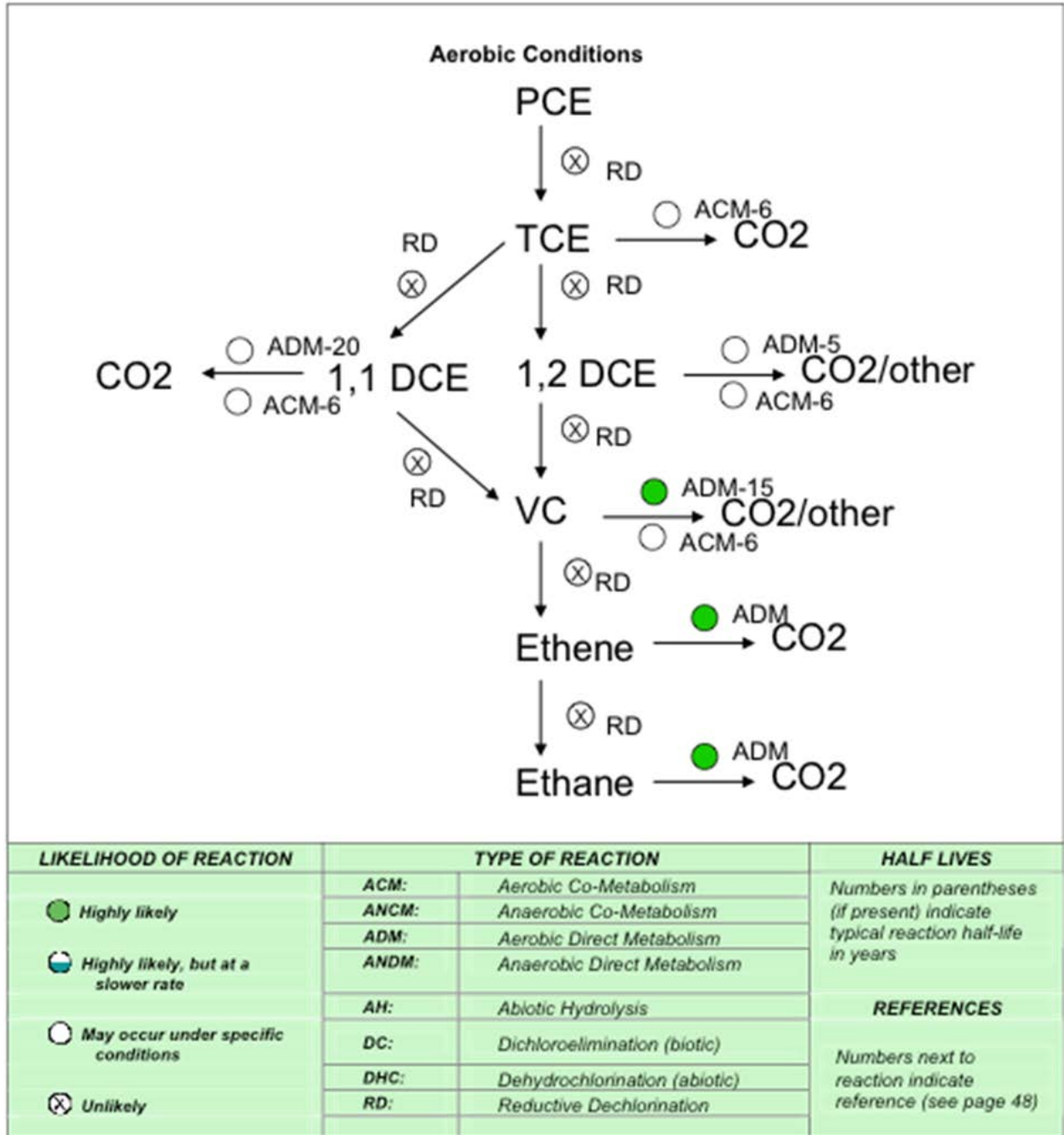


Figure 2-1. Dechlorination Reactions for PCE under the Aerobic Geochemical Setting. Excerpted from (Truex, Newell et al. 2007).

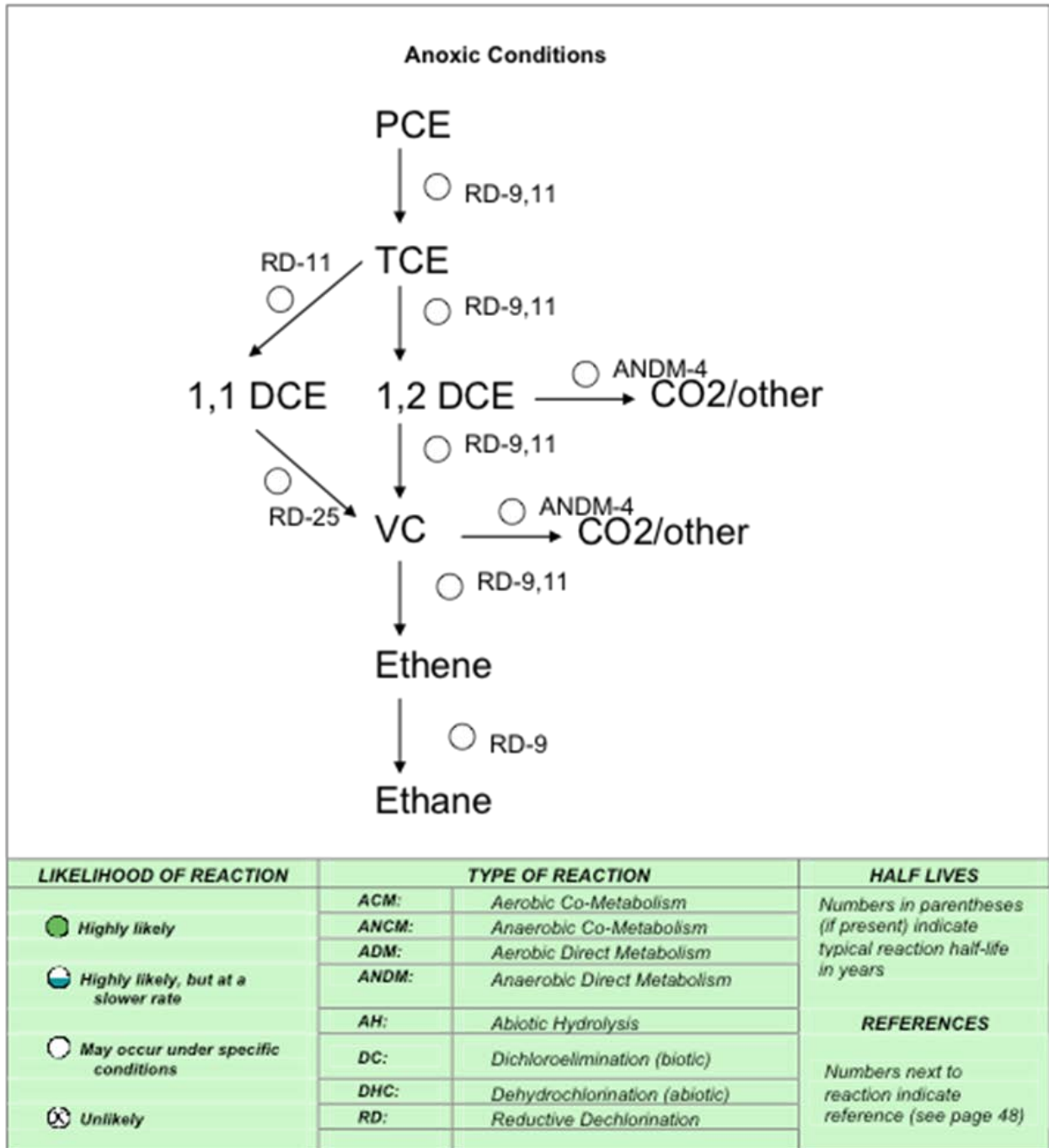


Figure 2-2. Dechlorination Reactions for PCE under Anoxic Geochemical Setting. Excepted from (Truex, Newell et al. 2007).

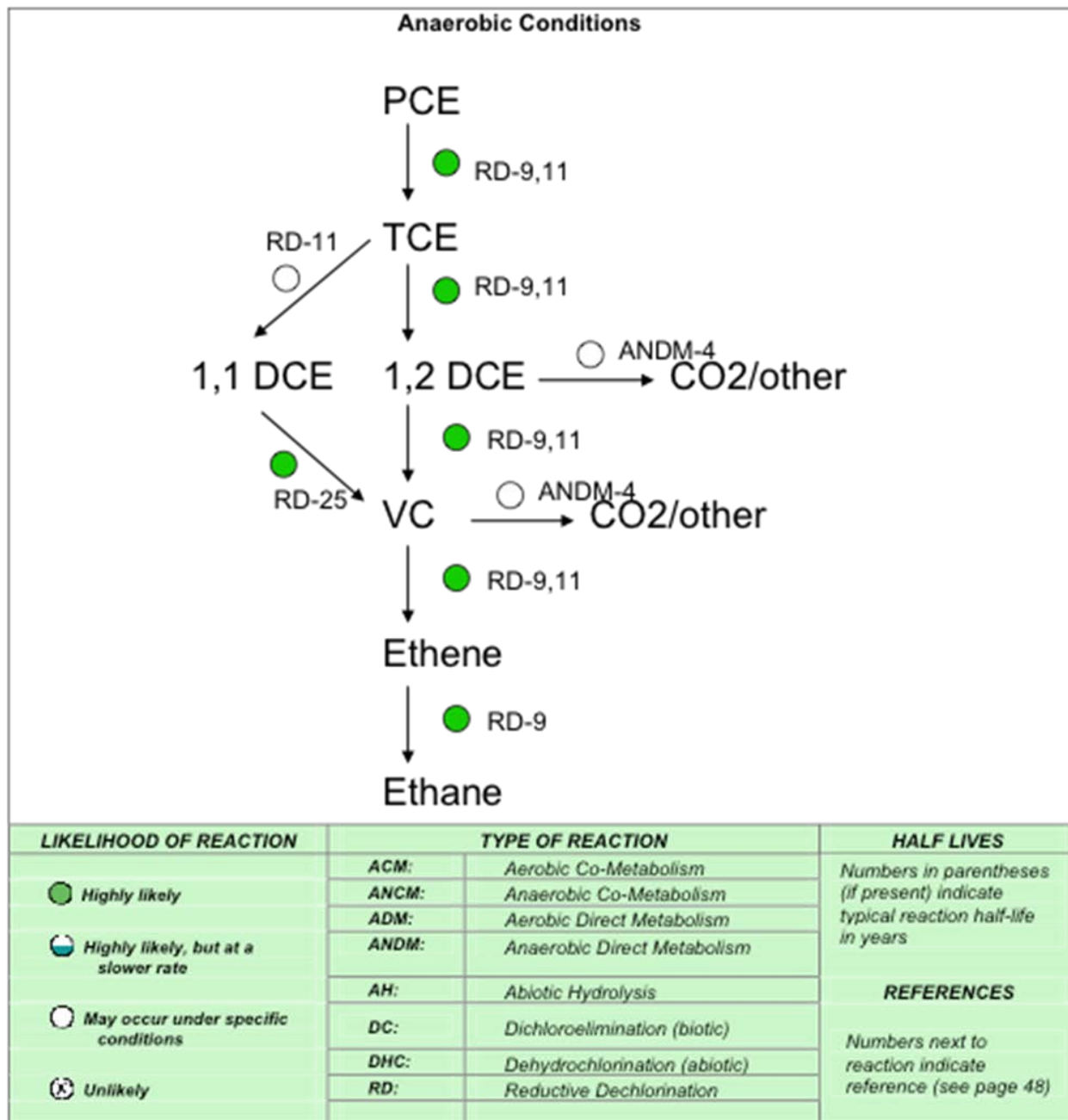


Figure 2-3. Dechlorination Reactions for PCE Under Anaerobic Geochemical Setting
 Excepted from (Truex, Newell et al. 2007).

2.1.8 Volatilization

CE's released to soil tend to migrate downward under the influence of gravity until contacting a dense or very low porosity layer. However, CEs are volatile and can diffuse from contaminated media into the vapor phase, particularly in the unsaturated or vadose zone. Once in the vapor phase of the vadose zone, CEs can move by diffusion or advection (induced by spatial differences in soil gas pressure) spreading contamination. Factors influencing the horizontal and vertical distance over which vapors may migrate in the subsurface include source concentration, depth, soil porosity and moisture content, and time since the release occurred. Saturation or high moisture levels in the vadose can impede transport of CE vapors as can low-permeability zones. Biodegradation in the vadose may reduce concentrations, thus preventing exposure to potential receptors.

In recent years, potential exposure through vapor intrusion into buildings has been a focus of research and regulation (DoD 2009; Eklund, Beckley et al. 2012). Support for MNA remedies may require vapor investigations to determine if vapor exposure pathways are controlled by site conditions. CSIA methods have been used to distinguish vapor intrusion from contaminated subsurface media from indoor sources of CEs (McHugh, Kuder et al. 2011,) and may provide important information for the development of CSMs for MNA remedies at sites where vapor intrusion is a concern.

2.2 Key Methods for Demonstrating Generation 1 MNA Studies

2.2.1 Concentration vs. Time Data and Statistical Trend analysis

The first line of evidence in evaluating natural attenuation at a site is the development of graphs showing historic concentration vs. time at various points within the plume. For most sites, at least 2 years of quarterly data or 8 semi-annual samples are required for a preliminary evaluation; however, many sites have significantly larger datasets. Concentration at individual wells versus time can be plotted as straight values or as log-transformed quantities. The slope of the line through the data can then be evaluated to determine if the trend is increasing, decreasing, or stable or non-parametric methods such as Mann-Kendall analysis can be used to evaluate a trend. In addition, plume stability analysis and plume-level total dissolved mass estimates can be plotted versus time to demonstrate plume-wide reduction in mass (Vanderford 2010; NJDEP 2012). Recently, mass flux and mass discharge calculations have been applied to demonstrate plume control and risk reduction (Farhat, Newell et al. 2006; NJDEP 2012).

2.2.2 Daughter Products

As illustrated in **Figures 2-1** through **2-3**, biological decay chains for CEs produce a variety of secondary products. The presence of dechlorination daughter products is one of the key supports for MNA at CE sites. One potentially confusing decay process is production of TCE by the elimination of one Cl atom from PCE. For sites with limited historic information on sources, determining whether PCE or TCE is the primary parent compound can be challenging. For TCE, the primary anaerobic degradation product is *cis* 1,2-DCE. Depending on the microbial community, varying amounts of *trans* 1,2-DCE and 1,1-DCE can also be generated. The anaerobic dechlorination process can produce VC from DCE congeners, but the process is less favored than the initial steps when parent compounds remain. When DCE apparently builds up in a CE affected aquifer without further transformation to VC, this is referred to as 'stalling' and is a major concern of stakeholders reviewing MNA remedies.

2.2.3 Conventional Attenuation Rate Estimates

First-order attenuation rate constant calculations can be an important tool for evaluating NA processes at groundwater contamination sites. Specific applications identified in USEPA guidelines (USEPA, 1999) include use in characterization of plume trends (shrinking, expanding, or showing relatively little change), as well as estimation of the time required for achieving remediation goals. However, the use of the attenuation rate data for these purposes is complicated as different types of first-order rate constants represent very different attenuation processes. The figure below illustrates two different approaches to calculating rate constants:

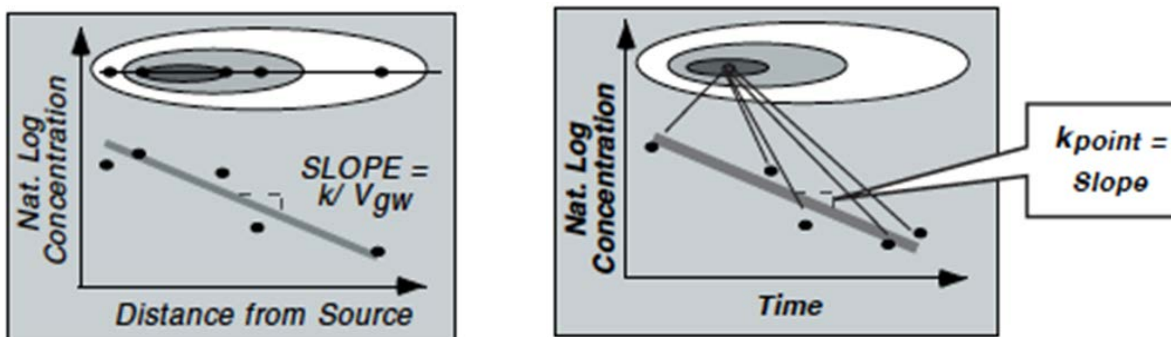


Figure 2-4. Calculation method for concentration versus time (k_{point}) and concentration vs. distance (k) rate constants. (Newell, Rifai et al. 2002)

2.2.4 Geochemical Indicators

Naturally occurring geochemical constituents and processes affect and are affected by anthropogenic releases. Several geochemical parameters can indicate the status of biodegradation processes within groundwater plumes. Hydrocarbon constituents (for example BTEX) are degraded aerobically, but, in the process, oxygen is depleted from areas of high metabolism. Conversely, CEs are more labile under anaerobic conditions, where oxygen and other terminal electron acceptors (TEAs) have already been depleted. The 2003 USGS *Methodology for Estimating Times of Remediation Associated with Monitored Natural Attenuation* describes several geochemical constituents and conditions under which CE biodegradation, particularly by RD, are favored (USGS 2003). The geochemical conditions of an aquifer, particularly those focusing on the presence of TEAs, are considered a secondary line of evidence for MNA remedies.

The most common TEAs in groundwater are oxygen (O_2), nitrate (NO_3), ferric or oxidized iron ($Fe(III)$ or Fe^{+3}), sulfate (SO_4) and carbon dioxide (CO_2). Many TEAs are included as field parameters in routine groundwater sampling events to confirm 'stable' conditions for low-flow sampling (Puls and Barcelona 1996). A thorough geochemical investigation of MNA at a site would include a monitoring program including the following constituents:

- **Oxygen** – Dissolved oxygen (DO) in groundwater is primary driver of many aerobic biodegradation processes, but can impede processes that rely on anaerobic conditions. Oxygen provides microbes with the most energetically favored electron acceptor for degradation of fuels, but inhibits RD of higher chlorinated CEs. DO is the key determinant of the type and diversity of microbial communities in the subsurface. Concentrations of oxygen can help categorize and environment as aerobic, micro-aerophilic, and anaerobic and determine the likelihood of CE degradation by RD.

- **Oxidation-Reduction Potential (ORP)** – ORP is related to DO. Redox potentials of +100mV or less, corresponding to a DO < 1 mg/L, are indicative of conditions appropriate for RD.
- **Nitrate** – organisms will consume NO₃ in the absence of oxygen. Indicators of anoxic conditions include a depletion of NO₃ in favor of nitrite (NO₂). Generally, NO₃ concentrations below 1.0 mg/L are favorable to RD and, as NO₂ is unstable, any detections of NO₂ indicate anaerobic conditions.
- **Iron** –The oxidized form of iron (Fe(III) or ferric iron) can be used as an electron acceptor during anaerobic biodegradation of CEs, generating Fe(II) (ferrous iron). Reduced iron concentrations can be monitored in the aquifer as a potential indicator of conditions conducive to anaerobic biodegradation of cVOCs.
- **Sulfate** – Sulfate is a common TEA in marine environments and sulfate reduction is a pathway used by a number of microbial genera. Sulfate reduction results in high sulfide concentrations and generation of ferrous sulfide minerals.
- **Methane** – Detection of methane (>0.5 mg/L) in environmental samples indicates that methanogenesis is occurring either through reduction of CO₂ as a TEA or direct reduction of organic compounds.
- **Alkalinity** – Alkalinity, under neutral pH conditions is primarily composed of bicarbonate (HCO₃), the dominant inorganic carbon species at neutral pH. When evaluating potential biodegradation scenarios, elevated alkalinity can be associated with microbial oxidation of organic compounds.
- **Physical parameters** – Temperature, conductivity and pH can fluctuate in response to active microbial degradation as well as influxes or drawdown of the aquifer.
- **Chloride** – Chloride can be released as CEs are reduced. Elevated levels of chloride relative to background levels can indicate ongoing RD.

However favorable geochemical indicators appear, they provide only indirect evidence of NA processes and have to be interpreted with other lines of evidence.

2.2.5 Laboratory and Molecular Biological Tools

Laboratory microcosms and an expanding array of MBTs (also called Environmental Molecular Diagnostics [EMD]) are considered a tertiary line of evidence supporting adoption of MNA remedies. Historically, laboratory tests were used to demonstrate that microbes capable of degrading specific contaminants were present in aquifer materials. Laboratory testing has been applied at sites with recalcitrant or persistent constituents. Increasingly, laboratory tests are being supplanted by direct measurement of microbial biomarkers through DNA amplification and other molecular techniques (ITRC 2013).

In many cases, CSIA is considered along with MBTs and laboratory studies as a tertiary line of evidence supporting MNA (NJDEP 2012). CSIA has been applied along with MBTs to characterize CE contaminated sites (Hunkeler, Abe et al. 2011; Damgaard, Bjerg et al. 2013).

2.3 When to Use CSIA to support MNA Decisions

A 2007 survey on application of MNA remedies found that MNA was determined to be feasible as a remedy or remedy component at over 75% of sites where it was evaluated using conventional

methods described above (Truex, Newell et al. 2007). The survey found that MNA could be used as a sole remedy at 36% of sites and in combination with other remedies at 46% of sites. MNA was determined to be infeasible at 23% of sites. In the survey, almost 70% of respondents stated that anaerobic degradation is the primary NA process occurring in the plume. While geochemical indicators were used extensively to support MNA efforts, the primary line of evidence supporting use of MNA was the presence of daughter products and evidence of reduction in dissolved contaminant mass.

The survey results suggest the conditions under which MNA for CEs, supported by conventional analysis, may not be accepted as a component of the site remedy. These conditions include:

- Sites where daughter products such as DCE and VC are not found in high concentrations.
- Sites with anaerobic cores that may still have aerobic or microaerophilic plume fringes, or
- Sites with largely aerobic conditions.
- Sites where advection is strong process may present concerns of plume growth, particularly in areas where the plume migrates off site. MNA may be approved as a source treatment, but stakeholders may still be skeptical of its capacity to control spread of the plume.
- Sites where DCE and VC appear to be persistent.
- Sites with multiple primary sources of CEs and where different fate processes may be affecting contaminants from the various sources.

The decision to conduct CSIA analysis is usually made when insufficient daughter product and geochemical evidence is present to demonstrate complete anaerobic decay. Many sites with aerobic or partially aerobic groundwater plumes cannot attain regulatory acceptance of an MNA remedy even when there is evidence of decreasing contaminant mass. This situation arises when stakeholders are skeptical about the strength, speed or contaminant-destructive nature of attenuation processes. CSIA can also be applied to evaluate the efficacy of enhanced biodegradation remedies including *in situ* biostimulation or bioaugmentation. CSIA can be used to monitor the progress of natural attenuation or active biological remediation, and identify remedies that are not performing as expected. In the case where multiple sources of CEs are suspected, CSIA can be used to identify sources to strengthen the CSM.

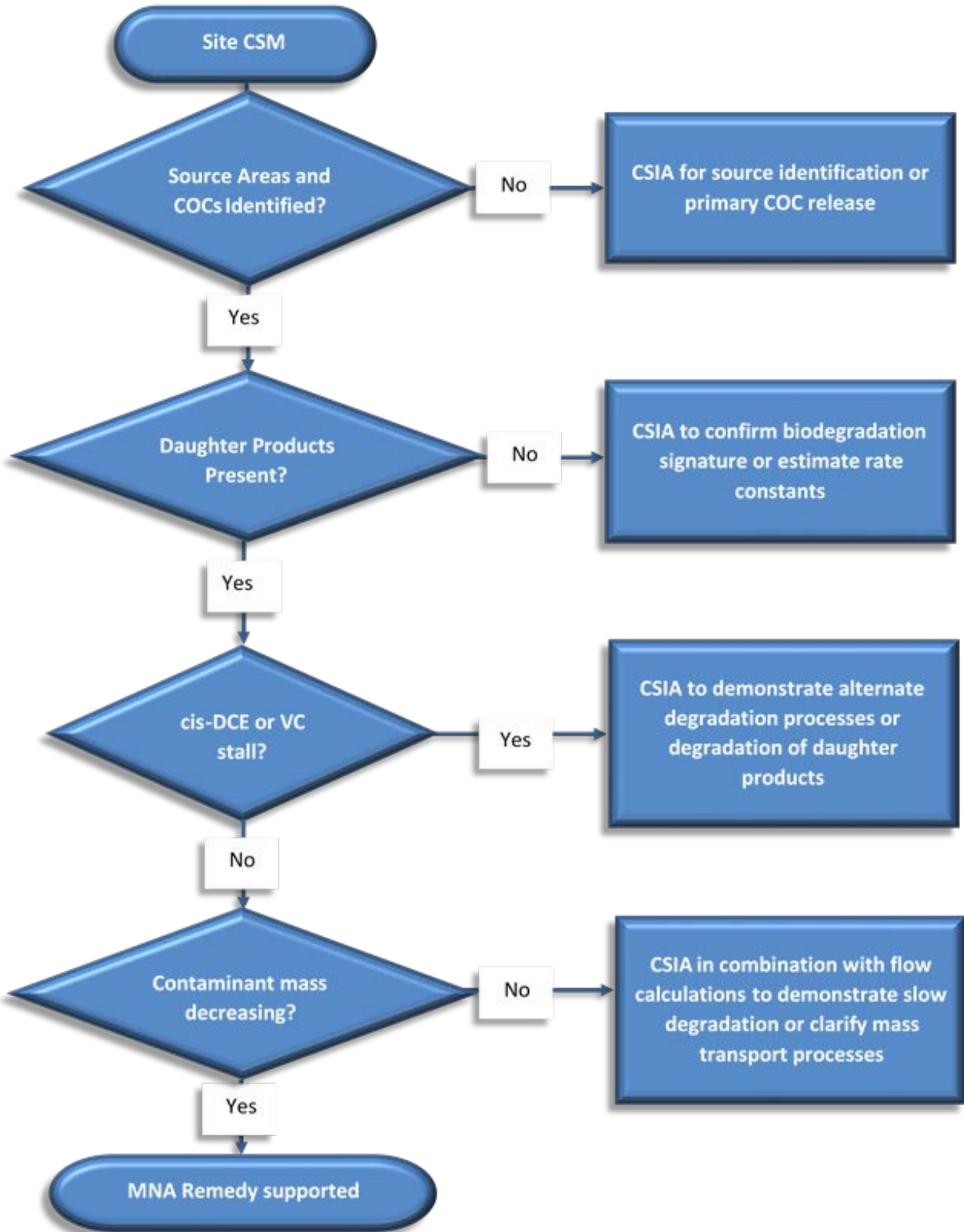


Figure 2-5. Decision matrix for applying CSIA for MNA.

3.0 BACKGROUND: CSIA FOR CSM DEVELOPMENT AND MNA (GENERATION 2 MNA)

CSIA (Compound-Specific Isotope Analysis) combines chromatography and mass spectrometry to determine isotope ratios of elements within individual chemical compounds, for example, the ratio of $^{13}\text{C}/^{12}\text{C}$ in TCE in a groundwater sample. While the ability to analyze isotope ratios in single-compound samples dates back to the first half of the 20th century, CSIA is still a relatively new approach. Commercially available CSIA instrumentation was introduced two decades ago, initially for C and N isotopes (Sessions, 2006). CSIA for H became available a decade ago (Sessions, 2006), and CSIA for Cl became available even more recently (Sakaguchi-Soder, Jager et al., 2007).

Application of CSIA to environmental contaminant studies appeared shortly after the instrumentation became available (for example, [Lollar, 1999]). Since the 1990's, CSIA has evolved from purely academic research to a technique with widespread application in environmental remediation projects. CSIA has been applied to the analysis of contaminated groundwater samples to identify sources of contamination and to confirm biological degradation processes (Hunkeler, Chollet et al. 2004; Kuder, Georgi et al. 2005; Lollar, Slater et al.). In such applications, stable isotope ratios of carbon ($^{13}\text{C}/^{12}\text{C}$), hydrogen (2H/1H), and at lesser scale, also nitrogen ($^{15}\text{N}/^{14}\text{N}$), chlorine ($^{37}\text{Cl}/^{35}\text{Cl}$), and bromine ($^{81}\text{Br}/^{79}\text{Br}$) have been utilized to identify sources and fate of fuel, solvent, and munitions contaminants. An excellent summary of these applications is provided in "A Guide for Assessing Biodegradation and Source Identification of Organic Ground Water Contaminants using Compound Specific Isotope Analysis (CSIA)" published by the USEPA in 2008 (Hunkeler, et al. 2008).

The isotope composition of given chemical compound in the environment reflects the compound's origin and, in part, determines its fate. The initial isotope compositions of industrial chemicals reflect their manufacturing feedstocks (e.g., for C isotopes these include crude oil, natural gas, and biomass) and the manufacturing processes (e.g., petroleum distillation, distillate reforming or chemical synthesis). Given those variables, isotope compositions of different lots of a given chemical manufactured at different facilities and/or at different dates often vary.

CSIA Definitions

Isotopologue: molecules of the same chemical species with different isotope composition.

Isotope fractionation: a change of the bulk compound's isotope ratio, occurring over time or space due to a (bio-) chemical transformation or due to non-destructive physical processes.

Isotopomer: isotopologues with the same number of heavy isotopes, but located at different positions within the molecule.

Primary isotope effects: atoms or functional groups directly involved in the chemical transformation influence the rate of reaction.

Secondary isotope effects: atoms or functional groups remote from the reacting atoms in the chemical transformation influence the rate of reaction.

Isotopic shift: the difference between the isotopic ratio at the source and a point downgradient or the ratio at an initial time and a later time ($\Delta^{13}\text{C}$).

Kinetic isotope fractionation: isotopic fractionation resulting from non-reversible (bio)-chemical reactions.

After the chemicals are released into the environment, physical attenuation and (most importantly) *in situ* biological degradation lead to alterations of the initial isotope ratios. To discuss those changes, it is convenient to introduce the concept of **isotopologue** (molecules of the same chemical species with different isotope composition are referred to as isotopologues). During (bio-)chemical transformations, isotopologues often react at slightly different rates. Typically, the heavy isotope (e.g., ^{13}C , ^2H , ^{37}Cl) present at a reaction center slow down the reaction rate. Also, certain pathways of physical (non-degradative) attenuation in the environment favor movement or sequestration of compounds with specific isotope characteristics. A simple example of the latter is provided by comparison of gas diffusion coefficients of isotopologues, where the rate of diffusion is inversely proportional to the square root of the molecular mass of the molecule.

These isotope-specific reaction rates and/or physical coefficients lead to **isotope fractionation**. Isotope fractionation is a change of the bulk compound's isotope ratio, occurring over time or space due to a (bio-)chemical transformation or due to non-destructive physical processes. In the case of environmental contaminants, the single most significant driver of isotope fractionation is *in-situ* biodegradation (Hunkeler et al., 2008).

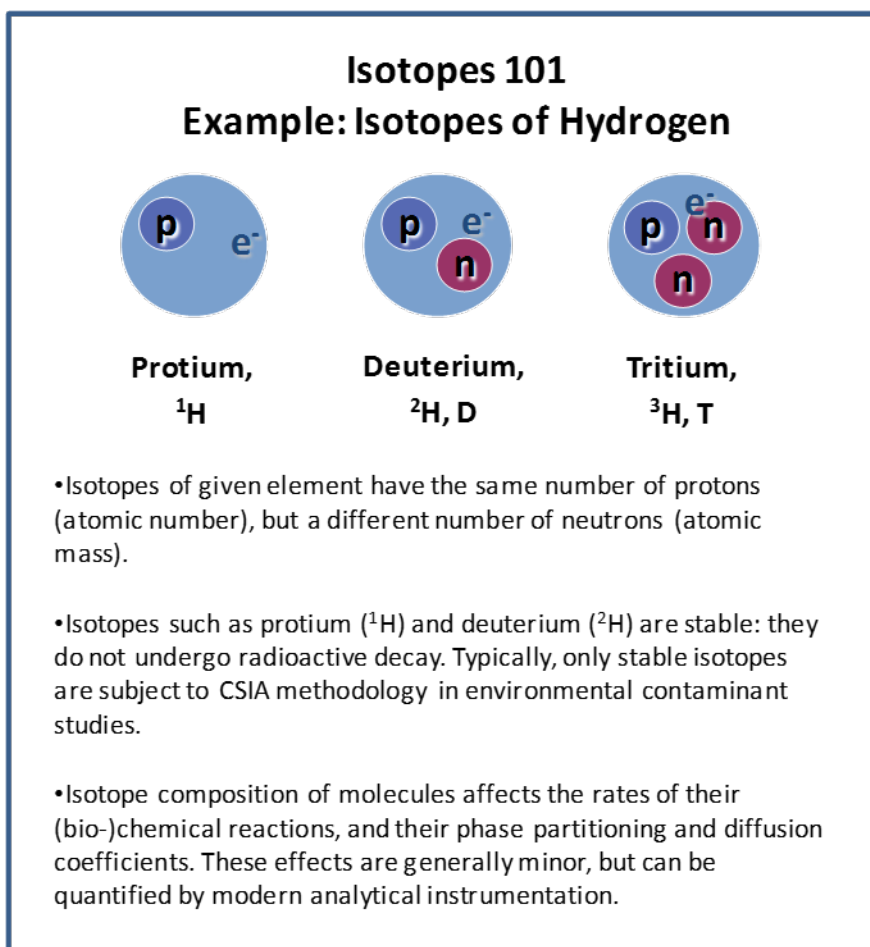


Figure 3-1. Explanation of stable isotopes.

The patterns of isotope fractionation resulting from contaminant attenuation can be determined using appropriate analytical chemistry methods and used as evidence to characterize attenuation processes outlined in **Section 2**. The following sections will address: 1) CSIA methodology; 2) interpretation of CSIA data; and 3) implementation of CSIA in contaminated site assessment.

3.1 CSIA Methodology: How are Isotope Ratios Determined?

3.1.1 CSIA Analytical Method

The isotope ratios are measured using an analytical technique known as Gas Chromatography–Isotope Ratio Mass Spectrometry (GC-IRMS). A schematic diagram of a GC-IRMS is shown in Figure 3.2. In this technique, compounds mixed within a medium are separated from the mixture using traditional methods such as gas chromatography (GC). In C and H CSIA, separated compounds eluting from the GC are fed into an in-line reactor and converted to carbon dioxide (CO₂) and hydrogen (H₂), respectively. These conversion products enter the IRMS for determination of their isotope ratios. The values of ¹³C/¹²C and 2H/1H are obtained by integration of peaks of the isotopologues of CO₂ and H₂, respectively. For Cl CSIA, the analytes are passed from the GC into the mass spectrometer and ionized in the electron source. The isotope ratio of ³⁷Cl/³⁵Cl is determined on a pair (or pairs) of isotopologue ions, with and without ³⁷Cl.

The isotope ratios are obtained by integration of at the isotopologue peaks, for the “heavy isotope” and “light isotope” isotopologues, respectively. These isotope ratios must be normalized, using a standard of known isotope composition. In C and H CSIA, pulses of CO₂ and H₂, respectively, are introduced into the IRMS during analysis as internal references and their isotope ratios are obtained alongside those of the target analytes. The raw output of the mass spectrometer is then mathematically corrected, to force the raw isotope ratios of the internal reference gas pulses to match the known isotope composition of the internal reference gas.

In Cl CSIA, the reference must be identical to the compound being analyzed (e.g., determination of ³⁷Cl/³⁵Cl of TCE requires using a TCE reference). The Cl reference compound is introduced into the mass spectrometer during analysis or reference samples are inserted into the daily sequence of samples for so-called standard isotope bracketing.

In environmental sciences, isotope ratios are reported using delta (δ) notation (**Equation 3-1**, where HE/ LE represent the heavy/light isotope ratio of element E). The δ notation shows a difference of the measured sample from an international standard (the international standards of the relevant elements are shown in **Table 3.1**). Small fractional δ values are usually expressed in permil (‰) by multiplying Equation 3-1 by 1000 (e.g., δ¹³C = 0.0032 is written as δ¹³C = 3.2 ‰).

$$\delta^{\text{HE}} = \frac{\text{HE}/\text{LE}_{\text{sample}}}{\text{HE}/\text{LE}_{\text{standard}}} - 1 \quad (3-1)$$

Table 3-1. Reference Standards and Isotopic Abundances of Common Elements

Element Isotope Ratio	Reference Standard	Ratio in Standard	Abundance Heavy Atom (%)	Abundance Light Atom (%)
$^2\text{H}/^1\text{H}$	Vienna Standard Mean Ocean Water (VSMOW)	1.5575e-4	0.015	99.985
$^{13}\text{C}/^{12}\text{C}$	Carbonate - Vienna Pee Dee Belemnite (VPDB)	1.1237e-2	1.11	98.89
$^{15}\text{N}/^{14}\text{N}$	Air (AIR)	3.677e-3	0.366	99.634
$^{37}\text{Cl}/^{35}\text{Cl}$	Standard Mean Ocean Chloride (SMOC)	0.319766	24.23	75.77
$^{81}\text{Br}/^{79}\text{Br}$	Standard Mean Ocean Bromide (SMOB)	0.97	49.31	50.69

For analysis of isotope ratios of typical VOCs sample pretreatment is typically limited to extraction/preconcentration of the analytes from the groundwater, soil or air. The methodology of extraction can be similar to those included in the EPA SW846 methods. For VOC-class contaminants in groundwater and sediment samples, the recommended extraction approach is the use of purge and trap (P&T). Alternative VOC extraction techniques (including solid-phase micro-extraction (SPME) and direct sampling of headspace) can also be successfully integrated into CSIA methodology. A schematic diagram of an instrumentation used for CSIA of environmental VOCs is shown in **Figure 3.2**.

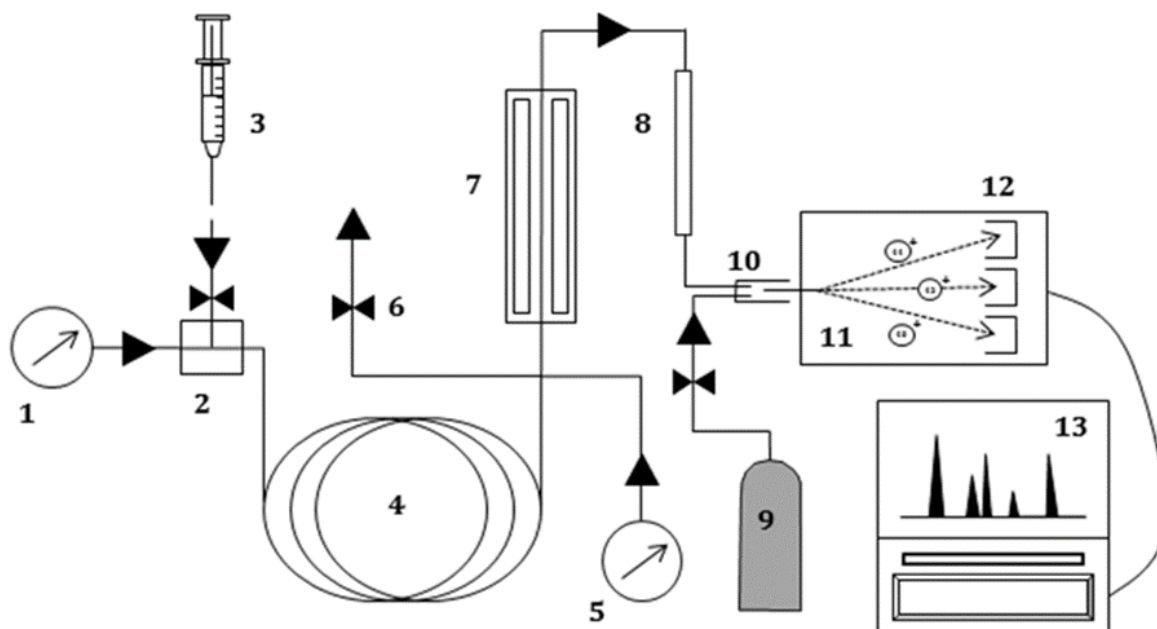


Figure 3-2. Schematic diagram of the GC-IRMS instrumentation. This is the basic instrumental configuration for general analyses. See **Figure 3-3** for information of the configurations used for environmental VOCs. Components: 1) GC carrier gas pressure regulator; 2) GC injector; 3) Sample (configuration for manual injection, see **Figure 3-3** for schematics of extraction/preconcentration train for analysis of VOCs in environmental matrices); 4) GC column; 5) Oxygen pressure regulator ($^{13}\text{C}/^{12}\text{C}$ mode only); 6) Backflush valve; 7) Thermal conversion reactor (combustion to CO_2 in $^{13}\text{C}/^{12}\text{C}$ mode, pyrolysis to H_2 in $2\text{H}/1\text{H}$ mode); 8) Nafion membrane for water removal; 9) Reference standard gas (CO_2 or H_2); 10) Open split interface; 11) IRMS: ion source and ion optics; 12) IRMS: Faraday cups set for different isotope species (shown for $^{13}\text{C}/^{12}\text{C}$ mode, where 44, 45 and 46 represent $^{12}\text{C}^{16}\text{O}_2$, $^{13}\text{C}^{16}\text{O}_2$ and $^{12}\text{C}^{16}\text{O}^{18}\text{O}$); 13) Data acquisition and processing.

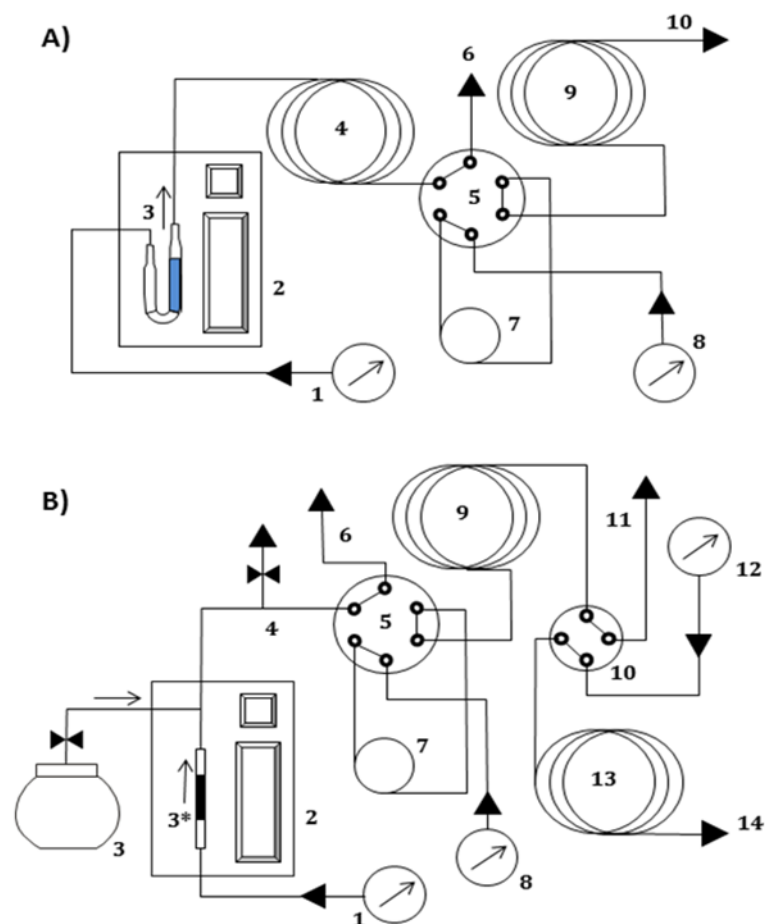


Figure 3-3. Diagram of the CSIA instrumentation as applied to analysis of environmental VOCs. A) Basic configuration for analysis of VOCs in environmental samples, aqueous sample configuration shown: 1) Desorption & Column #1 gas pressure regulator; 2) Purge and Trap unit; 3) Aqueous VOCs sample in sparge vessel; 4) GC column #1 (optional, precolumn used for water separation); 5) Switching valve; 6) Vent with capillary flow restrictor; 7) Cryotrap (LN₂); 8) GC column #2 carrier gas pressure regulator; 9) GC column #2; 10) Extension to the thermal conversion reactor. B) Configuration for analysis of complex matrix VOCs with 2-D GC, airborne VOCs sample configuration shown: 1) Desorption & Column #1 gas pressure regulator; 2) Purge and Trap unit; 3-3*) VOCs sample in Summa canister as in TO-15 or in thermal desorption tube* as in TO-17 [for vapor analysis]; 4) Splitter; 5) Switching valve; 6) Vent with capillary flow restrictor; 7) Cryotrap (LN₂); 8) GC column #1 carrier gas pressure regulator; 9) GC column #1; 10) Switching valve; 11) Vent with capillary flow restrictor; 12) GC column #2 carrier gas pressure regulator; 13) GC column #2; 14) Extension to the thermal conversion reactor.

3.1.2 Quality Assurance Project Planning: CSIA Perspective

Quality Assurance/Quality Control (QA/QC) for CSIA analyses are required to control the analytical precision and accuracy of isotope ratio determination. The precision reflects the stability and linearity of the mass spectrometer detector. The detector can be adversely affected by electronic noise and by fluctuations of water and oxygen present in trace amounts in the mass spectrometer source. Precision is also influenced by fluctuations of baseline noise that affect the quantitation of individual isotope peak areas required for calculation of isotope ratios. The overall accuracy can be adversely affected by less than ideal thermal conversion of the analyte to the IRMS-amenable surrogate, by the quality of GC peak separation and by isotope species disproportionation by incomplete recovery from sample matrix. The latter applies specifically to environmental samples run by methods involving techniques such as P&T and thermal desorption. Laboratory control samples of known isotope composition are analyzed under identical conditions as the environmental samples of interest, to determine the analytical bias. The same control samples serve as one line of evidence to determine the analytical precision.

GC separation quality poses a separate challenge that cannot be addressed adequately by lab matrix spikes, because the GC interferences in real samples are usually more abundant and diverse than in a lab matrix spike. The quality of GC separation has to be assessed by a trained operator, who can identify compromised peaks by examination of peak geometry and the geometry of isotope ratio output (**Figure 3.4**). Minor coelutions are acceptable (and unavoidable). The net analytical uncertainty should account for all these potential problems, including those caused by minor coelutions and peak integration deficiencies. Stated uncertainty for different isotopes is typically higher than the performance for clean matrix spikes, because it allows for additional factors present in actual samples. Stated uncertainty should be given for specific analytes analyzed by particular method. The performance for the same isotope for different analytes and for the same analyte and isotope for different analytical methods is not necessarily identical.

Unlike the analytical methodologies used to collect evidence for “first generation” MNA (e.g., U.S. EPA SW846 methods for contaminant concentration analysis), there is no standard CSIA methodology endorsed by regulatory or government agencies. Consequently, the QA and deliverables tend to vary among the different CSIA laboratories. **Table 3.2** summarizes Data Quality *Measures* applicable to CSIA work. Table 3.2 is intended to provide a general guidance of what type of QA data can be requested from the analytical laboratory. At the minimum, it is recommended that the report should document the analytical precision using laboratory control samples (Item 2) and lab duplicates of field samples (Item 6) and disclose all identified data quality problems (e.g., flag samples where the analyzed compound were poorly separated by the GC, Item 7). The report should also specify whether the reported data have been corrected for analytical bias and whether the isotope ratios are traceable to the international references (compare **Table 3-1**).

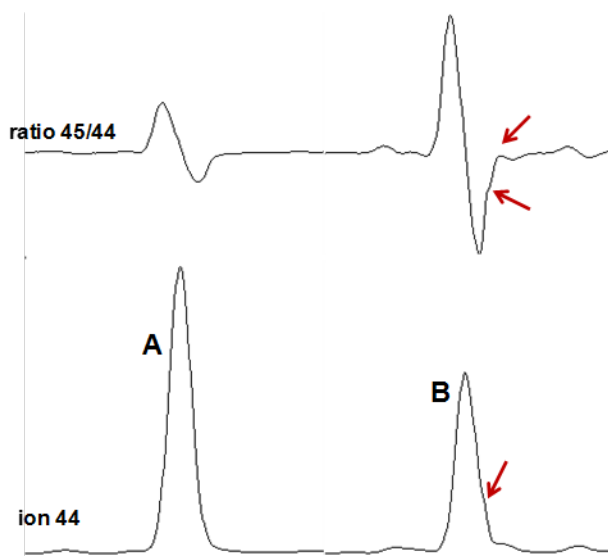


Figure 3-4. An example of a CSIA chromatogram. The lower trace is a chromatogram drawn for mass 44 ($^{12}\text{C}^{16}\text{O}_2$). The upper trace is drawn for the ratio of masses 45/44 ($^{13}\text{C}^{16}\text{O}_2/^{12}\text{C}^{16}\text{O}_2$). The characteristic sinusoid appearance of the ratio trace results from slightly faster travel of ^{13}C species through the GC column. Compound A is well-resolved, permitting accurate definition of isotope ratio. Compound B overlaps (coelutes) with another unidentified compound, mostly hidden underneath peak B. The coelution problems can be usually identified by careful examination of the geometry of the GC peak and the corresponding 45/44 ratio trace (arrows point asymmetries resulting from such coelution). Samples affected by coelution problems should be always flagged in data reports.

3.1.3 CSIA Service Providers

Currently, CSIA services are available on commercial basis from several laboratories in North America and Europe. Unlike the analytical methodologies used to collect evidence for “first generation” MNA (e.g., US EPA SW846 methods for contaminant concentration analysis), no formal certification is issued for CSIA methods. Consequently, the QA and deliverables may vary among the different CSIA laboratories. Potential clients are advised to discuss the details of the planned work with the CSIA laboratory contacts. Contact information for the major CSIA laboratories is provided in **Appendix D**.

Table 3.2. List of Data Quality Measures Applicable to CSIA

#	Data Quality Indicator	QC Sample or Activity	Frequency/ Number	QC Acceptance Limits (Measurement Performance Criteria)	Corrective Action
1	Analytical Precision	Laboratory Control Sample; Determine Linear Range	Performed for new method/analyte; should be repeated if the performance of laboratory control samples deteriorates	Must contain all available target analytes and be matrix-specific (aq.); A minimum of 3 different concentration standards across the amplitude range	NA

#	Data Quality Indicator	QC Sample or Activity	Frequency/ Number	QC Acceptance Limits (Measurement Performance Criteria)	Corrective Action
2	Analytical Precision & Accuracy	Laboratory Control Sample; Initial calibration	≥1 before starting a batch of samples ¹ .	Must contain all available target analytes and be matrix-specific (aq.); precision < stated precision of the method; accuracy < stated accuracy of the method	Re-analyze; if still out, maintenance/troubleshooting
3	Analytical Precision & Accuracy	Laboratory Control Sample; Daily calibration	Daily prior to sample analysis; repeat after < 10 field samples	Must contain all available target analytes and be matrix-specific (aq.); precision < stated precision of the method	Re-analyze; if still out, hardware maintenance/troubleshooting
4	Analytical Accuracy & Sensitivity (Contamination)	Method Blank	After processing samples with analytes present at unusually high concentrations	Target analyte peaks should be absent; Use professional judgment (acceptable limit varies at < 1-5 % relative to the lower limit for reportable analytes)	Re-analyze; if still out, may require equipment cleaning
5	Sampling Accuracy & Sensitivity (Contamination)	Trip Blank	Optional; recommended 1 per each shipping container	Target analyte peaks should be absent (the blanks can be analyzed using a standard GCMS methods for the presence of the analytes as opposed to CSIA); Use professional judgment (acceptable limit varies at < 1-5 % relative to the lower limit for reportable analytes)	Lab narrates outliers. Potential data usability issue
6	Analytical Precision	Laboratory Duplicate (of a field sample) ²	For each analyte, 1 per < 10 field samples	Preferably, use a sub-sample from the same container as the original analysis. Duplicate precision < stated precision of the method	Re-analyze, qualify data.
7	Analytical Precision and Accuracy	Evaluate GC resolution	Every sample	Professional judgment (evaluate geometries of chromatographic peaks and the corresponding isotope ratio traces).	Lab flags the compromised results. Samples may require reanalysis using a different GC method.
8	Overall Precision & Representativeness	Field Duplicate Sample	Optional; recommended 1 per < 10 field samples	Precision < stated precision of the method	Low precision suggests sample heterogeneity
9	Preservation	Sample preservation	Every field sample	Follow the protocol appropriate for given analyte; check pH of the samples.	Lab narrates outliers. Potential data usability issue
10	Data Completeness	Calculate from valid/usable data collected	Not applicable	Not applicable	Potential data usability/data gap issue
11	Comparability	Assure that the laboratory standards are traceable to international isotope scale references ³	Not applicable	Not applicable.	Potential data usability issue

- 1 The number varies depending on the analyte and the isotope ratio; e.g., Initial calibration of H-CSIA tends to require more analytical runs and initial calibration of C-CSIA.
- 2 Note that the lab duplicate using material from a separate sample container (e.g., VOA) can be also impacted by sample heterogeneity
- 3 If the CSIA standard cannot be traced to international isotope ratio scale, data from different laboratories using different lots of the standard lack comparability. If a traceable standard cannot be obtained, the reported deltas for the analyzed field samples (eq 3-1, using an arbitrary $^{15}\text{E}/^{14}\text{E}$ standard) would be precise, but the accuracy bias would be unknown.

3.1.4 Data Management

Due to their size and complexity, groundwater analytical datasets are increasingly being managed in relational databases. Standard formats for groundwater databases include component tables that contain sampling location data (e.g., X, Y coordinates, sample depth, screen interval, lithology), sample tables (e.g., sample names, laboratory name, analytical method, analysis date, collection date, collection method) and results tables (e.g. sample location, sample date, constituent name, result, detection limit, data flags). Geochemical data can be stored along with constituent concentrations or in separate tables. Frequently, hydrogeologic data such as groundwater elevations should be maintained in databases to assess how concentrations or isotope ratios may correlate with hydrogeologic parameters.

Data deliverables for CSIA laboratory analyses differ somewhat from standard environmental data products. CSIA datasets can contain both the name of the molecule and the element analyzed within the molecule. In some cases, the laboratory will develop unique names for the analyte including the element evaluated for isotope ratio (e.g., methane = 'd¹³C C1). 'For this reason, standard database formats may need to be expanded to store and analyze CSIA data. Prior to CSIA field studies, the format of the data deliverable should be discussed with the laboratory performing the analyses. Data management standard operating procedures and database architecture should be developed in detail prior to commencing field studies.

Table 3.3. Data Dictionary for CSIA Data Management

Field Name	Data Type	Description
Location ID	Text	Location ID – Well name or sampling location, unique identifier of sampling location – can be linked to Sample Location Table with location coordinates, depth, well construction, etc.
Sample ID	Text	Laboratory sample ID – can connect to Sample Table including QA/QC data, laboratory information, analytical methods
Constituent Name	Text	Name of molecule or constituent of concern, full name or abbreviation (e.g. trichloroethene, cDCE);
Alternate Constituent Name	Text	A field for alternate constituent names may be required if the laboratory has a unique name for the constituent or if unusual abbreviations are used
CAS No.	Text (or number)	Chemical Abstract Service Number – unique identifier of constituent name
Element	Text	Symbol or text indicating element analyzed e.g., C, H, Cl
Ratio Result	Number (can be negative)	Result of CSIA Ratio analysis – ratio of heavy to light isotope
Detection Limit	Number	Detection Limit of analysis
Units	Text	Units of analysis
Qualifiers	Text	Data qualifiers from laboratory analysis indicating values below detection limits, laboratory artifacts, sample irregularities

3.2 Interpretation of CSIA Results

3.2.1 Understanding Isotope Fractionation

As briefly indicated above, during chemical reaction, molecular bonds containing the lighter isotopes are usually broken at slightly faster rates than those containing the heavier isotopes. Biodegradation and chemical degradation commonly cause isotope fractionation, owing to lower activation energy barrier for the lighter isotope species (See **Figure 3-5**). Note that within a molecule, the isotope effects are strongest at atoms or functional groups directly involved in the chemical transformation (so-called **primary isotope effects**). Measurable isotope effects can also occur at atoms remote from the reaction center (so-called **secondary isotope effects**). While secondary isotope effects are usually minor and are often neglected in data interpretation, they are postulated as one of the key factors controlling the Cl isotope fractionation in the chlorinated ethenes reductive dechlorination chain (Abe et al., 2009; Kuder van Breukelen et al., 2013). As discussed in the following sections, the numerical model of Cl fractionation requires accounting for the primary and secondary Cl isotope effects.

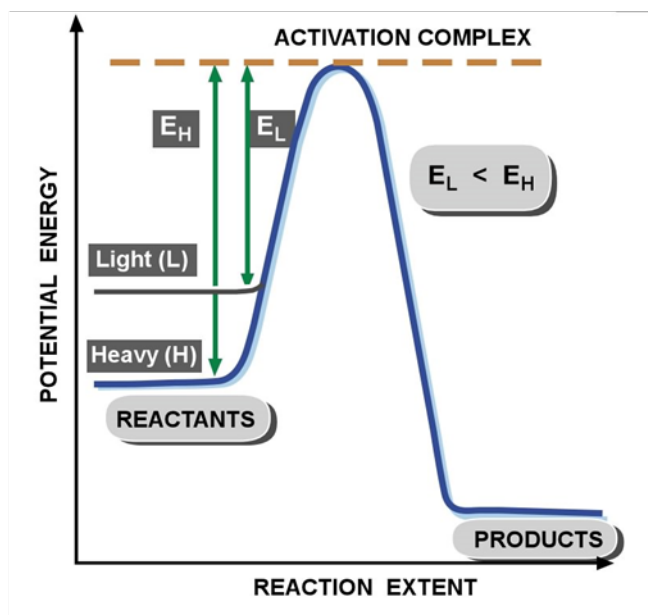


Figure 3-5. Thermodynamic basis for isotope fractionation during (bio-)chemical reactions. Isotope fractionation effects occur mainly because of larger activation energy requirements for molecules with heavier isotopes (E_H) than for molecules with lighter isotopes (E_L). The larger activation energy for molecules with a heavier stable isotope results from the stronger bonds formed by the heavier isotope, evident in the larger bond dissociation energy requirement for the molecule with the heavier isotope. (Galimov, 1985)

Isotope fractionation in (bio-)chemical reactions progressing from parent compound to daughter compound, that is for processes that are not reversible, the isotope fractionation is referred to as **kinetic isotope fractionation**, following the so-called Rayleigh fractionation model described below in more detail. Kinetic fractionation is normally observed in contaminant degradation, and also in certain physical processes, including gas and aqueous diffusion. Another type of isotope fractionation occurs in phase partitioning and in certain reversible chemical reactions. The so-called **equilibrium isotope fractionation** results from isotope-dependent changes of vibrational energies and in intermolecular forces of molecules in phase equilibria.

Kinetic effects lead to progressive enrichment (or less frequently, depletion) of the heavy isotope species in the unreacted parent compound over the progress of reaction. In the case of an equilibrium effect, there is a constant offset of isotope compositions between the compounds in equilibrium.

Equilibrium effects are usually not directly observed in chemical reactions of interest in VOC contaminant assessment, but are important in certain environmental applications, specifically that of anionic species such as perchlorate (Ader, 2008).

3.2.2 Rayleigh Model of Isotope Fractionation

Kinetic isotope fractionation is described by the Rayleigh fractionation model. The model applies to fractionation occurring in closed systems (e.g., batch reactors, microcosms etc.), where changes of reactant concentrations result exclusively from the reaction of interest. However, the model is also useful to describe fractionation in less than ideal environments. The limitations of the Rayleigh model in interpretation of isotope data from contaminated sites will be discussed below.

The basic premise of the model is that over the progress of a reaction, at point of time t , isotope compositions of the parent and product follow the relationship shown in **Equation 3-2**, where α is a constant, reaction-specific **fractionation factor**; $R_{\text{product},t}$ and $R_{\text{parent},t}$ are instantaneous heavy/light isotope ratios of given element in the parent and the product, respectively. Expressed in another way, α represents the ratio of reaction rates of the heavy versus the light isotope species, Hk and Lk . In most cases, molecules with light isotopes react faster ($\alpha < 1$).

$$\alpha = R_{\text{product},t} / R_{\text{parent},t} = {}^Hk / {}^Lk \quad (3-2)$$

Equation 3-2 can be transformed into **Equation 3-3** (to relate R , the isotope ratio of the parent reactant remaining at time t to the decrease of the mass of the reactant. The fraction of the reactant mass remaining (f) is defined in **Equation 3-4**. The isotope ratios are also shown using delta notation for element “E”. **Equation 3-3** is typically used in scientific CSIA literature to present experimental data.

$$\ln R_t / R_0 = \ln ((\delta^H E_t / 1000 + 1) / (\delta^H E_0 / 1000 + 1)) = (\alpha - 1) \times \ln f \quad (3-3)$$

$$f = C_{\text{time} = t} / C_{\text{time} = 0} \quad (3-4)$$

Equation 3-3 is often simplified to **Equation 3-5** to present CSIA data for most audiences. The latter equation uses the enrichment factor notation (ϵ) instead of α . The enrichment factor is related to the fractionation factor (α) by **Equation 3-6**. Epsilon (ϵ) is usually expressed in permil (‰) by multiplying **Equation 3-6** by 1000. The larger the isotope fractionation effect during the reaction, the more negative the value of ϵ . **Equation 3-5** is accurate in describing the fractionation in the majority of degradation systems, including those reported in all CE studies to date, but the accuracy decreases for the certain reactions with exceptionally strong kinetic H isotope fractionation (Dorer, 2014).

$$\delta^{13}C = \epsilon \times \ln f + \delta^{13}C_0 \quad (3-5)$$

$$\epsilon = \alpha - 1 \quad (3-6)$$

Equations 3-3 or **3-5** permit determination of α or ϵ by fitting experimental data consisting of isotope ratios and concentrations of the parent reactant. These parameters can be readily determined in a controlled laboratory degradation study (see **Appendix B** for values and references). In the case of contaminant degradation, the fraction of reactant remaining (f) can be determined in laboratory settings from $C_{\text{time}} = t$, the concentration at a time after initiation of transformation, and the original concentration ($C_{\text{time}} = 0$). The δ values for the contaminant at time = 0 and time = t can be determined by CSIA.

Figure 3-5 illustrates an idealized data set from a degradation experiment following the Rayleigh model of fractionation. The parent reactant (TCE) becomes exponentially enriched in the heavy isotope (^{13}C) in proportion to a linear decrease of TCE mass. The product (DCE) is relatively depleted in the heavy isotope. Note the difference between the instantaneous and the cumulative isotope ratios of DCE. While the instantaneous isotope ratio of DCE follows that of the evolving isotope ratio of TCE with a constant depletion (equal to ϵ), the cumulative isotope ratio of DCE progresses for the depleted value at the onset of transformation to the final value matching the initial isotope ratio of TCE upon complete transformation. In a closed degradation system, the cumulative isotope ratio of all remaining reactants and products (isotope ratios normalized by the molar concentrations of individual compounds) is always identical to the initial isotope ratio of the parent (See **Section 3.3.5** for description of **Carbon isotope mass balance (C-IMB)** approach that is based on the conservation of the average isotope ratio).

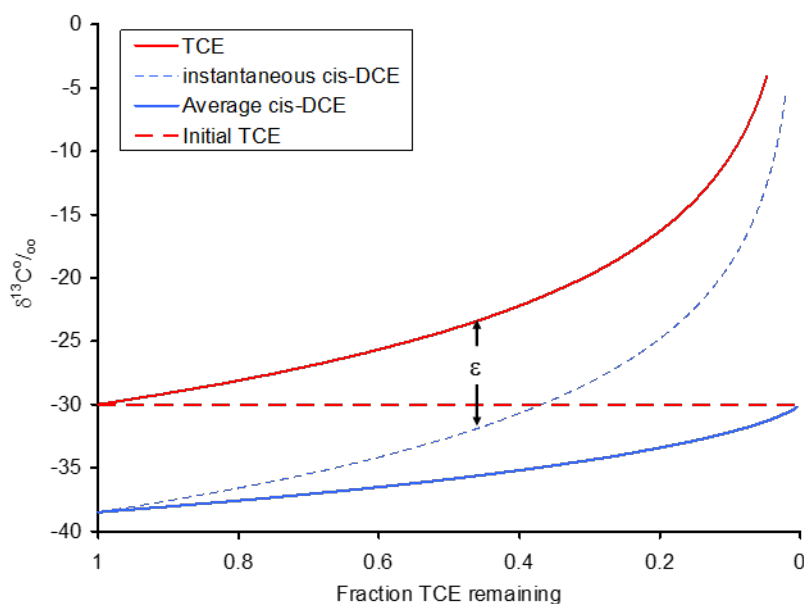


Figure 3-5 Typical Rayleigh-type fractionations in degradation. Isotope ratios of parent (TCE) and single daughter product (cis-DCE) degradation simulated over time. TCE becomes enriched in the heavy isotope ^{13}C as cis-DCE is formed, while cis-DCE is initially highly depleted in ^{13}C , but shows values closer to the original release over time. (Excerpted from EPA Guidance **Figure 7-1**) Note that the same data plotted with the X-axis expressed in logarithmic scale would show a linear trend for TCE isotope ratios. For the X-axis expressing the natural logarithm of 'f', the slope of such linear regression line would be equal to ϵ . See **Figure 3-9** for an example of the latter type of format.

3.2.3 *Isotope Fractionation in Alternative Attenuation Pathways*

Estimating the values of ϵ for relevant attenuation processes is critical to interpreting the results of CSIA analysis. Epsilons have been determined in laboratory settings with various microbial communities and geochemical conditions, for abiotic degradation systems and also for certain non-degradative attenuation systems, by fitting the experimental data to the Rayleigh fractionation model (**Equation 3-3**). Many of laboratory-determined values for ϵ are listed in the scientific literature and in the EPA CSIA Guidance (Hunkeler, 2008). An updated list of literature ϵ values is included in this report as **Appendix B**. On the other hand, ϵ cannot be determined from field data using the same approach, as multiple attenuation mechanisms are occurring simultaneously and the parameter f in **Equation 3-3** does not exclusively represent degradation.

In conventional interpretation of CSIA data, a representative value (or a range of values) for ϵ must be chosen to estimate contaminant degradation. **Figure 3.6** illustrates the range of ϵ values for several constituents and biodegradation conditions. It is apparent that various degrading organisms can be associated with very different magnitudes of isotope effects (e.g., note the wide range of ϵ for aerobic degradation of TCE).

In practice, it is very difficult to justify picking a single accurate value of ϵ for a specific set of field samples. To do so, strong independent evidence would be needed to confirm that the degradation is mediated by a single degrader organism or a single abiotic degradation process. More realistically, data interpretation would consider the minimum and the maximum values of ϵ that apply to the studied contaminant. One of the most extreme cases of that uncertainty is aerobic degradation of TCE, where studies on different aerobic cultures yielded ϵ values of approximately -1‰ and -20‰ . For the same isotope ratio of TCE determined in a field sample, the calculated extent of degradation (see the following section) would be much higher than the value calculated for ϵ of -20‰ . The conservative approach in data interpretation should always consider the strongest fractionation (the most negative epsilon) applicable for a given degradation pathway.

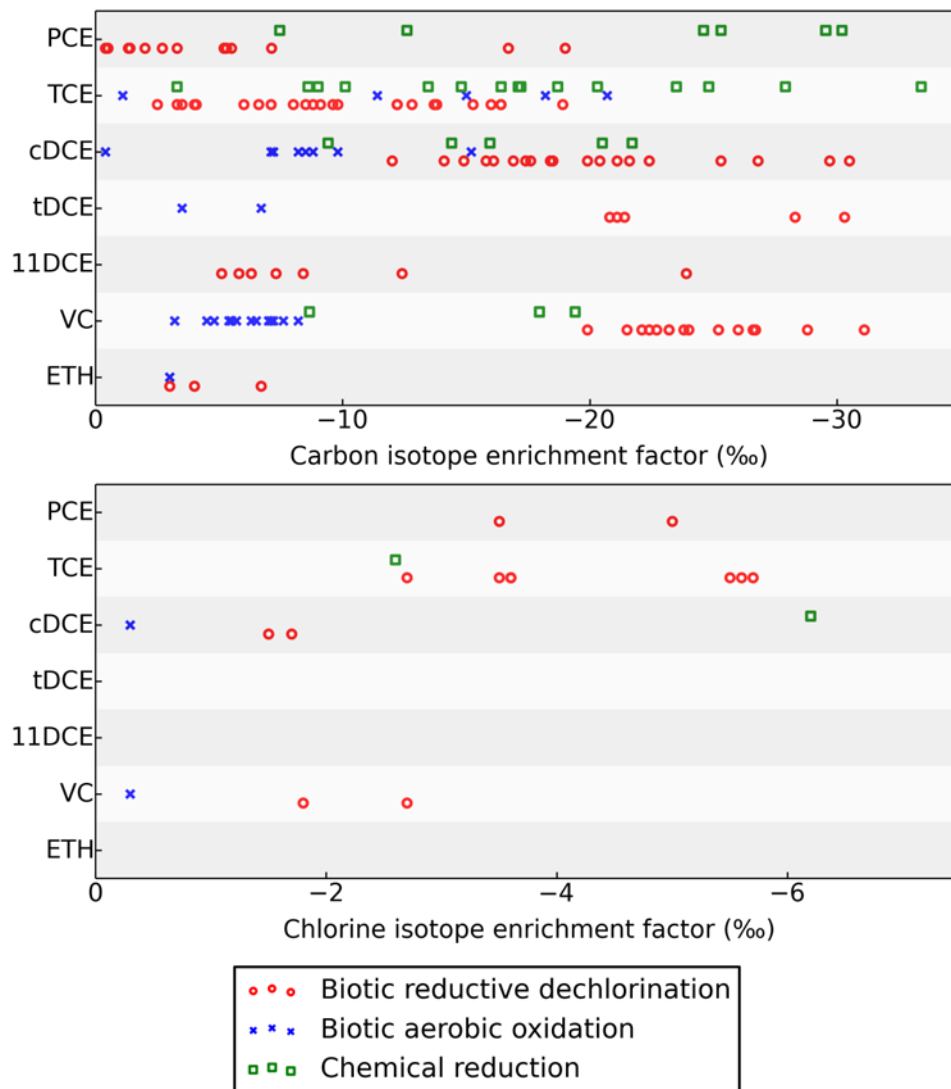


Figure 3-6. Carbon and chlorine isotopic enrichment factors (ϵ) for several contaminants and degradation processes. (for full list of data and literature sources, see Appendix B)

3.2.4 Do Physical Processes Cause Isotope Fractionation?

One of the key questions in the use of CSIA in assessing contaminant attenuation is whether isotope fractionation results strictly or primarily from compound degradation. While the answer to this question is affirmative in most situations, measurable isotope effects can also result from certain non-degradative or physical processes.

Potential isotope fractionation should be considered for physical processes including diffusion and phase partitioning. Scenarios conducive to fractionation from physical processes include: significant mass attenuation by vapor phase flux (fractionation due to isotope effects in phase partitioning combined with the effects from gas diffusion); contaminant sorption in expanding plumes, prior to attaining the solute/sorbent equilibrium (fractionation due to isotope effect in phase partitioning) and sites with significant proportion of the contaminant diffusing into low permeability zones (fractionation by diffusion in aqueous medium).

All experimental data available up to this point show that the values of ϵ associated with various volatilization scenarios of VOCs were not detected or were relatively low (Bouchard, Hohener, and Hunkeler 2008 ;Bouchard et al., 2008;Kuder, Philp and Allen 2009). For TCE (the single CE-class compound studied to date), the C fractionation in volatilization was absent (Jeannotat and Hunkeler, 2012). On the other hand, volatilization of TCE produced a Cl isotope effect of a magnitude approximately one half of those in TCE biodegradation (Jeannotat and Hunkeler, 2012). This suggests that at the CE sites where volatilization is a major element of the CSM, chlorine fractionation alone should be not automatically used as evidence of CE degradation, but should be considered together with other lines of evidence.

It was proposed previously that relatively low levels of isotope fractionation of aqueous solutes can result from diffusion into low permeability strata (low-K zones) along the flow path of a plume or due to lateral dispersion (LaBolle et al., 2008; Rolle et al., 2010). The actual significance of fractionation due to partitioning into low-K zones depends on the relative difference of the aqueous diffusion coefficient for the different isotopologues. While the coefficients calculated based on the molecular mass difference between the isotope species suggested relatively strong fractionation potential, experimental data available to date show much lower isotope effects. A single study reported Cl fractionation for TCE (ϵ -0.5 to -0.8‰) and cDCE (-1.5 to -2‰) (Jin et al., 2014) vs. predicted values of -10 ‰ and -8‰. No similar data are available for C isotope fractionation of VOCs, but studies of aqueous diffusion of hydrocarbon gases and CO₂ show even more negligible C isotope fractionation (O'Leary, 1984; Zhang, 2001).

Studies of sorption phenomena available to date suggest a possibility of transient fractionation at the front of an expanding plume (Kopinke, 2005; Qiu, 2013). Generally, contaminant plumes in steady state with respect to sorption are no longer affected by isotope fractionation from this mechanism. However, this phenomenon may be relevant when developing and interpreting the site history for the CSM.

Similar to isotope effects from degradation, the significance of isotope effects from physical processes depends on the fraction of contaminant mass remaining. Even for a small isotope effect, attenuation of a high fraction of the original mass may lead to a measurable change of the contaminant isotope ratios. In evaluating field sites, relatively small changes of δ for a given element at a site where there is a possibility of significant non-degradative mass attenuation should be evaluated in the context of other lines of evidence. For example, sites where vapor extraction remedies have been installed or sites with high potential of retention of CEs in low permeability sediments should be evaluated for potential isotope fractionation effects from physical processes.

3.2.5 How do I Estimate the Rate and Extent of Degradation Using the Rayleigh Model?

In the field, contaminant concentrations decrease as the result of in situ degradation but also due to non-degradative processes (dilution, dispersion, sorption etc.). CSIA results can be used to estimate the extent of biodegradation or abiotic degradation as opposed to the overall contaminant concentration attenuation. As discussed in the preceding section, the estimated extent of biodegradation has to consider the uncertainty of the magnitude of isotope effect (ϵ). The conservative estimate avoiding overprediction of the extent of degradation would be based on the strongest fractionation (the most negative epsilon) applicable for a given degradation pathway.

The fraction of contaminant remaining in groundwater after degradation can be estimated using **Equation 3-6**, where ϵ is the isotope effect assumed to be representative for given site, $\delta^{13}C_0$ is the pre-degradation isotope ratio of the contaminant (see **Section 3.2.6**, on determination of δ_0)

and $\delta^{13}\text{C}_{\text{GW}}$ is the isotope ratio of degraded contaminant determined by CSIA of a groundwater sample.

$$f = \exp((\delta^{13}\text{C}_{\text{GW}} - \delta^{13}\text{C}_0)/\epsilon) \quad (3-7)$$

The extent of degradation (D) is obtained by **eq. 3-7**, using f determined from **equation 3-6**.

$$D = 1 - f \quad (3-8)$$

Combining **equations 3-6** and **3-7** yields the following:

$$D = 1 - \exp((\delta^{13}\text{C}_{\text{GW}} - \delta^{13}\text{C}_0) / \epsilon) \quad (3-9)$$

Calculated values of f can be used to roughly predict downgradient concentrations and estimate first order degradation rate constants in a manner similar to that described in Newell et al., 2002 and referred to in **Section 2.2.3** above (cf. **equation 4.7** in U.S. EPA CSIA protocol).

$$\lambda = -\ln(f)/(d/v) \quad (3-10)$$

In **equation 3-10**, λ is the first order degradation rate constant for the contaminant, d is the distance between the source and the observation well, and v is the average groundwater flow velocity. Note this equation assumes that the observation well and the source well are connected through a flow line parallel to the groundwater flow direction. Values of λ can be used to estimate concentrations downgradient at hypothetical receptor points or regulatory boundaries or can be used to estimate a maximum extent of a plume. Rate constants calculated from CSIA data can be compared with those calculated from concentration data to refine estimates of attenuation by various mechanisms.

3.2.6 How do I Estimate the Isotope Signature of the Original Release?

One common uncertainty in applying CSIA for MNA is estimating the isotope ratio of the primary contaminant release. Often, the original release occurred over an extended period of time with CE solvents from a variety of manufactured sources. The isotope ratios at the source area usually reflect the average delta values representative of the source history over time. Under field conditions, the original (pre-degradation) values of $\delta^{13}\text{C}$, $\delta^{37}\text{Cl}$, or $\delta^2\text{H}$ in CEs at the top of the degradation chain can be estimated by the following lines of evidence:

1. Direct determination of the source signatures by CSIA of DNAPL from an identified primary release area.
2. Estimate based on CSIA of dissolved phase CEs in the vicinity of the primary release area. Caution is necessary. Frequently, CEs have been released along with organic co-contaminants such as BTEX, which stimulate biodegradation in the source area, leading to isotope fractionation. Dissolved phase CEs should meet the following criteria: (i) the observed δ values should show relatively low fractionation as compared to the samples collected elsewhere within the plume; (ii) no significant amounts of degradation daughter products are observed; (iii) the CEs occur at relatively high concentrations as compared to the samples collected elsewhere within the plume.

3. The range (most negative δ to the least negative) of feasible source signatures can be taken from the literature for the manufactured solvents. Note that the number of manufactured products with known isotope compositions is limited. The data coverage is relatively good for C isotopes in TCE and PCE, but fewer samples were characterized for their Cl isotope and H isotope composition. It is possible that the initial isotope ratios at individual CE spills may fall beyond the currently defined limits.
4. Apply the carbon isotope mass balance (C-IMB) approach discussed in **Section 3.3.5**. A consistent C-IMB in wells throughout the plume indicates that the estimated value of source signature is reliable.

Simultaneous transport of parent compounds downgradient and biodegradation in the source can complicate estimation of original isotope ratios in plume-wide CSIA studies. A conservative approach may be to estimate source ratios using all applicable methods described above and develop a range of probable isotope ratios to compare with sample results. The Case Study presented in **Appendix A** provides an example of estimation of source isotope ratios at a complex field site.

CSIA can also assist in correlation/discrimination between the sources of environmental contaminants, among other lines of evidence. In those applications, isotope ratios may provide a unique fingerprint of the primary contaminant source. This subject is discussed in more detail in the 2008 EPA guidance (Hunkeler, 2008), but is not a primary topic for this Guidance.

3.3 Conventional Data Interpretation for CSIA

The first step in data interpretation from any sampling program is to confirm that data collection and laboratory analyses have met data quality objectives (DQOs) and QA/QC objectives established for the project. Data quality reviews for CSIA are discussed in detail in the 2008 EPA CSIA Guidance (Hunkeler, 2008) as are conventional approaches to interpreting CSIA data. Data analysis methods commonly used in CSIA studies are summarized below and presented in more detail in the EPA Guidance.

3.3.1 Is the Observed Shift of Isotope Ratios Significant?

If isotope fractionation is occurring, the difference between the source, pre-degradation isotope ratio and the isotope ratio determined by CSIA in a groundwater sample (following **eq 3-5**, the difference between $\delta^{13}\text{C}$ and $\delta^{13}\text{C}_0$) is referred to as isotopic shift ($\Delta^{13}\text{C}$).

For CSIA results, it is important to determine a minimum detectable difference in isotope ratios that will signal a significant difference between results.

The analytical uncertainty for C CSIA of CEs is generally 0.5‰ so the $\Delta^{13}\text{C}$ between sampling locations or time frames should exceed the sum of the analytical CSIA uncertainties of both the data points. Therefore, following the EPA recommendations (Hunkeler, 2008), a significant isotope shift is defined as the sum of sample and source CSIA uncertainties, plus an arbitrary value of 1‰ to minimize erroneous interpretations. In this case, the significant isotopic shift should be 2‰ for C in total when the sample has an uncertainty of 0.5‰. At complex plumes with probable multiple, poorly defined sources, a more conservative approach is to increase the limit of uncertainty. Similar logic is used to determine significant shifts for other elements. Clear demonstration that two data points or datasets are significantly different is a critical step when

developing evidence of contaminant degradation and for distinguishing samples from different primary sources.

In practice, C enrichment factors (ϵ) due to biodegradation are in the range of -2 to -30‰ for CEs. A degradation pathway characterized by a small C isotope enrichment factor will lead to a significant degradation only after a large fraction of the compound mass is degraded. For example, an enrichment factor of about -3‰ will lead to a significant enrichment of 2‰ only after 50% of the compound is degraded.

Enrichment factors for H and Cl have not been as well studied as C in laboratory settings. Abe et al. (2009) reported average Cl enrichment factors of -0.3‰ for Cl in cDCE and VC. Kuder and van Breukelen, et al. (2013) found ϵ_{CL} for RD to be between -3.6 and -2.7‰. The H isotope enrichment factor for TCE conversion to DCE from the same study was found to be in the range of +34 ‰ (inverse fractionation) (Kuder and van Breukelen et al., 2013). A summary of published enrichment factors can be found in **Appendix B**.

3.3.2 Comparison of Results in Space and Time

CSIA results can be plotted on two-dimensional graphs or on maps or cross sections to visualize and communicate the relative isotope ratios over time and space. Concentration results, molar ratios and geochemical analyses can be plotted along with CSIA results to support interpretation of the data. Several simple plot styles provide effective qualitative review of CSIA data. Preliminary data plots may be used in an adaptive sampling strategy to support decisions for additional samples or sample locations or to confirm or refute assumptions about CE fate processes.

Isotope results can be plotted against horizontal or vertical distance or over time. **Figures 3-7 and 3-8** show examples of how isotope and concentration data can be visualized to interpret site processes.

A qualitative initial review of the data may compare isotope ratios at various locations in a plume and for both parent and daughter compounds against isotopic ratios estimated for the source. Molar ratios of the parent and daughter CEs can be displayed adjacent to CSIA results to visualize the extent of degradation (as shown in **Figure 3-8**).

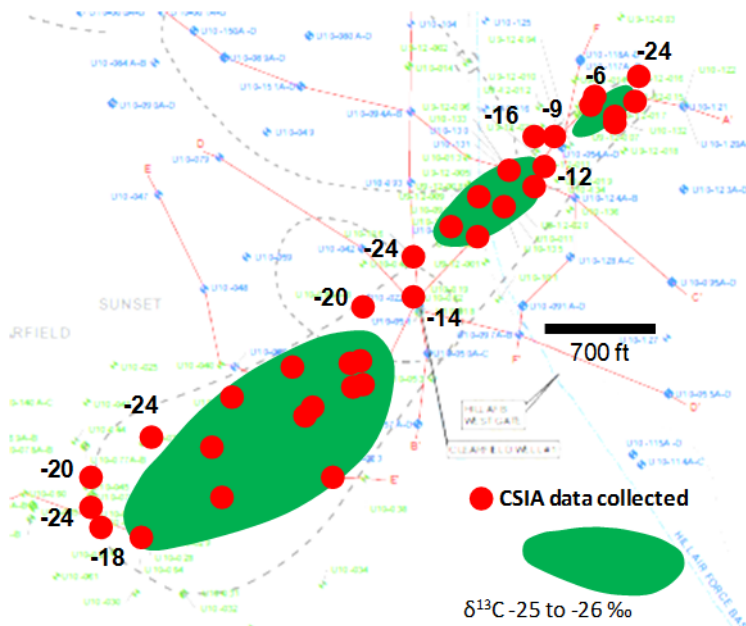


Figure 3-7. An example of a map plot of isotope data (taken from this study; TCE in the Shallow OU10 Plume). The map shows positions of CSIA sampling points and the distribution of samples with and without meaningful enrichments of ^{13}C . The localized evidence of isotope fractionation is not consistent with classic model of 1st order degradation within a contaminant plume.

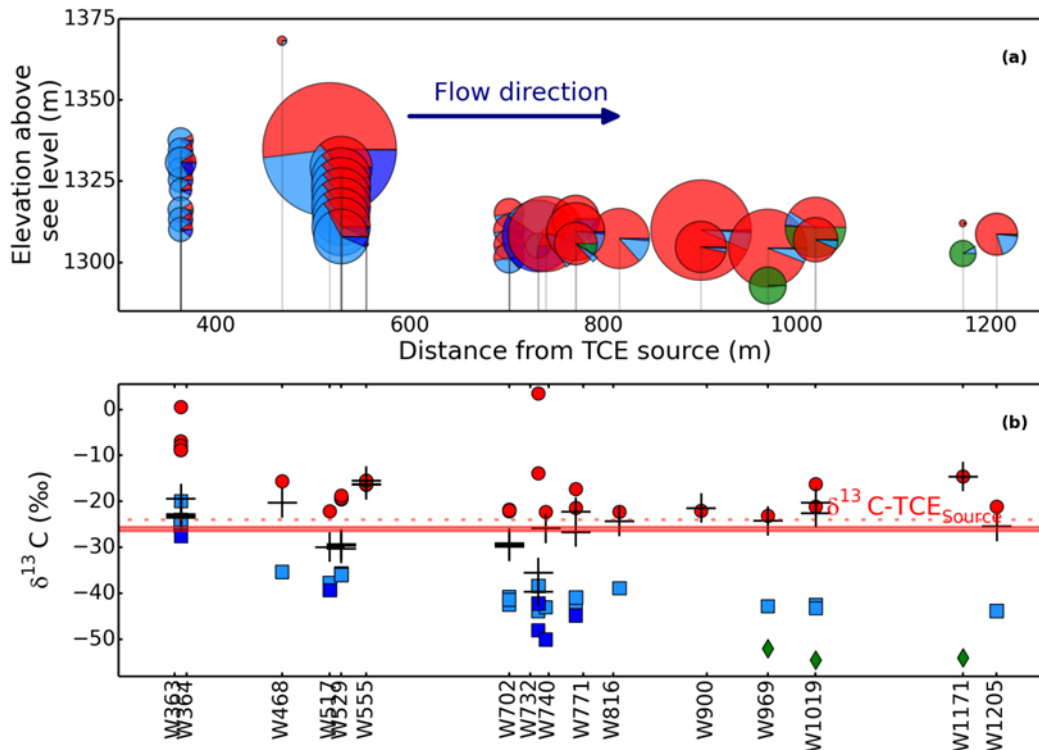


Figure 3-8. Examples of spatial plots of isotope data. Figures (a) and (b) show concentration and isotope data of CEs in the Deep TCE Plume at OU10 plotted against the distance from the source. (a) Pie graphs of the molar ratio of TCE (red) to DCE (blue) (c-DCE, light blue, t-DCE dark blue) and ethene (green) versus distance downgradient, and (b) the C isotope ratio for each

constituent versus distance (by sample location) with the source isotope ratio estimate indicated by the solid red line for TCE. Parent compound (TCE) signatures are enriched in ^{13}C throughout the site, with most enrichment near the source area. The daughter products (DCEs), are in most part depleted in ^{13}C , which is consistent with the normal trend of fractionation between the parent and the product (see **Figure 5**). However, DCEs enrichment vs. the source is observed in certain samples near the source area. If the daughter product continues to degrade, the isotope ratio will approach and eventually exceed that the initial source value (see **Figure 3-12**). Finally, the TCE degradation evidence is consistent between the isotope ratios (^{13}C enrichments) and the CEs concentration data (high proportion of DCEs vs. TCE).

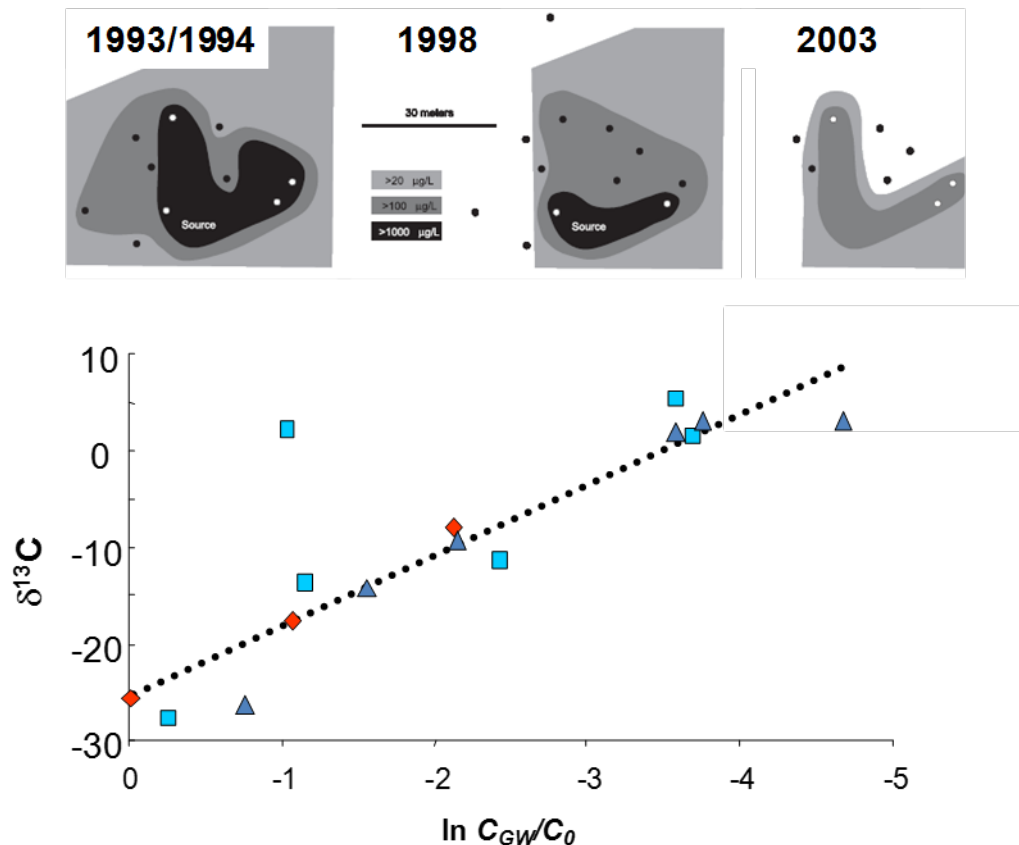


Figure 3-9. Example of a Rayleigh-type plot of field CSIA data, (an MtBE site, data after Wilson et al., 2005 and Kolhatkar et al., 2002). Historical concentration data (top panel) suggested effective MNA remediation of the MtBE release. CSIA data (bottom panel) collected for three different sampling events (indicated by separate symbols) show a good linear relationship of δ vs. the log of MtBE concentration, consistent with MtBE degradation. The steep slope of the regression line (-8, similar to that obtained for degradation of MtBE in sediment microcosms) suggests that the degradation is the dominant attenuation pathway. Note that the present regression slope is not equivalent to the epsilon determined in batch degradation experiment. While the quality of the regression is very good, the unknown contribution from non-degradative attenuation impacts on MtBE concentrations must be acknowledged. The single outlier shows relatively stronger isotope fractionation than the remaining samples. The true epsilon characteristic of the MtBE-degrading culture is more negative than -8.

3.3.3 *Rayleigh-type Plots (Isotope Ratios vs. Concentration)*

Field CSIA and concentrations data can be plotted using the format of **Figure 3-9**. The X axis represents the fraction of the contaminant remaining after degradation. To obtain the fraction remaining, use the highest historical concentration of the parent CE or the highest historical concentration of the sum of all CEs (to use the latter approach, the concentrations of individual CEs and ethene have to be converted to molar concentrations). Alternatively, the concentrations may be normalized simply to the largest concentration within the plume recorded at the time of current sampling. **Figure 3-9** illustrates the information potential of such plots: data distribution consistent with Rayleigh fractionation model (strong regression line) offers robust evidence of plume-wide degradation. Ideally, if degradation is the sole attenuation process, the slope of the plot would be identical to the slope in a corresponding microcosm experiment and would be identical to the enrichment factor of the degradation process responsible for contaminant removal. In reality, a slope obtained by plotting field data is always lower than the ideal value. If the data show isotope enrichments, but there is no apparent relationship between the isotope ratios and the decrease of concentrations, spatial heterogeneity of the degradation processes within the plume is suggested.

A specific variant of the Rayleigh-type plot is shown in **Figure 3-10**. The figure helps to visualize the evidence of degradation (or lack thereof) by overlaying the field sample result with various attenuation scenario lines. The proximity of a sample to a scenario line shows relative significance of this attenuation mechanism for this specific sample. A numerical treatment of the same topic is discussed by van Breukelen (2007).

The X-axis of the figure shows the concentrations normalized to a conservative estimate of the historical maximum for any monitoring point at the contaminated site. If adequate historical data are available, the maximum can be based on these data. In the absence of such data, the maximum can be based on solubility of the contaminant or on the concentrations of the contaminant in equilibrium with a NAPL source. **Figure 3-10** used an example of cis-DCE, which is a RD product, rather than a parent compound. In such situations, the maximum (molar) concentration of the parent compound should be used. If based on historical concentration data, the maximum is obtained for the sum of molar concentrations of all compounds in the RD chain. Solid lines are drawn corresponding to different values of ϵ from the literature corresponding to different geochemical or microbial environments. The horizontal line reflects attenuation with no isotope effect (“dilution”). The attenuation scenario lines intercept the Y axis at the best estimate or range of the isotope ratio of the original material.

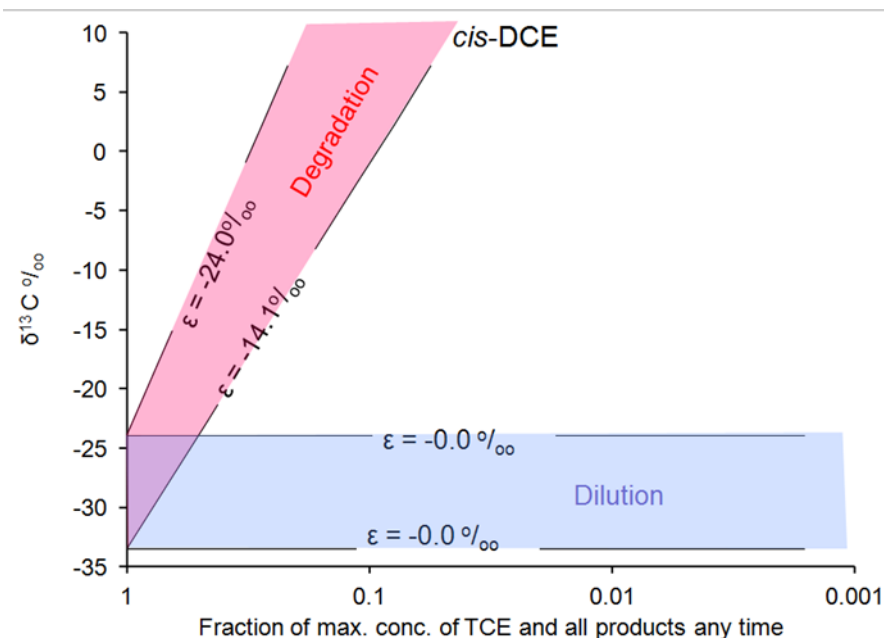


Figure 3-10. Plot of changes in isotope ratio vs. fraction contaminant mass remaining expected from biodegradation and dilution attenuation processes. The range defined for biodegradation is determined from epsilon values in the literature. Excerpted from (Wilson, 2011).

3.3.4 Dual Isotope Plots

For sampling programs that include CSIA of multiple elements, dual isotope plots such as $\delta^{13}\text{C}$ vs $\delta^{37}\text{Cl}$ or $\delta^{13}\text{C}$ vs $\delta^2\text{H}$ can be developed to provide powerful visualizations for interpreting degradation mechanisms (**Figure 3-11**). So-called 2-D (C and Cl or C and H) or 3-D datasets (C, Cl and H) can be collected by performing CSIA for all elements for each CE in a groundwater sample. The rationale for multi-element analyses is that isotope fractionation pathways for a single element may appear similar for various degradation pathways. However, isotopic fractionation factors for different elements often vary widely among different degradation pathways, allowing pathway discrimination based on a value of, e.g., $\delta^{13}\text{C} / \delta^2\text{H}$ for C+H CSIA. By plotting dual isotope values, different microbial pathways can be identified based on different fractionation patterns seen by comparing fractionation for multiple elements for various VOCs. (Fischer et al., 2008; Kuder, Georgi et al., 2005; Zwank et al., 2005).

Recently, introduction of Cl and H CSIA permits analysts to apply the 2D-CSIA approach to CEs. The data published so far suggest that the 2D approach can help to differentiate aerobic degradation from RD (Abe, 2009) and likely to differentiate attenuation pathways for other CEs (Wiegert, 2012) 2D-CSIA may also help to identify non-degradative processes. Currently, it is not clear to what extent can various RD pathways (e.g., biological vs. abiotic) be identified by 2D-CSIA. The results from the laboratory experiments on TCE volatilization and aqueous diffusion (Jeannotat, 2012; Jin, 2014) suggest that Cl fractionation in samples impacted by these processes should be proportionally larger (vs C fractionation) than that in degradation.

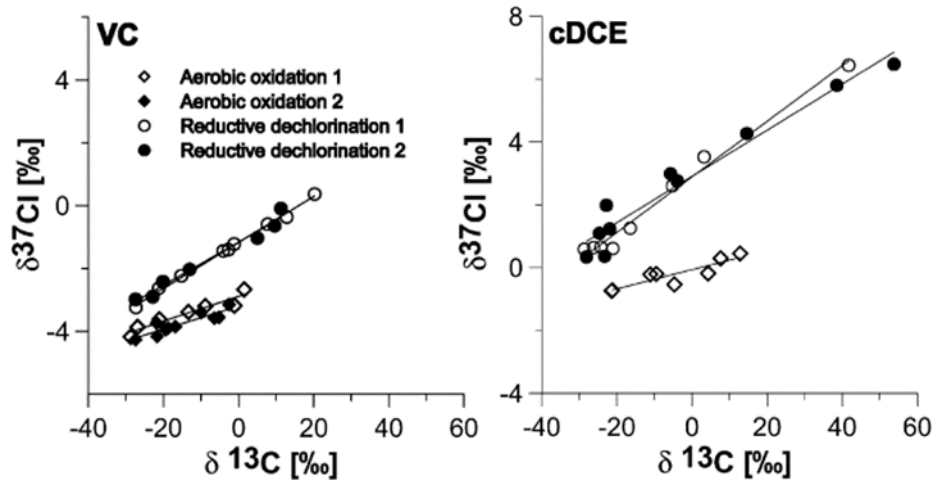


Figure 3-11. Dual isotope plots of C and Cl illustrating various degradation pathways. (Excerpted from [Abe, 2009 #21]).

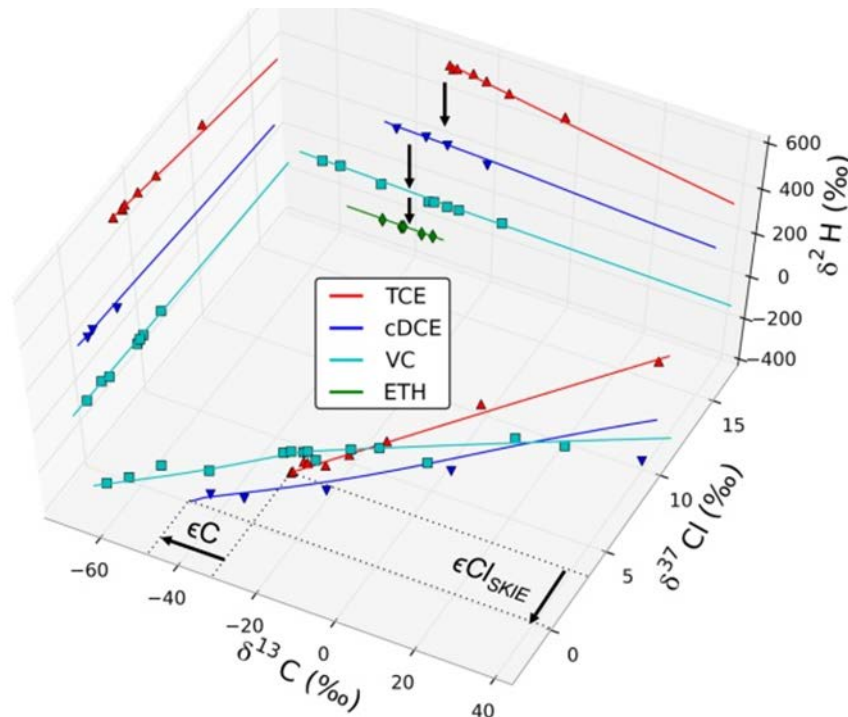


Figure 3-12. Examples of 2D-CSIA and 3D-CSIA plots. Top: C+Cl plot of isotope fractionation in aerobic degradation and RD or VC and cis-DCE (Abe et al., 2009); Bottom: C+Cl+H plot of isotope fractionation in RT transformation of TCE to ethene (CSIA data after Kuder van Breukelen et al., 2013).

3.3.5 Carbon Isotope Mass Balance

Carbon isotope mass balance (C-IMB) calculation is a method that can be used to assess CE degradation. The method relies on multiplying the C isotope signature for each compound by the molar concentration divided by the sum of CEs plus ethene concentrations: The method of calculating the C-IMB is illustrated by **Equation 3-11**.

$$C-IMB(\text{‰}) = \frac{\sum_i \delta^{13}C_i \times C_i}{\sum_i C_i} \quad (3-11)$$

Where C_i is the molar concentration and $\delta^{13}C_i$ is the isotope ratio of each parent and daughter compound and $\sum_i C_i$ is the sum of all CEs, including ethene, in the degradation chain (Aeppli, 2010). During RD, the C skeleton of the parent compound is retained through multiple transformation steps, so that C-IMB remains constant and equal to the source signature as the C atoms are transferred to the daughter products through ETH (**Figure 3-13**, see also **Figures in Section 4**). If ETH or any other compounds of the dechlorination chain are degraded (mineralized to CO_2) by alternative mechanisms (e.g., cometabolic oxidation), C-IMB becomes progressively enriched in ^{13}C . A positive deviation of C-IMB from the initial source value can be used as an evidence of additional degradation pathways competing with RD.

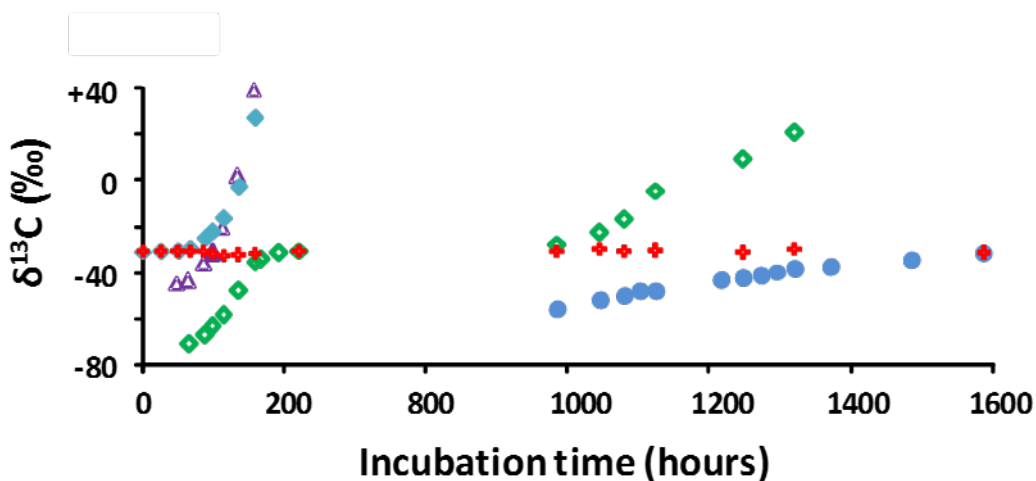


Figure 3-13. Evolution of individual C isotope ratios and C-IMB in transformation of TCE to ethene in the BDI microcosm (after Kuder and van Breukelen et al., 2013; van Breukelen et al., in prep). TCE (\blacklozenge), cDCE (\blacktriangle), VC (\blacklozenge), ethene (\bullet), C-IMB ($+$). Note that C-IMB remains nearly identical to the initial isotope composition of TCE.

3.4 Practical Aspects of CSIA Implementation

3.4.1 CSIA Sample Plan Design

As with all sampling plans, strategies for CSIA investigations should be based on the current CSM and the goals and objectives of site stakeholders. Field sampling strategies for conventional data interpretation and analysis by RTM are similar.

For support of MNA remedies, the CSIA study goals often include:

1. Demonstration that parent contaminants are degraded in the subsurface.
2. Demonstration that the rate of degradation is sufficient to control the extent of the plume and reduce toxicity over time.

3. Demonstrate the presence of multiple degradation reaction mechanisms in the subsurface (e.g. anaerobic RD, aerobic cometabolism, abiotic RD).
4. Demonstrate that cis-DCE and VC are ‘stalling’ or failing to degrade further.
5. Demonstrate biodegradation in the source zone.
6. Confirm assumptions in the CSM including hydrogeologic connection, sources and fate

In addition, CSIA can be used to confirm degradation kinetics for enhanced in situ biodegradation remedies. Data from CSIA may also confirm hydrogeologic assumptions in the CSM by providing a geochemical signal of transport pathways and may help in detecting matrix diffusion processes as further support for a comprehensive CSM. CSIA is also frequently used as one line of evidence in identifying discrete sources of CEs (Hunkeler, 2004). Source distinction objectives can often overlap with site characterization and assessments of biodegradation.

An adaptive or tiered sampling approach is recommended for most CSIA studies. Preliminary samples for CSIA can be collected during routine groundwater monitoring for concentrations. After the preliminary data are reported, and results evaluated, the sampling plan can be expanded or modified to address outstanding questions.

Methods for groundwater sampling for CSIA are essentially the same as those for conventional CE concentration analysis. Any method that provides an adequate sample volume, minimizes losses due to volatilization and provides a representative sample is suitable (Hunkeler et al. 2008). Groundwater samples can be collected from existing wells without specialized equipment and can be performed simultaneously with concentration measurements. Sampling methods that include measurement of field parameters such as DO, ORP, pH and temperature (and parameters listed in **Section 2.2.4**) provide additional lines of evidence for biodegradation pathways.

In some cases, existing groundwater monitoring wells may not be sufficient to characterize isotope fractionation in a complex plume. Additional, temporary, groundwater sampling locations may be required. The need for temporary sampling locations can be assessed after preliminary analysis from existing wells and a review of monitoring objectives. Temporary locations may be required in plume fringe areas and areas where there are transitions in lithology, geochemistry, recharge or where plumes comingle.

The primary difference between conventional groundwater sampling and sampling for CSIA is that the volume of sample required for CSIA may be much larger. The sample volume will depend on the concentration of constituents in groundwater and the detection limit of the CSIA instrument method. Specific recommendations on sample collection and preservation techniques as well as data quality objectives (DQOs) for CSIA are discussed in 2008 USEPA Guidance.

3.4.2 Where should I sample?

General Recommendations

The density, location and frequency of samples for CSIA are dependent on the objectives of the study and the size, geometry and heterogeneity of the plume. Prior to initiating a CSIA investigation, data from site investigation and routine monitoring should be reviewed carefully to identify candidate areas for CSIA sampling. **Table 3.2** lists plume areas and potential monitoring objectives that would prompt CSIA sampling.

Generally, CSM elements and site history should be reviewed to identify:

1. **Sources** – primary sources such as tanks and industrial processes, DNAPL, secondary sources, including residual contamination in the vadose zone and sewer line areas; Source history may be important in the case where different primary solvents (e.g. PCE, TCE, 1,1,1-TCA) have been used over time.
2. **Locations with Sufficient Concentration of Parent and Daughter Compounds.** For analyses such as C-IMB, it can be important to have high concentrations of daughter products to compare with source area isotope signatures. It is also important to have some high concentration daughter product samples if Cl and H ratios are evaluated. Review the method detection limits with the lab to identify target concentrations for target COCs and choose sampling locations where concentrations exceed the method detection limit. Locations with no detection of most CEs should be avoided.
3. **Potential Areas of Anaerobic Degradation** including locations with hydrocarbon co-contaminants, low DO and anaerobic biodegradation geochemical indicators (**Section 2.2.4**).
4. **Hydrogeology** – identify areas of likely transport of solutes and the strength of each transport mechanism.
5. **Plume Fringe Areas** – Areas outside of the primary flow line represent solutes transported by both advection and dispersion and may be more aerobic than center zones. Sampling in plume fringes may provide data to support conclusions of aerobic destruction of cis-DCE and VC and may help estimate the maximum extent of plume migration.
6. **Depth Discreet Heterogeneity** – Concentrations and degradation processes may vary by depth. Monitoring well construction, including screen length, should be reviewed to identify sampling depths supporting the goals of the study. CSIA results may vary significantly by lithology, showing stronger degradation or matrix diffusion signals in low-porosity sediments.
7. **Transitional Areas** – Locations that mark transitions between high and low porosity zones, co-mingling plumes, flow barriers or between aerobic and anaerobic zones can provide important information supporting CSM development.
8. **Past and Ongoing Remediation Activities** – Certain activities conducted at the site complicate implementation of CSIA. For example, active physical remediation (vapor extraction etc.) can potentially imprint isotope fractionation that will mask or mimic the effects of in situ degradation at the area. One critical element is former in situ application of heavy isotope-labeled surrogates to detect evidence of *in situ* degradation. Inevitably, trace concentrations of such surrogates remain in the aquifer and mask the isotope signatures of the unlabeled contaminants. The surrogates can persist longer than expected based on groundwater seepage rates, due to their retention in low permeability sediments and matrix desorption.

For most MNA applications, sampling in the source area or from source material (i.e., DNAPL) is essential. Source area sampling is often the best indication of the isotope ratios of the original release material (**Section 3.1.2**). Samples should be collected from groundwater wells with the maximum COC concentrations or closest to the known original release. If multiple source areas are present, sampling in each area is important to distinguish isotope ratio signatures and distinguish fractionation effects from differences in releases from various locations and processes (Hunkeler, 2008). Samples of dissolved CEs collected near or immediately downgradient from the primary source area can indicate the level of source attenuation relative to DNAPL samples.

For the plume body, the sampling density should be proportional to the complexity of the aquifer. If there are multiple interbedded layers, discontinuities or other complex hydrogeological features, many samples, fairly closely spaced may be required to identify dominant processes in each stratum. It is important to remember that source areas are three dimensional and that a thorough investigation of source history (Newell, 2013) can provide details of migration of contaminants into the subsurface that can guide precise CSIA sampling.

Table 3.4. Monitoring Objectives for CSIA Investigations

Plume Area	CSIA Monitoring Objective
Source	<ul style="list-style-type: none"> • Determine isotope ratio of original contaminant release; and highest total CE concentration (C_0) to estimate extent of degradation • Identify sources, distinguish between multiple sources • Demonstrate source attenuation by biodegradation
Centerline of Plume	<ul style="list-style-type: none"> • Demonstrate degradation of CEs outside of source, including degradation of daughter products • Estimate rate constants for degradation of individual CEs and daughter products • Estimate potential plume control from biodegradation • Identify potential alternate biodegradation mechanisms • Correlate biodegradation mechanisms with geochemical and concentration data
Lateral Plume Fringe	<ul style="list-style-type: none"> • Demonstrate ‘alternative’ plume biodegradation mechanisms (e.g., aerobic cometabolism) • Quantify effects of hydrodynamic dispersion on estimates of biodegradation
Leading Edge of Plume	<ul style="list-style-type: none"> • Data for prediction of future migration of plume • Demonstrate ‘alternative’ plume biodegradation mechanisms (e.g., aerobic cometabolism)
Low-porosity zones	<ul style="list-style-type: none"> • Evaluate effects of matrix diffusion on isotope signals • Evaluate biodegradation in low-porosity zones

Typically, CSIA samples are collected from locations downgradient from the source along the groundwater flowpath. For plumes in simple hydrogeologic environments, including sandy, homogeneous sediments with diffuse flow, sampling from a few points (4-5) along the primary flow path will support demonstration of degradation and simple rate calculations. Additional samples can be collected in plume fringe areas including lateral areas various depths. *The total number of samples for most plumes will be dictated, not by the length of the plume but by the heterogeneity of the subsurface environment and the isotopic shifts in preliminary samples.*

For more complex, geologically heterogeneous, plumes, at least three samples should be collected from each region representing a distinct hydrogeologic regime (e.g. saturated unit, flow path, flow direction) as a preliminary screening step. If isotopic ratios are similar (that is showing an isotopic shift below the level of significance [Section 3.2.1]) along flow paths or in distinct areas, additional sampling may be conducted at locations farther down or cross-gradient.

If monitoring well screens transect more than one lithologic layer or are very long (20 ft or greater), several discreet depths may be sampled. Concentration and isotopic data taken together can indicate if groundwater over depths is well mixed. In the Hill AFB Case Study (Appendix A), samples taken from multiple locations in a long screen were found to be very similar, indicating that the plume was not highly stratified over the length of the screen.

An adaptive sampling strategy can be used to evaluate the need for further spatial sample coverage. After results of preliminary sampling of a subset of wells has been evaluated, additional spatial samples can be taken to confirm results and test the sensitivity of biodegradation and rate constants estimated from preliminary results.

Recommendations for CSIA with RTM

Figure 3-13 illustrates how the type of degradation kinetics results in different isotope enrichment isolines across a pollution plume. The Scenarios A and B are based on actual observations and numerical modeling results (van Breukelen and Prommer, 2008; Atteia et al., 2008; Prommer et al., 2009). First-order degradation where the degradation rate only depends on the pollutant concentration results under homogeneous conditions in a steady linear increase in isotope ratio in the groundwater flow direction. With depth, the isotope ratios should be identical (not shown). Under these conditions samples are best taken along the plume center line to be sure concentrations are sufficiently high to enable CSIA. Because the isotope signal increases away from the source and might be below the recommended 2 permil enrichment near the source area, it is recommended to apply the highest sampling density at the plume front area provided concentrations are sufficiently high to allow CSIA. In case degradation conditions are not expected to be homogeneous but, for example, layered with depth. It is recommended to sample along flowlines at multiple depths to identify aquifer layers with high and low first-order degradation rate constants.

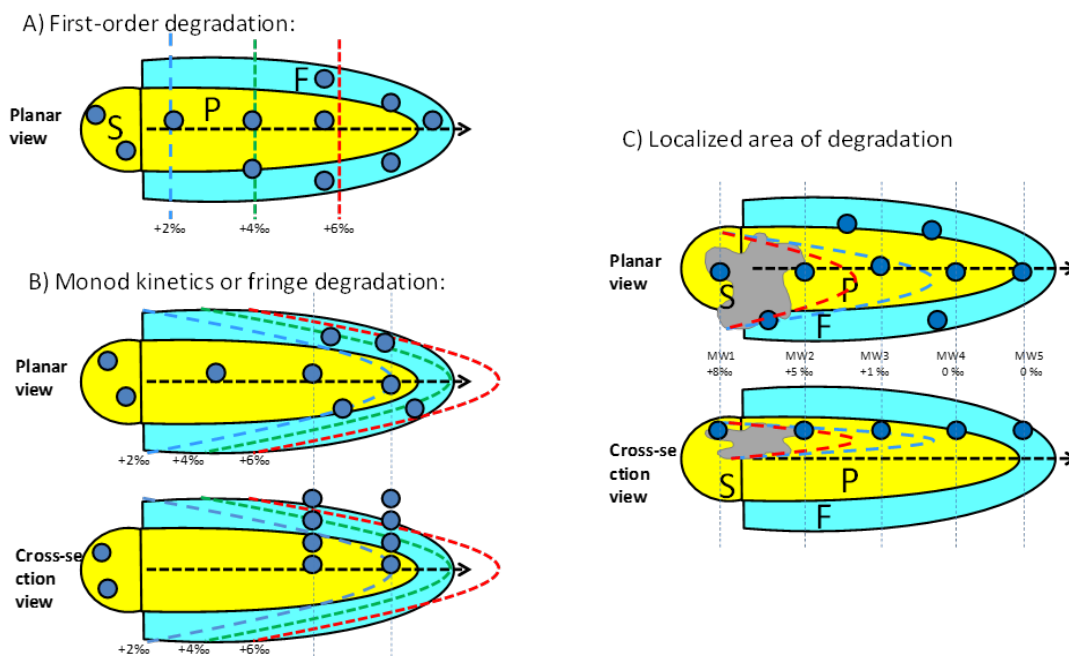


Figure 3-13. Isotope enrichment patterns versus degradation kinetics and strategies for CSIA monitoring network design. *S* defines the source zone, *P* defines the plume area, and *F* the fringe area around the main plume with strongly reduced concentration levels. Blue dots roughly indicate the spatial coverage and density of recommended CSIA sampling locations. The dark patch shown in Panel C represents a commingled hydrocarbon product.

Usually the assumption of first-order kinetics is fair provided concentration levels are not too high. However, Monod kinetics might be more applicable in case source concentrations are very high (near NAPL solubility). Monod kinetics would therefore, better describe the transition of pseudo zero-order kinetics at high concentration levels to pseudo first-order kinetics at low concentration levels. The result of Monod kinetics is a relatively high extent of degradation at lower concentration levels as the rate is high compared to the concentration level. As a result, isotope enrichment isolines become curved and somewhat tend to follow concentration gradients (**Figure 3-13B**). A similar pattern is observed for so called fringe degradation, i.e., the oxidative transformation of pollutants contained in anoxic plumes. Degradation is enhanced at the fringe areas where pollutants and oxidants mix leading the steep isotope ratio gradients across the fringe areas (**Figure 3-13B**). A similar isotope enrichment pattern should also evolve at the fringes of the plume as depicted in cross-section (**Figure 3-13B**). For these kinds of kinetics, it is strongly recommended to sample especially at the fringes of plumes provided concentration levels permit CSIA. A multilevel sampling strategy across the plume fringe may also aid in obtaining proof for this process.

Scenario C (**Figure 3-13C**) shows a localized zone of degradation producing a localized zone of enhanced isotope enrichment. This scenario can occur at CEs plumes commingled with hydrocarbon electron donor plumes (such as BTEX), where vigorous RD is limited to strongly reducing areas with abundant electron donors. Away from the zone of degradation, the fractionated CEs can eventually be diluted and mixed with undegraded CEs moving along flow lines that bypass the zone of degradation. The Hill AFB data set discussed in Appendix A. Figure 3-13 shows localized zones of highly fractionated CEs, where the distribution of the degradation zones is controlled by aquifer lithology.

3.4.3 How many samples do I need?

Sampling density for CSIA is likewise dependent on the goals and objectives of the study. The more limited the goals and the simpler the hydrogeology and geochemistry, the fewer samples are normally required. The EPA Guidance recommends between 12-20 or more groundwater well locations (Hunkeler, 2008), however, a contaminant plume envisioned in that guidance was relatively homogenous (approximated by Scenario A in **Figure 3-13**). Many features of the site could affect the final sample count.

For highly heterogeneous subsurface environments, multiple CSIA analyses may be required to identify predominant attenuation mechanisms. For many sites, an adaptive or tiered sampling program is recommended. The initial sampling program can be prioritized based on monitoring goals listed in **Sections 3.4.1** and **3.4.2** above. As data are collected, the need for further sampling and CSM refinement may become clearer.

CSIA sampling DQOs often require replicate samples QA/QC. In general, duplicate samples should be collected for one out of every 10 sampling locations.

3.4.4 Which Isotope Ratios do I Evaluate?

All isotopes ratios ($^{13}\text{C}/^{12}\text{C}$, $^{37}\text{Cl}/^{35}\text{Cl}$, and $^2\text{H}/^1\text{H}$) of CEs are accessible for CSIA. For most CE applications, C isotope ratios are analyzed as these are most likely to provide strong evidence of both mass destruction and a distinct source of the primary contaminant, and the carbon C=C skeleton is conserved through most of the degradation sequence. However, multi-dimensional analyses can provide more specific information on fate processes of CEs. Potentially,

characterization of two or more isotope ratios may be invaluable to identify different microbial strains (or enzyme systems) or abiotic agents responsible for CE degradation (Abe et al., 2009) (Cretnik, 2013) (see **Section 3.3.4** for rationale of this approach).

Multi-dimensional CSIA may be the best option for identification of distinct sources of the primary contaminants, because C isotope ratios fractionate readily if part of the contaminant is degraded. The net changes (in permil) of Cl isotope ratios are small in comparison, and distinct source signatures may be resolved even if C data alone are inconclusive. H isotope signatures may be very different depending whether the CE is the parent compound or degradation product (e.g., TCE released as a parent contaminant vs. TCE product of PCE dechlorination). Ultimately, the decision to incorporate multiple elements depends on the goals of the CSIA study and the budget.

3.4.5 How often do I perform CSIA?

As with questions of spatial sampling, temporal sampling for CSIA depends on the type and frequency of site management decisions that must be made. CSIA is normally conducted as part of the site characterization/remedy investigation stage of site management. CSIA for site characterization may involve an adaptive (tiered) approach to sampling where the need for additional sampling is determined after preliminary samples are analyzed and interpreted. CSIA during site characterization may include repeat sampling events separated by several months to confirm reproducibility of results. Additional sampling events may be required after major construction (e.g., pump and treat, capping or excavation) or cessation of active remedies (e.g., shut down of pump and treat systems or soil vapor extraction) or in the case of major hydrogeochemical changes to the aquifer (e.g., significant drawdown or flux of organic matter into the system).

CSIA analyses can be used as part of remedy performance monitoring, particularly in the case where reductants are applied to a CE plume to stimulate RD of CEs. Baseline CSIA prior to installation or application of a remedy should be performed with follow-up analyses performed at intervals after remedy installation. CSIA can be used to demonstrate on-going biodegradation after injections have ceased or to evaluate if further injections or reductant are necessary. CSIA can demonstrate RD of parent compounds, as well as daughter products, which can potentially address questions of stalling of sequential degradation at intermediate products.

After MNA is chosen as all or part of a site remedy, routine (conventional) monitoring of groundwater concentrations and geochemical indicators is normally sufficient to demonstrate MNA remedial performance. In some cases, remedy performance evaluations for MNA, such as Five-Year Reviews for EPA programs, may require subsequent CSIA to confirm that subsurface processes are still active. Remedy performance reviews may also be required during property transactions. In the case of remedy performance reviews, monitoring locations from the initial investigation should be identified that provide the best data supporting dominant attenuation processes in each area of the plume.

3.5 When to Move to CSIA with Reactive Transport Models

CSIA results from individual locations within a plume combined with conventional interpretation methods (e.g., Rayleigh equation) have the potential to demonstrate and quantify biological destruction of CEs. The conditions under which conventional CSIA is most likely to be productive include assessments for a single parent compound (e.g., PCE or DCE), one degradation pathway or one isotopic fractionation factor. CSIA has been shown to work well to support MNA where

the CSM is straightforward and complete and where the sources are well delineated in space and time and where hydrogeology is fairly simple.

However, application of the Rayleigh equation requires the assumption that the plume is an idealized, closed and well mixed system (Van Breukelen, 2008). For sites with complex hydrogeology including interbedded sediments with varying porosity, variable flow directions, complex pumping regimes, source uncertainty and multiple degradation pathways, CSIA data interpreted using the simple Rayleigh equation may not be definitive. Conventional analysis of CSIA data does not account for sequential degradation of intermediates well or with competing degradation pathways (e.g., VC degradation by both aerobic and anaerobic mechanisms). Conventional CSIA interpretation does not account for sorption or matrix diffusion effects where solutes with more degraded isotope ratios mix with less degraded solutes through physical processes (Aeppli, 2009). Conventional CSIA also may not account for hydrodynamic dispersion or diffusion-induced fractionation (DIF).

For some sites, RTM of isotope effects can potentially combine the benefits of traditional CSIA (robust compound-specific signal of in-situ degradation) with improved quantitative assessment of chemical reaction with mass transport (Van Breukelen et al. 2005; Atteia et al. 2008). Several example scenarios of using RTM to interpret CSIA data are presented in **Section 4**. The scenarios include using RTM to demonstrate the strength of contaminant degradation versus attenuation effects from dispersion and dilution, detecting oxidation processes for cis-DCE and VC and simulation of RD in the core of plume with oxidation at the fringe.

The objective of this guidance is to help site managers apply a RTM approach for improved CSIA data interpretation and to use the models to estimate more accurate attenuation processes. The quantification of various destructive and transport processes and how they contribute to plume size and longevity may help extend MNA remedies to sites that have heretofore not been able to apply this important technology.

In comparison with traditional interpretation of the field isotope data based on Rayleigh equation, the approach presented below has several important benefits: (1) improvement of a CSM by identification and quantification of prevalent attenuation pathways (i.e., reductive biotic dechlorination vs. abiotic dechlorination vs. aerobic degradation) and identification of secondary inputs from DNAPL dissolution or non-degradative sinks such as sorption or volatilization, diffusion or dispersion. (2) a more accurate assessment of degradation of the parent contaminant. (3) quantitative assessment of the net degradation/accumulation of the dechlorination intermediates.

4.0 CSIA WITH REACTIVE TRANSPORT MODELS (GENERATION 3 MNA)

4.1 Introduction to Reactive Transport Models

A model is a simplified representation of the features of interest of a site. Models can be developed with varying levels of complexity to simulate a variety of conditions. Most groundwater models are developed around either physical processes (e.g. advection, dispersion, diffusion, and sorption, described above) or chemical reaction (e.g. spontaneous or enzymatically catalyzed Monod-type rate equations). *Reactive Transport Models (RTMs) constitute a set of interpretive tools to simulate complex interactions between linked chemical and physical processes across multiple space and time scales.* Models linking CSIA results with contaminant reaction and transport require integration of both a geochemical approach and physical processes and are, therefore, best approached through RTM.

The Stable Isotope Reactive Transport Modeling (SIRTM) approach outlined in the following section and in the Technical Manual (**Sections 5 – 7**) includes a number of strategies to support interpretation of CSIA data beyond those described in Section 3. Many of these strategies involve use of pre-existing modeling platforms and coding languages developed in the field of geochemical modeling.

RTMs, in principle, enable users to simulate complex reaction networks (sequential reductive dechlorination together with oxidative transformation) together with isotope fractionation (C, H, Cl), while accounting for physical processes that may influence isotope ratios such as hydrodynamic dispersion (Abe, 2009; Van Breukelen and Prommer, 2008), diffusion as part of vertical transverse dispersion (Jin et al., 2014 ; Van Breukelen and Rolle, 2012), and sorption (Eckert, 2013 ; Van Breukelen and Prommer, 2008). RTMs allow 3-D simulation of concentration and CSIA patterns at contaminated sites. However, as discussed below, RTMs also enable sound data interpretation through simulating fewer dimensions like 2-D cross-sections or 1-D flow paths. RTMs are essential tools in the interpretation of CSIA data and are not necessarily too complex to establish and run.

RTM model and software platforms used to develop modeling tools for CSIA interpretation for this project include:

- **PHREEQC** – A one dimensional (1D) geochemical transport model developed by the US Geological Survey (USGS).
- **PHAST** – A three dimensional (3D) groundwater flow and transport model capable of simulating the same set of reactions as PHREEQC. PHAST couples PHREEQC to the groundwater flow and solute transport model HST3D.
- **PHT3D** – A three dimensional (3D) groundwater flow and transport model capable of simulating the same set of reactions as PHREEQC. PHT3D couples PHREEQC to the groundwater flow model MODFLOW and the solute transport model MT3DMS.
- **Python** – A general purpose scripting language available for free download. Algorithms written in Python scripts have been developed for this project to visualize output from modeling programs.

More details on the RTM platforms, including download information is provided in the Technical Manual (Sections 5 -7).

4.1.1 RTM Spatial Dimensions

Figure 4-1 illustrates the number of spatial dimensions that can be simulated using RTM techniques. Site data occur in 3-D space. However, this does not imply that RTMs in 3-D are required to interpret concentrations and CSIA data. Many relevant site characterization questions can be answered by models created in 2 and 1-D formats.

Provided hydraulic head contours are more or less parallel (**Figure 4-1A**), observations can usually be projected to a 2-D cross-section of the pollution plume (**Figure 4-1B**), because a sampling network typically follows the groundwater flow direction. Monitoring of a 2-D cross-section is cost-effective and sound for many sites where environmental conditions are relatively homogeneous perpendicular to the groundwater flow direction at a certain depth level. Furthermore, 2-D model development is simpler and computationally less intensive. Still, a 2-D cross-sectional model is only required if degradation processes vary between the core and the fringe of the plume. **Figure 4-1B** shows the spreading of ethylbenzene and its degradation following anaerobic core and aerobic fringe degradation results in complex CSIA patterns and enrichment at the fringe (D’Affonseca, 2011). Clearly, for this case a 2-D model is required as well as multi-level sampling.

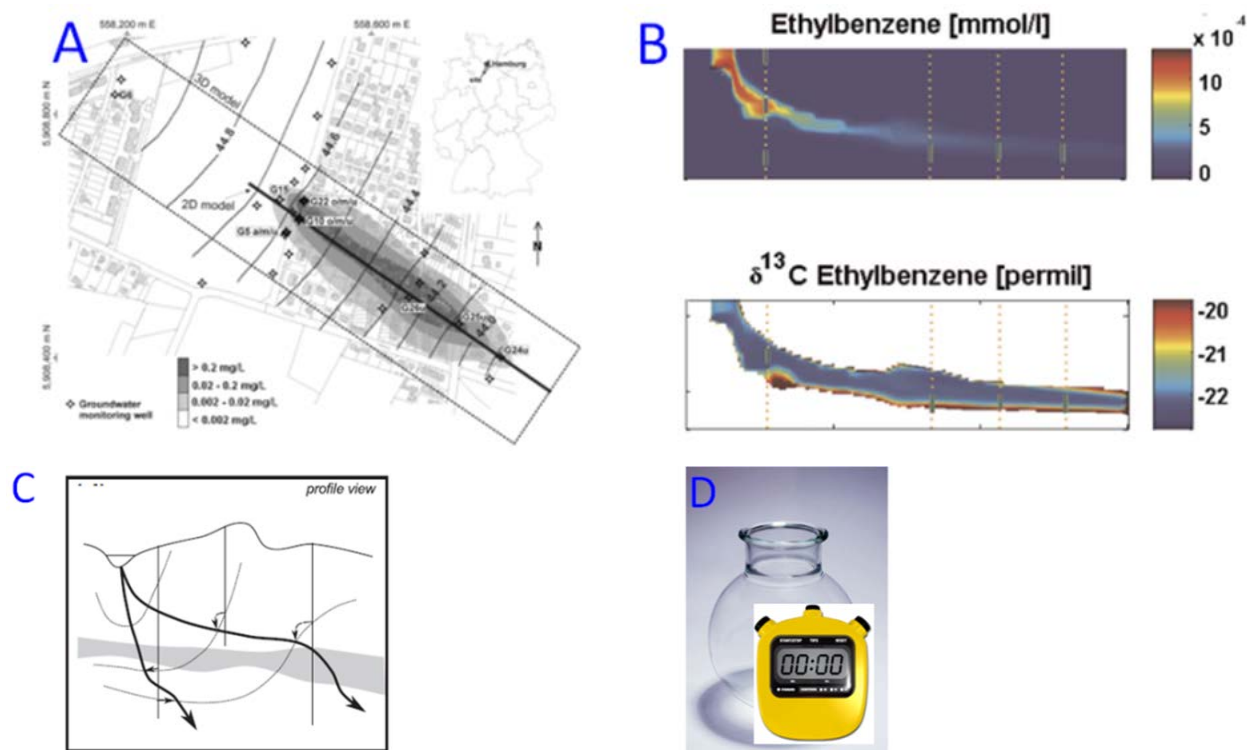


Figure 4-1. Spatial dimensions of RTM and application. A) 2-D plan view of 3-D pollution plume (D’Affonseca, 2011). The black line following the groundwater flow direction shows the position of a 2-D cross-section shown in B. B) 2-D cross-section of pollution plume depicted in A showing simulated ethylbenzene concentrations and C isotope ratios (D’Affonseca, 2011). C) 1-D flow paths simulating observations in 2-D space (Karlsen, 2012). D) A well-mixed closed 0-D batch system where the properties only change as function of time or reaction progress.

In the case where degradation processes are homogenous across the height of the plume, a 1-D flow path model may suffice to simulate observations as illustrated for Case 1 under Example Scenarios below (see **Section 4.2** with more detailed descriptions following in **Section 7**). Example Scenario Case 1 shows that a 1-D flow path RTM is not able to match concentration levels as transversal dilution processes are not accounted for in a 1-D model. Model calibration to molar concentration ratios instead of absolute CE concentrations provides a solution. Optionally, several flow paths can be modeled to simulate observations in 2-D cross section (**Figure 4-1c**). Flow path RTMs are easy to setup and are computationally fast. Another advantage is that heterogeneous conditions along the flow path such as aerobic transformation downgradient of a reductive dechlorination zone are easy to implement in the model.

A typical assumption in any 1-/2-/3-D model is spatially constant degradation rate constants. In fact this is a sound assumption to limit model complexity and to prevent non-uniqueness of the set of calibrated model parameters. However, it is questionable if rate constants are truly spatially homogeneous and, in reality, the spatial heterogeneity of reaction rates should reflect heterogeneities in the distribution of hydrogeochemical properties. For cases of high spatial heterogeneity in geochemical environments, it will be hard for a 1-D model to accurately simulate observations as a function of travel distance. A potential approach is to consider the subsurface as a black box reaction vessel and to apply a 0-D batch RTM (actually a RM, reaction model, as transport does not occur). In such a setup (**Figure 4-1D**) the changes in molar concentration ratios and CSIA data are evaluated versus reaction progress as previously performed by van Breukelen et al. (2005). Such a model setup enables a fast evaluation of the appropriateness of the conceptual reaction network, the proportion of degradation rate constants, and isotope fractionation factors. However, an important drawback to this approach is the omission of hydrodynamic dispersion as an attenuation process. Calibrated fractionation factors will, consequently, deviate somewhat from actual values. This latter 0-D approach was applied to interpret the field site data of the Case Study (**Appendix A**). Examples of 1-D and 2-D RTMs are illustrated with the Example Scenarios presented in Section 4.2.

4.1.2 Model Input Data

Several types of information are required to construct different types of RTMs (see **Table 4-1** and **Section 2.1** above). Basic categories of data include hydrogeologic data such as groundwater flow direction, porosity, gradient and hydraulic conductivity. Data sources for hydrogeologic characteristics include site-specific groundwater elevations, results of pump tests and boring logs. These types of data are normally collected during the site investigation and are part of the CSM. Lithology datasets are sometimes maintained in a relational database, like the concentration data, but other parameters are normally found in site characterization reports and regulatory decision documents.

The second category of model information includes transport data such as effective porosity, bulk density of soil and fraction of organic matter as well as longitudinal and transverse dispersivity. Often data in the second category are estimated for specific lithology from literature sources, but data derived from actual site conditions can improve the quality of the model.

The third category of site data includes contaminant concentrations over both space and time. CSIA and other analytical data collected from the site would be included in this category. These data are normally found in a site relational database including details of the media sampled, analytical methods and the dates and locations of samples collected.

For RTM models using CSIA results, a fourth category of data is required: reaction rates (k) and enrichment factors (ϵ) for reacting constituents. These input values can be taken from literature sources for the reactants and the geochemical conditions of the site. Values for ϵ for a number of elements and CEs have been collected from the literature and are shown in **Figure 3-3** based on the recent compilation shown in **Appendix B**. Estimates of rate constants are likewise available in the literature (For example, see for first-order rate constant van Breukelen et al., 2005 cf. **Table 1** and literature references herein).

Table 4-1. Information Required to Construct Reactive Transport Models

Conceptual Info	<ul style="list-style-type: none"> • Site history • Key contaminants • Base map 	<ul style="list-style-type: none"> • A good conceptual site model • Source identity and history
Hydrogeologic Data	<ul style="list-style-type: none"> • Hydraulic conductivity at several locations • Effective porosity • Configuration of the transmissive zone (layers, location of any no-flow boundaries) • Confined vs. unconfined conditions 	<ul style="list-style-type: none"> • Any recharge/discharge zones • Recharge rates to transmissive zone • Hydraulic gradient information • Location, pumping rate of any major wells
Transport Data	<ul style="list-style-type: none"> • Bulk density of soil in aquifer matrix • Total porosity of soils in aquifer matrix • Fraction organic carbon in aquifer matrix • Partition coefficients 	<ul style="list-style-type: none"> • Estimates of longitudinal and transverse dispersivity • Diffusion coefficient estimates • Tortuosity or effective diffusion coefficients • General ranges of expected degradation coefficients
Reaction Data	<ul style="list-style-type: none"> • Reaction rates (k) for various CEs under different biogeochemical conditions 	<ul style="list-style-type: none"> • Isotope fractionation factors (ϵ)
Contaminant Data	<ul style="list-style-type: none"> • Decay chain for the contaminants of interest • Parent compound concentration at multiple locations and multiple times • Daughter compound concentration at multiple locations and multiple times 	<ul style="list-style-type: none"> • Carbon isotope (^{13}C) data at multiple locations (probably 10 or more) for at least one sampling event. • Chlorine isotope (Cl) data at multiple locations (probably 10 or more) for at least one sampling event. • Hydrogen isotope data (optional)

Different RTM software platforms have been developed for CSIA data interpretation, and require different types of input data. (Key model platforms are described in detail in **Section 5**). **Table 4-2** indicates more specifically which general input data or information are needed for the various types of RTMs (0/1/2/3-D) relevant to CSIA interpretation. Specific attributes of the reaction network and type of kinetics are usually fine-tuned during model development. Once the reaction network is properly determined, the values of degradation rate constants and isotope fractionation factors can be fine-tuned within literature ranges in the process of model calibration. All models need prior information on the source composition. Detailed information on hydrogeological properties is needed to develop 2-D and 3-D models, whereas for 1-D models information on the average groundwater flow velocity and trajectory of the flow path are sufficient.

Table 4-2. Input Data for Various Model Levels

<i>Input data/information</i>	<i>0-D Batch</i>	<i>1-D Flow path</i>	<i>2-D Cross-section</i>	<i>3-D Aquifer</i>
Model platform	PHREEQC	PHREEQC	PHAST, PHT3D	PHAST, PHT3D
Reaction network	Y (MD)	Y (MD)	Y (MD)	Y (MD)
Reaction kinetics	Y (MD)	Y (MD)	Y (MD)	Y (MD)
Degradation rate constants	Y (MC)	Y (MC)	Y (MC)	Y (MC)
Isotope Fractionation factors	Y (MC)	Y (MC)	Y (MC)	Y (MC)
Source composition	Y	Y	Y	Y
Source concentrations	Y	Y	Y	Y
Source isotope ratios	Y	Y	Y	Y
Age of source	na	Y	Y	Y
Time	Y	na	na	na
Groundwater flow velocity	na	Y	na	na
Hydraulic heads	na	na	Y	Y
Hydraulic permeability	na	na	Y	Y
Porosity	na	na	Y	Y
Hydrogeological architecture	na	y	Y	Y
Solid-water partitioning coefficient	Y	Y	Y	Y
Longitudinal dispersion coefficient	na	Y	Y	Y
Transverse dispersion coefficients	na	na	Y: αV	Y: αV & αH
Concentration and CSIA data	Y	Y	Y	Y
Y = Yes na = not applicable (MD) = will also follow out of model development (MC) = could also be determined through model calibration				

4.1.3 Calibration

Model calibration is the systematic adjustment of model input parameters so that model outputs more accurately reflect field or ‘ground truth’ conditions. Calibration involves the estimation of values of constants and parameters used in the model algorithms. This is normally accomplished by solving approximation equations for the desired constants and parameters using values of field observed variables. All models require some level of calibration to be useful for a specific site. **Table 4-3** provides a brief summary of calibration processes for the RTMs used to interpret CSIA data.

Table 4-3. Calibration process for various models

<i>Model Name</i>	<i>Model Type</i>	<i>Calibration Process</i>
PHREEQC	0-D	Adjusting degradation rate constants and isotope fractionation factors to fit isotope ratio versus molar concentration ratio plots
	1-D	Adjusting degradation rate constants, isotope fractionation factors, and the longitudinal dispersion coefficient to fit isotope ratio and molar concentration ratio versus travel distance plots
PHAST/ PHT3D	2-D	Assuming the flow field has been properly calibrated: Adjusting degradation rate constants, isotope fractionation factors, and the longitudinal and transverse vertical dispersion coefficients to fit CSIA and concentration data in the 2-D cross-section. Fitting should be regarded as approximately reproducing the observed concentration and CSIA patterns.
	3-D	The same as for 2-D. However, also the horizontal transverse dispersion coefficient should be fitted. The model-data comparison will be a considerably larger challenge than for a 2-D model. Fitting should be regarded as roughly reproducing the observed concentration and CSIA patterns.

4.1.4 Model Output

After the trial-and-error process of model calibration indicated in **Table 4-3**, the model results can be presented as illustrated in the four example case models described in **Section 4.2**, and as illustrated for the field site interpretation (**Appendix A**). Furthermore, degradation rate constants and isotope fractionation factors can be summarized into a table (various examples in **Section 4.2**).

4.1.5 Model Validation

Models developed for this project were validated based on microcosm experiments. Details of the microcosm experiments are presented in the Final Report for this project (ESTCP ER-201029) and in Kuder van Breukelen et al. (2013). **Figure 4-2** shows the results of the model developed and calibrated with microcosm experimental observations obtained as part of this project. The template models presented in example cases 1-4 below are based on this model. The user can therefore rely on accurate and valid model predictions provided the input data are correct.

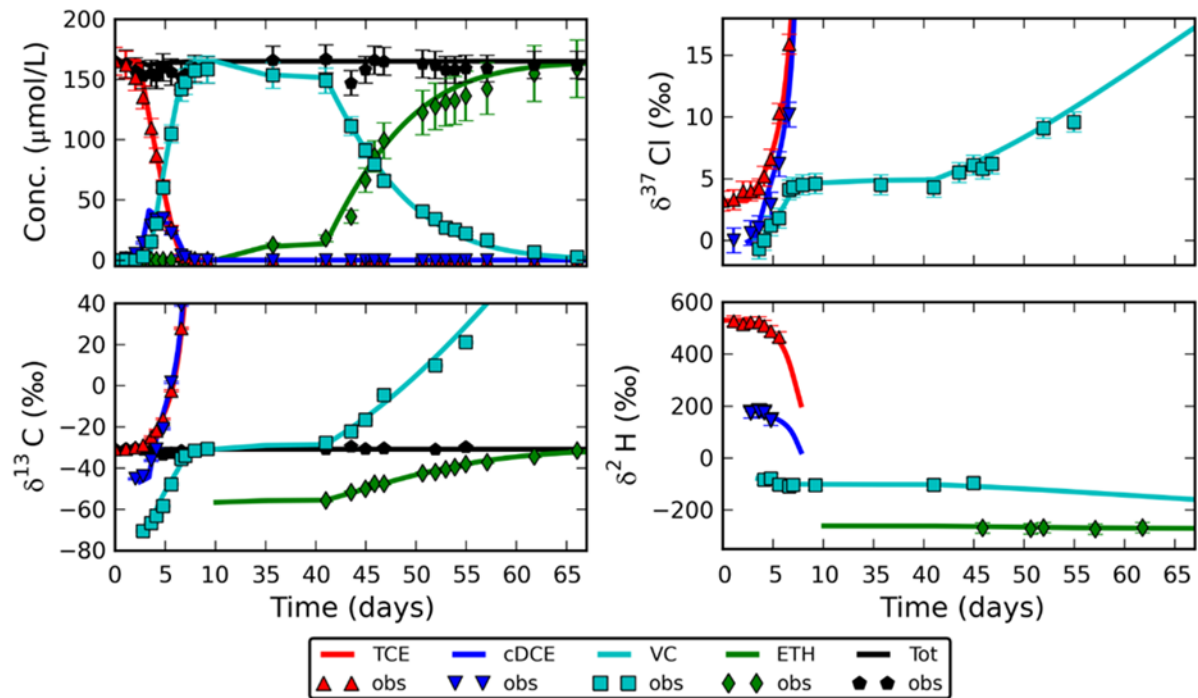


Figure 4-2. Model validation of the ‘Microcosm’ Model (see **Section 5.3**). The model developed to support interpretation of CSIA data accurately simulates concentrations, and C, Cl, and H isotope ratios of CEs and ETH over the course of sequential dechlorination. The observations were obtained in the microcosm experiment on complete reductive dechlorination of TCE as part of this project (Kuder, van Breukelen et al. 2013). The model applied Monod kinetics with lag-phases and SKIEs during Cl isotope fractionation.

4.2 Example Scenarios

To help users understand the Generation 3 MNA approach using CSIA and RTM, the following example scenarios have been developed to illustrate:

- What input data are needed?
- What models are used?
- How the results are interpreted?

Simulations presented below and discussed in more detail in **Section 7**, provide a basis for identifying patterns of isotope enrichment characteristic of different attenuation processes for comparison to field data. The models can be used to identify and judge the strength of different attenuation processes to support MNA remedies.

4.2.1 Case 1: Reductive Dechlorination Under Anaerobic Conditions

For example Case 1, a 1-D PHREEQC model is used to simulate concentrations, molar ratios, and C isotope ratios for complete dechlorination of PCE to ETH. In Case 1A, ETH is modeled as a stable end product of dechlorination (in other words, there is no further degradation of ETH). For Case 1B, the effects of further degradation of ETH are simulated to illustrate the effect of the loss of the original C skeleton of the molecule on C isotope signatures. (The model input files needed to run the model are explained in detail in **Section 7.1**)

In example Case 1, a model source zone was generating a PCE plume at 166 mg/L (1 mmol/L) in an anoxic (partially anaerobic) homogeneous aquifer with groundwater flowing at 65.8 ft/yr (20 meters per year) (**Figure 4-3**). The model illustrates changes in contaminant concentrations and isotope ratios as CEs are simultaneously transported and transformed over 500 m of plume length. Contaminant concentration and CSIA data have been generated with PHAST to simulate conventional anaerobic environments. *The site-management goal of the modeling effort is to determine if daughter products are degrading all the way to non-toxic end points.*

Figure 4-2 illustrates the simplified hydrogeological model setup and **Table 4-4** lists the input parameter values selected for the degradation and isotope fractionation processes. Input parameters are estimated for each constituent including kRD (per year), the degradation rate per year for the RD pathway only and εC (‰) the isotope enrichment factor for C for each transformation reaction. Values in **Table 4-4** represent average literature values. Data are entered into the PHREEQC model as described in **Section 7.1**.

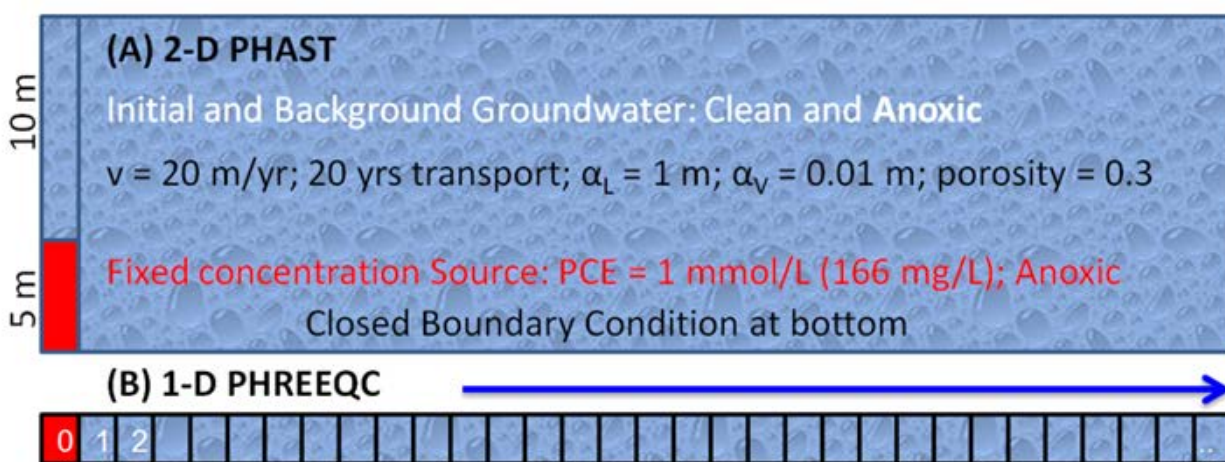


Figure 4-3. Model setup for complete dechlorination under anoxic conditions. The 2-D PHAST model was used to create an artificial dataset. PHREEQC was applied to simulate and interpret this artificial dataset.

Table 4-4. Parameter values selected for Case 1A, B

	PCE	TCE	DCE	VC	ETH
kRD (per year)	1.5	1	0.75	0.5	0*1 0.25*2
εC (‰)	-4	-12	-20	-25	-5
*1 Case 1A: ETH acts as stable end-product					
*2 Case 1B: ETH degrades slowly					

k_{RD} (per year) = degradation rate per year for RD pathway only εC (‰) – isotope enrichment factor for C

Case 1A: Modeling Complete Dechlorination of PCE to ETH using PHREEQC

Figure 4-4 presents the output of the PHAST model used to create a dataset for Case 1. The model predictions along the central flow path (at a depth of zero m) were used as artificial data for the 1-D PHREEQC model.

Figure 4-5 presents output from the PHREEQC 1-D model representing the classical concentrations and isotope patterns for complete dechlorination of PCE to ETH. **Figure 4-5(a)**

shows concentration vs time for the parent and daughter products. Panel (b) plots molar ratios (moles of each constituent normalized by total moles of all decay chain components) over distance. (Note in ‘conventional’ MNA approaches, the molar mass balance does not close). Panel (c) charts the enrichment of the heavy isotope ($\delta^{13}\text{C}$) over distance for each component. Calibration data shown as points on the graphs have been generated artificially to demonstrate how field data may be incorporated into the visualization.

The concentration–distance plot (b) shows the conventional sequential degradation of PCE to ETH via TCE, DCE, and VC. The C isotope ratio of the PCE parent compound (shown in panel c), steadily increases during degradation. The daughter products that are formed initially near the source show a depleted C isotope ratio as the heavy C atoms from PCE are transformed at a slightly slower rate relative to molecules with the light C isotopes. With distance away from the source zone, however, the $\delta^{13}\text{C}$ of the daughter products also steadily increases, and, at some point, attain the $\delta^{13}\text{C}$ of PCE in the original source zone. After complete dechlorination of all constituents, ETH will have the same C isotope ratio as PCE in the source.

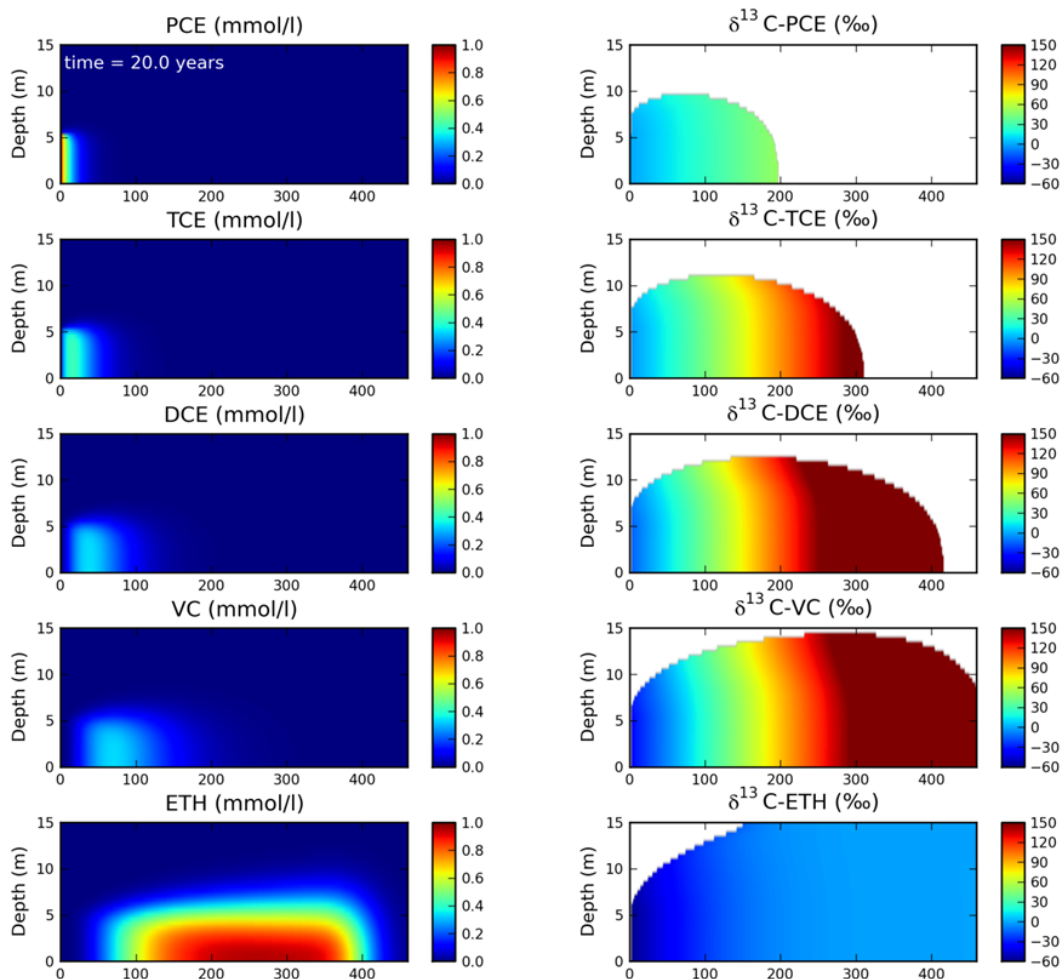


Figure 4-4. PHAST model 2-D cross-sectional simulation results of Case 1A: complete reductive dechlorination with ETH as stable reaction product. The simulation results along the central flow path in the core of the plume (at a reference depth of zero m) were used as artificial data for the 1-D PHREEQC model.

Whereas the extent of degradation of the parent compound, PCE, can be quantified with the Rayleigh equation, a RTM approach is required to quantify the extent of transformation of the daughter products as their isotope ratio is influenced by the combination of production and consumption reactions.

The isotope ratios – distance slopes of the different chlorinated ethenes vary and depend on the associated isotope fractionation factors and degradation rate constants. The behavior of ETH illustrates that an accumulating compound, *not further degraded or mineralized*, will never exceed the original source isotopic signature. At some distance away from the source, all daughter products exceed $\delta^{13}\text{C-PCE}_{\text{Source}}$, providing definite proof of their continuing transformation. *This can be considered as positive proof of the continuing degradation of daughter products -- a phenomenon that can be hard to demonstrate with just concentration or CSIA data alone. (See example Case 2 below).*

The 2-D PHAST model includes dilution by transverse and longitudinal dispersion, whereas the 1-D PHREEQC model only accounts for longitudinal dispersion which only results in dilution at the leading edge of the plume front. The 1-D PHREEQC model therefore cannot predict the decreasing concentrations in the spreading direction. However, 1-D PHREEQC predicts the molar ratios which do not depend on the degree of dilution.

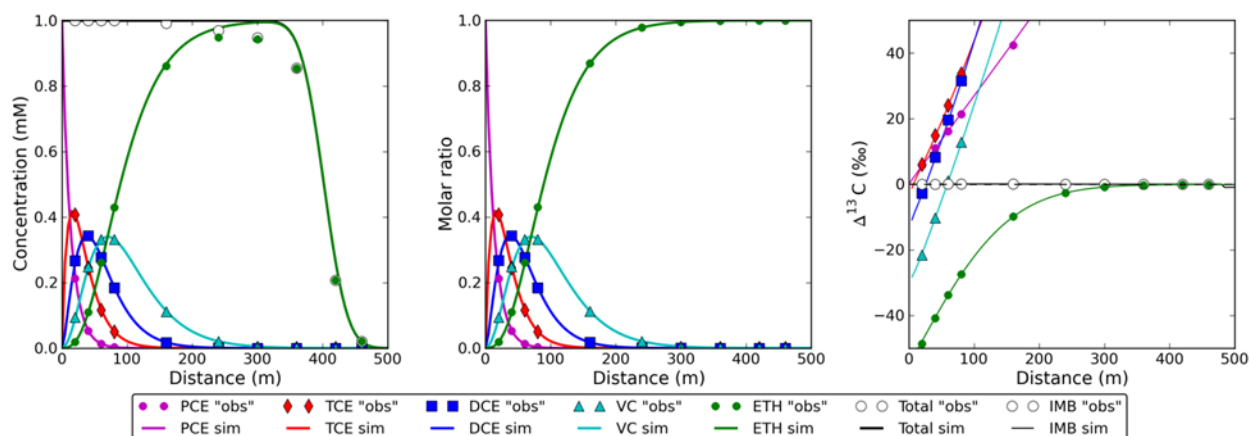


Figure 4-5. Model simulation results of Case 1A: complete reductive dechlorination with ETH as stable reaction product. Results are shown along the central flow path in the core of the plume. The “observations” (“obs”; symbols) were created with 2-D PHAST, the simulations (simulation (sim) lines) were done with 1-D PHREEQC. Panel ‘a’ shows concentration with distance, panel ‘b’ the molar ratio of parent and daughter products with distance and panel ‘c’ illustrates the change in C isotope ratio with distance. The horizontal line in panel ‘c’ is the isotope ratio of the source CE.

Figure 4-6 shows the effect of the longitudinal dispersion coefficient on simulation results. The αL taken for the 1-D PHREEQC simulation was five times higher than actual valid estimates (5 m versus 1 m), other model parameters were not changed. Concentrations become more dispersed: simulated concentration peaks become lower and downgradient tails become higher and longer. Hydrodynamic dispersion attenuates isotope signals (Abe, 2009; Van Breukelen, 2008; Van Breukelen, 2012). Predicted $\delta^{13}\text{C-PCE}$ is clearly lower than observed, especially downgradient. The same effect can be observed for TCE and DCE. However, $\delta^{13}\text{C}$ of these daughter products is overestimated near the source as a result of less enriched PCE. This second effect is particularly

clear for VC and ETH. The longitudinal dispersion coefficient is thus an important fitting parameter.

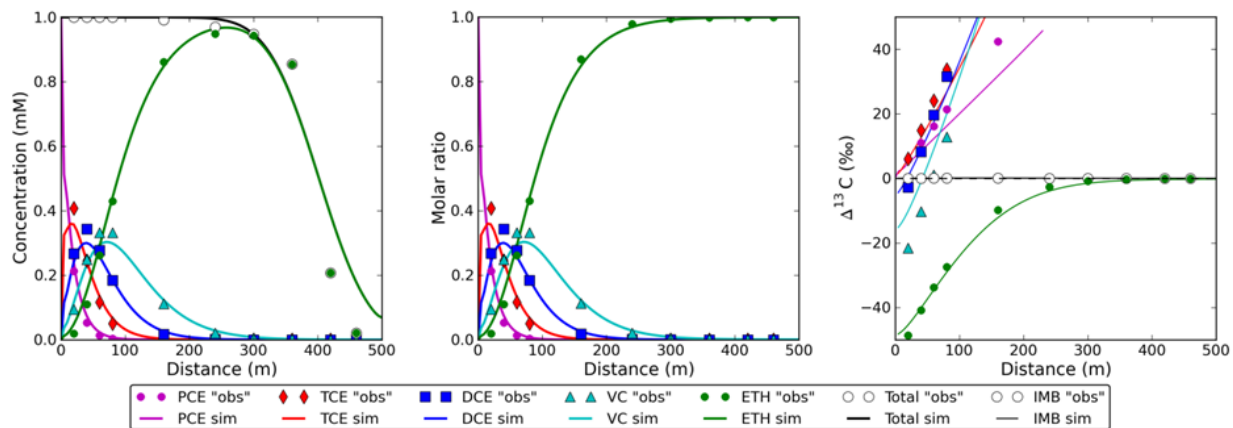


Figure 4-6. Model simulation results of Case 1A: complete reductive dechlorination with no ETH degradation. The model settings were the same as for **Figure 4-4** but the longitudinal dispersion coefficient was increased to 5 m. Because of large dispersion, the concentration data (left panel) shows a false degradation signal of ETH.

Case 1B: Confirming that Ethene is Degrading

For example Case 1B, a second simulation was generated where ETH continues to degrade as it is transported downgradient (**Figure 4-7**). In this section we compare the results of Case 1A with no ETH degradation and Case 1B where ETH is degrading slowly under anaerobic conditions. While ETH is not a regulated compound, it is the final organic degradation product of chlorinated solvent biodegradation, and its accurate simulation can help support demonstrations of complete mass destruction of the parent compound or, eventually, all daughter products.

In the model output results, the molar ratio patterns (**Figure 4-7 [b]**) look very similar to Case 1A without ETH degradation. Concentration data (a) show a strong decrease of ETH near the plume edge but this decrease may also be interpreted as a result of stronger dilution at the distal parts of the plume. Note Case 1A also showed decreases of ETH near the plume edge due to dilution. **Figure 4-6 (c)** provides conclusive evidence that ETH is degrading rather than attenuating by physical processes. The C isotope ratio for ETH increases and surpasses that of the source, indicating isotope enrichment due to further degradation of molecules containing the light isotopes.

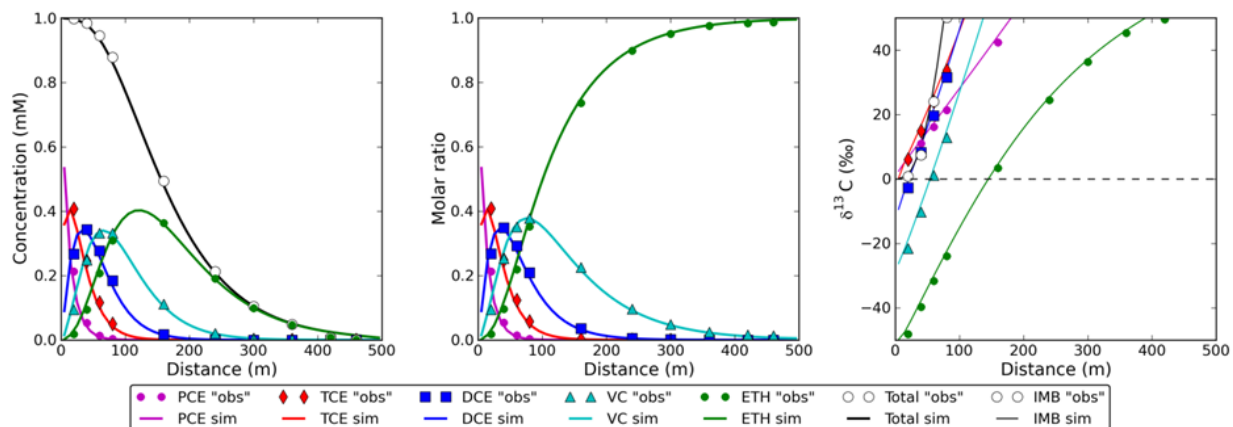


Figure 4-7. Model simulation results of Case 1B: complete reductive dechlorination but with further anaerobic degradation of ETH. Results are shown along the central flow path in the core of the plume. The isotope mass balance (IMB) is multiplied with a factor of 10.

Summary Case Study 1A, 1B

When comparing these two scenarios 1A and 1B (**Figures 4-5, 4-6 and 4-7**), it is clear that a concentration-based interpretation using only the leftmost panels (a) would have missed the occurrence of further ETH degradation.

ETH degradation can be assessed if C isotope ratios of ETH are measured and/or modeled. For scenario 1B, the C isotope ratio exceeds the source signature at around 150m from the source area. *When a supposed stable end product exceeds the source signature, this is strong evidence supporting further transformation of this daughter product.* The same applies if, for example, DCE or VC accumulates. Even stronger support for the occurrence of ETH transformation can be developed by calculating the C-IMB (see **Section 3.3**). **Figure 4-6** shows the C-IMB (panel c) exceeds the source signature relatively quickly at 2‰ around 50m downgradient from the source area. A 2‰ isotope shift is generally accepted as proof for occurrence of transformation (See **Section 3**).

Example of Incorrect Interpretation Without Key Isotope Data

Figure 4-8 presents the results of an RTM ignoring ETH degradation, fitted to concentrations and CSIA observations without $\delta^{13}\text{C}$ -ETH data. The model clearly fits the molar ratios and C isotope ratios of PCE-VC. Produced ETH approaches the source signature after full dechlorination but actual further ETH conversion goes unnoticed without having $\delta^{13}\text{C}$ -ETH observations. The model calibration was possible because the first-order degradation rate constants of DCE and VC were underestimated (DCE: 0.6/yr [actually 0.75/yr]; VC: 0.3/yr [actually 0.5/yr]) and the ϵ_{C} , VC was overestimated (-35 ‰ instead of -25 ‰). Since part of the ETH is degraded but undocumented, the molar ratios of the other CEs are overestimated and the molar ratio of ETH underestimated in the mass balance calculation. As a consequence, the rate constants are too conservative. To achieve a fit for the C isotope ratios of VC, ϵ_{C} will be set higher than is actually valid. The potential occurrence of ETH degradation thus results in conservative estimates of overall chlorinated ethene degradation.

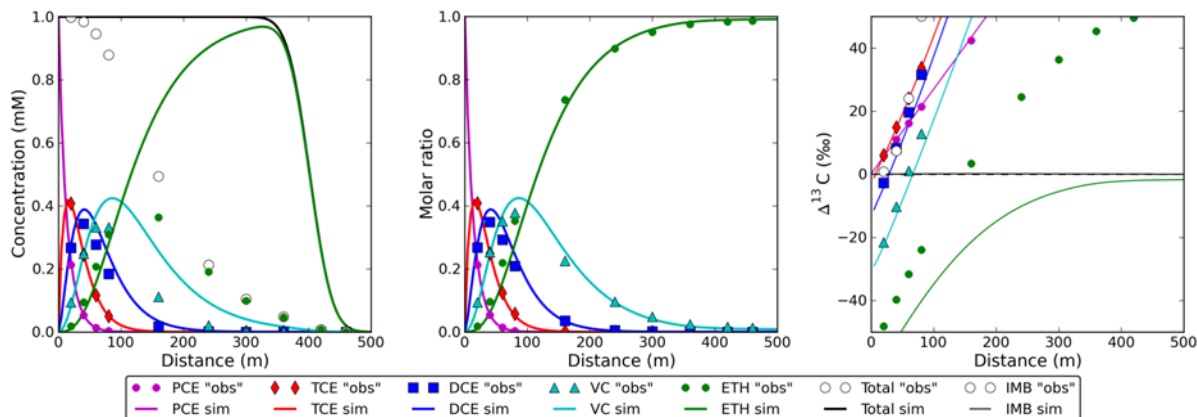


Figure 4-8. Results of Case 1B but calibrated to fit with a model disregarding ETH degradation and without the availability of $\delta^{13}\text{C}$ -ETH data.

4.2.2 Case 2: Stall of DCE/VC: Detection of Potential Oxidation

Reductive dechlorination of PCE or TCE often does not lead to complete conversion to ETH and CO_2 but rather to a ‘stall’ or apparent stall after DCE or VC formation. This can occur when geochemical conditions are not sufficiently anoxic and/or the relevant microorganisms are absent. However, apparently accumulating DCE or VC may also degrade slowly further via (an) aerobic oxidation. Such processes may be ongoing, but are difficult to detect and confirm as concentrations can decrease by physical processes such as dilution, and characteristic reaction products are not formed. The goal of example Case 2 is to illustrate how dual C-Cl CSIA can aid in detecting the occurrence of oxidative transformation, confirming that there is not a VC ‘stall’.

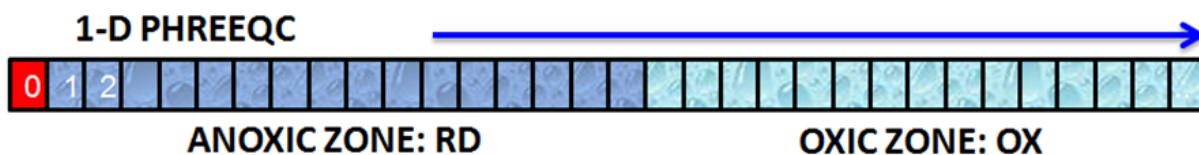


Figure 4-9. Model setup (1-D PHREEQC) for incomplete dechlorination under anoxic conditions (RD= reductive dechlorination) resulting in a stall of VC with potential an (aerobic) oxidation (OX) further downgradient.

Case 2 simulates a TCE plume flowing first through an anoxic zone (approximately 250 m) amenable to RD of TCE and DCE (but not of VC) followed by an aerobic zone where only slow oxidative VC transformation occurs (**Figure 4-9**). For simplicity this case was simulated by assigning two different sets of kinetic reactions to the spatially fixed anoxic and oxic zones, respectively.

The model requires preliminary estimates of the first order degradation rate constants for TCE and DCE for the RD pathway (k_{RD} [per year]), the bulk isotope enrichment factor for C (ϵ_C [‰]), enrichment factors for Cl for both primary KIE ($\epsilon_{Cl, KIE}$ [‰]) and SKIE ($\epsilon_{Cl, SKIE}$ [‰]), the first order degradation rate constant of VC for the OX pathway (k_{OX} [per year]), and the bulk isotope enrichment factor for Cl (ϵ_{Cl} [‰]). The input parameters of this example are shown in **Table 4-5**.

The technical details (including the software method) for example Case 2 are explained in **Section 7.2** and summarized below.

Table 4-5. Parameter values selected for Case 2

	TCE	DCE	VC
Anoxic Zone			
k_{RD} (per year)	1	0.5	0
ϵ_C (‰)	-16.7	-28.8	
$\epsilon_{Cl, KIE}$ (‰)	-4.2	-4.5	
$\epsilon_{Cl, SKIE}$ (‰)	-3.3	-1.7	
Oxic Zone			
K_{OX} (per year)	0	0	0.25
ϵ_C (‰)			-0.3
ϵ_{Cl} (‰)			-7.2

The results of the simulation are plotted in Figure 4-9 and show the accumulation of VC (**Figure 4-10 [a]** and **[b]**) until 300 m downgradient, consistent with RD of TCE and DCE forming VC. Farther downgradient, VC concentrations decrease, but, based on concentration data alone, it cannot be determined whether these concentration reductions are caused by transformation or by dilution.

The fact that the C isotope ratio of VC has started to exceed that of the source TCE (-30‰) at 300 m downgradient (**Figure 4.10 [c]**) is a definite indicator of further VC conversion, as a reaction product that accumulates without degrading cannot exceed the original source signature. Another powerful indicator of further degradation is the C-IMB (discussed in **Section 3.3.5**). The C-IMB (shown in **Figure 4-10 [c]**) by the black dashed line) shows that VC upgradient is highly depleted in heavy isotopes; however, at 300 m downgradient, $\delta^{13}C$ for VC equals the source isotope signature and then steadily increases through the aerobic zone, indicating mineralization of the VC molecules containing the lighter C isotopes. Since the reaction product of VC oxidation (inorganic carbon) is not part of the C-IMB, the C-IMB increases with continuing VC oxidation.

Similar as for C, the Cl isotope ratios are more depleted in the order TCE to VC at any distance. Secondary KIEs cause this stepwise pattern. If SKIEs were zero, the initial Cl isotope ratios of the various CEs would be identical because the Cl atoms that end up in the lower chlorinated ethenes have not reacted and thus have not experienced isotope fractionation (Hunkeler, van Breukelen, and Elsner 2009). Note the Cl-IMB is not a useful indicator as during RD of CEs it will gradually increase since the chloride ion that splits off is depleted but not part of the Cl-IMB. The change in Cl-C CSIA slope (**Figure 4-10 [e]**) downgradient indicates a change in dominant transformation process: from VC generation by RD (steep slope) to VC oxidative transformation (gentle slope; related to low ϵ_{Cl} of VC oxidation; **Table 4-5**).

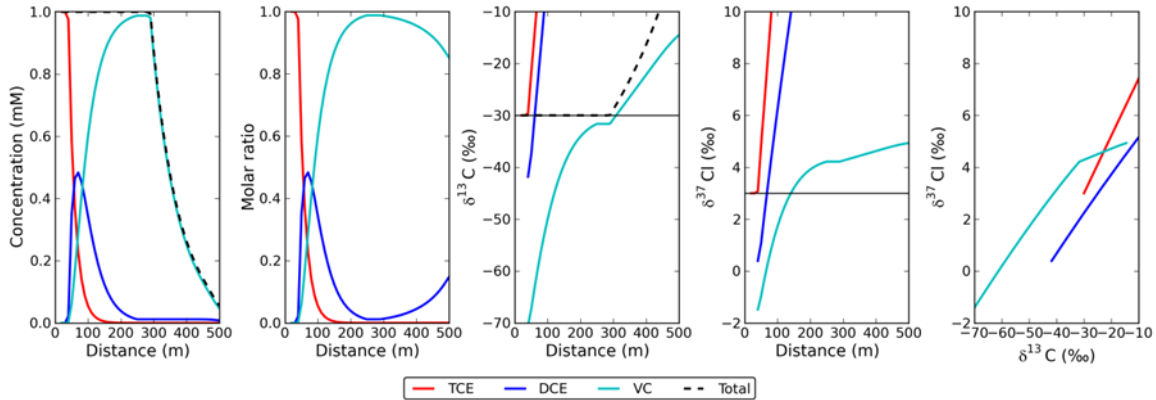


Figure 4-10. Case 2: Model results simulating slow VC oxidation downgradient of a reductive dechlorination zone with a VC ‘stall’. Shown are the simulated concentrations (a), molar ratios (b), C (c) and Cl (d) isotope ratios versus distance and a 2-D plot of C to Cl isotope ratios (e).

4.2.3 Case 3: 2-D Simulation of Reductive Dechlorination in Core and Oxidation at Fringe

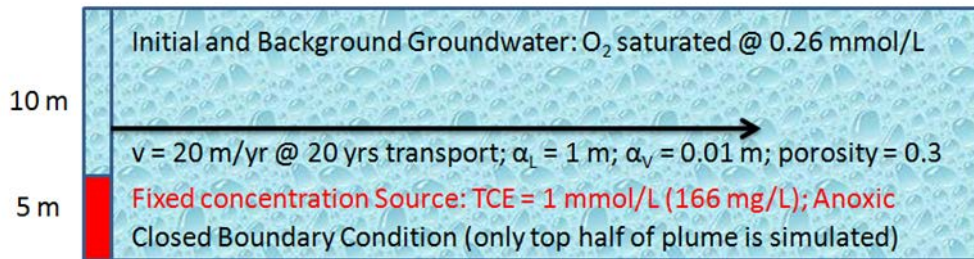


Figure 4-11. Case 3: Model setup for reductive dechlorination of TCE to ETH under anoxic conditions in the core of the plume together with oxidative transformation of VC at the fringe of the plume under aerobic conditions.

Table 4-6. Parameter values selected for Case 3

	TCE	DCE	VC
k_{RD} (per year)	1	0.5	0.25
ϵ_C (‰)	-12	-20	-25
ϵ_{Cl} (‰)	-3	-2	-2
k_{OX} (per year)	-	-	2
ϵ_C (‰)	-	-	-7.2
ϵ_{Cl} (‰)	-	-	-0.3

k_{RD} (per year) = degradation rate per year for RD pathway; k_{OX} (per year) = degradation rate per year for oxidative transformation pathway; ϵ_C (‰) – isotope enrichment factor for C; ϵ_{Cl} (‰) – isotope enrichment factor for Cl

For example Case 3, a 2-D PHREEQC-based model is used (PHAST and PHT3D) to simulate concentrations, molar ratios, and C and Cl isotope ratios for complete dechlorination of TCE to ETH together with oxidative transformation of VC at the plume fringe. Both PHAST and PHT3D were applied in 2-D and compared in performance. The goal was to illustrate that the developed model is able to simulate complex situations (core and fringe degradation) in 2-D and should, therefore, be applicable as PHT3D in actual complex groundwater solute transport models setup with the widely used MODFLOW-MT3DMS codes. The model input files needed to run the model are explained in detail in **Section 7.3**. The developed model can simulate complete dechlorination

of PCE to ETH together with oxidative transformation of DCE and VC under aerobic conditions. However, because the number of solutes which can be simultaneously simulated with the PHT3D graphical user interface (GUI) PMWIN was limited to 60, the PCE to TCE RD step and DCE oxidation step were discarded. The complete model worked without problems in PHAST (results not shown).

In example Case 3, a model source zone was generating a TCE plume at 166 mg/L (1 mmol/L) in an oxic homogeneous aquifer with groundwater flowing at 65.8 ft/yr (20 meters per year) (**Figure 4-3**). The model illustrates changes in contaminant concentrations and isotope ratios as CEs are simultaneously transported and transformed over 500 m of plume length (only first 300 m depicted). Contaminant concentration and C and C1 CSIA data have been generated with PHAST and PHT3D to simulate a special case of an anoxic plume flowing through an aerobic aquifer. *The site-management goal of the modeling effort is to evaluate how CSIA patterns can aid in detecting oxidative transformation for such cases.*

Figure 4-11 illustrates the hydrogeological model setup and **Table 4-6** shows the input parameter values selected for the degradation and isotope fractionation processes. Input parameters are estimated for each constituent including k_{RD} (per year), the degradation rate per year for the RD pathway only, k_{OX} (per year), the degradation rate per year for the OX pathway, ϵ_C (‰) the isotope enrichment factor for C for each transformation reaction, and ϵ_{Cl} (‰) the isotope enrichment factor for Cl for each transformation reaction. Occurrence of SKIEs was not assumed. Values in **Table 4-6** represent literature values (See **Appendix B**). Data are entered into the model as described in **Section 7.3**.

Figures 4-12 and **4-13** presents output from the PHAST and PHT3D models, respectively, applied in cross-sectional 2-D mode. The model output shows (i) concentration peaks increasingly downgradient in the order TCE to ETH; (ii) relatively high levels of TCE and DCE in the top fringe area where reductive dechlorination is impeded by elevated oxygen concentrations; (iii) correspondingly the C isotope ratios of TCE and DCE increase downgradient but decrease upwards due to increasing inhibition of RD by oxygen; and (iv) in contrast for VC an enrichment is noticeable in the diluted top parts of the fringe where its oxidative transformation is promoted by higher oxygen levels.

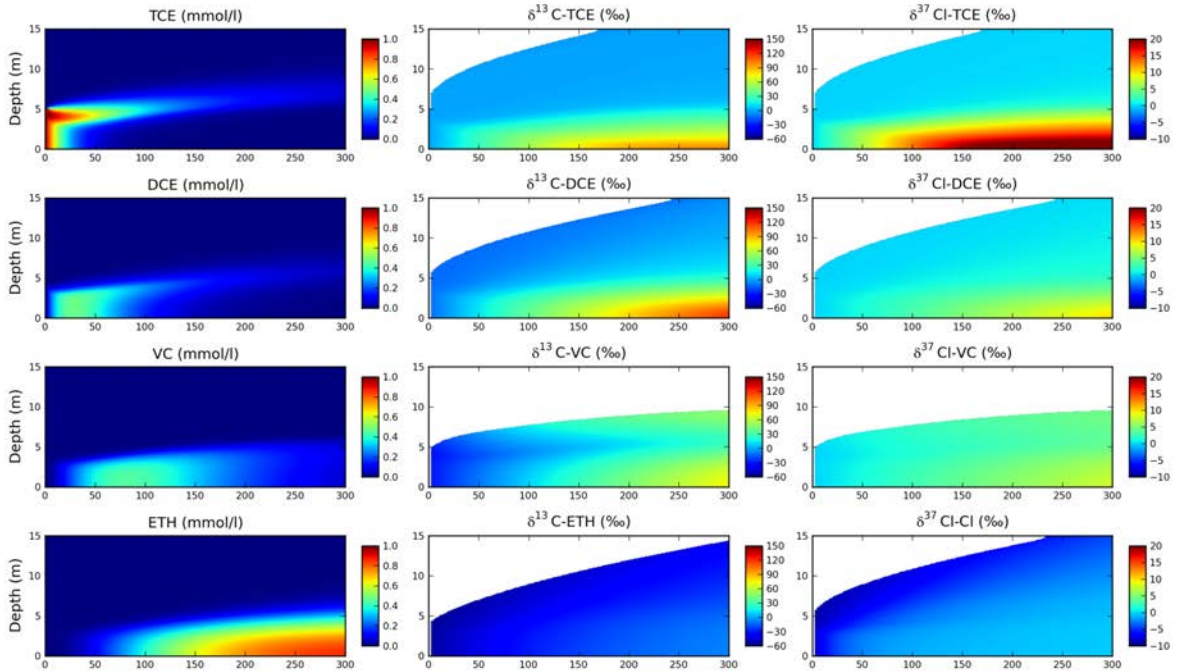


Figure 4-12. Results of 2-D PHAST simulation for C and Cl isotope fractionation following reductive dechlorination (TCE to ETH) in the core of the plume and aerobic oxidation of VC at the fringe.

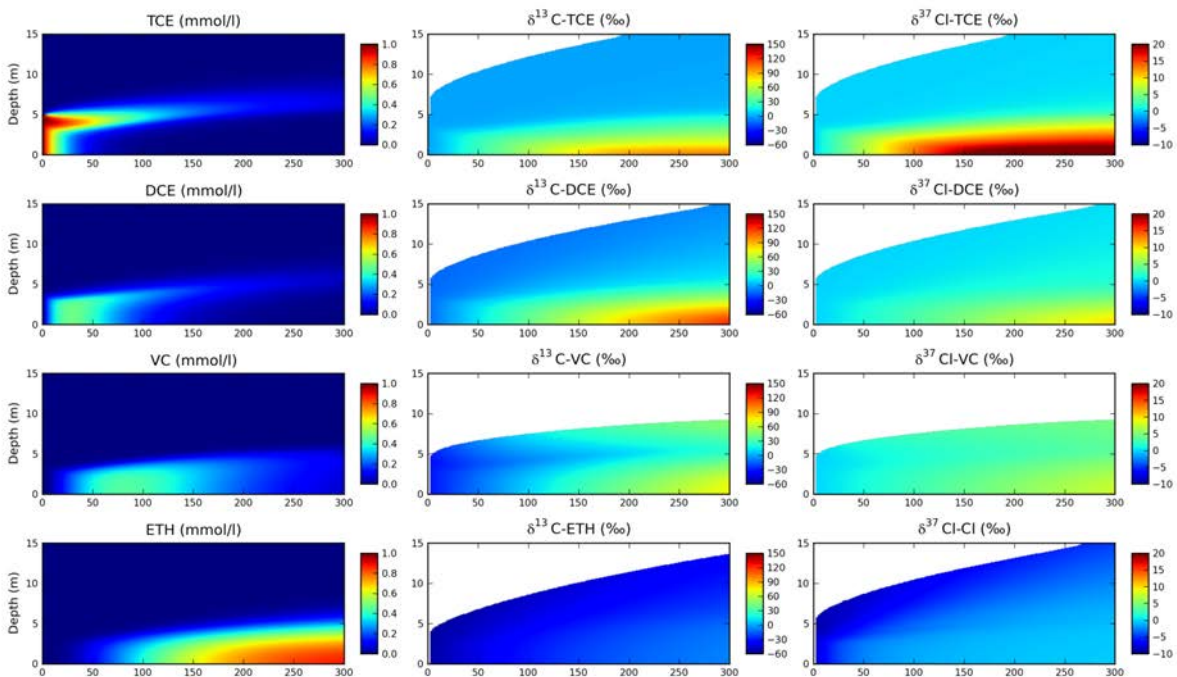


Figure 4-13. Results of 2-D PHT3D simulation for C-Cl isotope fractionation following reductive dechlorination (TCE to ETH) in the core of the plume and aerobic oxidation of VC at the fringe.

The spatial and temporal discretization was equal for both the PHAST and PHT3D model: 0.1 m and 2.0 m spatial resolution (node spacing) in vertical and horizontal direction, respectively, and a time step of 0.1 year. PHT3D has a better solver (TVD) than PHAST to simulate transverse dispersion accurately. Indeed numerical dispersion seems a bit larger in the PHAST model as the fringe in the PHT3D model seems slightly sharper. However, the small differences are probably not relevant in practical applications.

4.2.4 Case 4: Hydrogen Isotope Fractionation During Reductive Dechlorination of PCE/TCE

For example Case 4, a 1-D PHREEQC model is used to simulate concentrations and H isotope ratios during complete reductive dechlorination of TCE, PCE, or a mixed PCE/TCE source. The summed concentration of PCE and TCE in the source was 1 mmol/L in all three simulations. The groundwater flow velocity was 20 m per year. The model illustrates changes in contaminant concentrations and H isotope ratios as CEs are simultaneously transported and transformed over 300 m of plume length.

The hydrogeological setup is identical to the one of Case 1 (**Figure 4-3**). **Table 4-7** shows the input parameter values selected for the degradation and H isotope fractionation processes. Input parameters are estimated for each constituent including k_{RD} (per year), the degradation rate per year for the RD pathway only, $\epsilon H_{bulk\ SKIEs}$ (‰) the H bulk isotope enrichment factor of H atoms transferred to the corresponding daughter product, and $\epsilon H_{protonation}$ the overall H isotopic enrichment factor expressed with respect to δ^2H_{water} during protonation for each transformation reaction. Values in **Table 4-7** represent values obtained through model validation to the microcosm experimental data on complete reductive dechlorination of TCE as conducted as part of this ESTCP project (see Final Report ESTCP Project ER-201029). Only the value of $\epsilon H_{protonation}$ was not known for the PCE to TCE step and was taken equal to the TCE to DCE step. δ^2H-H_2O was taken as -42‰, δ^2H-TCE was taken as +500‰, within the range (+467‰ to +682‰) of published values for manufactured TCE (Shouakar-Stash et al., 2003). δ^2H-H_2O is not a very sensitive model parameter as the $\epsilon H_{protonation}$ values are large. If not available at a site, an estimate for δ^2H-H_2O can be obtained from global or regional maps on the isotopic composition of precipitation. Data are entered into the PHREEQC model as described in **Section 7.4**.

Table 4-7. Parameter values selected for Case 4

	PCE	TCE	DCE	VC	ETH
k_{RD} (per year)	1.5	1	0.5	0.5	0
$\epsilon H_{bulk\ SKIEs}$ (‰)	na	+34	0	0	na
$\epsilon H_{protonation}$ (‰)	-170	-170	-580	-740	na
na = not applicable					

k_{RD} (per year) = degradation rate per year for RD pathway only; $\epsilon H_{bulk\ SKIEs}$ (‰) – hydrogen bulk isotope enrichment factor (SKIEs) of hydrogen atoms transferred to daughter product; $\epsilon H_{protonation}$ overall hydrogen isotopic enrichment factor expressed with respect to δ^2H_{water} during protonation. See **Section 5.4.5** for an explanation of simulation of hydrogen isotope fractionation.

Figure 4-13 presents output from the PHREEQC 1-D model representing concentrations and H isotope patterns for complete dechlorination of TCE to ETH along the simulated flow path. The parent compound TCE becomes depleted in δ^2H during reductive dechlorination due to the inverse isotope fractionation observed for this reaction step (Kuder and Philip, 2013). Daughter products are increasingly depleted the less they are chlorinated. During protonation strongly depleted hydrogen atoms replace the C1 atoms resulting in strong depletion of the final metabolite, ETH.

Figure 4-15 shows model results if PCE instead of TCE is taken as source compound. Note PCE does not contain H atoms and consequently H isotope ratios are not shown for PCE. In this case, strongly depleted $\delta^2\text{H}$ -TCE is produced, about 700‰ more depleted than source PCE of the previous simulation (**Figure 4-13**). Correspondingly, the other daughter products are also considerably more depleted than in the TCE as parent compound scenario. In this scenario $\delta^2\text{H}$ -DCE exceeds $\delta^2\text{H}$ -TCE because of (i) the inverse H isotope fractionation effect during the TCE to DCE step; and (ii) the isotope fractionation effects associated with protonation are assumed similar for both the PCE to TCE and the TCE to DCE steps. As a result, both H atoms added during protonation in the sequential steps PCE to TCE are equally depleted and their $\delta^2\text{H}$ will, on average, increase in the TCE to DCE step related to the inverse fractionation effect. It might be that the fractionation factor related to protonation is in fact different and probably smaller than assumed for the PCE to TCE step. In that case, $\delta^2\text{H}$ -DCE and $\delta^2\text{H}$ -TCE will be more similar along the flow path.

Concluding, provided source TCE is strongly enriched, H isotope analysis could be useful to distinct among source TCE and TCE produced through PCE reductive dechlorination. Besides $\delta^2\text{H}$ -TCE, also $\delta^2\text{H}$ of lower chlorinated daughter products could be informative about their source compound (PCE or TCE) as their $\delta^2\text{H}$ is strongly different between the two scenarios.

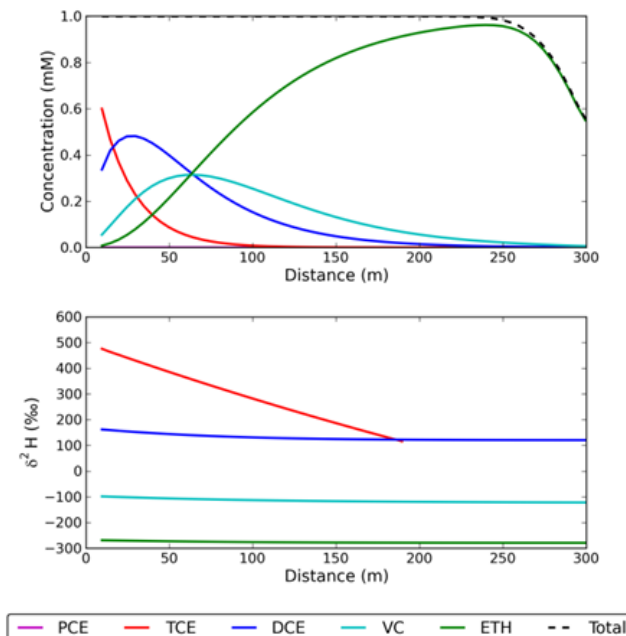


Figure 4-14. Results of 1-D PHREEQC flow path simulation on hydrogen isotope fractionation during complete reductive dechlorination of TCE.

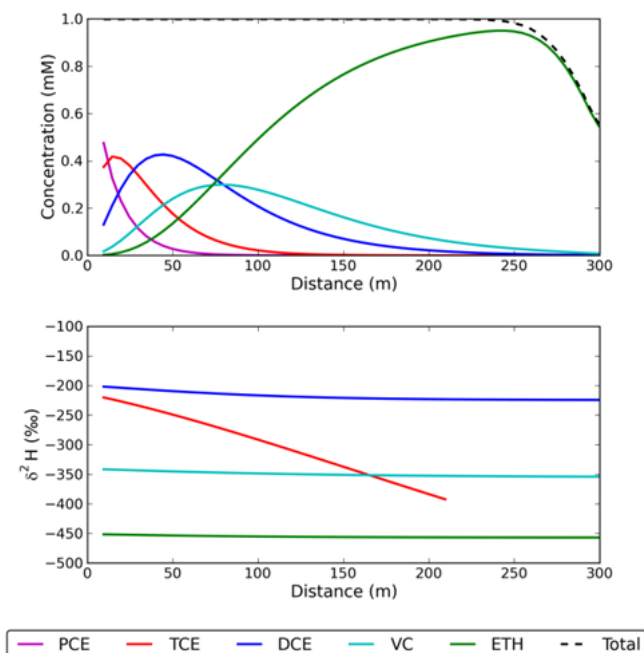


Figure 4-15. Results of 1-D PHREEQC flow path simulation for H isotope fractionation during complete reductive dechlorination of PCE.

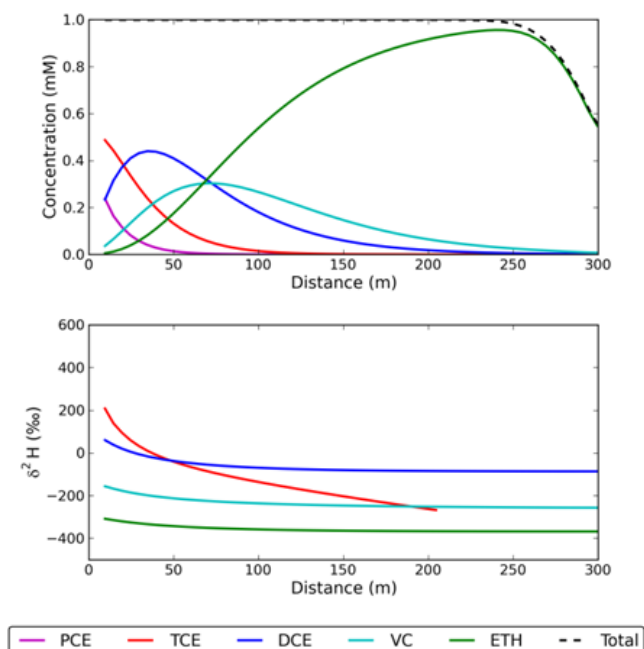


Figure 4-16. Results of 1-D PHREEQC flow path simulation for H isotope fractionation during complete reductive dechlorination of a mixed 1:1 molar ratio PCE/TCE source.

Finally, **Figure 4-16** shows the simulation results of a mixed PCE/TCE source (1:1 molar ratio). PCE reductive dechlorination produces strongly depleted $\delta^2\text{H}$ -TCE which mixes with the pool of strongly enriched source TCE. As a result $\delta^2\text{H}$ -TCE values intermediate between the first two scenarios are produced.

In application of the template model of Case 4 to actual field site data, it is warranted that very little is known about hydrogen isotope fractionation effects during transformation of CEs especially at field sites.

OVERVIEW MANUAL

5.0 CSIA WITH RTM: OVERALL MODELING APPROACH

5.1 Software and System Requirements

Key models and programming languages developed or used for the SIRTM approach include:

- **PHREEQC** – A one dimensional (1D) geochemical transport model developed by the U.S. Geological Survey (USGS) that can also simulate irreversible kinetic reactions such as the degradation of CEs. PHREEQC can be used to simulate advection, longitudinal dispersion, and to model kinetic reactions with user-supplied rate expressions. The software is free and can be downloaded along with documentation at http://wwwbrr.cr.usgs.gov/projects/GWC_coupled/PHREEQC/ (USGS web page; PHREEQC 3 version) or at <http://pfw.antipodes.nl/download.html> (PHREEQC 2 for Windows version). All work for this project was done with the latter PHREEQC for Windows program but the models run as well with PHREEQC 3.
- **PHAST** – A three dimensional (3-D) groundwater flow and transport model capable of simulating the same set of reactions as PHREEQC. PHAST couples PHREEQC to the groundwater flow and solute transport model HST3D. PHAST is a practical platform to run 2-D simulations of plume cross-sections or even fully 3-D simulations. A freely available graphical user interface (GUI) is available. For simple conceptual models a GUI is however not needed. PHAST models are very simple to develop once the user understands the 1-D PHREEQC version of the model. PHAST can be downloaded at http://wwwbrr.cr.usgs.gov/projects/GWC_coupled/phast/
- **PHT3D** – A three dimensional (3D) groundwater flow and transport model capable of simulating the same set of reactions as PHREEQC. PHT3D couples PHREEQC to the groundwater flow model MODFLOW and the solute transport model MT3DMS. PHT3D is mostly practical to run 2-D simulations of plume cross-sections or even fully 3-D simulations. The potential advantage of PHT3D with respect to PHAST is the option to simulate isotopologue diffusion which is not possible with PHAST. Diffusion-induced isotope fractionation might be relevant at the upper/lower fringes of pollution plumes. PHT3D can be downloaded at <http://www.pht3d.org>. However, to run PHT3D a commercial GUI is practically required which is a disadvantage compared to PHAST if the goal is to make a simple model. PHT3D takes more time to setup than PHAST. A large advantage of PHT3D is that the model is part of some commercially available GUIs like Visual Modflow or Processing Modflow (PMWIN; <http://www.simcore.com/>), which, in principle implies endless possibilities to simulate contaminant transport including isotope fractionation.
- **Python** – A general purpose scripting language designed to be highly readable and easy to use. For viewing model results of the template files, Python scripts have been developed for this project and are available for download from the project website (see below). Python is a free alternative for MATLAB and enables plotting of graphs and 2-D contour plots in a programming environment. Alternatively, plots can be made with PHREEQC for Windows or with Microsoft (MS) Excel. Python implementations can be downloaded for free as open-source softwares which run in a variety of Windows, Macintosh or Linux environments. Python can be downloaded at <http://code.google.com/p/pythonxy/>.

The software applications listed above run on any windows PC (windows XP, 7, 8). All software is freely available from the internet (URLs shown above). **Section 6** gives detailed download and installation instructions for the softwares.

Programs, example input files and software tools developed for this project are available for download from the project website (under construction http://www.gsi-net.com/en/software/free-software/CSIA_RTM.html).

5.2 User Qualification and Training Recommendation

Users should have a basic level of training in groundwater flow modeling, solute transport modeling, and programming. The level reached after completion of a commercial training course in these skills should be sufficient. Specific PHREEQC experience is not required but recommended.

5.3 Aims and Overview of Models Developed

At the start of this ESTCP project the state of isotope fractionation reactive transport modeling was as follows:

- A 1-D PHREEQC model simulating C isotope fractionation during sequential RD of CEs was developed by Van Breukelen et al. (2005) and validated to a microcosm experiment.
- A 1-D PHREEQC model simulating Cl isotope fractionation during sequential RD of CEs was developed by Hunkeler et al. (2009). The model was not yet validated to experimental data and did not account for potential secondary kinetic isotope effects (SKIEs).
- 3-D PHT3D models (PHREEQC coupled to MODFLOW-MT3DMS) were developed for 2-D simulations of C isotope fractionation of aromatic hydrocarbons (Prommer et al., 2009; Van Breukelen and Prommer, 2008).

The goal of this project was to continue this model development with the following aims:

- Development of a PHREEQC model simulating H isotope fractionation during sequential RD of CEs.
- Validation of both the Cl and H models to experimental data of reductive dechlorination of TCE to ethene.
- Development of 3-D PHT3D and 3-D PHAST (PHREEQC coupled to HST3D) models to simulate C and Cl isotope fractionation during both RD and oxidative transformation of DCE and VC at fringes of plumes.

Two main models were developed for this project (see **Table 5-1**). First, the ‘Plume’ model was developed that simulates C and Cl isotope fractionation during sequential RD of PCE to ETH and during oxidation of DCE and VC. The model was implemented in PHAST and partially in PHT3D as the number of solutes was limited in the applied PHT3D GUI PMWIN such that only TCE to ETH could be simulated for both C and Cl. Secondary KIEs related to Cl isotope fractionation were not simulated as these were not known to be relevant at the time. C isotope fractionation was simulated with the isotopologue method to optionally account for potential isotope diffusion effects. Isotopologue-dependent diffusion can be simulated with PHT3D but not with PHAST. The model assumed first-order kinetics with respect to CE concentration and was extended with Monod terms to describe either oxygen inhibition of RD or oxygen dependent DCE and VC oxidation.

Second, the ‘Microcosm’ model was developed to simulate the microcosm experiment performed as part of this ESTCP project (Kuder van Breukelen, et al., 2013). This model simulates TCE to ETH sequential RD and C/Cl/H isotope fractionation. The model is implemented in PHREEQC and application in 3-D PHAST is, thus, straightforward. The model applied the C isotope method (see **Section 5.4.3**) as diffusion effects are not relevant in a microcosm. However, it is a simple procedure to apply the C isotopologue method instead. The model also simulated secondary KIEs related with Cl isotope fractionation as this was observed in the experiment. The model was extended with oxidative transformation of VC together with C and Cl isotope fractionation (see **Section 4.2.2**). The model simulates concentration-dependent Monod kinetics and optional lag phases for reactions to occur as this appeared needed. The model does not accommodate oxygen dependent inhibition/promotion of RD/oxidation, respectively. However, oxidation of VC was added in Case 2 (see **Section 4.2.2** above) and degradation processes can be simulated for specific and fixed model domains. Note the models are not cast in stone and can be adjusted by an experienced user for specific needs and model parts can be exchanged.

Table 5-1. Principle differences between the First ‘Plume’ and Second ‘Microcosm’ Model

	First (Initial) ‘Plume’ Model	Second ‘Microcosm’ Validation Model
Codes	1-D PHREEQC, 3-D PHAST, 3-D PHT3D	1-D PHREEQC
Prime Goal	Theoretical simulation of C-Cl isotope patterns of pollution plumes in groundwater	Simulation of microcosm experiment and model validation
Calibrated	-	Microcosm study
Reductive Dechlorination (RD)	PCE to ETH	TCE to ETH
Oxidation (OX)	DCE, VC	VC (Case 2).
Kinetics	First-order versus CE concentration together with an oxygen-dependent Monod term (inhibition of RD, promotion of OX)	Monod kinetics versus CE concentration; lag phases
Aerobic/Anaerobic Zones	Spatially/Temporarily Dynamic	Spatially Fixed
Carbon Isotope Fractionation	Yes, isotopologue model	Yes, isotope model
Chlorine Isotope Fractionation	Yes, but only KIEs (bulk enrichment factors as input), not SKIEs	Yes, KIEs & SKIEs
Hydrogen Isotope Fractionation	-	Yes

5.4 Model Reaction Network and Equations

This section explains the isotope/isotopologue reaction networks and the mathematical equations to simulate C, Cl and H isotope fractionation, as performed for this project. At the end of the section it is also explained how initial isotope/isotopologue concentrations are calculated and how isotope ratios are calculated based on absolute concentrations of isotopes/isotopologues.

5.4.1 Reaction Kinetics

Figure 5-1 presents the general reaction network of the models developed. The available template files (introduced in **Section 4.2** and expanded in **Section 7**) present minor variations to the overall reaction network. Note the models simulate the concentrations of CEs and ETH by simulating their isotopes/isotopologues. The sum of the isotopes/isotopologues concentrations gives the compound

concentration. Each isotope pair (C, H, Cl) is simulated with a different and independent reaction network. The degradation rate of a parent compound is equal to the production rate of the associated daughter product (only the sign is opposite).

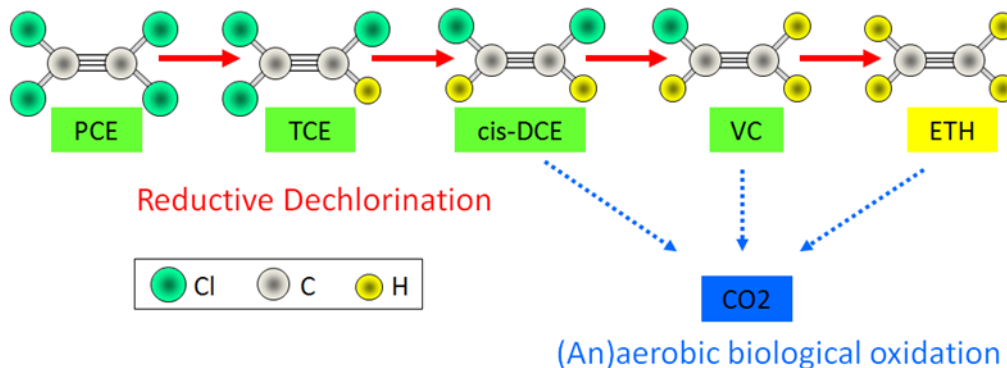


Figure 5-1. General reaction network simulated: RD of PCE to ETH, and optional oxidative transformation (OX) of cDCE, VC, or ETH.

First (Initial) 'Plume' Model

This model assumes first-order degradation. The anaerobic (i.e., RD) rate, r_{anoxic} [M L⁻³ T⁻¹], is inhibited in the presence of oxygen with a Monod inhibition term (**Equation 5-1**). The aerobic rate, r_{oxic} [M L⁻³ T⁻¹], is multiplied with a Monod term for oxygen availability (**Equation 5-2**).

$$-r_{\text{anoxic}} = -k_{\text{anoxic}} \cdot [C_m] \cdot \frac{K_I}{K_I + [C_{O_2}]} \quad (5-1)$$

$$-r_{\text{oxic}} = -k_{\text{oxic}} \cdot [C_m] \cdot \frac{[C_{O_2}]}{[C_{O_2}] + K_{O_2}} \quad (5-2)$$

Where k_{anoxic} [T⁻¹] is the rate constant for RD, k_{oxic} [T⁻¹] is the rate constant for oxidative transformation, C_m [M L⁻³] is the concentration of the degradable organic contaminant which is the sum of all isotopologues (or isotopes) of the considered element, C_{O_2} [M L⁻³] is the oxygen concentration, K_I is the inhibition constant for oxygen [M L⁻³], and K_{O_2} is the half-saturation constant for oxygen [M L⁻³]. The values for K_I and K_{O_2} are fixed in the database file (download file ESTCP_CSIA.dat in Case 1 folder) but can, in principle, be modified via a search and replace action.

The degradation rate of a parent compound is explicitly simulated and is equal to the production rate of its daughter product. However, the sign (+/-) is opposite (negative for degradation, positive for production). Only degradation rates are explicitly simulated but as these rates are multiplied by the stoichiometrical numbers of the reactions (e.g., box 7.2B), the production rates are inherently simulated.

Second 'Microcosm' Model

The Monod kinetic equation (**Equation 5-3**) was applied without growth for all reactions:

$$Rate_m = -V_{max} \times \left(\frac{C_m}{K_s + C_m} \right) \quad (5-3)$$

Where $Rate_m$ is the reaction rate of molecule m ($-Rate_m$ is production rate of its daughter product), V_{max} is the maximum degradation rate constant [$M L^{-3} T^{-1}$], C_m is the concentration of the molecule [$M L^{-3}$], and K_s is the half saturation constant [$M L^{-3}$]. Individual lag periods, i.e., the period before which the reaction in question did not occur [T], were used for all reactions.

Monod kinetics is typically observed in microcosm studies and also at field sites if concentration levels are high. However, under most field conditions with low contaminant concentration levels, a first-order kinetic model usually applies. **Equation 5-3** can be applied in such a way that first-order kinetics is simulated as explained in the following. The approach is to set the half-saturation constants much larger than the concentration ranges (i.e., $K_s \gg [C_m]$) and then select the V_{max} as follows: $k_1 \approx V_{max}/K_s$, where k_1 is the first-order rate constant. For example, K_s values of 1 (M) could be taken to establish first-order rate constants of 1 and 0.5 per year, for TCE and DCE, respectively, if V_{max} values of 1 and 0.5 M per year, respectively, are adopted. This approach is applied for example scenario Case 2.

5.4.2 Definitions of Isotope Effects

Different expressions are available to describe isotope effects and are widely used in this report and the model input files. These definitions are explained in this section with examples.

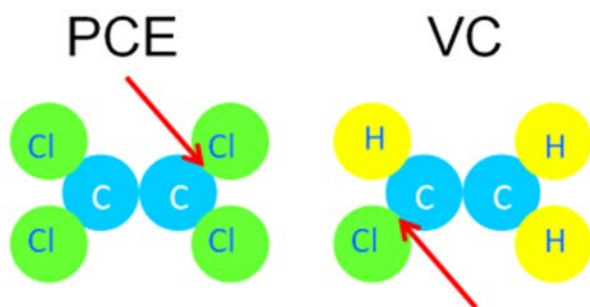


Figure 5-2. Isotope effects at PCE and VC.

Figure 5-2 shows a PCE molecule where a C-Cl bond is broken (red arrow). With respect to C isotope effects, a KIE is expressed at the C atom of the C-Cl bond. As isotope fractionation does not occur at the other C atom, the average or bulk isotope effect as observed by CSIA is a factor 2 smaller than the KIE_C. In other words: $\epsilon_{CKIE} \approx \epsilon_{C_{bulk}} \times 2$. With respect to Cl isotope effects, a KIE is expressed at the Cl atom of the C-Cl bond. As isotope fractionation does not occur at the other 3 Cl atoms (neglecting potential secondary KIEs), the average or bulk isotope effect as observed by CSIA is a factor 4 smaller than the KIE_{Cl}. In other words: $\epsilon_{ClKIE} \approx \epsilon_{Cl_{bulk}} \times 4$. In the case of VC and for Cl, a C-Cl bond is broken with a KIE_{Cl}. As other Cl atoms are not present, the KIE_{Cl} is not 'diluted'. Therefore, $\epsilon_{ClKIE} \approx \epsilon_{Cl_{bulk}}$. The table below explains the various measures of isotope effects with numerical examples.

Table 5-2. Measures of isotope fractionation illustrated with the example of C isotope fractionation during RD of a CE.

Measure of isotope fractionation	Name	Definition	Example value
α (bulk)	Kinetic isotope fractionation factor	as observed by CSIA for the entire molecule	0.9945
ϵ (bulk; ‰)	Kinetic isotope enrichment factor	$\epsilon = (\alpha - 1) \times 1000$	-5.5‰
ϵ KIE (‰)	KIE expressed as ϵ at the reactive position	ϵ KIE $\approx \epsilon$ bulk $\times (n/x)$ a	-11‰
α KIE	KIE expressed as α at the reactive position	α KIE = ϵ KIE + 1	0.9890
KIE	Kinetic Isotope Effect	Lk/Hk = $1/\alpha$ KIE	1.011
a n is number of atoms of the element (carbon) = 2; of which x are located at the reactive site = 1			

5.4.3 Simulation of Carbon Isotope Fractionation

C isotope fractionation can be simulated in two ways: with the (bulk) isotope model or the C isotopologue model as explained in the following. The C isotopologue model is only needed if diffusion-induced isotope fractionation effects are expected to be relevant, for example, at the top fringes of contaminant plumes. In order to simulate diffusion all isotopologues need to be simulated explicitly. If diffusion is not relevant, both models can be applied and give equal outcomes. The first ‘Plume’ model applied the C isotopologue model to enable simulation of diffusion effects in 2-D simulations of cross-sections (results not shown), whereas the second ‘microcosm’ model applied the (bulk) C isotope model (Van Breukelen, 2005).

The Carbon Isotope Model

Figure 5-3 illustrates the concept of the C isotope model. For each compound, a light and heavy C isotope species is defined representing the absolute concentration in the compound of the light and heavy C isotope, respectively.

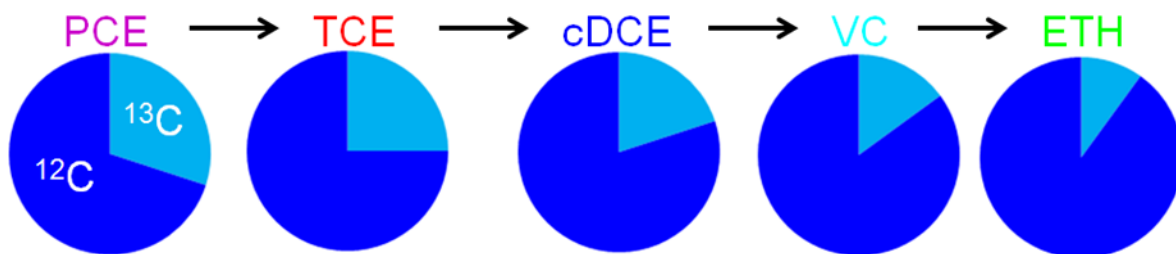


Figure 5-3. The C (bulk) isotope model for RD of PCE to ETH.

The initial concentration of each isotope species is calculated from the isotope ratio and the compound's concentration (see **Section 5.4.6** for a description of the spreadsheet tool to perform this calculation). Reaction rates are calculated as follows:

$$Rate_L = Rate_m \cdot \left(\frac{C_L}{C_m} \right) \quad (5-4)$$

$$Rate_H = Rate_m \cdot \left(\frac{C_H}{C_m} \right) \cdot [\varepsilon_{(bulk)} - 1] \quad (5-5)$$

Where $Rate_L$ and $Rate_H$ are the rates of the light and heavy C isotopes, respectively [$M L^{-3} T^{-1}$], $Rate_m$ is the reaction rate of molecule m (**Equation 5-3**), C_m is the concentration of the molecule (**Equation 5-3**), C_L and C_H are the concentrations of the light and heavy C isotopes, respectively [$M L^{-3}$], and $\varepsilon_{(bulk)}$ is the bulk kinetic C isotope enrichment factor of the reaction step.

The Carbon Isotopologue Model

Figure 5-4 illustrates the C isotopologue model where the concentrations of each of the three C isotopologues of each CE and ETH are simulated. Instead of 10 isotope species for the isotope model, 15 isotopologue species are needed for the C isotopologue model.

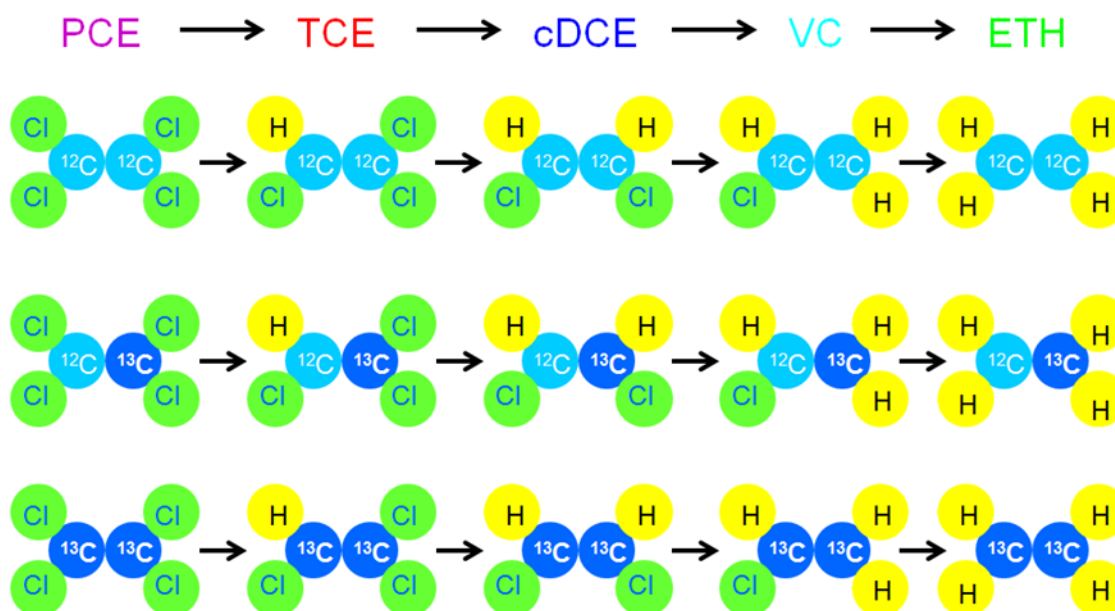


Figure 5-4. The C isotopologue model for RD of PCE to ETH.

The initial concentration of each isotopologue species is calculated from the isotope ratio and the compound's concentration (see **Section 5.4.6**). Degradation rates of the isotopologues are calculated by multiplying the degradation rate of the molecule times the isotopologue fraction times the isotope effect. Mathematically the reaction rates are as follows:

$$Rate_{LL} = Rate_m \cdot \left(\frac{C_{LL}}{C_m} \right) \quad (5-6)$$

$$Rate_{LH} = Rate_m \cdot \left(\frac{C_{LH}}{C_m} \right) \cdot [1 + (\varepsilon_{KIE} + 1)/2] \quad (5-7)$$

$$Rate_{HH} = Rate_m \cdot \left(\frac{C_{HH}}{C_m} \right) \cdot [\varepsilon_{KIE} + 1] \quad (5-8)$$

Where $Rate_{LL}$, $Rate_{LH}$, and $Rate_{HH}$ are the degradation rates of the C isotopologues containing 2 light (L) C atoms, 1 light and 1 heavy (H) C atom, and 2 heavy C atoms, respectively [$M L^{-3} T^{-1}$], $Rate_m$ is the reaction rate of molecule m (**Equation 5-3**), C_m is the concentration of the molecule (**Equation 5-3**), C_{LL} , C_{LH} , and C_{HH} are the concentrations of three C isotopologues [$M L^{-3}$], and ε_{KIE} is the KIE expressed as ε at the reactive position of the reaction step (see **Section 5.4.2** for a definition of the various isotope effects). The model input files need a bulk C enrichment factor; internally, the applicable ε_{KIE} is calculated.

5.4.4 Simulation of Chlorine Isotope Fractionation

At the start of this project, the available model of Cl isotope fractionation during RD assumed that isotope fractionation involves only the Cl atoms positioned at the reacting molecular bonds, i.e., that only the primary KIEs are significant (Hunkeler, 2009). However, the isotopic fractionation of Cl during degradation of TCE and cDCE was best described for the experimental microcosm data obtained in this project by incorporating multiple secondary KIEs (SKIEs), in addition to the primary KIE for a heavy isotope at the reactive position (**Figure 5-5**). SKIEs as result of presence of a heavy Cl isotope attached to the reacting C atom are referred to as α SKIEs, and those attached to the non-reacting C atom are prefixed with a ' β ', followed by a 't' or 'c' depending on whether the isotope is *trans* or *cis*, respectively, relative to the reacting bond (see **Figure 5-5**).

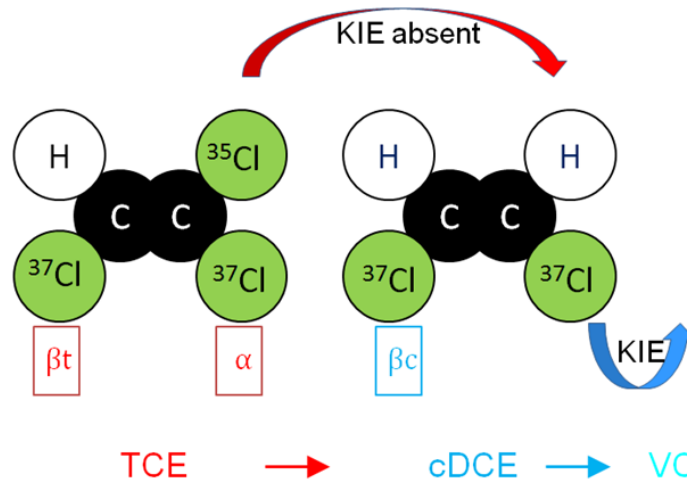


Figure 5-5. A schematic illustrating the three types (α , β_c , β_t) of Cl SKIE that occurs during sequential RD of TCE to VC.

To simulate Cl isotope fractionation, the isotopologue approach was applied (Hunkeler, 2009) which considers all isotopologues in the reaction network, and for TCE also all Cl isotopomers (i.e., isotopologues with same number of heavy isotopes but located at different positions). **Figure 5-6** illustrates the reaction network.

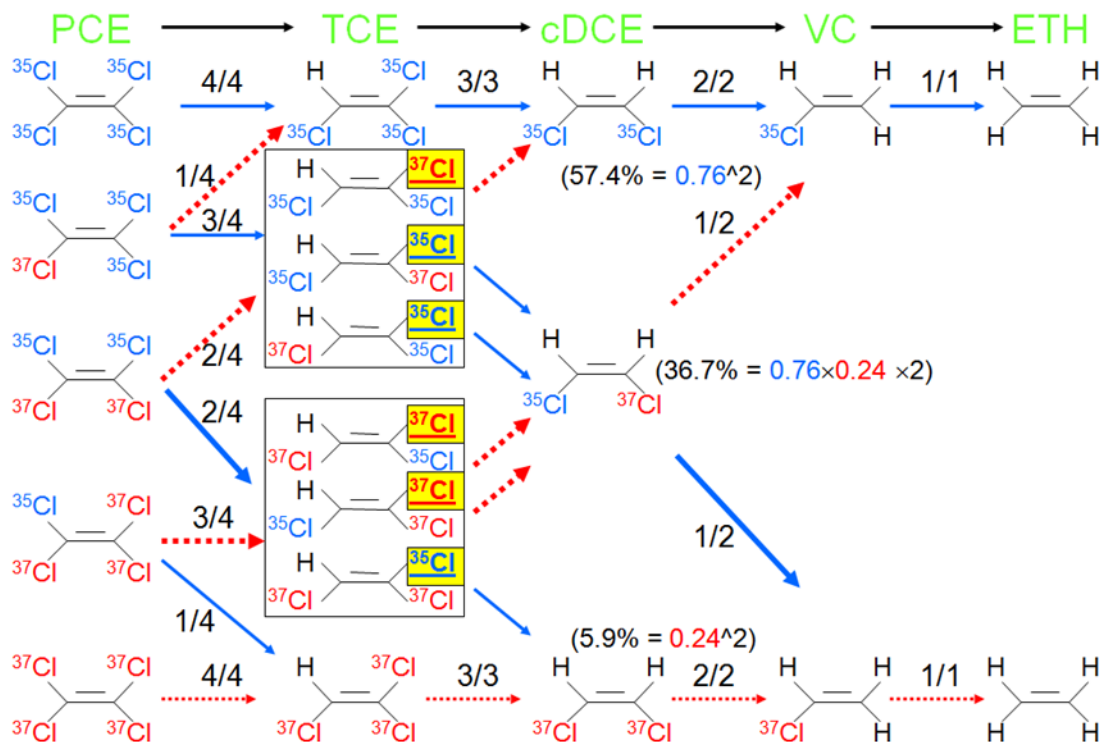


Figure 5-6. Schematic indicating the complex reaction network including all Cl isotopologues and isotopomers during RD of PCE. Blue solid arrows indicate (the approximate chance of) reaction pathways without primary KIEs, (but with potential SKIEs), whereas red dashed arrows indicate (the approximate chance of) reaction pathways where a primary isotope effect occurs (together with potential SKIEs). The two boxes show the TCE isomers containing 1 and 2 heavy Cl isotopes, respectively. Note only the yellow highlighted Cl atom reacts in the formation of cDCE. Potential secondary isotope effects are not shown in this schematic but listed in **Table 8**.

The model illustrated in **Figure 5.6**, developed by Hunkeler et al. (2009), was extended in this project to account for SKIEs. The initial Cl isotopologue concentrations were calculated according to a probability mass function, as described in **Section 5.4.6**. The reaction rate of each isotopologue/isotopomer ($Rate_{mi}$) was obtained by:

$$Rate_{mi} = Rate_m \cdot \left(\frac{C_i}{C_m} \right) \cdot \left[\frac{n_i - H_i}{n_i} \prod \alpha_{SKIE_i} + \frac{H_i}{n_i} \prod \alpha_{(S)KIE_i} \right] \quad (5-9)$$

Where C_i ($M L^{-3}$) is the concentration of the isotopologue/isotopomer of interest, n_i is the number of Cl atoms at reactive positions in the isotopologue/isotopomer, H_i is the number of heavy Cl isotopes at reactive positions in isotopologue/isotopomer i , and $\prod \alpha_{(s)KIE_i}$ is the multiplication of the inverse (α) of the applicable primary and secondary KIEs during transformation of isotopologue/ isotopomer i to either one or two daughter isotopologues. In case of Cl isotope

fractionation, a single daughter isotopologue is formed if $H_i = 0$ or if $H_i = n_i$, whereas two daughter isotopologues are formed if $H_i > 0$ and $H_i \neq n_m$ (**Figure 5-6**). A single daughter isotopologue is thus formed during transformation of entirely heavy or light isotopologues and of all TCE isotopomers. The first part of the last term of **Equation 5-9** describes the chance that a C-35Cl bond of an isotopologue is broken together with the potential applicable secondary KIEs, whereas the second part of this term describes the chance a C-37Cl bond is broken together with the primary and potential secondary KIEs that may apply. Note the following conversions used: $\alpha_{(S)KIE} - 1 = \epsilon_{(S)KIE}$; $\alpha_{(S)KIE} = 1/_{(S)KIE}$; and $\epsilon_{Cl(bulk)} \approx \sum \epsilon_{(S)KIE} / (n_m/x)$ (Elsner, 2005), where n_m is the total number of Cl atoms in the molecule, x is the number of these atoms in reactive positions (1 for all reactions). The sum of $\epsilon_{(S)KIEs}$ gives a nearly equal outcome as their multiplication (in $\alpha_{(S)KIEs}$ equivalents; outcomes not shown). The model input files need either bulk Cl enrichment factors for the ‘Plume’ model or KIE and SKIEs values for the ‘Microcosm’ model that considers secondary KIEs (see **Table 5-8**).

5.4.5 Simulation of Hydrogen Isotope Fractionation

Figure 5-7 illustrates H isotope fractionation during sequential RD lacks primary KIEs and only involves various types of secondary KIEs. The model only considered the averages of the applicable hydrogen SKIEs of each reaction step to limit model complexity. As the H atoms transferred to the daughter products experience little isotope fractionation (except for TCE as was found in the microcosm study conducted for this project [Kuder van Breukelen, et al., 2013]) due to solely SKIEs, the bulk δ^2H of a daughter product is mostly affected by the δ^2H of the H atom replacing the Cl atom during dechlorination/protonation (Ertle et al., 1998; Shouakar-Stash et al., 2003).

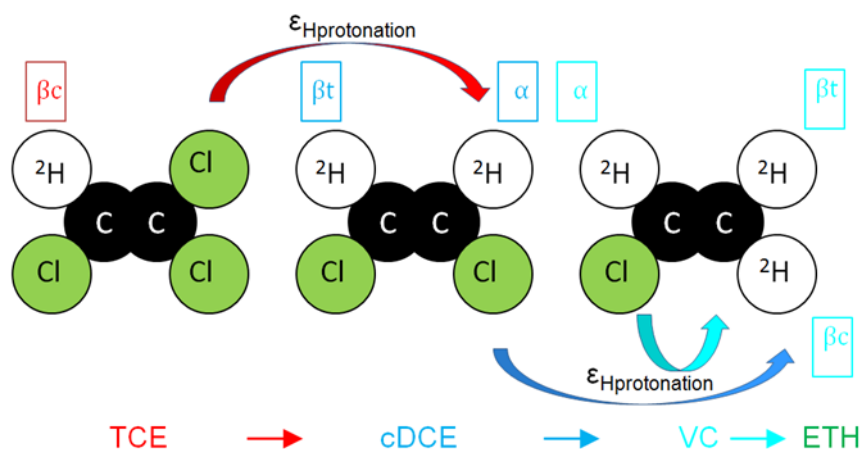


Figure 5-7. A conceptual model indicating the three types of H SKIEs that occur during RD of TCE to ETH. Arrows indicate reacting Cl atoms. The H isotope fractionation effect with respect to δ^2H-H^2O during protonation is called $\epsilon_{Hprotonation}$.

Hydrogen isotope ratios were simulated with an extended “bulk isotope” method. To simulate δ^2H of a daughter product, the model considered (i) isotope fractionation of the H atoms transferred from the parent to daughter product (**Equations 5-4** and **5-5** used with $\epsilon_{(bulk)}$ consisting of solely SKIEs); and (ii) the rates of the light, $Rate_{1H}$, and the heavy, $Rate_{2H}$, H isotopes replacing the Cl atom of the parent compound, *i.e.*, through protonation, at each dechlorination step calculated as the total rate multiplied with the hydrogen isotopic abundance:

$$Rate_{e_H} = -Rate_{e_m} \cdot \left[1 + \left(\delta^2H_{\text{water}} + \varepsilon_{H_{\text{protonation}}} + 1 \right) \cdot VSMOW \right]^{-1} \quad (5-10)$$

$$Rate_{e_{2_H}} = -Rate_{e_m} \cdot \left[1 - \left[1 + \left(\delta^2H_{\text{water}} + \varepsilon_{H_{\text{protonation}}} + 1 \right) \cdot VSMOW \right]^{-1} \right] \quad (5-11)$$

Where $Rate_m$ (**Equation 5-3**) is the degradation rate of the corresponding parent compound, $\varepsilon_{H_{\text{protonation}}}$ is the overall H isotopic enrichment factor expressed with respect to δ^2H_{water} and associated with this reaction step, and VSMOW is the international standard for the isotopic composition of water. The rates of H addition through protonation and of H transfer from the parent compound were weighted to account for the different numbers of H atoms involved. For example, in case of VC having three H atoms, two H atoms are transferred from DCE, whereas one H atom is added via protonation. Consequently, the H transfer flux is multiplied by $\frac{2}{3}$ and the protonation flux by $\frac{1}{3}$.

5.4.6 Calculation of initial isotope or isotopologue concentrations

The models need initial or starting concentrations of the individual isotope or isotopologue species, mostly to define the source concentration and isotope ratio. The model zip file (in the project web download) contains an Excel spreadsheet ‘Calculation of Initial Isotope or Isotopologue Concentrations.xls’ that can be used to perform these calculations. The theory is explained in the following.

Isotopes

The box below indicates the series of equations used to calculate absolute concentrations of isotopes based on the isotope ratio and the compound concentration.

<ul style="list-style-type: none"> • $\delta^{13}C\text{-PCE} = -30.8 \text{ ‰}$ • $[PCE] = 165 \text{ } \mu\text{M}$ • $VPDB = 1.1237\text{e-}2$ 	<p>B: Calculate Isotope Abundances</p> $R_A = 13C / 12C \quad 13C + 12C = 1$ $13C = 12C \times R_A$ $12C \times R_A + 12C = 1$ $12C \times (1 + R_A) = 1$ $12C = 1 / (1 + R_A)$ $13C = 1 - 12C$ $[12C] = 12C \times [PCE]$ $[13C] = 13C \times [PCE]$
<p>A: Calculate Isotope Ratio, R_A of Sample, from its δ:</p> $\delta_{Air} = \frac{R_A - R_r}{R_r} = \frac{R_A}{R_r} - 1$ $-30.8 / 1000 = \frac{R_A}{R_r} - 1$ $-30.8 / 1000 + 1 = \frac{R_A}{R_r}$ $R_A = (-30.8 / 1000 + 1) \times VPDB$	

Figure 5-8. Series of equations to calculate absolute concentrations of isotope species from the isotope ratio and concentration of the compound. An example is shown for the light and heavy C isotope of PCE having a concentration of 165 μM and a $\delta^{13}C$ of -30.8‰.

Isotopologues

The probability mass function enables calculation of the concentration distribution of each isotopologue and isotopomer based on the initial Cl isotope ratio of a compound and its total concentration. The theory applies as well for C isotopologues but is explained here for the Cl isotopologues. Assuming a binomial distribution of the light and heavy Cl isotopes, the distribution of the various isotopologues of a compound is given by, e.g., (Hofstetter et al., 2007)

$$P_i = \frac{n_i!}{H_i!(n_i - H_i)!} \cdot \pi_R^{H_i} \cdot (1 - \pi_R)^{n_i - H_i} \quad (5-12)$$

Where n_i is the total number of Cl atoms and H_i is the number of heavy ^{37}Cl -atoms of isotopologue i . Consequently, the difference $n_i - H_i$ corresponds to the number of ^{35}Cl atoms. π_R is the relative abundance of ^{37}Cl defined as:

$$\pi_R = \frac{{}^{37}\text{Cl}}{{}^{35}\text{Cl} + {}^{37}\text{Cl}} = \frac{{}^{37}R_{RO}}{{}^{37}R_{RO} + 1} = \frac{(\delta^{37}\text{Cl}_{RO} / 1000 + 1) {}^{37}R_{std}}{(\delta^{37}\text{Cl}_{RO} / 1000 + 1) {}^{37}R_{std} + 1} \quad (5-13)$$

The last term in **Equation 5-13** is obtained by substituting ${}^{37}R_{RO}$ by $\delta^{37}\text{Cl}_{RO}$ and the isotope ratio of international standard, ${}^{37}R_{std}$ (= SMOC = 0.319766), respectively (Hofstetter et al., 2007) based on **Equation 5-14**:

$$\delta^{37}\text{Cl}_{RO} = \left(\frac{{}^{37}R_{RO}}{{}^{37}R_{std}} - 1 \right) \cdot 1000 \quad (5-14)$$

Table 5-3. Chlorinated Ethene Isotopologues and (TCE) Isotopomers and Their Initial Abundance as Percentage in the Cl Isotopologue Model.

Pce_III (32.96)	Pce_IIIh ^a (42.16)		Pce_IIhh (20.22)		Pce_Ihhh (4.31)		Pce_hhhh (0.34)
Tce_III (43.50)	Tce_IIIh (13.91)	Tce_IIhl (13.91)	Tce_hII (13.91)	Tce_IIhh (4.45)	Tce_hIhh (4.45)	Tce_hIIh (4.45)	Tce_hhhh (1.42)
Dce_II (57.41)	Dce_Ih (36.72)						Dce_hh (5.87)
Vc_I (75.77)							Vc_h (24.23)

^a I denotes a light and h a heavy chlorine isotope, respectively.

Table 5-3 shows the relative abundances (as percentages) of all isotopologues of the four CEs produced in sequential RD including the six TCE isotopomers given a $\delta^{37}\text{Cl}$ -signature of 0‰ ($\pi_R = 0.2423$). For VC, containing one Cl atom, the distribution of its two isotopologues directly reflects the abundances of the heavy and light Cl isotopes (**Table 5-3**). For PCE, the isotopologue containing one heavy Cl atom is most abundant (42%). However, even PCE containing exclusively heavy Cl atoms still accounts for 0.3% of the total number of PCE molecules. Clearly, the high natural abundance of the heavy Cl atom results in high abundances of isotopologues containing multiple heavy Cl atoms. On the contrary, the chance that organic molecules contain multiple

heavy C atoms is highly unlikely. Therefore, in order to simulate Cl isotope fractionation during sequential degradation of CEs, the consumption and production rates of all isotopologues need to be taken into account. Calculated isotopologue concentrations were specified in input files to 10 significant digits.

5.4.7 Calculation of isotope ratios from absolute isotope/isotopologue concentrations

Isotope ratios can be calculated after each time step from the isotope/isotopologue concentration. The equations below give some examples:

$$\delta^{13}\text{C} - \text{TCE} = 1000 \times \left(\left(\frac{[\text{Tce}_h]}{[\text{Tce}_l]} \right) / \text{VPDB} \right) - 1 \quad (5-15)$$

$$\delta^{13}\text{C} - \text{TCE} = 1000 \times \left(\left(\frac{2[\text{Tce}_{hh}] + [\text{Tce}_{lh}]}{2[\text{Tce}_{ll}] + [\text{Tce}_{lh}]} \right) / \text{VPDB} \right) - 1 \quad (5-16)$$

$$\delta^3\text{H} - \text{TCE} = 1000 \times \left(\left(\frac{[\text{Tce}_{h_h}]}{[\text{Tce}_{h_l}]} \right) / \text{VSMOW} \right) - 1 \quad (5-17)$$

$$\begin{aligned} \delta^{37}\text{Cl} - \text{TCE} = 1000 \times & \left(\left(\frac{[\text{Tce}_{llh}] + [\text{Tce}_{lhl}] + [\text{Tce}_{hll}] + \right. \right. \\ & 2[\text{Tce}_{lhh}] + 2[\text{Tce}_{hlh}] + 2[\text{Tce}_{hhl}] + 3[\text{Tce}_{hhh}] \\ & \left. \left. \right) / (3[\text{Tce}_{lll}] + 2[\text{Tce}_{llh}] + 2[\text{Tce}_{lhl}] + 2[\text{Tce}_{hll}] + [\text{Tce}_{lhh}] + [\text{Tce}_{hlh}] + [\text{Tce}_{hhl}]) \right) \\ & / \text{SMOC} - 1 \end{aligned} \quad (5-18)$$

Where **Equation 5-15** gives the C isotope ratio based on the C isotope concentrations, **Equation 5-16** gives the C isotope ratio based on the C isotopologue concentrations, **Equation 5-17** gives the H isotope ratio based on the H isotope concentrations, and **Equation 5-18** gives the Cl isotope ratio based on the Cl isotopologue concentrations. VPDB, SMOW, and SMOC are the abbreviations of the international isotope standards of C, H, and Cl, respectively (see **Table 3-1**).

5.5 Model Limitations

A set of template models has been provided as part of this project (summarized in **Section 4.2**, and explained in more detail in **Section 7**), files available for download [insert web site]. For certain conditions, it might be necessary to develop a site or process-specific model by combining parts of the template models. The set of template models does not include details on the optional simulation of sorption and associated isotope fractionation nor the simulation of diffusion induced isotope fractionation. However, these processes have been simulated with these models before (Van Breukelen and Prommer, 2008; Van Breukelen and Rolle, 2012) and Dr. van Breukelen can be contacted to discuss specific wishes. Also chemical reduction has not been included but is planned to add to the models in the near future. The chosen model platform (PHREEQC, PHAST, PHT3D) is state-of-the-art and enables complex solute transport simulations. The template models assume homogeneous spatial conditions in degradation rate constants but this can also be adjusted as explained in Case 2. The general model limitations are similar to any general groundwater flow and solute transport model.

The main limitation of ‘RTM with CSIA’ models is the availability of process specific isotope fractionation factors. The literature database of those for C is extensive but limited for Cl and only just developing for H. See **Appendix B** for a list of references.

5.6 Additional Information

Table 5A-4. Names of Isotope/Isotopologue Species as Defined in the Models

Species	Compound	Element	Method	# Light	# Heavy	Isotope/Isotopologue
Carbon Isotopologues						
Pce_c ll	PCE	Carbon	Isotopologue	2	0	12C-12C-PCE
Pce_c lh	PCE	Carbon	Isotopologue	1	1	12C-13C-PCE
Pce_c hh	PCE	Carbon	Isotopologue	0	2	13C-13C-PCE
Tce_c ll	TCE	Carbon	Isotopologue	2	0	12C-12C-TCE
Tce_c lh	TCE	Carbon	Isotopologue	1	1	12C-13C-TCE
Tce_c hh	TCE	Carbon	Isotopologue	0	2	13C-13C-TCE
Dce_c ll	DCE	Carbon	Isotopologue	2	0	12C-12C-DCE
Dce_c lh	DCE	Carbon	Isotopologue	1	1	12C-13C-DCE
Dce_c hh	DCE	Carbon	Isotopologue	0	2	13C-13C-DCE
Vc_c ll	VC	Carbon	Isotopologue	2	0	12C-12C-VC
Vc_c lh	VC	Carbon	Isotopologue	1	1	12C-13C-VC
Vc_c hh	VC	Carbon	Isotopologue	0	2	13C-13C-VC
Eth_c ll	ETH	Carbon	Isotopologue	2	0	12C-12C-ETH
Eth_c lh	ETH	Carbon	Isotopologue	1	1	12C-13C-ETH
Eth_c hh	ETH	Carbon	Isotopologue	0	2	13C-13C-ETH
Carbon Isotopes						
Pce l	PCE	Carbon	Isotope	1	0	12C-PCE
Pce h	PCE	Carbon	Isotope	0	1	13C-PCE
Tce l	TCE	Carbon	Isotope	1	0	12C-TCE
Tce h	TCE	Carbon	Isotope	0	1	13C-TCE
Dce l	DCE	Carbon	Isotope	1	0	12C-DCE
Dce h	DCE	Carbon	Isotope	0	1	13C-DCE
Vc l	VC	Carbon	Isotope	1	0	12C-VC
Vc h	VC	Carbon	Isotope	0	1	13C-VC
Eth l	ETH	Carbon	Isotope	1	0	12C-ETH
Eth h	ETH	Carbon	Isotope	0	1	13C-ETH
Chlorine Isotopologues						
Pce_cl llll	PCE	Chlorine	Isotopologue	4	0	35Cl-35Cl-35Cl-35Cl-PCE
Pce_cl llhh	PCE	Chlorine	Isotopologue	3	1	35Cl-35Cl-35Cl-37Cl-PCE
Pce_cl llhh	PCE	Chlorine	Isotopologue	2	2	35Cl-35Cl-37Cl-37Cl-PCE
Pce_cl lhhh	PCE	Chlorine	Isotopologue	1	3	35Cl-37Cl-37Cl-37Cl-PCE
Pce_cl hhhh	PCE	Chlorine	Isotopologue	0	4	37Cl-37Cl-37Cl-37Cl-PCE
Tce_cl ll	TCE	Chlorine	Isotopologue	3	0	35Cl-35Cl-35Cl-TCE
Tce_cl lh	TCE	Chlorine	Isotopologue	2	1	35Cl-35Cl-37Cl-TCE
Tce_cl hl	TCE	Chlorine	Isotopologue	2	1	35Cl-37Cl-35Cl-TCE
Tce_cl hll	TCE	Chlorine	Isotopologue	2	1	37Cl-35Cl-35Cl-TCE
Tce_cl lhh	TCE	Chlorine	Isotopologue	1	2	35Cl-37Cl-37Cl-TCE
Tce_cl hhl	TCE	Chlorine	Isotopologue	1	2	37Cl-35Cl-37Cl-TCE
Tce_cl hll	TCE	Chlorine	Isotopologue	1	2	37Cl-37Cl-35Cl-TCE
Tce_cl hhh	TCE	Chlorine	Isotopologue	0	3	37Cl-37Cl-37Cl-TCE
Dce_cl ll	DCE	Chlorine	Isotopologue	2	0	35Cl-35Cl-DCE
Dce_cl lh	DCE	Chlorine	Isotopologue	1	1	35Cl-37Cl-DCE
Dce_cl hh	DCE	Chlorine	Isotopologue	0	2	37Cl-37Cl-DCE
Vc_cl l	VC	Chlorine	Isotopologue	1	0	35Cl-VC
Vc_cl h	VC	Chlorine	Isotopologue	0	1	37Cl-VC

Species	Compound	Element	Method	# Light	# Heavy	Isotope/Isotopologue
Hydrogen Isotopes						
Pce a	PCE					PCE
Tce h l	TCE	Hydrogen	Isotope	1	0	H-TCE
Tce h h	TCE	Hydrogen	Isotope	0	1	D-TCE
Dce h l	DCE	Hydrogen	Isotope	1	0	H-DCE
Dce h h	DCE	Hydrogen	Isotope	0	1	D-DCE
Vc h l	VC	Hydrogen	Isotope	1	0	H-VC
Vc h h	VC	Hydrogen	Isotope	0	1	D-VC
Et h l	ETH	Hydrogen	Isotope	1	0	H-ETH
Et h h	ETH	Hydrogen	Isotope	0	1	D-ETH

a Pce is used in the hydrogen isotope model to simulate PCE to TCE reductive dechlorination; the rate of this step is required to simulate the protonation of TCE.

Table 5A-5. Sets of isotope fractionation reactions ^{a, b}

Reaction ID c	Process name and set of kinetic reactions					
Carbon Isotopologue Fractionation						
Reductive Dechlorination						
111B	# PCE Reductive Dechlorination Carbon Isotopologue Fractionation: Pce_ci_ll_rd; -formula Pce_c_ll 1 Tce_c_ll -1 Pce_ci_lh_rd; -formula Pce_c_lh 1 Tce_c_lh -1 Pce_ci_hh_rd; -formula Pce_c_hh 1 Tce_c_hh -1					
112B	# TCE Reductive Dechlorination Carbon Isotopologue Fractionation: Tce_ci_ll_rd; -formula Tce_c_ll 1 Dce_c_ll -1 Tce_ci_lh_rd; -formula Tce_c_lh 1 Dce_c_lh -1 Tce_ci_hh_rd; -formula Tce_c_hh 1 Dce_c_hh -1					
113B	# DCE Reductive Dechlorination Carbon Isotopologue Fractionation: Dce_ci_ll_rd; -formula Dce_c_ll 1 Vc_c_ll -1 Dce_ci_lh_rd; -formula Dce_c_lh 1 Vc_c_lh -1 Dce_ci_hh_rd; -formula Dce_c_hh 1 Vc_c_hh -1					
114B	# VC Reductive Dechlorination Carbon Isotopologue Fractionation: Vc_ci_ll_rd; -formula Vc_c_ll 1 Eth_c_ll -1 Vc_ci_lh_rd; -formula Vc_c_lh 1 Eth_c_lh -1 Vc_ci_hh_rd; -formula Vc_c_hh 1 Eth_c_hh -1					
Oxidative Transformation						
123B	# DCE Oxidation Carbon Isotopologue Fractionation: Dce_ci_ll_ox; -formula Dce_c_ll 1 Ox_c_i 2 Dce_ci_lh_ox; -formula Dce_c_lh 1 Ox_c_i 2 Dce_ci_hh_ox; -formula Dce_c_hh 1 Ox_c_i 2					
124B	# VC Oxidation Carbon Isotopologue Fractionation: Vc_ci_ll_ox; -formula Vc_c_ll 1 Ox_c_i 2.5 Vc_ci_lh_ox; -formula Vc_c_lh 1 Ox_c_i 2.5 Vc_ci_hh_ox; -formula Vc_c_hh 1 Ox_c_i 2.5					
125B	# ETH Anaerobic Oxidation Carbon Isotopologue Fractionation: Eth_ci_ll_anox; -formula Eth_c_ll 1 Eth_ci_lh_anox; -formula Eth_c_lh 1 Eth_ci_hh_anox; -formula Eth_c_hh 1					
Carbon Isotope Fractionation						
Reductive Dechlorination						
111A	# PCE Reductive Dechlorination Carbon Isotope Fractionation: Pce_l_rd; -formula Pce_l 1 Tce_l -1 Pce_h_rd; -formula Pce_h 1 Tce_h -1					

Reaction ID c	Process name and set of kinetic reactions
112A	# TCE Reductive Dechlorination Carbon Isotope Fractionation: Tce_l_rd; -formula Tce_l 1 Dce_l -1 Tce_h_rd; -formula Tce_h 1 Dce_h -1
113A	# DCE Reductive Dechlorination Carbon Isotope Fractionation: Dce_l_rd; -formula Dce_l 1 Vc_l -1 Dce_h_rd; -formula Dce_h 1 Vc_h -1
114A	# VC Reductive Dechlorination Carbon Isotope Fractionation: Vc_l_rd; -formula Vc_l 1 Eth_l -1 Vc_h_rd; -formula Vc_h 1 Eth_h -1
	Oxidative Transformation
124A	# VC Oxidative Carbon Isotope Fractionation: Vc_c_l_ox; -formula Vc_l 1 Vc_c_h_ox; -formula Vc_h 1
Chlorine Isotopologue Fractionation	
	Reductive Dechlorination
211B	# PCE Reductive Dechlorination Chlorine Isotopologue Fractionation: Pce_cl_III_to_Tce_cl_III_RD;-formula Pce_cl_III 1 Cl_l -1 Tce_cl_III -1 Pce_cl_IIIh_to_Tce_cl_III_RD;-formula Pce_cl_IIIh 1 Cl_h -1 Tce_cl_III -1 Pce_cl_IIIh_to_Tce_cl_IIh_RD;-formula Pce_cl_IIIh 1 Cl_l -1 Tce_cl_IIIh -0.33333 Tce_cl_IIh -0.33333 Tce_cl_hII -0.33333 Pce_cl_IIIhh_to_Tce_cl_IIh_RD;-formula Pce_cl_IIIhh 1 Cl_h -1 Tce_cl_IIIhh -0.33333 Tce_cl_IIh -0.33333 Tce_cl_hII -0.33333 Pce_cl_IIIhh_to_Tce_cl_IIh_RD;-formula Pce_cl_IIIhh 1 Cl_l -1 Tce_cl_IIIhh -0.33333 Tce_cl_IIh -0.33333 Tce_cl_hII -0.33333 Pce_cl_IIIhhh_to_Tce_cl_IIh_RD;-formula Pce_cl_IIIhhh 1 Cl_h -1 Tce_cl_IIIhhh -0.33333 Tce_cl_IIh -0.33333 Tce_cl_hII -0.33333 Pce_cl_IIIhhh_to_Tce_cl_IIIh_RD;-formula Pce_cl_IIIhhh 1 Cl_l -1 Tce_cl_IIIh -1 Pce_cl_IIIhhh_to_Tce_cl_IIIh_RD;-formula Pce_cl_IIIhhh 1 Cl_h -1 Tce_cl_IIIh -1
212B	# TCE Reductive Dechlorination Chlorine Isotopologue Fractionation: Tce_LLL_to_Dce_LL_RD; -formula Tce_III 1 Cl_l -1 Dce_II -1 Tce_LLH_to_Dce_LL_RD; -formula Tce_IIIh 1 Cl_h -1 Dce_II -1 Tce_LHL_to_Dce_LH_RD; -formula Tce_IIIh 1 Cl_l -1 Dce_IH -1 Tce_HLL_to_Dce_LH_RD; -formula Tce_IIIh 1 Cl_l -1 Dce_IH -1 Tce_LHH_to_Dce_LH_RD; -formula Tce_IIIh 1 Cl_h -1 Dce_IH -1 Tce_HLH_to_Dce_LH_RD; -formula Tce_IIIh 1 Cl_h -1 Dce_IH -1 Tce_HHL_to_Dce_HH_RD; -formula Tce_IIIh 1 Cl_l -1 Dce_HH -1 Tce_HHH_to_Dce_HH_RD; -formula Tce_IIIh 1 Cl_h -1 Dce_HH -1
213B	# DCE Reductive Dechlorination Chlorine Isotopologue Fractionation: Dce_LL_to_Vc_L_RD; -formula Dce_II 1 Cl_l -1 Vc_cl_l -1 Dce_LH_to_Vc_L_RD; -formula Dce_IH 1 Cl_h -1 Vc_cl_l -1 Dce_LH_to_Vc_H_RD; -formula Dce_IH 1 Cl_l -1 Vc_cl_h -1 Dce_HH_to_Vc_H_RD; -formula Dce_HH 1 Cl_h -1 Vc_cl_h -1
214B	# VC Reductive Dechlorination Chlorine Isotopologue Fractionation: Vc_L_to_Eth_cl_RD; -formula Vc_cl_l 1 Cl_l -1 Eth_cl -1 Vc_H_to_Eth_cl_RD; -formula Vc_cl_h 1 Cl_h -1 Eth_cl -1
	Oxidative Transformation
223B	# DCE Oxidative Transformation Chlorine Isotopologue Fractionation: Dce_cl_II_ox; -formula Dce_cl_II 1 Cl_l -2

Reaction ID c	Process name and set of kinetic reactions
	Dce_cl_lh_ox; -formula Dce_cl_lh 1 Cl_l -1 Cl_h -1 Dce_cl_hh_ox; -formula Dce_cl_hh 1 Cl_h -2
224B	# VC Oxidative Transformation Chlorine Isotopologue Fractionation: Vc_cl_l_ox; -formula Vc_cl_l 1 Cl_l -1 Vc_cl_h_ox; -formula Vc_cl_h 1 Cl_h -1
Hydrogen Isotope Fractionation	
Reductive Dechlorination	
312A	# To simulate TCE: Tce_h_l_rd; -formula Tce_h_l 1 Dce_h_l -0.5 Tce_h_h_rd; -formula Tce_h_h 1 Dce_h_h -0.5 # also add reactions below if PCE is present and transforms to TCE Tce_h_l_added; -formula Tce_h_l -1 Tce_h_h_added; -formula Tce_h_h -1 Pce_rd; -formula Pce 1
313A	# To simulate DCE: Dce_h_l_added; -formula Dce_h_l -0.5 Dce_h_h_added; -formula Dce_h_h -0.5 Dce_h_l_rd; -formula Dce_h_l 1 Vc_h_l -0.6666666666 Dce_h_h_rd; -formula Dce_h_h 1 Vc_h_h -0.6666666666
314A	# To simulate VC: Vc_h_l_added; -formula Vc_h_l -0.3333333333 Vc_h_h_added; -formula Vc_h_h -0.3333333333 Vc_h_l_rd; -formula Vc_h_l 1 Et_h_l -0.75 Vc_h_h_rd; -formula Vc_h_h 1 Et_h_h -0.75
315A	# To simulate ETH: Et_h_l_added; -formula Et_h_l -0.25 Et_h_h_added; -formula Et_h_h -0.25
<p>a To add a reaction to a model the whole set of isotope/isotopologue reactions part of that specific reaction step needs to be added beneath a KINETICS keyword. For example, to simulate carbon isotope fractionation during the PCE to TCE reductive dechlorination step with the carbon isotopologue model all three carbon isotopologue reactions of PCE must be included (reaction set 111B).</p> <p>b The databases may contain more species as part of the reaction stoichiometries such as chloride during reductive dechlorination and chloride and inorganic carbon during oxidative transformation (C isotope/isotopologue models). These species are not required to include in the model and for simplicity they are left out the overview in this table.</p> <p>c The reaction ID is defined as follows: First number: C [1], Cl [2], H [3] isotope fractionation; Second number: reductive dechlorination [1] or oxidative transformation [2]; Third number: PCE [1], TCE [2], DCE [3], VC [4], ETH [5]; Fourth capital letter: type of model: isotope [A], isotopologue [B].</p>	

Table 5A-6. Overview of Model parameter names as defined in the 'Plume' model^a and sets of kinetic reactions to which they apply

Parameter name	Compound	Kinetics	Process	Reaction set	Case
Rate constants					
PCE_RD_k1	PCE	k1 (per year) & O2 inhibition	reductive dechlorination	111B, 211B	1
TCE_RD_k1	TCE	k1 (per year) & O2 inhibition	reductive dechlorination	112B, 212B	1, 3
DCE_RD_k1	DCE	k1 (per year) & O2 inhibition	reductive dechlorination	113B, 213B	1, 3
VC_RD_k1	VC	k1 (per year) & O2 inhibition	reductive dechlorination	114B, 214B	1, 3
DCE_OX_k1	DCE	k1 (per year) & O2 dependent	oxidation	123B, 223B	na
VC_OX_k1	VC	k1 (per year) & O2 dependent	oxidation	124B, 224B	3
ETH_anOX_k1	ETH	k1 (per year) & O2 inhibition	anaerobic oxidation	125B	1B
Carbon Isotope Enrichment Factors					
PCE_RD_e_C	PCE	ϵ_C (‰)	reductive dechlorination	111B	1
TCE_RD_e_C	TCE	ϵ_C (‰)	reductive dechlorination	112B	1, 3
DCE_RD_e_C	DCE	ϵ_C (‰)	reductive dechlorination	113B	1, 3
VC_RD_e_C	VC	ϵ_C (‰)	reductive dechlorination	114B	1, 3
DCE_OX_e_C	DCE	ϵ_C (‰)	oxidation	123B	na
VC_OX_e_C	VC	ϵ_C (‰)	oxidation	124B	3
ETH_anOX_e_C	ETH	ϵ_C (‰)	anaerobic oxidation	125B	1B
Chlorine Isotope Enrichment Factors					
PCE_RD_e_Cl	PCE	ϵ_{Cl} (‰)	reductive dechlorination	211B	na
TCE_RD_e_Cl	TCE	ϵ_{Cl} (‰)	reductive dechlorination	212B	3
DCE_RD_e_Cl	DCE	ϵ_{Cl} (‰)	reductive dechlorination	213B	3
VC_RD_e_Cl	VC	ϵ_{Cl} (‰)	reductive dechlorination	214B	3
DCE_OX_e_Cl	DCE	ϵ_{Cl} (‰)	oxidation	223B	3
VC_OX_e_Cl	VC	ϵ_{Cl} (‰)	oxidation	224B	3
<i>a Use the ESTCP_CSIA.dat database: C & Cl isotopologue methods; first-order concentration-dependent kinetics plus oxygen dependent Monod term</i>					

Table 5A-7. Overview of Model Parameter Names as Defined in the ‘Microcosm’ Model and Sets of Kinetic Reactions they apply to.

Parameter name	Compound	Kinetics	Process	Reaction set	Case
Rate constants					
PCE to TCE k max	PCE	V_{max} (M/yr)	reductive dechlorination	111A, 311A	4
PCE to TCE K Sat	PCE	K_s (M)	reductive dechlorination	111A, 311A	4
PCE_to_TCE_lag	PCE	Lag phase (days)	reductive dechlorination	111A, 311A	4
TCE to cDCE k max	TCE	V_{max} (M/yr)	reductive dechlorination	112A, 212B, 312A	2
TCE to cDCE K Sat	TCE	K_s (M)	reductive dechlorination	112A, 212B, 312A	2
TCE_to_cDCE_lag	TCE	Lag phase (days)	reductive dechlorination	112A, 212B, 312A	2
cDCE k max	DCE	V_{max} (M/yr)	reductive dechlorination	113A, 213B, 313A	2
cDCE K Sat	DCE	K_s (M)	reductive dechlorination	113A, 213B, 313A	2
cDCE_lag	DCE	Lag phase (days)	reductive dechlorination	113A, 213B, 313A	2
VC k max	VC	V_{max} (M/yr)	reductive dechlorination	114A, 214B, 314A	2
VC K Sat	VC	K_s (M)	reductive dechlorination	114A, 214B, 314A	2
VC_lag	VC	Lag phase (days)	reductive dechlorination	114A, 214B, 314A	2
VC_OX_k1	VC	k_1 (per year)	oxidation	124A, 224B	2
Carbon Isotope Enrichment Factors					
PCE to TCE C e	PCE	ϵC (‰)	reductive dechlorination	111A	na
TCE to cDCE C e	TCE	ϵC (‰)	reductive dechlorination	112A	2
cDCE C e	DCE	ϵC (‰)	reductive dechlorination	113A	2
VC C e	VC	ϵC (‰)	reductive dechlorination	114A	2
VC_OX_e_C	VC	ϵC (‰)	oxidation	124A	2
Chlorine Isotope Fractionation Effects					
TCE to cDCE Cl eKIE	TCE	ϵCl_{KIE}	reductive dechlorination	212B	2
TCEtoDCE SKIE A	TCE	$\epsilon Cl_{SKIE} (\alpha)$	reductive dechlorination	212B	2
TCE_to_cDCE_SKIE_B t	TCE	$\epsilon Cl_{SKIE} (\beta t)$	reductive dechlorination	212B	2
cDCE Cl eKIE	DCE	ϵCl_{KIE}	reductive dechlorination	213B	2
cDCE to VC SKIE Bc	DCE	$\epsilon Cl_{SKIE} (\beta c)$	reductive dechlorination	213B	2
VC Cl eKIE	VC	$\epsilon Cl_{KIE} = \epsilon Cl_{bulk}$	reductive dechlorination	214B	2
VC_OX_e_Cl	VC	$\epsilon Cl_{KIE} = \epsilon Cl_{bulk}$	oxidation	224B	2
Hydrogen Isotope Fractionation					
TCE to cDCE H e	TCE	$\epsilon H_{bulk SKIEs}$	reductive dechlorination	312A	4
cDCE H e	DCE	$\epsilon H_{bulk SKIEs}$	reductive dechlorination	313A	4
VC H e	VC	$\epsilon H_{bulk SKIEs}$	reductive dechlorination	314A	4
dH water		δ^2H-H^2O (‰)	reductive dechlorination	312A-315A	4
TCE added H e	TCE	$\epsilon H_{protonation}$	reductive dechlorination	312A	4
cDCE added H e	DCE	$\epsilon H_{protonation}$	reductive dechlorination	313A	4
VC added H e	VC	$\epsilon H_{protonation}$	reductive dechlorination	314A	4
Eth added H e	ETH	$\epsilon H_{protonation}$	reductive dechlorination	315A	4
a Use the Microcosm-C-Cl-H-PCE-ETH.dat database (Case 4): C & H isotope methods, chlorine isotopologue method; Monod kinetics					

Table 5A-8. Chlorine Isotope Fractionation Effects (‰)^d

Reaction	$\epsilon_{\text{Cl}_{\text{KIE}}}$	$\epsilon_{\text{Cl}_{\text{SKIE}} (\alpha)}$	$\epsilon_{\text{Cl}_{\text{SKIE}} (\beta)}$	$\epsilon_{\text{Cl}_{\text{SKIE}} (\beta\epsilon)}$	$\epsilon_{\text{Cl}_{\text{SKIE}} (\text{MEAN})}$	$\epsilon_{\text{Cl}_{\text{bulk}}}$
TCE → cDCE	-4.2e	-3.3a	-3.3a	na	-3.3	-3.6
cDCE → VC	-4.5c	na	na	-1.7	-1.7	-3.1
VC → Ethene	-2.7	na	na	na	na	-2.7

a Note only the average of $\epsilon_{\text{Cl}_{\text{SKIE}} (\alpha)}$ and $\epsilon_{\text{Cl}_{\text{SKIE}} (\beta)}$ can be determined and should equal $\epsilon_{\text{Cl}_{\text{SKIE}} (\text{MEAN})}$.
b $\epsilon_{\text{Cl}_{\text{KIE}}}$ of the TCE to cDCE step follows from $3 \times \epsilon_{\text{Cl}_{\text{bulk}}} - 2 \times \epsilon_{\text{Cl}_{\text{SKIE}} (\text{MEAN})}$
c $\epsilon_{\text{Cl}_{\text{KIE}}}$ of cDCE to VC follows from $-2 \times (\delta^{37}\text{Cl-VC}_{\text{final}} - \delta^{37}\text{Cl-TCE}_{\text{initial}}) + \epsilon_{\text{Cl}_{\text{SKIE}} (\beta\epsilon)}$ (cf. Eq S1 in Kuder et al. 2013a)
d Indicative values are shown and were the result of model calibration of the microcosm experiment
na = not applicable

6.0 DOWNLOADING AND INSTALLING OF SOFTWARE

This section explains where to access the software tools required to perform various levels of RTM modeling for CSIA and how to run the models. Most software tools can be downloaded as free-ware. In all cases, the PHREEQC model is used to simulate the coupled reactions. Users can use the PHAST or the PHT3D model to simulate 2-D or 3-D groundwater contaminant transport. Finally, modeling results can be analyzed with internal graphing routines in PHREEQC, or data can be exported and visualized in Excel, MATLAB, or Python applications.

6.1 PHREEQC Batch or Flow path Reaction Model

Isotope fractionation calculations are done with PHREEQC in 0-D (Batch) or 1-D (Flow path) setup. Although PHREEQC was developed to simulate inorganic geochemical reactions, the model code is versatile enough to simulate transformation reactions of organic chemicals including isotope fractionation as done for many cases in the literature (Hunkeler et al., 2009; Pooley et al., 2009; Van Breukelen et al., 2005; Van Breukelen and Prommer, 2008; Van Breukelen and Rolle, 2012). Users can define their own reaction network and are completely free to define any kinetic reaction. PHREEQC was also selected as model software because it is freely available, widely used and many geochemists and solute transport modelers have at least some experience with the software.

6.1.1 Software Installation and Execution

PHREEQC for Windows can be downloaded as freeware from the following website: <http://pfw.antipodes.nl/download.html>

To install run psetup21800.exe and follow the instructions. Note: you will need to set the ‘tab stops’ to 8 instead of 4 with edit > preferences > input > tab stops. This makes inputting the files prepared for this project easier to read.

PHREEQC was developed by David Parkhurst from the USGS and Tony Appelo, author of the textbook on use of the model course. More information about PHREEQC is available at the following links:

- USGS: < http://wwwbrr.cr.usgs.gov/projects/GWC_coupled/phreeqc/index.html >
- Tony Appelo’s home page: < <http://www.xs4all.nl/~appt/> >

The two links above lead to PHREEQC version 3. All template models run as well with PHREEQC-3. For PHREEQC troubleshooting you can check: the PHREEQC get-going sheets in appendix A in the Appelo & Postma textbook on pages 599-615. There is also an extensive user’s manual available, which is distributed with the download.

The PHREEQC software code needs one **template input text file** and one **technical database file** to run. The structure and method of generating the template input text file and technical database files are discussed in Section 7 below. The model template input file essentially defines the model with a scripting language. The technical database file was developed for this project and is an extension of the default database file with the reactions needed to simulate isotope fractionation.

The Graphical User Interface (GUI) of PHREEQC for Windows can help to visualize the model output. The PHREEQC model output can be visualized in two different ways: (1) a graph can be directly plotted (instructions listed at end of PHREEQC input file) with PHREEQC for Windows or with PHREEQC-3; (2) the model output as written to a text file can be imported and visualized

in MS Excel or with a scientific programming software like MATLAB or the free, open-source alternative Python (see **Section 6.4.1**, below). In the user's guide, Python is used to visualize the model output results with prepared scripts.

6.2 Two Dimensional/Three Dimensional Simulations - PHAST

PHAST couples the PHREEQC biogeochemical model to the groundwater flow model MODFLOW/MT3DMS. PHAST simulates constant-density saturated flow, multicomponent transport, and essentially all PHREEQC chemical reactions. PHAST also is available as a parallel (multiprocessor) version. Installation is straightforward by following the installation program.

6.2.1 Software Installation and Execution

PHAST can be used with either Windows or Linux and can be downloaded at: http://wwwbrr.cr.usgs.gov/projects/GWC_coupled/phast/

PHAST input files are similar to the PHREEQC input files, and for simple geometries a GUI is not needed to create the input files. PHAST needs three data files for execution: (1) the flow and transport data file (*prefix.trans.dat*); (2) the chemistry data file (*prefix.chem.dat*); (3) the thermodynamic database file (*phast.dat* (identical to *phreeqc.dat* except ammonium is defined as N(-3) and not as Amm) or another user-defined constituent). *Prefix* stands for the name of the simulation. The chemistry data file can simply be made with PHREEQC for Windows or with any other editor, like the free and the highly recommended ConTEXT editor (<http://www.contexteditor.org/>). Details on creation of input files are discussed in **Section 7**.

The flow and transport data file can also be made with a simple editor (you simply adjust templates/examples that come with the PHAST distribution, following the PHAST manual). To make input files for more complex hydrogeological situations, two free GUIs from the USGS are available at the PHAST website: ModelMuse and Phast4Windows.

To run PHAST:

1. Place the three files in one project folder preferably having the same name as the simulation (i.e., *prefix*).
2. Start the command prompt (C:\): start > programs > accessories > Command Prompt
3. Go from here to the right disk (type "d:", for example). Go to the project folder directory ("cd folder name": change directory to folder name to go down the directory structure, or type in the full path directly after cd; note "cd .." moves one directory up).
4. When you are in the project folder, simply type: `phast prefix [database]`. You do not need to specify the database file in case you use the default *phast.dat* database.
5. Now PHAST will start calculating.

Visualization of the model results can be done with Model viewer (included with the PHAST distribution), or alternatively with programs like Python or MATLAB to have more versatility. Model viewer uses the *prefix.h5* file (HDF file) which is in compressed binary format. The data in this file can alternatively be extracted to an ASCII file with the program PHASTHDF (part of PHAST distribution) for visualization in spreadsheets or programs like Python. Data generated by PHAST can, however, most conveniently be written to *prefix.xyz.chem* files for visualization in spreadsheets, contouring programs, or most effectively in Python.

6.3 Two Dimensional/Three Dimensional Simulations - PHT3D

PHT3D couples the PHREEQC biogeochemical model to the groundwater flow model MODFLOW/MT3DMS, and is an alternative groundwater transport model to PHAST. The advantage of PHT3D is its inclusion in two widely used graphical user interfaces (GUIs) and its coupling to the widely used MODFLOW groundwater flow modeling software. PHT3D may, therefore, be preferred above PHAST if MODFLOW/MT3D models are already available for a site; the isotope fractionation model can then be, relatively simply, added with a PHT3D simulation in the same GUI.

To run PHT3D, a commercial graphical user interface like Processing Modflow must normally be purchased.

6.3.1 Software Installation and Execution

PHT3D can be downloaded at < <http://www.pht3d.org/> >. A recommended (commercial) GUI for PHT3D can be obtained here: < <http://www.simcore.com/pm8> >

To install the software follow the instructions of the manual. **Section 7.3.2.** summarizes the main differences between PHT3D and PHAST in model setup.

6.4 Python for Visualization of PHREEQC/PHAST Results

6.4.1 Software Installation and Execution

The Python programming language has become popular in environmental and geospatial analysis applications. The Python implementation is under an open source license and is **freely usable and its applications distributable, even for commercial use.** Python has many advantages in that it is widely used in GIS applications, focused on readability with clear syntax and is interoperable with other programming languages. Python can be downloaded from the following location.

Download: <http://code.google.com/p/pythonxy/> > Downloads > current release (2.7.6.1, September 3, 2014) > save file (~703 MB)

Installation: Install installer file > agree with license > ‘Choose Components’:

IMPORTANT:

1. Choose ‘recommended’ for ‘type of install’
2. Install for ‘all users’, otherwise you are not able to use it with your regular login if you installed the program as administrator or installer.
3. ‘Type of install’ now switches to ‘custom’ but that is ok.

> Continue with default steps until program is installed

Starting Python: Start > All Programs >

- A. Python(x,y) > Click on ‘Spyder’ button (at right side of Spyder: Options:)
- B. OR: Python(x,y) Folder > Spyder Folder > Spyder

Recommended Spyder settings:

1. View > Select: ‘Run toolbar’ (the green run button is now available)

2. Interactive console > Interactive console settings > Deselect: ‘Dockable figures’ (Figures will then pop-up as separate windows which is much more convenient than to dock them in the Spyder console)

Running Python script:

1. File > Open: Browse for file
2. Press the folder icon at right end of toolbar to select the folder where the python script is located as ‘Working directory’
3. Run script with green start button OR Source > Run in interactive console OR press F9.

6.4.2 A short introduction to Python

Making plots with Python:

1. Start Python with Spyder: Start > All programs > Python(x,y) > Spyder (Spyder is a graphical user interface for Python)
2. Select as working directory the exercise’s folder: use browse function in toolbar
3. File > open: Browse to working directory and open the py file for the exercise
4. Run script with green traffic light button (or: press F9; or: Interactive console > Run)
5. Inspect the results in the figure window

Short background on Python

Python (<http://www.python.org/>) is a programming language similar to MATLAB but is open-source and free. Python is easy to learn especially for those who have some programming experience. Matplotlib (<http://matplotlib.org/>) is a Python 2D plotting library which produces the same quality figures as with MATLAB. Python(x,y) (<http://code.google.com/p/pythonxy/>) is one of the several available Python distributions which has the advantage of being free, easy to install, and goes with the excellent graphical user interface called Spyder providing MATLAB-like features. Spyder enables advanced editing, interactive testing, debugging and visualization of Python scripts.

A very short introduction to the Python programming language

Like MATLAB, Python works with scripts having extension *.py*. A script contains several to many program lines to execute certain tasks, for this course, the plotting of model results and observations in figures. At the start of a script, you need to import advanced functions contained in modules to enable, for example, 2D plotting. Therefore, the first active program line reads in all python scripts for this course “from pylab import *”, meaning all (*) functions from module Pylab are imported and available to use in the script. The Pylab module contains all functions needed for MATLAB type of plotting (*pyplot*) and data handling (*numpy*). If you want to make use of special mathematical functions you can import these with the module *math*, while advanced statistical functions are available in the module *scipy*. The table below summarizes some key differences between MATLAB and Python. For further information the following website is recommended: [http://wiki.scipy.org/NumPy for Matlab Users](http://wiki.scipy.org/NumPy%20for%20Matlab%20Users).

<i>Some important differences between MATLAB and Python</i>		
Item	MATLAB	Python
	a = 1;	a = 1 [you do not need to place a semi colon (;) at end]
Division	1/2 = 0.5	1/2 = 0 → 1.0/2.0 = 0.5 or float(1)/2 = 0.5 [use decimals to indicate floats, otherwise Python takes them as integers]
Matrix	a = [1 2;3 4]	a = array([[1.,2.],[3.,4.]])
Indexing	1 (one) based indexing: a(1,2)=2	0 (zero) based indexing: a[0,1]=2: access element in first row, second column. Note brackets [] instead of parentheses ()
Element-wise multiply	a .* b	a * b [same for division and exponentiation]
	2^3=8	2**3=8
	[2:2:10]	arange(2.,12.,2.0) = array([2., 4., 6., 8., 10.])
	linspace(2,10,5)	linspace(2,10,5) = array([2., 4., 6., 8., 10.])
	zeros(3,4)	zeros((3,4))

Another major difference with MATLAB is the ‘for loop’ and the use of indents in Python instead of end commands in MATLAB:

MATLAB	Python
<pre>b = ones(1,10) for i is 1:10 b(i) = b(i)*i end print b</pre>	<pre>b = ones((1,10)) # array with 10 elements on one row with value 1 for i in range(0, 10): b[0,i] = b[0,i]*float(i) # note i is an integer print b b = array([[0., 1., 2., 3., 4., 5., 6., 7., 8., 9.]])</pre>

A short example

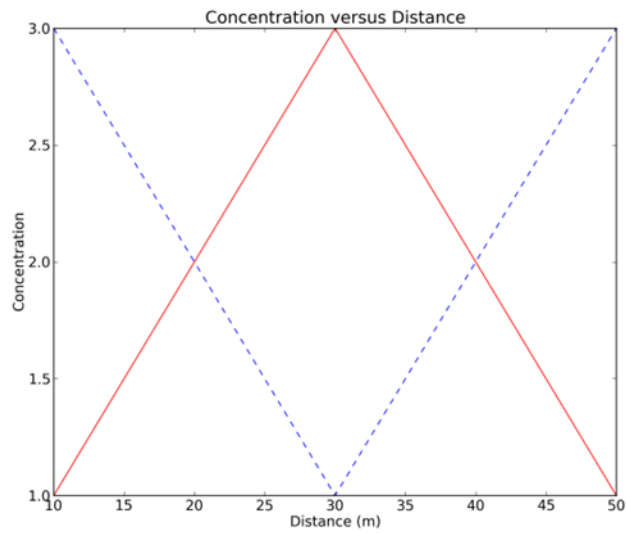
Distance	Parameter 1	Parameter 2
10	1	3
20	2	2
30	3	1
40	2	2
50	1	3

10	1	3
20	2	2
30	3	1
40	2	2
50	1	3

For example, the upper left table shows a spreadsheet with model results you want to plot. If you save the spreadsheet as a text (tab delimited) file, you can subsequently open this txt file with the command: `data = loadtxt('path and filename.txt', skiprows = 1)`. The first row of the file will be skipped (`skiprows = 1`) as it contains strings which cannot be part of a matrix (in Python a 2D array). The matrix (2D array) called *data* is shown in the upper right table.

Making a plot is now simple. The following sequence of program lines gives the plot below:

```
>>> plot(data[:,0], data[:,1], 'r') # : means all elements in this row or column
>>> plot(data[:,0], data[:,2], 'b--') # a blue dashed line, see help(plot) for all options
>>> xlabel('Distance (m)')
>>> ylabel('Concentration')
>>> title('Concentration versus Distance')
```



If you type the program lines above in a file which you save with extension *.py* (a Python script), you can simply run this script every time you modified a simulation to update the figure in a quick way.

7.0 STEP-BY-STEP EXPLANATION OF TEMPLATE MODELS

As part of this project, template model files developed on the PHREEQC format have been provided so that a model simulation project never needs to be started from scratch. The template models can be reviewed and then used as the rough drafts for site-specific simulations.

Note: All PHREEQC input files and other supplemental materials are contained in a zip file that can be downloaded from the project website (under construction http://www.gsi-net.com/en/software/free-software/CSIA_RTM.html).

7.1 Template Model Case 1: Full Dechlorination

This section explains step-by-step how to run the PHREEQC input file for this first template model. This manual assumes the reader has no prior experience with the PHREEQC software.

7.1.1 PHREEQC 1-D Model

Step 1: Inspecting the PHREEQC input file

- Start PHREEQC for Windows and open Case1A.phrq (from the project download) with File > Open, or double click on Case1A.phrq and the PHREEQC file opens automatically.
- PHREEQC runs with one input file and one database file (explained later). The input file is structured with a listing of KEYWORDS written in upper case letters and defining parts of the model (see **Table 7-1**). The PHREEQC input files contain numerous comments for explanation written behind the hatch sign (#) and automatically colored red by PHREEQC for Windows.

Table 7.1. Description of PHREEQC Keywords used in Input File

KEYWORD	Explanation
SOLUTION 0	Defines the chemical composition of the inflow/source water. The number of this solution is 0 by convention.
SOLUTION 1-n	Defines the chemical composition of the initial native/background water along the flow path. n is total number of cells.
CALCULATE VALUES	Here the values of most kinetic parameters are specified.
KINETICS 1-n	Here the kinetic reactions simulated are listed. n is total number of cells.
TRANSPORT	This keyword defines the setting for the 1-D transport simulation.
SELECTED_OUTPUT	Creates a result output file which can be imported in excel or python for visualization.
USER_PUNCH	This keyword is associated with the SELECTED_OUTPUT keyword and is used to create user defined output like isotope ratios.
END	A PHREEQC model always ends with END to tell PHREEQC it needs to run.

Step 2: Composition of the Source and Native Water

Table 7.1 lists and explains the KEYWORDS needed for a 1-D flow path simulation. For a 1-D flow path simulation, the composition of the inflow water and of the initial native water must be defined (see **Box 7.1**). In PHREEQC, a flow path consists of a series of cells. At each time step (called a shift in PHREEQC), the water from the one cell is moved to the neighboring cell. During the same time step, the model accounts for possible reactions and hydrodynamic dispersion. In template model 1, the total number of cells chosen was 50. This number is always an optimum between model calculation time and smoothness of the output results. The length of the contaminant flow path is therefore defined as **SOLUTION 1-50**, which specifies the initial

chemical composition of all 50 cells (pure water as no solutes are specified). The inflow solution has a value of 0 by definition if the flow direction is forward, i.e., from left to right.

Box 7.1	
SOLUTION 0	
units	umol/kgw
Pce_c_ll	977.8992135
Pce_c_lh	21.97730692
Pce_c_hh	0.123479498
SOLUTION 1-50	

The inflow solution (see Box 7.1 contains three solutes, which are the three C isotopologues of PCE: Pce_c_ll, Pce_c_lh, Pce_c_hh, see also illustration **Figure 5.4**), where “l” stands for presence of a light C atom (¹²C) and “h” stands for a heavy C atom (¹³C). The concentrations of these isotopologues follow from the total concentration of the solute (i.e., PCE, 1000 μmol/l) and its isotopic ratio ($\delta^{13}\text{C-PCE} = 0\%$) by means of the probability mass function (see **Section 5.4.6**). The isotopologue concentrations must be specified with a high number of digits (recommend a minimum of six) as the resulting isotope ratio may deviate from the input if too few digits are applied. The software download file contains an Excel spreadsheet ‘Calculation of Initial Isotope or Isotopologue Concentrations.xls’ where these calculations can be completed for any of the CEs and ETH for their C, H, and Cl isotopic ratios. All these isotopologues are defined and available in the ESTCP_CSIA.dat database file (explained below) and in **Table 5-4** of **Section 5.6**.

Step 3. Simulation of degradation processes including isotope fractionation

The values of the kinetic parameters are defined at the **CALCULATE_VALUES** keyword (see **Box 7.2**). With an inbuilt BASIC subroutine (starting with “-start” and finishing with “-end”), values are assigned parameter names. These parameter names are used as mathematical expressions, which describe the rates of the isotopologue transformation reactions. These are programmed beneath **RATES** in the database file (explained later). For example, parameter PCE_RD_k1 is assigned a value 1.5 (per year). Parameter PCE_RD_k1 is the first-order (k1) degradation rate constant for PCE transformation by reductive dechlorination (RD). Another example, ETH_anOX_e_C is the isotopic enrichment factor (ϵ : ϵ) for C isotope fractionation (C) during anaerobic oxidation (anOX) of ETH. With a one-line BASIC command (always starting with a number, here 10) the parameter value is assigned to the parameter name. Coding in PHREEQC can be shortened with the use of semi colons interpreted by PHREEQC as a hard return. A list of all model parameters is provided in **Table 5-6**.

Box 7.2	
CALCULATE_VALUES	
PCE_RD_k1 ; -start;	10 SAVE 1.5 ; -end
<i>is the same as</i>	
PCE_RD_k1	
-start	
10 SAVE 1.5	
-end	

The transformation reactions of the isotopologues are defined with two keywords: **KINETICS** and **RATES**. The stoichiometries of the reactions are defined beneath the **KINETICS** keyword (**Box 7.3**; see **Table 5-6** for an exhaustive list) and the mathematical rate equations beneath the **RATES** keyword (listed in the database file). As the present model considers all three C

isotopologues, three reactions need to be defined (described) for each CE. For example, Pce_ci_ll_rd means the transformation of the C isotopologue (ci) of PCE consisting of two light (ll) C isotopes via RD.

Box 7.3
KINETICS 1-50
Pce_ci_ll_rd; -formula Pce_c_ll 1 Tce_c_ll -1 Cl_c_i -1
Pce_ci_lh_rd; -formula Pce_c_lh 1 Tce_c_lh -1 Cl_c_i -1
Pce_ci_hh_rd; -formula Pce_c_hh 1 Tce_c_hh -1 Cl_c_i -1

With “-formula”, the reaction stoichiometry is defined as being negative for an isotopologue, which disappears from solution, and the overall rate is a multiplication of this reaction rate times the stoichiometric number, the stoichiometric numbers are positive for species that degrade and negative for species that are produced during the reaction. For this example, “Pce_c_ll” is consumed and both “Tce_c_ll” and “Cl_c_i” are produced. This latter species is the chloride (Cl) produced during the C (c) isotopologue (i) reaction. **Table 5-5** shows all isotope/isotopologue fractionation reactions as programmed for this project.

The mathematical formulations for the reaction rates can be found beneath the **RATES** keyword. These reactions can be specified in the input file and/or the database file (the definition stated in the input file will be used if another definition with the same rate name is present in the database file). The rate definitions are all kept in the database file for clarity and to reduce the length of the input files. **Box 7.4** gives an example for the rate definition of “Pce_ci_hh_rd”. After the rate name, the rate is defined with BASIC coding in between an “-start” and “-end” command to indicate the beginning and ending of the BASIC code definition. In lines 10-40 the rate of PCE RD is calculated. With calc_value (“PCE_RD_k1”) in line 40 the first-order rate constant of PCE RD is obtained from the input file as listed beneath **CALCULATE_VALUES**. The rate of the Pce_c_ll isotopologue is a multiplication of the overall PCE rate, the proportion of the Pce_c_ll, with respect to total PCE (line 45), and the kinetic isotope effect of the reaction (lines 50-60). The mathematics of all reactions is explained in **Section 5**.

Box 7.4
RATES
Pce_ci_hh_rd
-start
10 Pce_conc = tot("Pce_c_ll")+tot("Pce_c_lh")+tot("Pce_c_hh")
20 if Pce_conc < 1e-15 then goto 99
30 Monod_OxIb = (1e-3/32/1000)/(tot("Ox_c_i")+(1e-3/32/1000))
40 rate = -(calc_value("PCE_RD_k1")/(365*24*3600))*Pce_conc*Monod_OxIb
45 ratio = tot("Pce_c_hh")/Pce_conc
50 epsilon = calc_value("PCE_RD_e_C")
55 n = 2 # number of atoms to convert bulk epsilon to epsilon KIE
60 alpha = n*epsilon/1000+1
70 moles = ratio*rate*alpha * time
99 save moles
-end

Step 4. Simulation of 1-D transport

Beneath the **TRANSPORT** keyword the settings for a 1-D transport simulation are defined.

- Fifty cells were chosen to represent the 1-D flow path for this template model. From the length of the flow path (500 m, not specified), and `-cells` follows the cell length, `-lengths` (10 m).
- From the average groundwater flow velocity along the flow path (must be known; not specified; 20 m/yr) and the cell length, follows the residence time or `time_step` in a cell (10 m / 20 m/yr = 0.5 yr specified in seconds).
- From the total transport time along the flow path (must be known; not specified) and the `time_step`, follows the total number of shifts (i.e. time steps; 20 years / 0.5 yr = 40).
- PHREEQC assumes by default the assigned conditions for `-flow_direction` and `-boundary_conditions`.
- The `-dispersivities` must be specified.
- With `-punch_frequency`, results are only written to the output file with the indicated frequency. When the `-punch_frequency` equals the number of shift, results are only written to the output file for the last timestep.

Step 5. Creating the output file

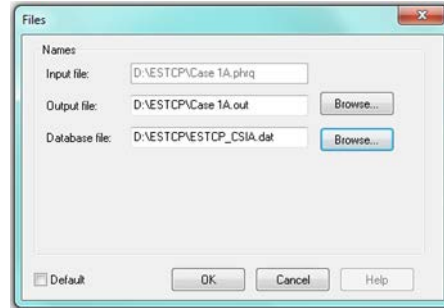
The layout of the calculation results output file is specified when `SELECTED_OUTPUT` is selected in combination with `USER_PUNCH`. With `USER_PUNCH`, the concentrations of the CEs are calculated from the sum of their isotopologues and multiplied by 1000 to convert from mol (“tot” gives total concentration in mol/kg water) to mmol/l. With the `punch` command the results are printed to the output file. BASIC coding language is used as for the KINETICS keyword.

The isotope ratios are calculated at the end from the relative concentrations of the isotopologues and the international standards ($C^{13}/C^{12} = 0.011237$). Isotope ratios are not calculated when total concentrations are very low ($\ll 1e-6$ of source concentration) as numerical errors produce unrealistic isotope ratios. In that case the value -9999 is printed, which can be replaced with a non-available number, NaN, in graphing programs. Section 5.4.6 explains in detail how isotope ratios are calculated from the absolute concentrations of the isotopes/isotopologues.

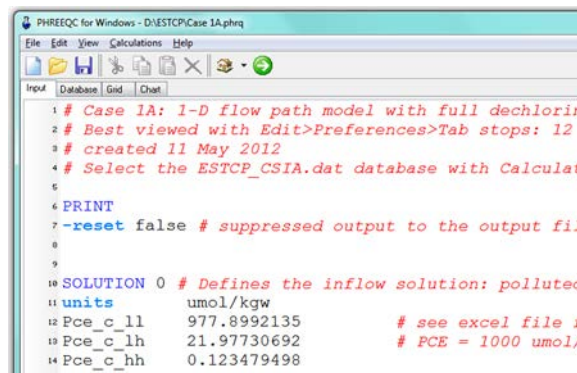
Step 6. Running the PHREEQC template model

The Case 1 template input file is ready to run. To run the model follow the substeps below:

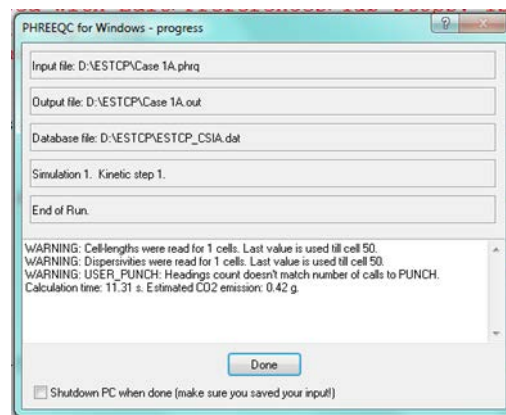
1. Select the ESTCP_CSIA.dat database with Calculations > Files > Browse for database file. See below:



2. Run the model with Calculations > Start, or by clicking on the green run button . See below:



3. The model is running and is finished if the screen below appears. “WARNINGS” are not a problem, only “errors” are. When finished (‘end of Run’), you can click the ‘Done’ button:



4. The next step is to visualize the model results.

Step 7: Visualization

Visualization can be done with the inbuilt graphing option in PHREEQC for Windows, Excel, or a scientific programming and visualization program like MATLAB or Python. This guide makes

use of Python as free alternative to MATLAB commercial software to make very nice plots of the model results. Section 6.4 explains the details of installing Python to your computer. After installing Python in the proper way follow the instructions below to make a plot of the model results:

1. Start Python(x,y) with All Programs > Python(x,y) > Python(x,y)
2. The screen below should open after 10 seconds:



3. Now open Spyder, a graphical user interface of Python, click this button: 
4. In Spyder, select as working directory the template model's folder: use the browse function in the toolbar:



5. File > open: Browse to working directory and open the *py* file for the exercise
6. Run script with green traffic light button (*or*: press F9; *or*: Interactive console > Run)
7. The figure window that opens shows **Figure 4-5**.

For those who have experience with MATLAB, understanding of the Python script is not too difficult with the 'short introduction to Python' in **Section 6.4**. The script available with the template files are heavily commented to explain most of the script.

PHREEQC reports results for the midpoints of the cells. However, the residence in a cell is valid for the full length of a cell. For kinetic reactions, the distance reported by PHREEQC is therefore better increased with half of the cell length for all the cells.

Step 8: Calibration

To demonstrate the calibration process of a RTM-CSIA 1-D PHREEQC model, a training dataset (tutorial) is provided which has been created with a 2-D PHAST model.

The virtual site has the following characteristics: a central flow path monitored along a stretch of 200 m length, a groundwater flow velocity of 50 m/yr, a PCE source concentration of 300 µg/L,

and a source $\delta^{13}\text{C}$ -PCE of -35‰. The longitudinal dispersion coefficient is not known for the site and needs to be calibrated as well as the rate constants and isotope enrichment factors.

The model parameters of template model Case 1A.phrq must be adjusted to calibrate the training dataset (all files available in the 'Calibration Training' subfolder of Case 1). This can be achieved following the general guideline below:

- 1) Adjust the concentrations of the PCE isotopologues in the input file:
 - a) Open the Excel file 'Calculation of Initial Isotope or Isotopologue Concentrations.xls'
 - b) Calculate the molar concentration from the weight concentration by dividing the weight concentration of 300 $\mu\text{g/L}$ with the molecular weight of PCE (165.83 g/mol) to obtain a molar concentration of 1.81 $\mu\text{mol/L}$ PCE.
 - c) Insert this value in cell E22 of the excel sheet
 - d) Adjust the source C isotope ratios as well in cell E23 of the excel sheet.
 - e) As we apply the C isotopologue model: copy and paste the values listed in cells E43-E45 to replace the values of SOLUTION 0 in the template model. Note cells E36-37 give the values if the C isotope model was applied.
- 2) Adjust the set-up of the flow part of 1-D PHREEQC model: -lengths, time_step, shifts:
 - a) In order to lower the computer running times we reduce the number of cells from 50 to 25. Adjust the total number of cells at 'cells' beneath TRANSPORT, but also at SOLUTION 1-n and KINETICS 1-n, where n should be the new number of total cells, 25.
 - b) As the flowpath has a length of 200 m and the total number of cells has changed as well we might need to adjust the cell length. However, it seems we could keep '-lengths' at 10 m to obtain a 25 cells \times 10 m cell length = 250 m long flow path. It is recommended to make the simulated flow path always a bit longer than the actual one.
 - c) Since the flow velocity is 50 m/yr and we chose a cell length of 10 m, the residence time in a cell is 10 m / 50 m/yr = 0.2 yr. Specify the time step in seconds: $0.2 \times 365 \times 24 \times 3600 = 6.3072\text{E}+06$ seconds.
 - d) As we do not know the exact age of the CE release we assume a steady-state situation and take a total simulation time of 7 years (note the transport time is 250 m / 50 m/yr = 5 yr). A total transport time of 7 years together with a time step of 0.2 years implies the number of shifts should be $7 / 0.2 = 35$. Also set the punch_frequency to 35 to only have output after 35 shifts.
- 3) The other model parameters are not known, yet, but these should follow from the calibration process. Run the adjusted PHREEQC model and compare the output with the artificial training dataset:
 - a) In PHREEQC for Windows, with Calculations > Files, select the ESTCP_CSIA.dat database, and run the model (see **Step 6** above)
 - b) Visualize the results with the Python script plotCase1C.py (see **step 7** above). The results of the model – virtual data comparison at this step are shown in **Figure 7-1**: rate constants and fractionation factors clearly need calibration. Note the total summed CE+ETH 'observed' concentration decrease downstream indicates either dilution through

transversal dispersion and/or oxidative transformation might occur. The CSIA C-IMB, however, shows constant values, thus, only reductive dechlorination occurs because the C skeleton of the CE is conserved. The total concentration decreases are thus due to dilution.

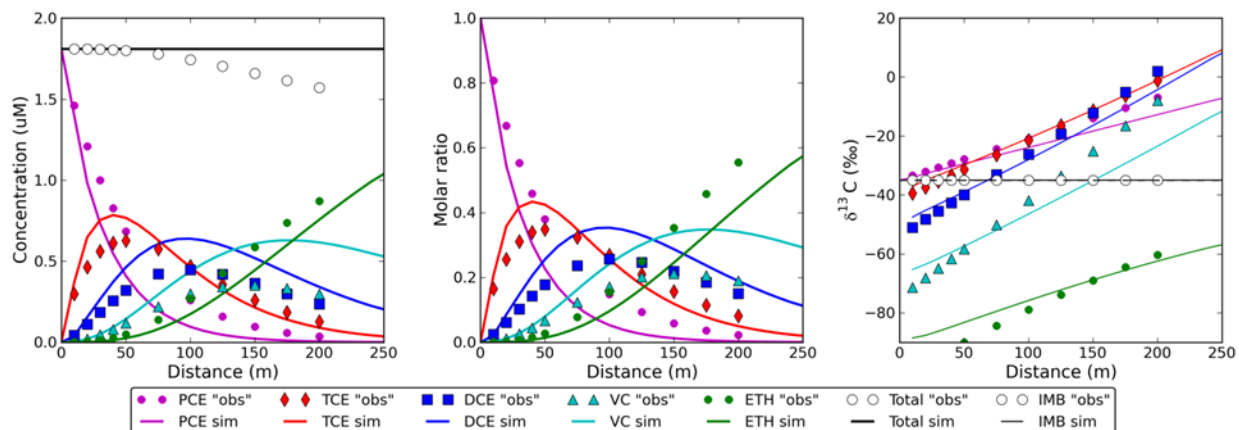


Figure 7-1: Simulation of virtual dataset at calibration guideline step 3.

- 4) First, calibrate the molar concentration ratios of the PCE and its daughter products in sequential order through changing the rate constants by trial and error
- 5) Second, calibrate the C isotope enrichment factors by trial and error also in sequential order from PCE to VC. See **Table 7-2** for the observed ranges of C isotope enrichment factors in the literature.
- 6) The effect of the longitudinal dispersion coefficient is subtle in this training exercise. Note that if you change its value it has a noticeable effect on the predicted C isotope ratios. With higher α_L the overall isotope enrichment downstream decreases. Thus to recalibrate the fractionation factors with a too high α_L selected means you tend to apply to large values for isotope enrichment factors, and vice versa.

Table 7-2. Carbon Isotopic Enrichment Factors, ϵ_C (‰), Reported in the Literature

PCE	TCE	cDCE	VC
-5.4* ¹	-10.6	-20.3	-24.6
[-0.4 – -19]* ²	[-2.5 – -18.9]	[-12 – -30.5]	[-19.9 – -31.1]
n=14	n=27	n=22	n=16

*1 Average value
*2 Range reported, see **Appendix B**

The model can also be calibrated automatically by means of PEST (Model Independent Parameter Estimation and Uncertainty Analysis software, example not included).

7.1.2 PHAST 2-D Model

PHAST was used to perform 2-D cross-sectional flow simulations for Case 1. The model set-up is depicted in **Figure 4.3** and is consistent with Example Scenario Case 1 in **Section 4.2.1**. The model has a length of 460 meters and a height of 15 meters. Groundwater contaminated with PCE occurs as a fixed concentration boundary at the lower 5 meters and clean anoxic water at the upper 10 meters of the left model boundary. Flow is from left to right. The initial domain is anoxic.

The template files for this Case 1 are available in the folder titled “Case1”. The flow and transport data file, chemistry data file, and database file are all composed of KEYWORD data blocks, like for PHREEQC. The keyword data blocks for chemistry are identical to PHREEQC, and any PHREEQC calculation can be performed. PHREEQC is run first when PHAST starts to define solutions, equilibrium-phase assemblages, exchange assemblages, surface assemblages, gas phases, and sets of kinetic reactions with associated identifying numbers. The numbered entities are used to set initial conditions in the model domain and to define boundary solutions.

1. Open the “*Case1.chem.dat*” file with PFW (or ConTEXT) as the editor. Inspect the file. As previously mentioned, it is similar to a PHREEQC input file with the exception that no transport or reactions are simulated; only solutions and kinetic reactions are defined.
 - a. SOLUTION 1 defines the clean anoxic water flowing through the model domain; SOLUTION 2 defines the anoxic with PCE polluted water. The different solutions in the model domain must have a unique number, which is used in the corresponding “*Case1.trans.dat*” file to indicate where in the model domain they occur.
 - b. The same definitions are used as for PHREEQC for the keywords CALCULATE_VALUES, KINETICS, and USER_PUNCH. For the SOLUTION definition, only a unique number needs to be assigned to the KINETICS reactions; the “*Case1.trans.dat*” file indicates this set of kinetic reactions and applies in the full model domain.
2. Open the “*Case1.trans.dat*” file with PFW or ConTEXT as the editor. Inspect the file. The keywords for the flow and transport data file have been devised for PHAST, but are based on input for the model HST3D (stripping out anything related to heat or density and using head in place of pressure). Most of the data blocks are related to the flow and transport parameters needed to simulate groundwater flow and solute transport. A more detailed explanation is provided in the files and below:
 - a. At UNITS, the units are defined and are valid for the whole file.
 - b. At GRID, the grid spacing is defined in three dimensions. For each direction X, Y or Z, the minimum and maximum value in the respective direction and the number of nodes in between these values are specified. The difference between the min and max value divided by the number of nodes minus one gives the node spacing. As you simulate an XZ cross-section you only specify the minimum number of two nodes for the Y direction, and indicate XZ as the dimensions for which the chemical reactions need to be calculated with –chemistry_dimensions XZ. The model has a length of 460 m with 2 m spacing and a height of 15 meters with 0.5 m spacing (more about the node spacing later).
 - c. At MEDIA, the physical properties of the model domain are specified such as hydraulic permeability in a (series) of zones. Here only one zone is specified, characterizing the whole model domain.
 - d. At FREE_SURFACE_BC, the top of the model is indicated to be confined.
 - e. At SPECIFIED_HEAD_BC, the fixed head boundaries and boundary solutions are specified. Read the explanation in the file. A fixed head of 1m is taken for the left boundary and the clean water as fixed solution. This fixed solution is overridden with one of polluted groundwater (solution 2) for the lower 5m of the model boundary. For the right boundary only the associated solution at time = 0 must be specified, which is clean water.

The head for the right boundary was chosen to obtain a groundwater velocity of exactly 20 m/yr with a K of 10 m/day and a porosity of 0.3.

- f. For the simulation of groundwater flow velocity in a hypothetical case like Case 1, it is easiest to first choose a desired velocity (v ; m/d), hydraulic conductivity (K ; m/d), and porosity (n ; -). The difference in hydraulic head (dh ; m) over the model length, dx (m), then follows from:

$$dh = \frac{v \times n \times dx}{K} \quad (7-1)$$

- g. At HEAD_IC, the initial head distribution is given as a linear function.
- h. At CHEMISTRY_IC, the main interaction between the flow and transport data file and the chemistry data file occurs. Here entity numbers (solutions, equilibrium-phase assemblages, etc., as defined in the chemistry data file) are assigned to spatial zones (rectangular parallelepipeds) to establish the initial conditions and reactions in the model domain. For Case 1, solution 1 (clean water) and kinetics 1 (all kinetic reactions specified) should be applied as initial conditions in the model domain.
- i. At SOLUTION_METHOD, the linear equation solver is selected and its options specified. Two linear equation solvers to solve the finite-difference flow and transport equations are available in PHAST: (1) a direct solver; and (2) an iterative solver. The iterative solver is used by default. Small problems of a few hundreds nodes are most efficiently solved with the direct solver; the iterative solver usually is more efficient for simulations with several thousands of nodes or more.
- j. Both spatial differencing for the advective term in the transport equation and time differencing for the flow and transport equations, matters. Centered-in-space or centered-in-time differencing has the potential for causing oscillations in the solutions as applied to the present exercise. Numerical oscillation, as a consequence of centered-in-space differencing, does not occur if

$$\frac{\Delta x}{\alpha} \leq 2 \text{ or } Pe \leq 2 \quad (7-2)$$

Where Δx is the cell size (m); α is the dispersivity (m); Pe is the Peclet number.

Numerical oscillation, as a consequence of centered-in-time differencing, does not occur if

$$\frac{\alpha v_x \Delta t}{\Delta x^2} \leq 1 \quad (7-3)$$

Where Δt is the time step.

- k. For Case 1, this means that Δx must be ≤ 2 for the chosen longitudinal dispersivity of 1 m. For the selected Δx of 2 m, this means that the time step must be ≤ 0.2 years (a time

step of 0.2 years was consequently selected). For the grid spacing in the vertical no clear rules of thumb are available. As the vertical dispersion coefficient is typically a factor 10-100 smaller than the longitudinal one (a value of 0.01 m was selected), it is therefore better to also select a much smaller grid spacing than applied for the X dimension (here 0.5 m was selected).

1. At PRINT_FREQUENCY, the printing frequency is specified to hdf files (which can be read with Modelviewer or converted to a prefix.xyz.chem file that can be read conveniently with Python or similar software to create nicer plots).
- m. At TIME_CONTROL, the total simulation time and the time step are specified.
3. Run the model as explained in the previous section. Results can be checked with Python by means of running the Python script plot2DPHAST_Case1.py as available in the Case1 folder (see **Section 7.1.1**, step 6 how to run a python script). This script creates 2-D, color images of all relevant results in one figure (see **Figure 4-4**).

7.2 Template Model Case 2: Stall of VC: Detection of potential oxidation (C&Cl-CSIA)

7.2.1 PHREEQC 1-D Model

Step 1: Inspecting the PHREEQC input file

- Start PHREEQC for Windows and open Case2.phrq with File > Open, or double click on Case2.phrq and the PHREEQC file opens automatically.
- PHREEQC runs with one input file and one database file (explained later). The input file is structured with a listing of KEYWORDS written in capitals and defining parts of the model (see **Table 7-3**). The PHREEQC input files contain numerous comments for explanation written behind the hatch sign (#) and automatically colored red by PHREEQC for Windows.

Table 7.3. Description of PHREEQC Keywords used in Input File

KEYWORD	Explanation
SOLUTION 0	Defines the chemical composition of the inflow/source water. The number of this solution is 0 by convention.
SOLUTION 1-n	Defines the chemical composition of the initial native/background water along the flow path,. n is total number of cells.
CALCULATE VALUES	Here the values of most kinetic parameters are specified
KINETICS 1-n	Here the kinetic reactions simulated are listed,. n is a specific cell number to which the kinetic zone extends. Note kinetic reactions can be different for different zones (as defined of series of cells).
TRANSPORT	This keyword defines the setting for the 1-D transport simulation
SELECTED_OUTPUT	Creates a result output file which can be imported in Excel or Python for visualization
USER_PUNCH	This keyword is associated with the SELECTED_OUTPUT keyword and is used to create user defined output like isotope ratios
END	A PHREEQC model always ends with END to tell PHREEQC it needs to run.

Step 2: Composition of the source and native water

Table 7.3 lists and explains the KEYWORDS needed for a 1-D flow path simulation. For a 1-D flow path simulation, the composition of the inflow water and of the initial native water must be defined (see **Box 7.5**). In PHREEQC, a flow path consists of a series of cells. At each time step (called a shift in PHREEQC), the water from the one cell is moved to the neighboring cell.

During the same time step, the model accounts for possible reactions and hydrodynamic dispersion. In template model 2, the total number of cells chosen was 50. This number is always an optimum between model calculation time and smoothness of the output results. The length of the contaminant flow path is therefore defined as SOLUTION 1-50, which specifies the initial chemical composition of all 50 cells (pure water as no solutes are specified). The inflow solution has a value of 0 by definition if the flow direction is forward, i.e., from left to right.

Box 7.5	
SOLUTION 0	
units	umol/kgw
Tce_l	989.2176366
Tce_h	10.78236342
Tce_lll	434.0727372
Tce_llh	139.2181079
Tce_lhl	139.2181079
Tce_hll	139.2181079
Tce_hhl	44.65076917
Tce_hlh	44.65076917
Tce_lhh	44.65076917
Tce_hhh	14.32063124
END	

The inflow solution (see **Box 7.5**) contains ten solutes, which are the two Cisotopes of TCE (Tce_l, Tce_h), where "l" stands for presence of a light C atom (¹²C) and "h" stands for a heavy C atom (¹³C), and the eight C1 isotopologues/isotopomers of TCE (Tce_lll to Tce_hhh), where "l" stands for presence of a light C1 atom (³⁵Cl) and "h" stands for a heavy C1 atom (³⁷Cl). Note: Case 2 uses the C isotope model instead of the C isotopologue model as done for Case 1. As explained in **Section 5.4.3**, the two models give identical results but the isotopologue model is capable of simulating isotope fractionation related to diffusion, which is not possible with the isotope model. Isotope-influenced diffusion might only be relevant at the fringes of thin plumes and is therefore not needed in this case.

The concentrations of these isotopologues follow from the total concentration of the solute (i.e., TCE, 1000 µmol/l) and its isotopic ratio ($\delta^{13}\text{C-TCE} = -30\text{‰}$; $\delta^{37}\text{Cl-TCE} = +3\text{‰}$) by means of the probability mass function (see section 5.4.6 and 'Calculation of Initial Isotope or Isotopologue Concentrations.xls'). The isotopologue concentrations must be specified with a high number of digits (recommended a minimum of six) as the resulting isotope ratio may deviate from the input if too few digits are applied. The model download file contains an Excel spreadsheet 'Calculation of Initial Isotope or Isotopologue Concentrations.xls' where these calculations can be completed for any of the CEs and ETH for their C, H, and Cl isotopic ratios. All these isotopologues are defined and available in the various database files (see below).

Step 3. Simulation of Degradation Processes including Isotope fractionation

The values of the kinetic parameters are defined at the **CALCULATE_VALUES** keyword (see **Box 7.6**). With an inbuilt BASIC subroutine (starting with “-start” and finishing with “-end”), values are assigned parameter names. These parameter names are used as mathematical expressions, which describe the rates of the isotopologue transformation reactions. These are programmed beneath **RATES** in the database file (explained below). For example, parameter TCE_to_cDCE_k_max is assigned a value 1 (per year). Parameter TCE_to_cDCE_k_max is the maximum degradation rate constant for TCE transformation by RD. Another example, TCE_to_cDCE_C_e is the isotopic enrichment factor (ϵ : ϵ) for C isotope fractionation (C) during RD. With a one-line BASIC command (always starting with a number, here 10) the parameter value is assigned to the parameter name. Coding in PHREEQC can be shortened with the use of semi colons interpreted by PHREEQC as a hard return. A complete list of all parameter names and their meaning is presented in 5-7.

Simulating First-order Kinetics with the Monod Model:

For simplicity we like to simulate first-order kinetics but the rate formulations are available as Monod kinetics in the database file Microcosm-C-Cl.dat. Of course we could modify the whole database to simulate first-order kinetics but this will take a lot of time and error checking. A simpler approach is to use the available Monod kinetics but take half-saturation constants much larger than the concentration ranges (i.e., $K_s \gg S$) and then select the k_{max} as follows: $k_1 \approx k_{max}/K_s$, where k_1 is the first-order rate constant (see also **Section 5.4.1**). See **CALCULATE_VALUES**: K_s values of 1 (M) were taken and to achieve first-order rate constants of 1 and 0.5 per year for TCE and DCE, respectively, k_{max} values of 1 and 0.5 M per year, respectively, were adopted.

Box 7.6		
CALCULATE_VALUES		
TCE_to_cDCE_k_max	; -start; 10 SAVE 1	; -end
TCE_to_cDCE_K_Sat	; -start; 10 SAVE 1	; -end
TCE_to_cDCE_lag	; -start; 10 SAVE 0	; -end
TCE_to_cDCE_C_e	; -start; 10 SAVE -16.7	; -end
TCE_to_cDCE_Cl_eKIE	; -start; 10 SAVE -4.2	; -end
TCEtoDCE_SKIE_A	; -start; 10 SAVE -3.3	; -end
TCE_to_cDCE_SKIE_Bt	; -start; 10 SAVE -3.3	; -end

The transformation reactions of the isotopologues are defined with two keywords: **KINETICS** and **RATES**. The stoichiometries of the reactions are defined beneath the **KINETICS** keyword, the mathematical rate equations beneath the **RATES** keyword (listed in the database file). As the present model considers the two C isotopes, two reactions need to be defined (described) for each chlorinated ethene. For example, Tce_l_rd means the transformation of the light (l) Cn isotope of TCE via RD.

With “-formula”, the reaction stoichiometry is defined as being negative for an isotopologue/isotope, which disappears from solution, and the overall rate is a multiplication of this reaction rate times the stoichiometric number, the stoichiometric numbers are positive for species which degraded and negative for species which are produced during the reaction. For this example (**Box 7.7**), “Tce_l” is consumed and both “Dce_l” and “Chl” (Cl-) are produced. A Table with all isotopologue fractionation reactions as programmed for this project can be found in **Table 5-5**.

Box 7.7**KINETICS 5-25**

Tce_l_rd;-formula	Tce_l	1	Chl	-1	Dce_l	-1
Tce_h_rd;-formula	Tce_h	1	Chl	-1	Dce_h	-1

Note different sets of kinetic reactions are specified in this model for two different reactive zones: reductive dechlorination (KINETICS 5-25) between 50-250 m downstream (cells 5-25; cell length = 10 m) followed by oxidative transformation of VC (KINETICS 30-50) between 300-500 m downstream (cells 30-50).

The mathematical formulations for the reaction rates can be found beneath the **RATES** keyword. These reactions can be specified in the input file and/or the database file (the definition stated in the input file will be used if another definition with the same rate name is present in the database file). The rate definitions are all kept in the database file for clarity and to reduce the length of the input files. **Box 7.8** gives an example for the rate definition of “Tce_h_rd”. After the rate name, the rate is defined with BASIC coding in between an “-start” and “-end” command to indicate the beginning and ending of the BASIC code definition. At line 30 the rate of TCE RD is calculated. With calc_value (“TCE_to_cDCE_k_max”) in line 30 the maximum rate constant of TCE RD is obtained from the input file as listed beneath **CALCULATE_VALUES**. As explained in **Section 5**, the degradation rate of the Tce_h isotope (line 50) is a multiplication of the overall TCE rate (line 30: rate), the proportion of the Tce_l with respect to total TCE (line 20: ratio), and the kinetic isotope effect of the reaction (line 40: alpha).

Box 7.8**RATES**

Tce_h_rd

-start

5 Tce_conc = tot("Tce_h")+tot("Tce_l")

10 if sim_time < calc_value("TCE_to_cDCE_lag") then goto 60

15 if Tce_conc < calc_value("dl_all") then goto 60

20 ratio = tot("Tce_h")/Tce_conc

30 rate = -(calc_value("TCE_to_cDCE_k_max")*Tce_conc)/(Tce_conc + calc_value("TCE_to_cDCE_K_Sat"))

40 alpha = ((calc_value("TCE_to_cDCE_C_e")/1000)+1)

50 moles = alpha * rate * ratio * time

60 save moles

-end

Step 4. Simulation of 1-D transport

Beneath the **TRANSPORT** keyword the settings for a 1-D transport simulation are defined.

- Fifty cells were chosen to represent the 1-D flow path for this template model. From the length of the flow path (500 m, not specified), and “-cells” follows the cell length,” – lengths” (10 m).
- From the average groundwater flow velocity along the flow path (must be known; not specified; 20 m/yr) and the cell length, follows the residence time or time_step in a cell (10 m / 20 m/yr = 0.5 yr specified in seconds).

- From the total transport time along the flow path (must be known; not specified) and the time_step, follows the total number of shifts (*i.e.*, time steps; 25 years / 0.5 yr = 50).
- PHREEQC assumes by default the assigned conditions for -flow_direction and -boundary_conditions.
- The -dispersivities (m) must be specified.
- With -punch_frequency, results are only written to the output file with the indicated frequency. When the -punch_frequency equals the number of shift, results are only written to the output file for the last timestep.

Step 5. Creating the output file

The layout of the calculation results output file is specified when **SELECTED_OUTPUT** is selected in combination with **USER_PUNCH**. With **USER_PUNCH**, the concentrations of the chlorinated ethenes are calculated from the sum of their isotopes/isotopologues and multiplied by 1000 to convert from mol (“tot” gives total concentration in mol/kg water) to mmol/l. With the punch command the results are printed to the output file. BASIC coding language is used as for the KINETICS keyword.

The isotope ratios are calculated at the end from the relative concentrations of the isotopologues/isotopes and the international standards ($C_{13}/C_{12} = 0.011237$; $C_{37}/C_{35} = 0.319766$). Isotope ratios are not calculated when total concentrations are very low ($\ll 1e-7$ of source concentration) as numerical errors produce unrealistic isotope ratios. In that case the value -9999 is printed, which can be replaced with a non-available number, NaN, in graphing programs. **Section 5.4.7** explains in detail how isotope ratios are calculated from the absolute concentrations of the isotopes/isotopologues.

Step 6. Running the PHREEQC template model

The Case 2 template input file is ready to run. To run the model, follow the substeps below:

- Select the Microcosm-C-Cl.dat database with Calculations > Files > Browse for database file. See Case 1 (**Section 7.2**) for the other steps.

Step 7: Visualization

See Case 1 (**Section 7.2**) for visualization. Case2.py in folder Case2 can be used to display the model results with Python. The explanation of the results is given in **Section 4.2.2**.

7.3 Template Model Case 3: Core Reductive Dechlorination and Fringe Oxidation (C&Cl-CSIA)

This guidance only briefly introduces the template models of Example Scenario Case 3. Only the differences with respect to the PHAST model of Case 1 will be discussed and how the PHT3D model evolved out of the PHAST model.

7.3.1 PHAST 2-D Model

With respect to the explanation of the PHAST model for Example Scenario Case 1 the following differences are relevant:

- All database information (SOLUTION_MASTER_SPECIES, SOLUTION_SPECIES, RATES) was placed in the Case3.chem.dat file instead of in a separate database file. To run the model the general phast database phast.dat should be used.
- Whereas the PHAST model of Case 1 used the CALCULATE_VALUES PHREEQC keyword to define all model parameter values, the PHAST model of Case 3 defined the parameter values with the setting '-parms' at the KINETICS keyword. The values after '-parms' agree with specific model parameters which are codes in the rate definitions beneath the RATES keyword at the end of the Case3.chem.dat file. The meaning of the parameter values beneath KINETICS is explained with comments after hatch signs. This procedure was done in this case as the complete database part of the file was also incorporated in the PHT3D database file. Thus in order to change model parameter values in this file take care to keep parameter values equal for each set of reactions simulating a specific process.
- Cl isotope fractionation does not include SKIEs; the user needs to specify bulk Cl isotope enrichment factors for the reactions.
- The Case3.trans.dat file is almost equal to the one used for Case 1.
- After running the model (see explanation of Case 1), the model results (PHASTmodelResult.png) can be plotted with the plot2DPHAST_Case3.py python script.

7.3.2 PHT3D 2-D Model

The user who wishes to apply the PHT3D version of the model should first get acquainted with PHT3D. We recommend reading the PHT3D user's manual (at www.pht3d.org) and use of PMWIN as GUI of PHT3D (www.simcore.com). An excellent textbook introducing modelling with PMWIN is "3D-Groundwater Modeling with PMWIN" by Wen-Hsing Chiang, 2nd edition, 2005, 397 p, Springer.

The two relevant PHT3D files are available in the model download file in the Case 3 folder. Note these two text files have the extension Case3 but they can be opened with any text editor.

The PHAST model files were changed into PHT3D model files as follows:

- PHT3D database file pht3d_datab.Case3: the only difference compared with a PHAST database file is the addition of the names of the kinetic reactions as SOLUTION_MASTER_SPECIES and SOLUTION_SPECIES to the database.
- PHT3D database file pht3d_datab.Case3: parameter values are retrieved with parm(n) in the rate formulations beneath the RATES keyword. The parameter values are defined in the PHT3D input file (see below).
- PHT3D input file pmwin_pht3dv210.Case3: The processes are simulated as immobile kinetic components [Component_immobile_kinetic], while all solutes are considered mobile equilibrium components [Component_mobile_equilibrium]. Also the process name must be part of the reaction stoichiometry (with number 0). However, as in PHT3D the processes in PHREEQC/PHAST become species, the process name should start with a capital only followed by lowercase letters. All subsequent upper case letters in the PHREEQC/PHAST process names were changed to lowercase with the search and replace function of the text editor.

- PHT3D input file pmwin_pht3dv210.Case3: the values of the rate parameters are listed beneath each other at each process. Thus in order to change model parameter values in this file take care to keep parameter values equal for each set of reactions simulating a specific process.

7.4 Template Model Case 4: Hydrogen Isotope Fractionation During Reductive Dechlorination of PCE/TCE

The PHREEQC template model of Example Scenario Case 4 is available as Case4.phrq in folder Case 4 and needs the Microcosm-C-Cl-H-PCE-ETH.dat database file to run. The input file of Case 4 is generally similar as the one of Case 1 or 2 with the exception that H instead of C isotope fractionation is simulated in this case. The following key differences compared to the template files of Case 1 or 2 are explained below.

Box 7.9	
SOLUTION 0	
units	umol/kgw
Tce_h_l	499.8832148
Tce_h_h	0.116785216
Pce	500

Box 7.9 presents the source composition defined as SOLUTION 0 in the model input file of the fourth scenario as discussed in **Section 4.2.4**. Tce_h_l and Tce_h_h are the light and heavy H isotope species of TCE, respectively. They sum to 500 $\mu\text{mol/l}$ and their absolute concentrations were calculated with ‘Calculation of Initial Isotope or Isotopologue Concentrations.xls’ as explained in **Section 5.4.6**. As PCE does not contain H atoms, H isotopic species for PCE are logically not defined. To simulate PCE degradation and associated TCE formation, PCE can be included as the species “Pce”.

Parameter names of the degradation rate constants are identical as for Case 2. Different are the isotope fractionation effects associated with H isotope fractionation. These are explained in **Section 5.4.5** and **Table 5-7**. The set of kinetic reactions that follows beneath KINETICS 1-60 is explained in **Section 5.4.5** and in **Table 5-5**, cf. reaction sets 312A-315A.

REFERENCES

- Abe, Y., R. Aravena, J. Zopfi, O. Shouakar-Stash, E. Cox, J. D. Roberts and D. Hunkeler (2009). "Carbon and Chlorine Isotope Fractionation during Aerobic Oxidation and Reductive Dechlorination of Vinyl Chloride and cis-1,2-Dichloroethene." Environmental Science & Technology **43**(1): 101-107.
- Abe, Y. and D. Hunkeler (2006). "Does the Rayleigh Equation Apply to Evaluate Field Isotope Data in Contaminant Hydrogeology?" Environ. Sci. Technol. **40**(5): 1588-1596.
- Adamson, D. T. and C. J. Newell (2014). Frequently Asked Questions about Monitored Natural Attenuation in Groundwater. Arlington, Virginia, Environmental Security and Technology Certification Program.
- Ader, M., S. Chadhuri, J. D. Coates and M. Coleman (2008). "Microbial perchlorate reduction: A precise laboratory determination of the chlorine isotope fractionation and its possible biochemical basis." Earth and Planetary Science Letters **269**: 605-613.
- Aeppli, C., M. Berg, O. A. Cirpka, C. Holliger, R. P. Schwarzenbach and T. B. Hofstetter (2009). "Influence of Mass-Transfer Limitations on Carbon Isotope Fractionation during Microbial Dechlorination of Trichloroethene." Environmental Science & Technology **43**(23): 8813-8820.
- Aeppli, C., T. B. Hofstetter, H. I. F. Amaral, R. Kipfer, R. P. Schwarzenbach and M. Berg (2010). "Quantifying In Situ Transformation Rates of Chlorinated Ethenes by Combining Compound-Specific Stable Isotope Analysis, Groundwater Dating, And Carbon Isotope Mass Balances." Environmental Science & Technology **44**(10): 3705-3711.
- AFCEE (2007). AFCEE Source Zone Initiative, Air Force Center for Environmental Excellence.
- Alvarez-Cohen, L. and G. E. Speitel, Jr. (2001). "Kinetics of aerobic cometabolism of chlorinated solvents." Biodegradation **12**(2): 105-126.
- Amos, B. K., K. M. Ritalahti, C. Cruz-Garcia, E. Padilla-Crespo and F. E. Löffler (2008). "Oxygen Effect on Dehalococcoides Viability and Biomarker Quantification." Environmental Science & Technology **42**(15): 5718-5726.
- Arp, D. J., C. M. Yeager and M. R. Hyman (2001). "Molecular and cellular fundamentals of aerobic cometabolism of trichloroethylene." Biodegradation **12**(2): 81-103.
- ASTM (2008). Standard Guide for Developing Conceptual Site Models for Contaminated Sites¹.
- Atteia, O., M. Franceschi and A. Dupuy (2008). "Validation of reactive model assumptions with isotope data: Application to the Dover case." Environmental Science & Technology **42**(9): 3289-3295.
- Barth, J. A., G. F. Slater, C. Schuth, M. Bill, D. C. Downey, M. Larkin and R. M. Kalin (2002). "Carbon isotope fractionation during aerobic biodegradation of trichloroethene by Burkholderia cepacia G4: a tool to map degradation mechanisms." Applied and Environmental Microbiology **68**(4): 1728-1734.
- Bloom, Y., R. Aravena, D. Hunkeler, E. Edwards and S. K. Frape (2000). "Carbon isotope fractionation during microbial dechlorination of trichloroethene, cis-1,2-dichloroethene and vinyl chloride: Implications for assessment of natural attenuation." Environmental Science and Technology **34**(13): 2768-2772.
- Bouchard, D., P. Höhener and D. Hunkeler (2008). "Carbon Isotope Fractionation During Volatilization of Petroleum Hydrocarbons and Diffusion Across a Porous Medium: A Column Experiment." Environmental Science & Technology **42**(21): 7801-7806.
- Bouchard, D., D. Hunkeler, P. Gaganis, R. Aravena, P. Höhener, M. M. Broholm and P. Kjeldsen (2008). "Carbon Isotope Fractionation during Diffusion and Biodegradation of Petroleum

- Hydrocarbons in the Unsaturated Zone: Field Experiment at Værløse Airbase, Denmark, and Modeling." Environmental Science & Technology **42**(2): 596-601.
- Boving, T. B. and P. Grathwohl (2001). "Tracer diffusion coefficients in sedimentary rocks: correlation to porosity and hydraulic conductivity." Journal of Contaminant Hydrology **53**(1-2): 85-100.
- Bradley, P. M. and F. H. Chapelle (1997). "Kinetics of DCE and VC Mineralization under Methanogenic and Fe(III)-Reducing Conditions." Environmental Science & Technology **31**(9): 2692-2696.
- Bradley, P. M. and F. H. Chapelle (2000). "Aerobic Microbial Mineralization of Dichloroethene as Sole Carbon Substrate." Environmental Science and Technology **34**(1): 221-223.
- CH2MHILL (2007). Aquifer Age Dating and Well Screen Profiling for Shallow and Deep Groundwater Plumes, Operable Unit 10, Hill AFB, Utah. Hill AFB, Utah, CH2M Hill for USAF.
- CH2MHILL (2009). Groundwater Flow and Transport Model Documentation. Salt Lake City, UT, AFCEE and the Environmental Management Division (75 CEG/CEVR) Hill Air Force Base, Utah.
- CH2MHILL (2009). Operable Unit 10 Remedial Investigation Report. Salt Lake City, UT, CH2M Hill for Air Force Center for Engineering and the Environment and Hill Air Force Base, Utah. CH2MHILL (2011). Hill AFB OU10 ERPIMS Database. C. M. f. U. A. Force.
- Chang, H. L. and L. Alvarez-Cohen (1996). "Biodegradation of individual and multiple chlorinated aliphatic hydrocarbons by methane-oxidizing cultures." Applied and Environmental Microbiology **62**(9): 3371-3377.
- Chapelle, F. H., M. A. Widdowson, S. J. Brauner, E. Mendez and C. C. Casey (2003). Methodology for Estimating Times of Remediation Associated with Monitored Natural Attenuation. Columbia, S.C., U. S. Geological Survey (USGS): 58.
- Chapman, S. W. and B. L. Parker (2005). "Plume persistence due to aquitard back diffusion following dense nonaqueous phase liquid source removal or isolation." Water Resources Research **41**(12): W12411(12411-12416).
- Charbeneau, R. J. (2000). Groundwater Hydraulics and Pollutant Transport. Upper Saddle River, NJ, Prentice Hall.
- Chen, W., K. Lakshmanan, A. T. Kan and M. B. Tomson (2004). "A Program for Evaluating Dual-Equilibrium Desorption Effects on Remediation." Ground Water **42**(4): 620-624.
- Chu, K.-H., S. Mahendra, D. L. Song, M. E. Conrad and L. Alvarez-Cohen (2004). "Stable carbon isotope fractionation during aerobic biodegradation of chlorinated ethenes." Environmental Science and Technology **38**(11): 3126-3130.
- Cretnik, S., K. A. Thoreson, A. Bernstein, K. Ebert, D. Buchner, C. Laskov, S. Haderlein, O. Shouakar-Stash, S. Kliegman, K. McNeill and M. Elsner (2013). "Reductive Dechlorination of TCE by Chemical Model Systems in Comparison to Dehalogenating Bacteria: Insights from Dual Element Isotope Analysis (13C/12C, 37Cl/35Cl)." Environmental Science & Technology **47**(13): 6855-6863.
- D'Affonseca, F. M., H. Prommer, M. Finkel, P. Blum and P. Grathwohl (2011). "Modeling the long-term and transient evolution of biogeochemical and isotopic signatures in coal tar-contaminated aquifers." Water Resources Research **47**.
- Damgaard, I., P. L. Bjerg, J. Bælum, C. Scheutz, D. Hunkeler, C. S. Jacobsen, N. Tuxen and M. M. Broholm (2013). "Identification of chlorinated solvents degradation zones in clay till

- by high resolution chemical, microbial and compound specific isotope analysis." Journal of Contaminant Hydrology **146**(0): 37-50.
- DeBruin, W. P., M. J. Kotterman, M. A. Posthumus, G. Schraa and A. J. Zehnder (1992). "Complete biological reductive transformation of tetrachloroethene to ethane." Applied and Environmental Microbiology **58**(6): 1996-2000.
- DoD (2009). DoD Vapor Intrusion Handbook. Washington, D.C., Department of Defense, Tri-Service Environmental Risk Assessment Workgroup: 171.
- Dorer, C., P. Höhener, N. Hedwig, H.-H. Richnow and C. Vogt (2014). "Rayleigh-Based Concept to Tackle Strong Hydrogen Fractionation in Dual Isotope Analysis—The Example of Ethylbenzene Degradation by *Aromatoleum aromaticum*." Environmental Science & Technology **48**(10): 5788-5797.
- Eckert, D., S. Qiu, M. Elsner and O. A. Cirpka (2013). "Model Complexity Needed for Quantitative Analysis of High Resolution Isotope and Concentration Data from a Toluene-Pulse Experiment." Environmental Science & Technology **47**(13): 6900-6907.
- Eklund, B., L. Beckley, V. Yates and T. E. McHugh (2012). "Overview of State Approaches to Vapor Intrusion." Remediation Autumn 2012: 7-20.
- Elsner, M., M. Chartrand, N. VanStone, G. Lacrampe Couloume and B. Sherwood Lollar (2008). "Identifying Abiotic Chlorinated Ethene Degradation: Characteristic Isotope Patterns in Reaction Products with Nanoscale Zero-Valent Iron." Environmental Science & Technology **42**(16): 5963-5970.
- Elsner, M., L. Zwank, D. Hunkeler and R. P. Schwarzenbach (2005). "A new concept linking observable stable isotope fractionation to transformation pathways of organic pollutants." Environmental Science and Technology **39**(18): 6896-6916.
- Ertle, S., L. Eichinger, F. H. Frimmel and A. Kettrup (1998). "The $^{13}\text{C}/^{12}\text{C}$ and $2\text{H}/1\text{H}$ Ratios of Trichloroethene, Tetrachloroethene and Their Metabolites." Isotopes in Environmental and Health Studies **34**(3): 245-253.
- Farhat, S. K., C. J. Newell and E. Nichols (2006). Mass Flux Toolkit. Houston, Texas, GSI Environmental: Freeware.
- Farhat, S. K., C. J. Newell, T. C. Sale, D. S. Dandy, J. J. Wahlberg, M. A. Seyedabbasi, J. M. McDade and N. T. Mahler (2012). Matrix Diffusion Toolkit. E. S. T. C. Program. Arlington, Virginia, Developed for the Environmental Security Technology Certification Program (ESTCP) by GSI Environmental Inc., Houston, Texas.
- Fetter, C. W. (1993). Contaminant Hydrogeology. New York, NY, Macmillan Publishing.
- Fischer, A., I. Herklotz, S. Herrmann, M. Thullner, S. A. B. Weelink, A. J. M. Stams, M. Schlömann, H.-H. Richnow and C. Vogt (2008). "Combined Carbon and Hydrogen Isotope Fractionation Investigations for Elucidating Benzene Biodegradation Pathways." Environmental Science & Technology **42**(12): 4356-4363.
- Freedman, D. L. and J. M. Gossett (1989). "Biological reductive dechlorination of tetrachloroethylene and trichloroethylene to ethylene under methanogenic conditions." Applied and Environmental Microbiology **55**(9): 2144.
- Galimov, E. M. (1985). The Biological Fractionation of Isotopes. Orlando, Academic Press / Harcourt Brace Jovanovich.
- Gorder, K. and C. Hobert (2010). Thiessen Area and Mass Calculator for Assessment of Plume Dynamics. Remediation of Chlorinated and Recalcitrant Compounds: Seventh International Conference on Remediation of Chlorinated and Recalcitrant Compounds, Monterey, CA, Battelle Memorial Institute.

- Habets-Crutzen, A. Q. H., L. E. S. Brink, C. G. vanGinkel, J. A. M. deBont and J. Tramper (1984). "Production of epoxide from gaseous alkenes by resting-cell suspensions and immobilized cells of alkene-utilizing bacteria." Applied Microbiology and Biotechnology **20**: 245-250.
- Hartmans, S. and J. A. DeBont (1992). "Aerobic vinyl chloride metabolism in *Mycobacterium aurum* L1." Applied and Environmental Microbiology **58**(4): 1220-1226.
- Hedges, J. I., W. A. Clark and G. L. Cowie (1988). "Organic matter sources to the water column and surficial sediments of a marine bay." Limnol. Oceanogr. **33**(5): 1116-1136.
- Hofstetter, T. B., C. M. Reddy, L. J. Heraty, M. Berg and N. C. Sturchio (2007). "Carbon and chlorine isotope effects during abiotic reductive dechlorination of polychlorinated ethanes." Environmental Science & Technology **41**(13): 4662-4668.
- Hunkeler, D., Y. Abe, M. M. Broholm, S. Jeannotat, C. Westergaard, C. S. Jacobsen, R. Aravena and P. L. Bjerg (2011). "Assessing chlorinated ethene degradation in a large scale contaminant plume by dual carbon–chlorine isotope analysis and quantitative PCR." Journal of Contaminant Hydrogeology **119**: 69-79.
- Hunkeler, D., R. Aravena and B. J. Butler (1999). "Monitoring Microbial Dechlorination of Tetrachlorethene (PCE) in Groundwater Using Compound-Specific Stable Carbon Isotope Ratios: Microcosm and Field Studies." Environmental Science and Technology **33**(16): 2733-2738.
- Hunkeler, D., R. Aravena and E. Cox (2002). "Carbon isotopes as a tool to evaluate the origin and fate of vinyl chloride: Laboratory experiments and modeling of isotope evolution." Environmental Science and Technology **36**(15): 3378-3384.
- Hunkeler, D., N. Chollet, X. Pittet, R. Aravena, J. A. Cherry and B. L. Parker (2004). "Effect of source variability and transport processes on carbon isotope ratios of TCE and PCE in two sandy aquifers." Journal of Contaminant Hydrogeology **74**(1-4): 265-282.
- Hunkeler, D., R. U. Meckenstock, B. S. Lollar, T. C. Schmidt and J. T. Wilson (2008). A Guide for Assessing Biodegradation and Source Identification of Organic Ground Water Contaminants using Compound Specific Isotope Analysis (CSIA). USEPA. Washington, DC, US Environmental Protection Agency Office of Research and Development National Risk Management Laboratory: 82.
- Hunkeler, D., B. M. Van Breukelen and M. Elsner (2009). "Modeling Chlorine Isotope Trends during Sequential Transformation of Chlorinated Ethenes." Environmental Science & Technology **43**(17): 6750-6756.
- ITRC. (2013). "Environmental Molecular Diagnostics." Retrieved June 30, 2014, 2014, from http://www.itrcweb.org/emd-2/#Welcome.htm%3FTocPath%3D_____1.
- Jeannotat, S. and D. Hunkeler (2012). "Chlorine and Carbon Isotopes Fractionation during Volatilization and Diffusive Transport of Trichloroethene in the Unsaturated Zone." Environmental Science & Technology **46**(6): 3169-3176.
- Jin, B. and M. Rolle (2014). "Mechanistic approach to multi-element isotope modeling of organic contaminant degradation." Chemosphere **95**: 131-139.
- Jin, B., M. Rolle, T. Li and S. B. Haderlein (2014). "Diffusive Fractionation of BTEX and Chlorinated Ethenes in Aqueous Solution: Quantification of Spatial Isotope Gradients." Environmental Science & Technology **48**(11): 6141-6150.
- Karlsen, R. H., F. J. C. Smits, P. J. Stuyfzand, T. N. Olsthoorn and B. M. Van Breukelen (2012). "A post audit and inverse modeling in reactive transport: 50 years of artificial recharge in the Amsterdam Water Supply Dunes." Journal of Hydrology **454**: 7-25.

- Kelley, C. A., B. T. Hammer and R. B. Coffin (1997). "Concentrations and Stable Isotope Values of BTEX in Gasoline-Contaminated Groundwater." Environmental Science & Technology **31**(9): 2469-2472.
- Klier, N. J., R. J. West and P. A. Donberg (1999). "Aerobic biodegradation of dichloroethylenes in surface and subsurface soils." Chemosphere **38**(5): 1175-1188.
- Kopinke, F.-D., A. Georgi, M. Voskamp and H. H. Richnow (2005). "Carbon Isotope Fractionation of Organic Contaminants Due to Retardation on Humic Substances: Implications for Natural Attenuation Studies in Aquifers." Environmental Science & Technology **39**(16): 6052-6062.
- Kuder, T. and P. Philp (2013b). "Demonstration of Compound-Specific Isotope Analysis of Hydrogen Isotope Ratios in Chlorinated Ethenes." Environmental Science & Technology **47**(3): 1461-1467.
- Kuder, T., P. Philp and J. Allen (2009). "Effects of Volatilization on Carbon and Hydrogen Isotope Ratios of MTBE." Environmental Science & Technology **43**(6): 1763-1768.
- Kuder, T., B. M. van Breukelen, M. Vanderford and P. Philp (2013). "3D-CSIA: Carbon, Chlorine, and Hydrogen Isotope Fractionation in Transformation of TCE to Ethene by a Dehalococcoides Culture." Environmental Science & Technology **47**(17): 9668-9677.
- Kuder, T., P. K. Wilson, R. Kolhatkar, P. Philp and J. Allen (2005). "Enrichment of stable carbon and hydrogen isotopes during anaerobic degradation of MTBE: microcosm and field evidence." Environmental Science and Technology **39**(1): 213-220.
- LaBolle, E. M., G. E. Fogg, J. B. Eweis, J. Gravner and D. G. Leaist (2008). "Isotopic fractionation by diffusion in groundwater." Water Resources Research **44**(7): W07405.
- Liang, X., Y. Dong, T. Kuder, L. R. Krumholz, R. P. Philp and E. C. Butler (2007). "Distinguishing Abiotic and Biotic Transformation of Tetrachloroethylene and Trichloroethylene by Stable Carbon Isotope Fractionation." Environ. Sci. Technol. **41**(20): 7094-7100.
- Liu, C. and W. P. Ball (2002). "Back Diffusion of Chlorinated Solvent Contaminants from a Natural Aquitard to a Remediated Aquifer Under Well-Controlled Field Conditions: Predictions and Measurements." Ground Water **40**(2): 175-184.
- Lollar, B. S., G. F. Slater, J. Ahad, B. Sleep, J. Spivack, M. Brennan and P. MacKenzie (1999). "Contrasting carbon isotope fractionation during biodegradation of trichloroethylene and toluene: Implications for intrinsic bioremediation." Organic Geochemistry **30**: 813-820.
- Lollar, B. S., G. F. Slater, B. Sleep, M. Witt, G. M. Klecka, M. Harkness and J. Spivack (2001). "Stable Carbon Isotope Evidence for Intrinsic bioremediation of tetrachloroethene and trichloroethene at Area 6, Dover Air Force Base." Environmental Science and Technology **35**(2): 261-269.
- Lutz, S. R. and B. M. Van Breukelen (2014). "Combined Source Apportionment and Degradation Quantification of Organic Pollutants with CSIA: 1. Model Derivation." Environmental Science & Technology **48**(11): 6220-6228.
- Lutz, S. R. and B. M. Van Breukelen (2014). "Combined Source Apportionment and Degradation Quantification of Organic Pollutants with CSIA: 2. Model Validation and Application." Environmental Science & Technology **48**(11): 6229-6236.
- Mancini, S. A., A. C. Ulrich, G. Lacrampe-Couloume, B. Sleep, E. A. Edwards and B. S. Lollar (2003). "Carbon and hydrogen isotopic fractionation during anaerobic biodegradation of benzene." Applied and Environmental Microbiology **69**(1): 191-198.

- Marco-Urrea, E., X. Gabarrell, G. Caminal, T. Vicent and C. Reddy (2008). "Aerobic degradation by white-rot fungi of trichloroethylene (TCE) and mixtures of TCE and perchloroethylene (PCE)." Journal of Chemical Technology and Biotechnology **83**: 1190-1196.
- McCarty, P. L. (1996). Biotic and abiotic transformations of chlorinated solvents in ground water. Symposium on Natural Attenuation of Chlorinated Organics in Ground Water, USEPA 540/R-96/509.
- McHugh, T., T. Kuder, S. Fiorenza, K. Gorder, E. Dettenmaier and P. Philp (2011). "Application of CSIA to Distinguish Between Vapor Intrusion and Indoor Sources of VOCs." Environmental Science & Technology **45**(14): 5952-5958.
- McRae, C., C. G. Sun, C. E. Snape, A. E. Fallick and D. Taylor (1999). "d13C values of coal-derived PAHs from different processes and their application to source appointment." Organic Geochemistry **30**: 881-889.
- Mundle, S. O. C., T. Johnson, G. L. Couloume, A. Perez-de-Mora, M. Duhamel, E. A. Edwards, M. L. McMaster, E. Cox, K. Revesz and B. S. Lollar (2012). "Monitoring Biodegradation of Ethene and Bioremediation of Chlorinated Ethenes as a Contaminated Site Using Compound-Specific Isotope Analysis (CSIA)." Environmental Science & Technology **46**(3): 1731-1738.
- Newell, C. J., D. T. Adamson, B. L. Parker, S. W. Chapman and T. C. Sale (2013). Final Report: Determining Source Attenuation History to Support Closure by Natural Attenuation. E. S. T. C. P. (ESTCP). Washington, D.C., Environmental Security Technology Certification Program (ESTCP).
- Newell, C. J., K. R. McLeod and J. R. Gonzales (1996). Bioscreen Natural Attenuation Decision Support System. San Antonio, TX, Air Force Center for Environmental Excellence.
- Newell, C. J., H. S. Rifai, J. T. Wilson, J. A. Connor, J. A. Aziz and M. P. Suarez (2002). Calculation and use of first-order rate constants for monitored natural attenuation studies. Washington, D.C., US Environmental Protection Agency: 27.
- NJDEP (2012). Monitored Natural Attenuation Technical Guidance. Trenton, NJ, New Jersey Department of Environmental Protection
- NRC (2012). Alternatives for Managing the Nation's Complex Contaminated Groundwater Sites. Washington, D.C., The National Academies Press.
- O'Leary, M. H. (1984). "Measurement of the isotope fractionation associated with diffusion of carbon dioxide in aqueous solution." The Journal of Physical Chemistry **88**(4): 823-825.
- Parkhurst, D. L. and C. A. H. Appelo (1999). Users Guide to PHREEQ (Version 2) -- A computer program for speciation, Batch-Reaction, One-Dimensional Transport and Inverse Geochemical Calculations. Denver, CO, US Department of Interior, US Geological Survey.
- Pignatello, J. J. and B. Xing (1996). "Mechanisms of slow sorption of organic chemicals to natural particles." Environmental Science and Technology **30**(1): 1-11.
- Pooley, K. E., M. Blessing, T. C. Schmidt, S. B. Haderlein, K. T. B. Macquarrie and H. Prommer (2009). "Aerobic Biodegradation of Chlorinated Ethenes in a Fractured Bedrock Aquifer: Quantitative Assessment by Compound-Specific Isotope Analysis (CSIA) and Reactive Transport Modeling." Environmental Science & Technology **43**: 7458-7464.
- Prommer, H., B. Anneser, M. Rolle, F. Einsiedl and C. Griebler (2009). "Biogeochemical and Isotopic Gradients in a BTEX/PAH Contaminant Plume: Model-Based Interpretation of a High-Resolution Field Data Set." Environmental Science & Technology **43**(21): 8206-8212.

- Puls, R. W. and M. Barcelona (1996). Low-flow (Minimal Drawdown) Groundwater Sampling Procedures. Washington D.C., USEPA: 12.
- Qiu, S., D. Eckert, O. A. Cirpka, M. Huenniger, P. Knappett, P. Maloszewski, R. U. Meckenstock, C. Griebler and M. Elsner (2013). "Direct Experimental Evidence of Non-first Order Degradation Kinetics and Sorption-Induced Isotopic Fractionation in a Mesoscale Aquifer: C-13/C-12 Analysis of a Transient Toluene Pulse." Environmental Science & Technology **47**(13): 6892-6899.
- Rolle, M., G. Chiogna, R. Bauer, C. Griebler and P. Grathwohl (2010). "Isotopic Fractionation by Transverse Dispersion: Flow-Through Microcosms and Reactive Transport Modeling Study." Environmental Science & Technology **44**: 6167-6173.
- Ryoo, D., H. Shim, K. Canada, P. Barbieri and T. K. Wood (2000). "Aerobic degradation of tetrachloroethylene by toluene-o-xylene monooxygenase of *Pseudomonas stutzeri* OX1." Nature America **18**: 775-778.
- Sakaguchi-Soder, K., J. Jager, H. Grund, F. Mattaus and C. Schuth (2007). "Monitoring and evaluation of dechlorination processes using compound-specific chlorine isotope analysis." Rapid Communications in Mass Spectrometry **21**(18): 3077-3084.
- Sessions, A. L. (2006). "Isotope-ratio detection for gas chromatography." Journal of Separation Science **29**(12): 1946-1961.
- Shouakar-Stash, O., S. K. Frape and R. J. Drimmie (2003). "Stable hydrogen, carbon and chlorine isotope measurements of selected chlorinated organic solvents." Journal of Contaminant Hydrology **60**: 211-228.
- Stelzer, N., G. Imfeld, M. Thullner, J. Lehmann, A. Poser, H.-H. Richnow and I. Nijenhuis (2009). "Integrative approach to delineate natural attenuation of chlorinated benzenes in anoxic aquifers." Environmental Pollution **157**(6): 1800-1806.
- Takeuchi, M., Y. Kawabe, E. Watanabe, T. Oiwa, M. Takahashi, K. Nanba, Y. Kamagata, S. Hanada, Y. Ohko and T. Komai (2011). "Comparative study of microbial dechlorination of chlorinated ethenes in an aquifer and a clayey aquitard." Journal of Contaminant Hydrology **124**(1-4): 14-24.
- Truex, M. J., C. J. Newell, B. B. Looney and K. M. Vangelas (2007). Scenarios Evaluation Tool for Chlorinated Solvent MNA. Aiken, S.C., Savannah River National Laboratory: 194.
- USEPA (1998). Technical Protocol for Evaluating Natural Attenuation of Chlorinated Solvents in Ground Water. Washington DC, US Environmental Protection Agency.
- USEPA (1999). Use of Monitored Natural Attenuation at Superfund, RCRA Corrective Action, and Underground Storage Tank Sites. Washington, D.C., United States Environmental Protection Agency.
- USEPA (2011). Environmental Cleanup Best Management Practices: Effective Use of the Project Life Cycle Conceptual Site Model. Washington, D.C., US Environmental Protection Agency.
- USGS (2003). Methodology for Estimating Times of Remediation Associated with Monitored Natural Attenuation, U.S. Department of Interior, U.S. Geological Survey.
- Van Breukelen, B. M., D. Hunkeler and F. Volkering (2005). "Quantification of Sequential Chlorinated Ethene Degradation by Use of a Reactive Transport Model Incorporating Isotope Fractionation." Environmental Science and Technology **39**(11): 4189 - 4197.
- Van Breukelen, B. M. and H. Prommer (2008). "Beyond the Rayleigh equation: Reactive transport modeling of isotope fractionation effects to improve quantification of biodegradation." Environmental Science & Technology **42**(7): 2457-2463.

- Van Breukelen, B. M. and M. Rolle (2012). "Transverse Hydrodynamic Dispersion Effects on Isotope Signals in Groundwater Chlorinated Solvents' Plumes." Environmental Science & Technology **46**(14): 7700-7708.
- Vanderford, M. (2010). "A Comprehensive Approach to Plume Stability." Remediation Winter 2010: 21-37.
- Verce, M. F., C. K. Gunsch, A. S. Danko and D. L. Freedman (2002). "Cometabolism of cis-1,2-dichloroethene by aerobic cultures grown on vinyl chloride as the primary substrate." Environmental Science and Technology **36**(10): 2171-2177.
- Vogel, T. M. and P. L. McCarty (1985). "Biotransformation of Tetrachloroethylene to Trichloroethylene, Dichloroethylene, Vinyl Chloride, and Carbon Dioxide under Methanogenic Conditions." Applied and Environmental Microbiology **49**(5): 1080-1083.
- Vogel, T. M. and P. L. McCarty (1987). "Abiotic and biotic transformations of 1,1,1-Trichloroethane under Methanogenic Conditions." Environmental Science and Technology **21**(12): 1208-1213.
- Wiedemeier, T. H., H. S. Rifai, C. J. Newell and J. T. Wilson (1999). Natural Attenuation of Fuels and Chlorinated Solvents in the Subsurface. New York, John Wiley and Sons, Inc.
- Wiegert, C., C. Aeppli, T. Knowles, H. Holmstrand, R. Evershed, R. D. Pancost, J. Macháčková and Ö. Gustafsson (2012). "Dual Carbon–Chlorine Stable Isotope Investigation of Sources and Fate of Chlorinated Ethenes in Contaminated Groundwater." Environmental Science & Technology **46**(20): 10918-10925.
- Wilson, J. T. (2011). Applications of Monitored Natural Attenuation in the USA 2011 International Conference on Groundwater Contamination and Water System Security, Beijing, China
- Xu, M. and Y. Eckstein (1995). "Use of Weighted Least-squares Method in Evaluation fo the Relationship Between Dispersivity and Field Scale." Ground Water **33**(6): 905 - 908.
- Zenker, M. J., R. C. Borden and M. A. Baralaz (2003). "Occurrence and Treatment of 1,4-Dioxane in Aqueous Environments." Environmental Engineering Science **20**(5): 423-432.
- Zhang, T. and B. M. Krooss (2001). "Experimental investigation on the carbon isotope fractionation of methane during gas migration by diffusion through sedimentary rocks at elevated temperature and pressure." Geochimica et Cosmochimica ACTA **65**(16): 2723-2742.
- Zwank, L., M. Berg, M. Elsner, T. C. Schmidt, R. P. Schwarzenbach and S. B. Haderlein (2005). "New Evaluation Scheme for Two-Dimensional Isotope Analysis to Decipher Biodegradation Processes: Application to Groundwater Contamination by MTBE." Environ. Sci. Technol. **39**(4): 1018-1029.

APPENDICES

APPENDIX A: CASE STUDY

1.0 OVERVIEW

The overall objective of the work proposed for ESTCP ER-201029 was to develop methodologies to reduce the uncertainty associated with the field application of Compound-Specific Stable Isotope Analysis (CSIA) to sites with chlorinated ethene (CE) contamination in groundwater. CSIA is a potentially powerful tool to refine conceptual site models (CSMs) by identifying the sources and fate of contaminants released to groundwater. Existing evidence has indicated that CSIA can provide data to support and quantify mass destruction of chlorinated solvents in the subsurface, supporting MNA remedies. However, interpretation of field-scale results can be difficult due to variability in data and complex flow and transport conditions in situ.

The specific goal of this project is to perform field validation of a reactive transport model (RTM) approach for improved interpretation of CSIA data in support of monitored natural attenuation (MNA) remedies. CSIA with RTM results in an improvement to CSMs by 1) identifying prevalent degradation pathways; 2) distinguishing non-destructive contaminant sinks such as sorption, dilution or volatilization from biological mass destruction; 3) localizing areas of strong degradation processes within the plume; 4) demonstrating and facilitating more accurate assessment of the rate and extent of degradation of the parent contaminant, and 5) allowing quantitative assessment of the net degradation/accumulation of the dechlorination intermediates.

The field site chosen to demonstrate CSIA with RTM was Operable Unit 10 (OU 10) at Hill Air Force Base in Utah (USA). Hill AFB is located in northern Utah, approximately 25 miles north of Salt Lake City and five miles south of Ogden, Utah, just west of the Wasatch Front mountain range (CH₂MHILL, 2009). The Base occupies approximately 6,700 acres in Davis and Weber counties. The land use west of Hill AFB is entirely urban, whereas the north and southeast sides are mostly rural. The Base is surrounded by the incorporated towns of South Weber, Washington Terrace, Riverdale, Roy, Sunset, Clearfield, and Layton.

The Site has over 100 groundwater monitoring locations screened at various depths. Site monitoring began in 1995 with semiannual sampling since 2002. The OU10 site was chosen for the case study due to the density of sampling locations, evidence of both anaerobic and aerobic geochemical conditions, the relative lack of active remedies installed and the completeness of the CSM.

2.0 HILL OU10 CONCEPTUAL SITE MODEL

The Hill OU10 site is the former location of industrial operations for aircraft, missile, vehicle, and railroad engine, maintenance and repair. The Hill OU10 site encompasses the Building 1200 Area along the western boundary of Hill AFB and extends off-Base into the cities of Clearfield, Sunset, and Clinton. Industrial activities at the Building 1200 Area began in approximately 1940 and continued through 1959, at which point the building complex was renovated for administrative offices. Due to historical operations, the aquifer system underlying the site has become contaminated by chlorinated ethene solvents (CEs) resulting in three chlorinated solvent plumes (**Figure A-1**). The primary contaminants of concern (COCs) at OU10 are PCE, TCE, and cis-1,2-DCE. Contamination has been detected in the soil, groundwater, and soil gas.

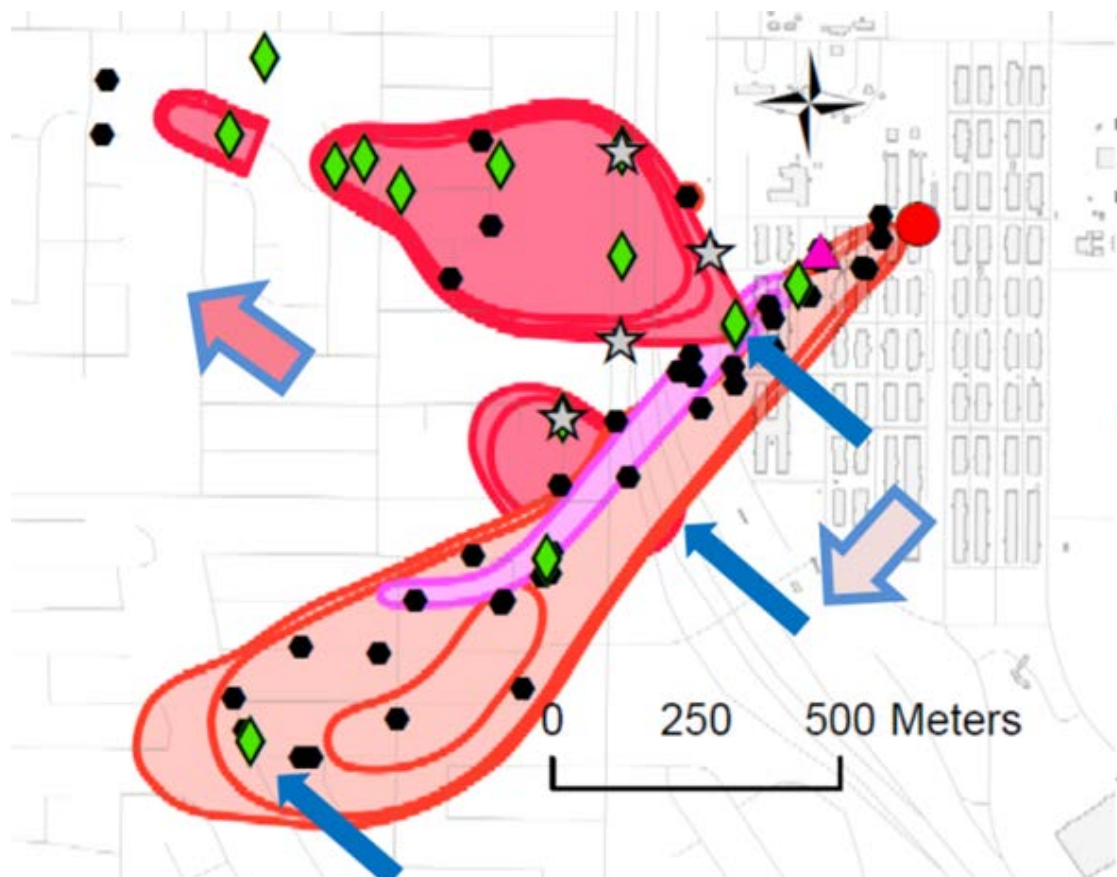


Figure A-1. Map of the Operable Unit (OU) 10 at the Hill Air Force Base (Utah, USA). Shown are the shallow PCE plume (purple) and the shallow TCE plume beneath (light red) flowing in SW direction, and the deep TCE plume (dark red), flowing in NW direction, following the groundwater flow directions (large arrows; deep, dark red; shallow, light red). The black dots represent the wells sampled during Winter 2012/2013. The estimated spill locations are signaled by a purple triangle for PCE and a red circle for TCE. The small blue arrows point to the leakage areas connecting the shallow with the deep plume. The green diamonds indicate wells where either VC or ethene was detected at least once since 2004.

The subsurface consists of two saturated upper units (Unit A and Unit C) separated by an aquitard (Unit B) of varying thickness (< 36 m). Below Unit C, a thick aquitard (Unit D) prevents further

downwards migration of pollutants. Cross-sections illustrating site lithology are shown in **Figures A-6 and A-7**.

In Unit A, a shallow PCE plume partially mixes with a shallow TCE plume. In the lower zone (Unit C), one deep TCE plume is divided in two lobes (called northern and southern) of different sizes. The Unit B aquitard is entirely eroded in some areas and leakage from the upper to the lower aquifer occurs. In the vicinity of those leakages, the shallow TCE plume is detected within Unit B. The shallow TCE plume is relatively thin (6-12 m) and appears to travel at the surface of Unit B between 7 m and 30 m BGS. The shallow TCE plume has the largest footprint (90 - 425 m) and has traveled at the surface of Unit B approximately 1,500 m in southwestern direction, including 1,000 m outside of the site's boundaries and underneath a residential area, before sinking into Unit C.

The deep TCE plumes flow towards the northwest. The deep plume is found between 53 m and 88 m BGS, and is up to 40 m thick. The northern lobe is 425 m wide at its maximum, and 800 m long. The southern lobe is defined as 245 m wide and 425 m long.

Chlorinated solvents were released during the period 1940-1959. Two primary sources of contamination have been identified. PCE was probably spilled incidentally on a parking lot the parking lot west of Building 1274. However, the shallow TCE plume originated from the continuous releases from an oil/water separator at the north end of Building 1244 (CH₂MHILL 2009). Active remedies at the OU10 site are limited. Some soil was excavated in the area of the oil/water separator in 2003. In 2007, an Enhanced Reductive Dechlorination (ERD) treatment was tested in an area of high dissolved TCE (approximately 900 m to 1000 m away from the assumed source area). Various lines of evidence (tracers, hydrochemical analysis, groundwater age dating, and hydraulic gradients) show that the shallow plume is leaking through the aquitard at three locations, two of those leakages forming the deep TCE plumes (**Figure A-1**).

During the 2012/2013 sampling round, the highest CEs concentrations were measured in the deep plume, with maximum concentrations of TCE (750 µg/L = 5.71 µmol/L) and cis-DCE (111 µg/L = 1.15 µmol/L) above regulatory standards. The other main DCE isomer, trans-DCE, reached a maximum concentration of 1.1 µmol/L, and constitutes on average 9% of total detected DCE, with large variations (0 – 100%). Only traces of 1,1-DCE were detected (< 0.8 µg/L = 0.008 µmol/L). In the shallow plume, PCE (136 µg/L = 0.82 µmol/L) and TCE (140 µg/L = 1.07 µmol/L) exceeded the regulatory standards, whereas cis-DCE was detected below standards (42 µg/L = 0.43 µmol/L).

DCE is present in most of the wells of Unit C, but is detected only in scattered locations in the shallow plume, mostly in wells screened in Unit B. VC has been detected historically (2001-2005) in one well in Unit B, and, until 2008, in multiple wells of Unit C, but with concentrations below the Maximum Contaminant Level (MCL = 2 µg/L/ 0.03 µmol/L). VC was not detected during the Winter 2012/2013 sampling event of the current study, except at one well in the deep plume at low concentrations. Ethene was only systematically analyzed during winter 2012/2013 and then only detected in Unit C, in 4 different wells, at concentrations up to 15 µg/L. Analyses from 2008 found traces of ethane (< 0.3 µg/L) at 8 wells in Unit C. Ethane and ethene were not detected in pristine areas of the plume, and are therefore potential degradation products from CEs. Previous sampling showed only traces of VC, ethene and ethane (**Figure A-1**). The only potential source of DCE and VC is their production through reductive dechlorination (RD) of TCE/PCE.

The CEs' total masses were estimated at 5 kg for the shallow PCE plume and about 90 kg for TCE in the shallow plume. TCE in the deep plume was estimated at 450 kg in 2009 (cf. % **7.1** in

[CH₂MHILL 2009]). 20% of the TCE remained in Unit A or B, while 80% sank to Unit C. PCE travels close to the groundwater surface. Conversely, TCE probably initially sank as a DNAPL because the shallow TCE plume travels at the surface of the aquitard, and occurs near the spill location only at the basal portion of the Unit A.

The TCE source zone is likely to be exhausted, as DNAPL was not detected in the probable source during the period of the site investigation (1995-2013), and since CEs concentrations are low in the vicinity of the source zone. Moreover, the highest TCE concentrations in the shallow plume are presently found away from the source (at 900-1300 m downgradient), which indicates that the source is depleted. Consequently, the water flowing in Unit C to form the upgradient part of the deep plume is also less polluted than in the past, as suggested by the decreasing concentrations at the well U10-131 (**Figure 4-19** in [CH₂MHILL 2009]), at the junction between the shallow plume and the northern deep plume.

Ascertaining the presence and activity of adequate microbial communities is a necessary step to assess biodegradation potential. The shallow TCE plume migrates through the largely aerobic Unit A. During a previous investigation, 12 wells in the shallow plume were tested for the presence and activity of TCE aerobic cometabolic microorganisms using molecular biological tools (MBTs) to detect genes for toluene and methane oxygenase. These enzymes catalyze TCE aerobic cometabolism when oxidizing toluene or methane in presence of oxygen. Enzyme analyses were performed (**Appendix J** in [CH₂MHILL 2009]) at 5 wells, 4 in Unit A and 1 in Unit B.

TCE cometabolism was shown to be possible in the shallow plume. Functional genes for methane monooxygenase were also investigated at 4 wells in Unit C. Relatively low estimated cell counts were detected at all wells in all aquifer units. CEs cometabolism during methane oxidation is considered possible when methane concentrations are relatively large compared to CEs concentrations. Since Unit C displays methane concentrations above 0.3 mg/L (18 µmol/L), which exceeds the highest CE concentration, aerobic cometabolism of CEs is theoretically possible in Unit C, if adequate aerobic/anaerobic interfaces occur.

In the Unit C, 3 wells were investigated for presence of bacteria capable of PCE and TCE RD, and functional genes that transcribe the competent enzyme for complete RD (TCE to VC, and VC reduction) (see **Table 5-22** in [CH₂MHILL 2009]). The targeted reductive bacteria are potentially capable of complete (through ethene; Dehalococcoides [Dhc]), or partial (through cis-DCE; Desulfomonas, and Dehalobacter) dechlorination. Bacterial activity was not confirmed in the study. Neither Dhc, nor adequate genes for complete RD were detected. Desulfomonas, and Dehalobacter were present at the well presenting the highest TCE concentrations (W517 - U10-094A), with a relatively low cell quantity. RD through cis-DCE in the Unit C is therefore likely, but further reduction is probably currently limited, despite the presence of VC and ethene traces.

An Enhanced Reductive Dechlorination (ERD) pilot test was conducted in a limited area in the shallow plume.

Details of site hydrogeology and aquifer characteristics are presented in the Materials and Methods section.

3.0 MATERIALS AND METHODS

3.1 Groundwater Sampling

Historical groundwater sampling data were obtained from Hill AFB (CH₂MHILL 2011). From the dataset, candidate wells were chosen for CSIA of carbon (C), chlorine (Cl) and hydrogen (H) (3-D CSIA) sampling based on contaminant concentrations. Samples were collected for CSIA analysis by the base sampling contractor (AEEC). Sample aliquots of 1L were collected from each well and shipped on ice to University of Oklahoma (UO) for analysis. All wells were sampled simultaneously for the routine base monitoring program, and sample analytical results were obtained from the contract commercial lab for comparison.

All wells in the shallow plume were sampled with Low-Flow Sampling (Puls and Barcelona 1996), while three different technologies were employed for the sampling of the deep plume:

- **Low-Flow Sampling** – Applied to most of the wells with screens of generally 3 to 6 m length. During sampling the drop in water level was limited and groundwater was drawn through flow-through cells until electrode measurements (pH, oxidation-reduction potential (ORP), dissolved oxygen (DO), turbidity, specific conductance, and temperature) stabilized.
- **Permeable Diffusion Bags (PDBs)** – Applied in 4 wells with exceptionally long screens (> 24 m). Field parameters cannot be collected at PDB sampling locations.
- **Barcad systems** – Barcad pumps are buried within a well screen placed in sand layers of 1 meter thickness or less, and separated from each other with bentonite. These smaller screens were generally monitoring thin interbedded sand zones.

The winter 2012/2013 sampling event included samples from 59 sampling points: 36 in the shallow plume and 23 in the deep plume. Barcad pumps placed in different screens within the same well were counted as different sampling points. PDBs placed at various depths in long-screened wells presented relatively stable concentrations and isotope ratios, without depth gradients or observable relation with lithology, and were, therefore, counted as one single sampling point per well. Since relatively strong vertical hydraulic gradients occur in Unit C, groundwater might travel through the long wells downwards explaining the lack of depth gradients.

Groundwater sample analysis included (i) on site field measurements (DO, oxidation-reduction potential (ORP), turbidity, electrical conductivity, pH, and temperature) where possible; (ii) analysis in the lab for chloride, ammonium, iron, nitrate, sulfate, sulfide, and dissolved organic carbon following standard methods; (iii) laboratory analysis for CEs concentrations and their carbon (C), chlorine (Cl), and hydrogen (H) isotopic composition following methods described by Kuder et al. (Kudervan Breukelen et al., 2013).

3.2 CSIA Laboratory Analysis

The concentrations and isotope ratios of CEs and ethene were performed using gas chromatography-quadrupole mass spectrometry (concentrations and Cl isotope ratios) or gas chromatography-isotope ratio mass spectrometry (C and H isotope ratios). H CSIA was performed using a custom chromium metal reactor (Kuder and Philp 2013) for conversion of the CEs and/or ethene to H₂. Details of the analytical methods are as described in Kuder et al. (2013) (Kuder, van Breukelen et al., 2013).

Laboratory analyses performed at University of Oklahoma were compared with duplicate samples analyzed at a commercial laboratory.

3.3 Source Isotope Ratios

Interpretation of CSIA data requires estimation of the isotope signatures of the original solvent spills as precisely as possible.

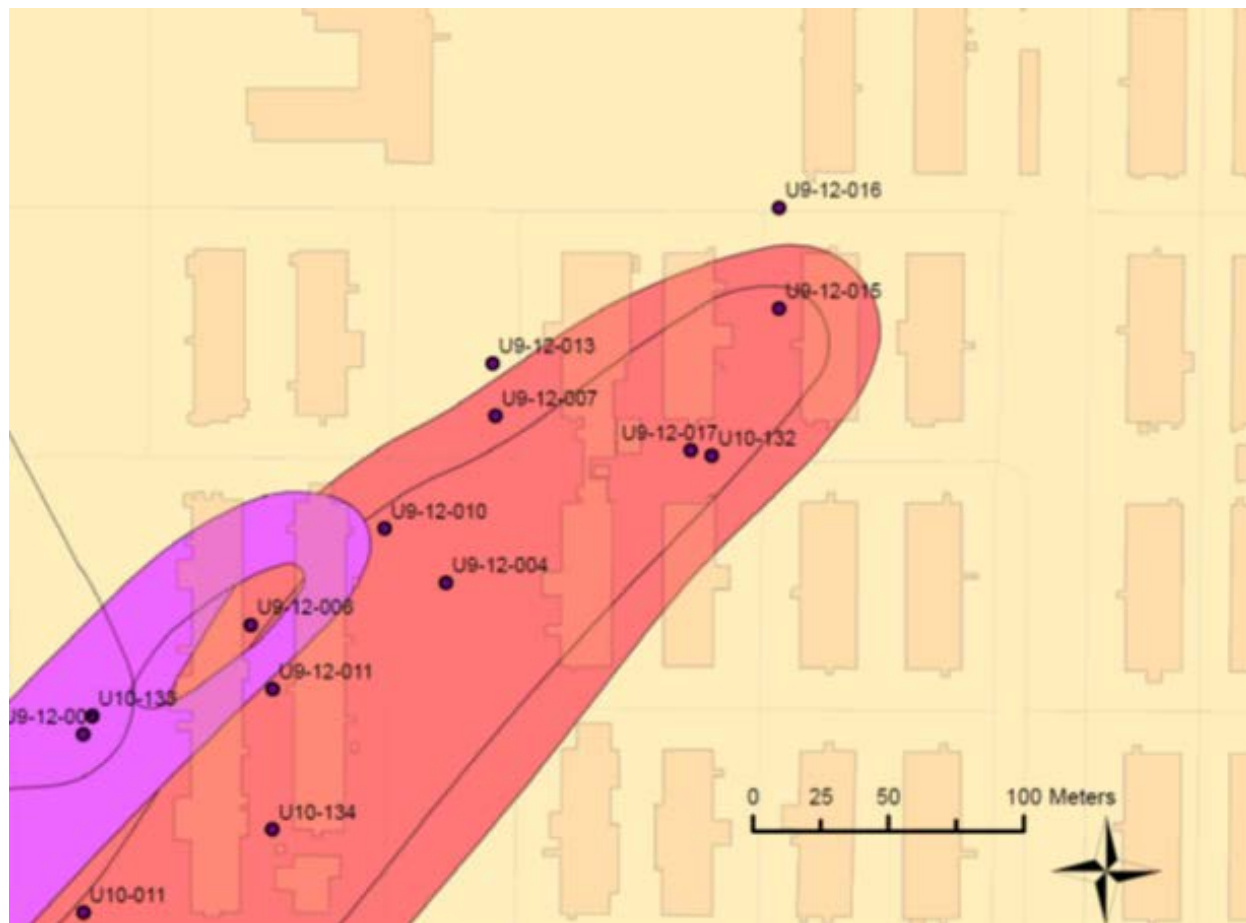


Figure A-2. Location of the potential primary spill zones of the PCE (purple) and TCE (red) plumes (CH₂MHILL 2009).

Site investigation at OU10 began in 1995, approximately 50 years after the both PCE and TCE spills. As the pure products were no longer available for investigation, the source isotope signatures had to be approximated. Candidate source samples were selected based on the following criteria: (i) carbon isotope ratio compared with known source values for industrial PCE and TCE (-30 to -25‰ (Sakaguchi-Soder, Jager et al. 2007; Kuder, van Breukelen et al. 2013); (ii) relatively high concentrations; (iii) relatively low (depleted) $\delta^{13}\text{C}$; (iv) absence of mixing between the TCE and PCE plumes (**Tables A-1** and **A-2**) for the shallow plume; or (iv) low DCE concentrations for the deep plume. Finally, a unique value was used for $\delta^{13}\text{TCE}$ without distinction between shallow and deep plumes.

Table A-1. Locations with the Potential Source Values for TCE

Location	Distance to TCE source (m)	$C_{TCE,average}$ ($\mu\text{mol/L}$)	$x_{TCE,average}$ (%)	$\delta^{13}\text{C-TCE}$	Comment	$\delta^{37}\text{Cl-TCE}$	$\delta^2\text{H-TCE}$
U10-011* W405	405	0.152	97	-26.2	Lowest carbon isotope ratio, but PCE is enriched ($\delta^{13}\text{C} = -20\text{‰}$). PCE degradation might, therefore, have depleted this TCE carbon isotope ratio.	2.7	-251
U09-12-015 W67	67	0.110	99	-26.0	Second most depleted isotope ratio for TCE	2.3	-256
U10-043 W971	971	0.719	98	-25.5	Second highest concentration and one of the most depleted carbon isotope ratio value, nearly pure TCE.	4.1	-260
U10-062 W881	979	0.135	100	-25.4		4.6	-193
U10-167 W895	895	0.749	88	-25.2	Highest concentration, relatively high carbon isotope ratio, XTCE < 90%	4.7	-192
U10_020 W1060	1248	1.05	100	-25.6		4.3	-259
U10-089C WD 900	900	2.72	94	-24.2		2.6	-266
U10-179B WD 771	771	0.822	85	-23.7		2.6	-247

* Lowest isotope ratio.
 $x_{TCE,average}$ (%) = average mole fraction TCE

Table A-2. Locations with the Potential “Source Values” for PCE.

Location	Distance to PCE source (m)	$C_{PCE,average}$ ($\mu\text{mol/L}$)	$X_{PCE,average}$ (%)	$\delta^{13}\text{C-PCE}$	Comment	$\delta^{37}\text{Cl-TCE}$
U10-133 W362*	197	0.078	99	-32.70	Lowest isotope ratio for PCE highest molar fraction.	-0.53
U09-12-006 W294**	132	0.771	89	-31.50	Highest concentration	-1.40
U10-107 W67	108	0.274	87	-31.38		-0.67

* Lowest isotope ratio.
 ** Selected source signature.
 $x_{PCE,average}$ (%) = average mole fraction PCE

The selected source signature ($\delta^{13}\text{C-TCE} = -26\text{‰}$, $\delta^{37}\text{Cl-TCE} = -2.5\text{‰}$, $\delta^2\text{H-TCE} = -255\text{‰}$) for the TCE plumes (both shallow and deep), based on the manual fitting of the model described in the following sections, is similar to the signature of wells such as U9-12-015, upgradient from the PCE plume (**Figure A-3**). The uncertainty on the source value was set arbitrarily to be equal to the standard analytic uncertainty (i.e., C \pm 0.5‰, Cl \pm 1‰ and H \pm 15‰).

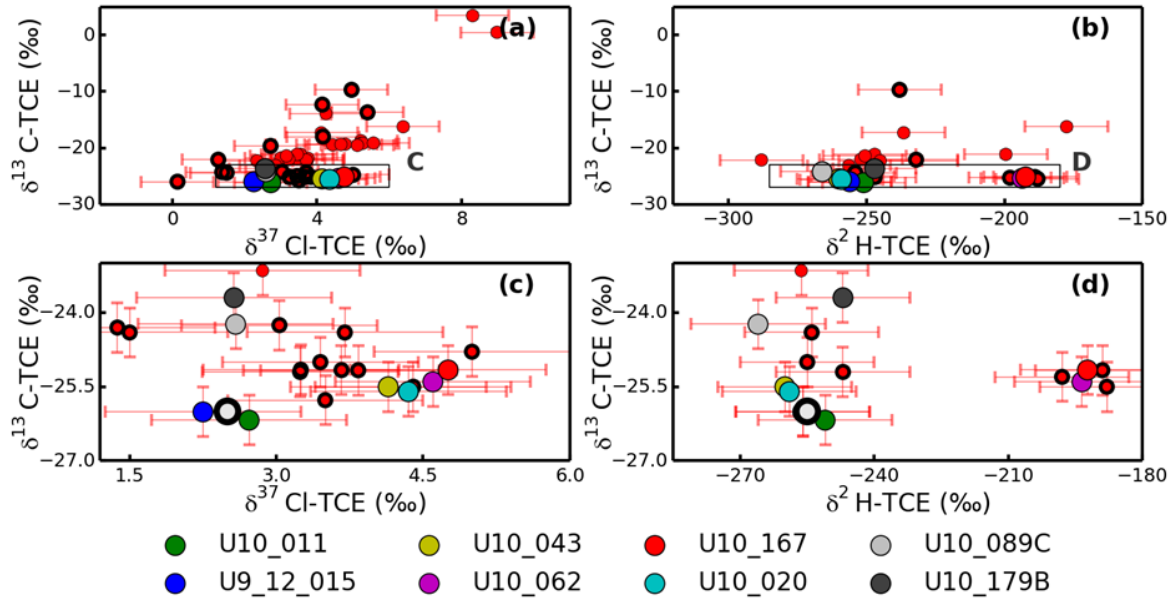


Figure A-3. TCE potential source values on 2D-CSIA plots. (a) C vs Cl ratios for TCE sample locations; (b) C vs H ratios for TCE sample locations; (c) Detail of plot (a); and (d) detail of plot (b). Final source value (white circle with back contour) was finally chosen after fitting the data as presented in the Case Study.



Figure A-4. Map of the wells with TCE $\delta^{13}C$ and $\delta^{37}Cl$ potentially similar to the original solvent signatures indicated in **Figure A-3**. Well location colors are those presented in **Figure A-3**.

3.4 Aquifer Parameters

Groundwater velocities were determined using conductivity values from slug or pump tests and groundwater ages performed during site investigation (CH₂MHILL 2009). The effective porosity, n_e , was estimated as 0.2 for the whole aquifer based on average literature for sand aquifer matrix. The hydraulic gradients $\delta h/\delta x$ were obtained from the groundwater elevation detected in the monitoring wells (Section 3.7 in [CH₂MHILL 2009]). The resulting flow velocities were averaged with the value calculated from the groundwater age, determined with tritium/helium-3 (Table A-3). The final groundwater velocities are presented Figure A-5.

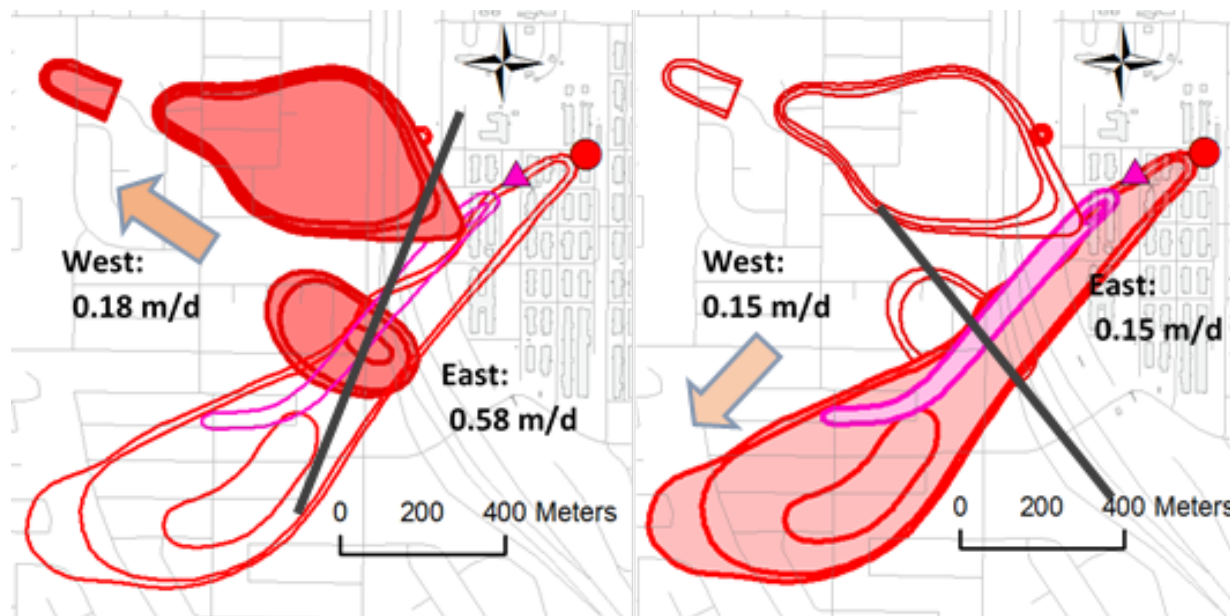


Figure A-5. Final averaged groundwater velocities based on data from Table A-3. The grey line represents the approximate separation between the “eastern” and “western” area.

Unit A is unconfined, perched, and composed of fine to medium coarse sand and clay lenses, with an average groundwater flow velocity of about 0.15 m/d (Table A-3). The calculated retardation factors for PCE, TCE, c-DCE, and t-DCE, were relatively low (≤ 3.1 , 1.7, 1.6, and 2.0, respectively, Table A-4), due to the low organic carbon content (sand, 0.03% - silty sand, 0.07%) of Unit A. In Unit C the groundwater velocity decreases abruptly with the hydraulic gradients between the eastern most part (0.58 m/d), where the sand layers are thin and interbedded with clay layers of low permeability, and the west (0.18 m/d), where the sand packages are thicker. Since the organic carbon content of Unit C is higher (0.2%), sorption is more important and TCE migrates at half the rate of DCE (Table A-4). Cross sections of different aquifer units are illustrated in Figures A-7 and A-8, a map of the cross-section locations is presented in Figure A-6.

Table A-3. Estimation of the Groundwater Velocities Based on the Aquifer Conductivities and Groundwater age at the Hill Site (Figure 3-20 in [CH₂MHILL 2009]).

	West	East
<i>Unit A</i>	0.15 m/d (slug) 0.36 m/d (pump) 0.06 m/d (age)	0.18 m/d (slug) 0.12 m/d (age)
<i>Unit C</i>	0.15 m/d (pump) 0.18 m/d (age)	1.06 m/d (pump) 0.09 m/d (age)

Table A-4. Parameters for the Calculation of the Retardation Factors, and Retardation Factors (Table 5-4 in [CH₂MHILL 2009]).

	Molar mass (g/mol)	Koc (mL/g)	R – Mixed values (foc 0.07%) (no unit)	R – sand zones (foc 0.03%) (no unit)	Unit C (foc 0.2%)
PCE	166	360	3.08	1.89	
TCE	131	120	1.69	1.30	3.0
Cis-DCE	97	36	1.20	1.1	1.58
Trans-DCE	97	59			1.98
VC	62	8			1.14
Eth	28	-			~1

Redox parameters such as Dissolved Oxygen (DO) were thoroughly investigated during summer 2007 (**Table 5-8** [CH₂MHILL 2009]). Based on those parameters, Unit A was qualified as overall oxic, while Unit B and C were qualified as mildly reducing (3.7.1.28 [CH₂MHILL 2009]). Since the shallow TCE plume evolves both within the Unit A and at the surface of the Unit B, the shallow plume enters in contact with different redox conditions. The 2007 investigation combined the redox parameters for Unit A and B. For those units, DO reached an average value of 3.9 mg/L (standard deviation (std) = 2.1 mg/L), but the unit presented large ranges for nitrate (0.0 to 50.9 mg/L) and sulfate (0.0 – 80.0 mg/L) concentrations. Unit C was qualified as mildly reducing, with lower concentrations of oxygen (2.0 mg/L, std = 1.2 mg/L), sulfate (average = 25.7 mg/L, std = 26.5 mg/L), and nitrate (average = 1.9 mg/L, std = 6.3 mg/L) and a negative average oxidation-reduction potential. Presence of methane (0.2 - 1.2 mg/L, measured in 2007) in some wells in Unit C signals methanogenic conditions, while other wells in Unit C present high nitrate concentrations. Therefore, Unit C also presents large redox heterogeneities.



Figure A-6. Map of the cross-sections A-A' and C-C'.

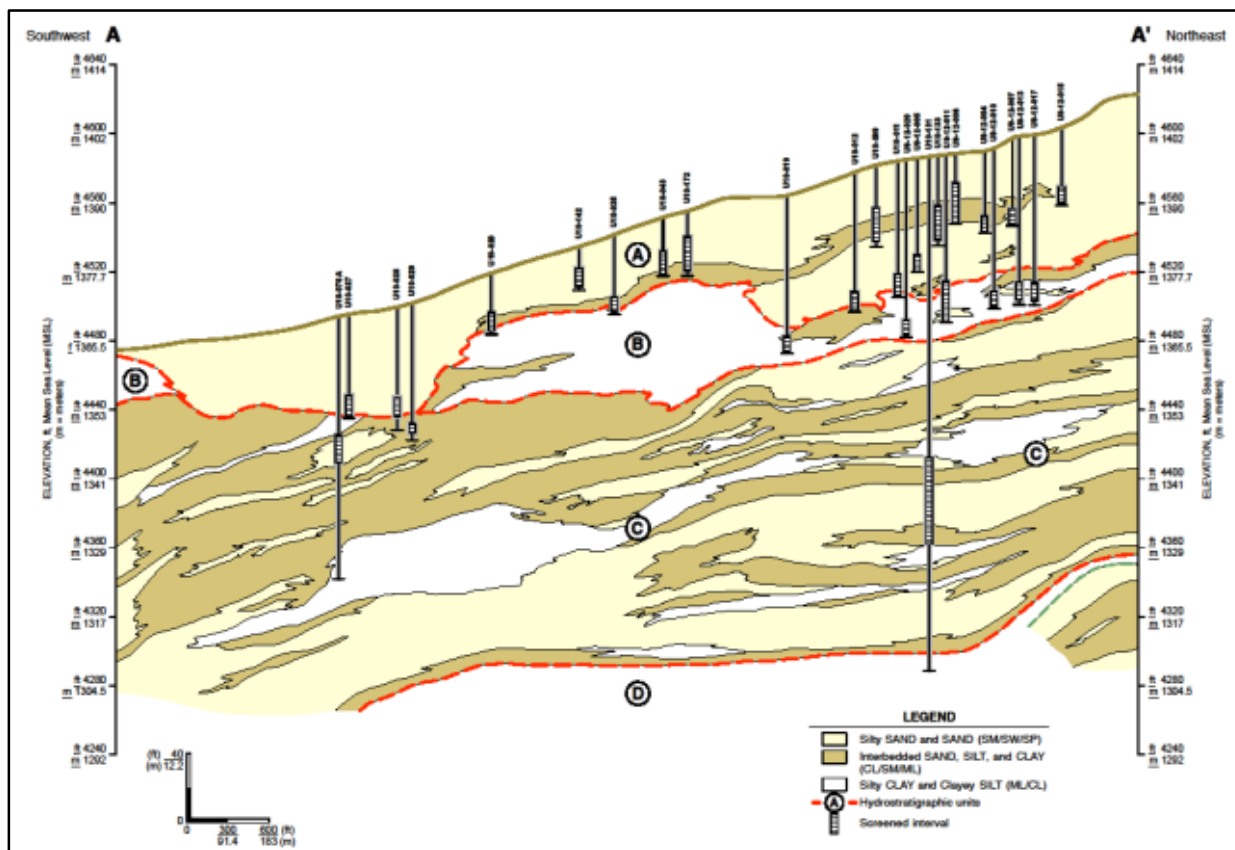


Figure A-7. Transect A-A' lithology. Taken from Figure G1-3 (CH₂MHILL 2009).

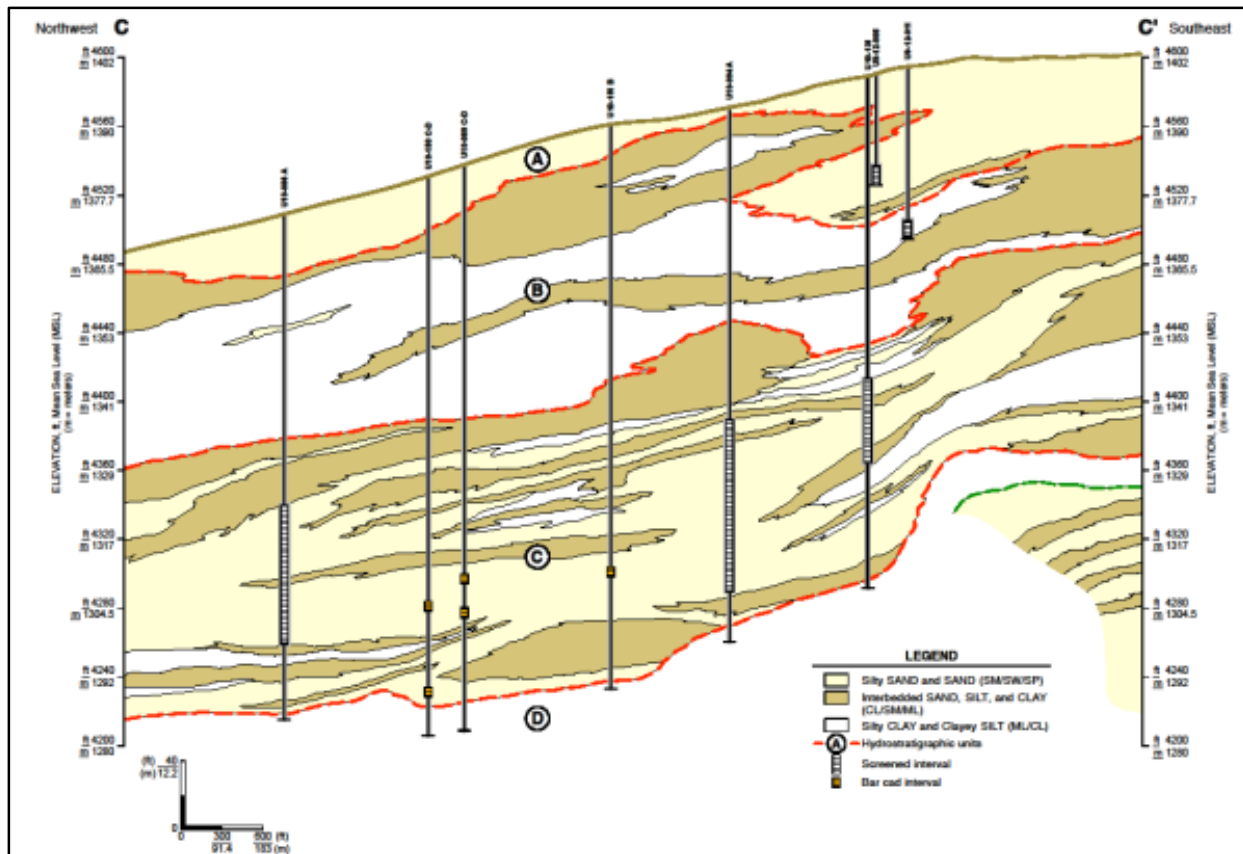


Figure A-8. Transect C-C' lithology. Taken from Figure G1-4 (CH₂MHILL 2009).

3.5 CSIA Preliminary Data Interpretation

Results of CSIA analysis can be complicated to interpret. For the Hill OU10 field site case study several data interpretation methods have been employed in order to clarify and simplify, where possible, the complex C, Cl, and H isotopic signatures for CEs.

3.5.1 Setting Rules for CSIA Degradation Signals

Parent CEs showing C isotope ratios significantly more enriched than the source isotope signature were interpreted to indicate biological transformation. Physical processes do not cause the same degree of fractionation. As enzymatic processes on near-term time scales. Note that daughter products might be depleted in heavy isotopes below the source threshold value, initially. Due to the uncertainty of C-CSIA (generally 0.5‰, maximum 1‰), the difference or isotope shift ($\Delta^{13}\text{C}$) between $\delta^{13}\text{C}$ -CEs/ethene and $\delta^{13}\text{C}$ -source should exceed the sum of the analytical C-CSIA uncertainties of both the source and the sample. Therefore, following the U.S. EPA recommendations (Hunkeler, Chollet et al. 2004), a significant isotope shift is defined as the sum of sample and source CSIA uncertainties, plus an arbitrary value of 1‰ in order to minimize erroneous interpretations. The significant shift reaches 2‰ in total when the sample has an uncertainty of 0.5‰.

3.5.2 2-D Plots

Plotting $\delta^{13}\text{C}$ isotope ratios against $\delta^{37}\text{Cl}$ and $\delta^2\text{H}$ values can provide an insight into fate processes of the measured compounds. CSIA data were plotted for 2 elements for interpretation of source signatures and processes at various locations within the plume.

3.5.3 Carbon Isotope Mass Balance

The C isotope mass balance (C-IMB;‰) was calculated for most sampling locations by summing the products of the C isotope signatures, $\delta^{13}\text{C}_i$, of the CEs (and ethene where detected) by their molar concentrations, C_i :

$$C - \text{IMB}(\text{‰}) = \frac{\sum_i \delta^{13}\text{C}_i \times C_i}{\sum_i C_i} \quad (1)$$

During RD, the C-IMB remains constant and equal to the source signature as the carbon atoms are transferred to the daughter products through ethene. In the case of oxidative transformation and mineralization, the parent C skeleton is lost as CO_2 . In this case, C-IMB becomes enriched with either time or distance from the original release as CEs are mineralized. An enriched total C-IMB relative to the source, therefore, signals complete oxidative transformation. The C-IMB can also be used directly for source apportionment provided complete mineralization is absent. The uncertainty of the C-IMB was calculated following Stelzer et al. (Stelzer, Imfeld et al. 2009). C-IMB presents uncertainties in the range 0.5 to 1‰ as well. The approach used for determining significant enrichment relative to the source is similar to the one described above (**Section 3.5.1**).

3.6 RTM Model Description

To better interpret CSIA results from the Hill OU10 field site, a RTM for CSIA was developed. The model employed for this study is an extension of the model developed by van Breukelen et al. (under preparation) and includes C, Cl, and H isotope fractionation, through both RD (PCE \rightarrow TCE \rightarrow c-DCE/t-DCE \rightarrow VC \rightarrow ETH) and oxidation (c-DCE/t-DCE \rightarrow CO_2 , VC \rightarrow CO_2). Reaction kinetics are modeled as first-order and independent from the redox conditions.

The model was developed and validated in conjunction with data from microcosm experiments using the Bio-Dechlor Inoculum (BDI) culture, a consortium of at least three *Dehalococcoides* (Dhc) strains that is capable of complete dechlorination of PCE via TCE, DCE, and VC to ethene. (Amos, Ritalahti et al. 2008) Concentrations and (C, Cl, H) CSIA were measured until dechlorination was complete after 66 days. $\delta^2\text{H}$, $\delta^{13}\text{C}$, and $\delta^{37}\text{Cl}$ values were expressed relative to the international standards VSMOW, VPDB, and SMOC, respectively. This dataset validated the Cl isotopologue fractionation model developed by Hunkeler et al., (Hunkeler, Van Breukelen et al. 2009) and supported development and validation of a hydrogen isotope fractionation model.

The microcosm experiments demonstrated that the modeling of Cl and H isotope fractionation effects during RD is not as straightforward as is the modeling of the one-step alternative pathways. Therefore, the objectives of the model development were (i) to extend the current Cl isotope fractionation model with SKIE and intramolecular heterogeneity of the source compounds as necessary; (ii) to develop a completely novel model that describes hydrogen isotope fractionation

during RD; and (iii) to validate the developed model with the experimental data of Kuder et al. (Kuder, van Breukelen et al. 2013).

The model was developed with the PHREEQC code (Parkhurst and Appelo 1999). Details of the model development are provided in van Breukelen et al. (under preparation) and discussed in detail in the Technical Manual (**Sections 5-7**) of this CSIA/RTM Guidance. RD of TCE via DCE, VC, and eventually ETH was simulated. *cis*-DCE was the main DCE isomer modeled, but minor quantities of *trans*-DCE and 1,1-DCE were detected in the microcosms and field samples and are included in the model for completeness. For model simplicity, the sum of the latter two DCE isomers was explicitly simulated as *trans*-DCE. Two minor pathways were, therefore, added to the model: TCE to *trans*-DCE and *trans*-DCE to VC.

Due to the complexity of this aquifer system and the occurrence of localized contaminant degradation, we followed a similar modeling approach as van Breukelen et al. (2005). The aquifer was considered as a black-box and modeled with a batch model. Spatial and temporal dimensions were thus not explicitly simulated. However, neglecting transport processes such as hydrodynamic dispersion might lead to the underestimation of degradation, while neglecting sorption might lead to overestimation of degradation at the fringe of the plume (Van Breukelen and Prommer 2008; Abe, Aravena et al. 2009). By neglecting transport, the modeling still enabled (i) reduction of uncertainties about the occurrence of specific degradation pathways; and (ii) narrowing the range of field enrichment factors for C, Cl, and H. Herewith, the model of CEs sequential degradation improved the reliability of CEs degradation quantification at the site.

4.0 RESULTS

4.1 Isotope ratios, at the source and throughout the plume

The selected isotope signatures of the PCE and TCE primary releases are plotted in **Figure A-9**, which displays dual plots of isotope ratios of all wells in the shallow and deep plumes. Isotope analysis confirms that the deep TCE plume originates from leakages of the shallow TCE plume, since a unique TCE source signature is found for both plumes ($\delta^{13}\text{C-TCE}_{\text{Source}}$, $-26 \pm 0.5\text{‰}$, $\delta^{37}\text{Cl-TCE}_{\text{Source}}$, $2.5 \pm 1\text{‰}$; **Figure A-3**). TCE C1 and C isotope ratios are higher than those of the PCE source ($\delta^{13}\text{C-PCE}_{\text{Source}}$, $-31.5 \pm 0.5\text{‰}$; $\delta^{37}\text{Cl-PCE}_{\text{Source}}$, $-1.5 \pm 1\text{‰}$; **Table A-2**). The depleted $\delta^2\text{H-TCE}_{\text{Source}}$ (-255‰) is comparable with commercial products analyzed in the past, however, at the lower end of the range (Kuder and Philp 2013).

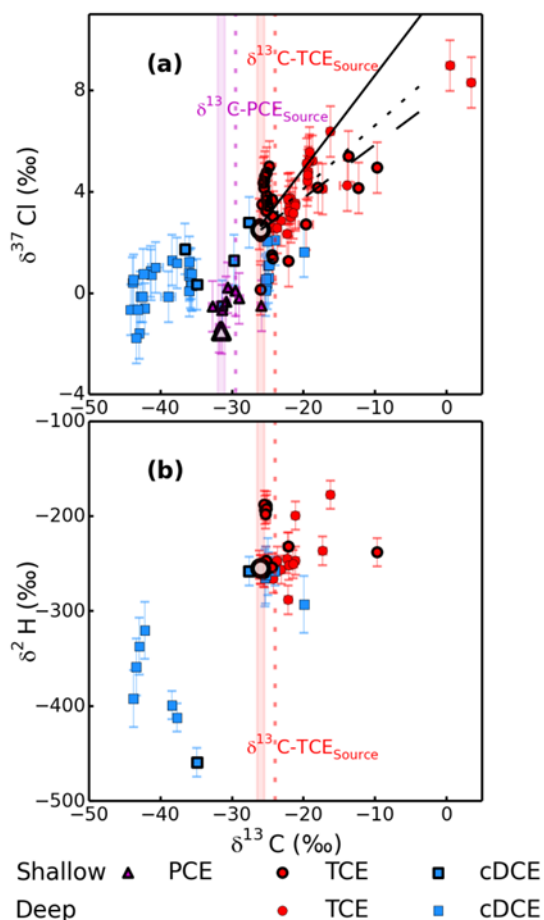


Figure A-9 (a) C/Cl and (b) C/H dual CSIA plots for PCE, TCE, and c-DCE for both the deep and shallow plumes. Each point represents results from one well location. Uncertainties of the C isotopes ratios are smaller than the marker. Selected TCE (black circle) and PCE (black triangle) source signatures were determined as explained in the SI. The red and purple vertical lines (labelled with $\delta^{13}\text{C-PCE}_{\text{source}}$ and $\delta^{13}\text{C-TCE}_{\text{source}}$) represent the uncertainty range of the source C signature ($\pm 0.5\text{‰}$). The dashed perpendicular lines correspond to the minimum $\delta^{13}\text{C}$ signal indicative of degradation (Wiegert, Aeppli et al. 2012). Uncertainty of CSIA was in general $\pm 0.5\text{‰}$ for C, $\pm 1\text{‰}$ for Cl, and $\pm 15\text{‰}$ for H. Black lines meeting at the TCE source signature represent literature values of $\epsilon_{\text{Cl}}/\epsilon_{\text{C}}$ for TCE reductive dechlorination: plain: 0.37 (Wiegert, Aeppli et al. 2012).; dashed (small): 0.25 (average from values displayed in [Cretnik, Thoreson et al. 2013]); dashed (long): 0.22 (Kuder, van Breukelen et al. 2013).

Significantly enriched $\delta^{13}\text{C-TCE}$ (i.e., $> -24\text{‰}$) occurs for 90% of the wells in the deep TCE plume versus 25% in the shallow plume (**Figures A-9, A-10**). PCE shows significantly enriched $\delta^{13}\text{C}$ values (i.e., $\delta^{13}\text{C-PCE} > -29.5\text{‰}$) at 5 out of 14 wells (**Figures A-9, A-10 [b]**).

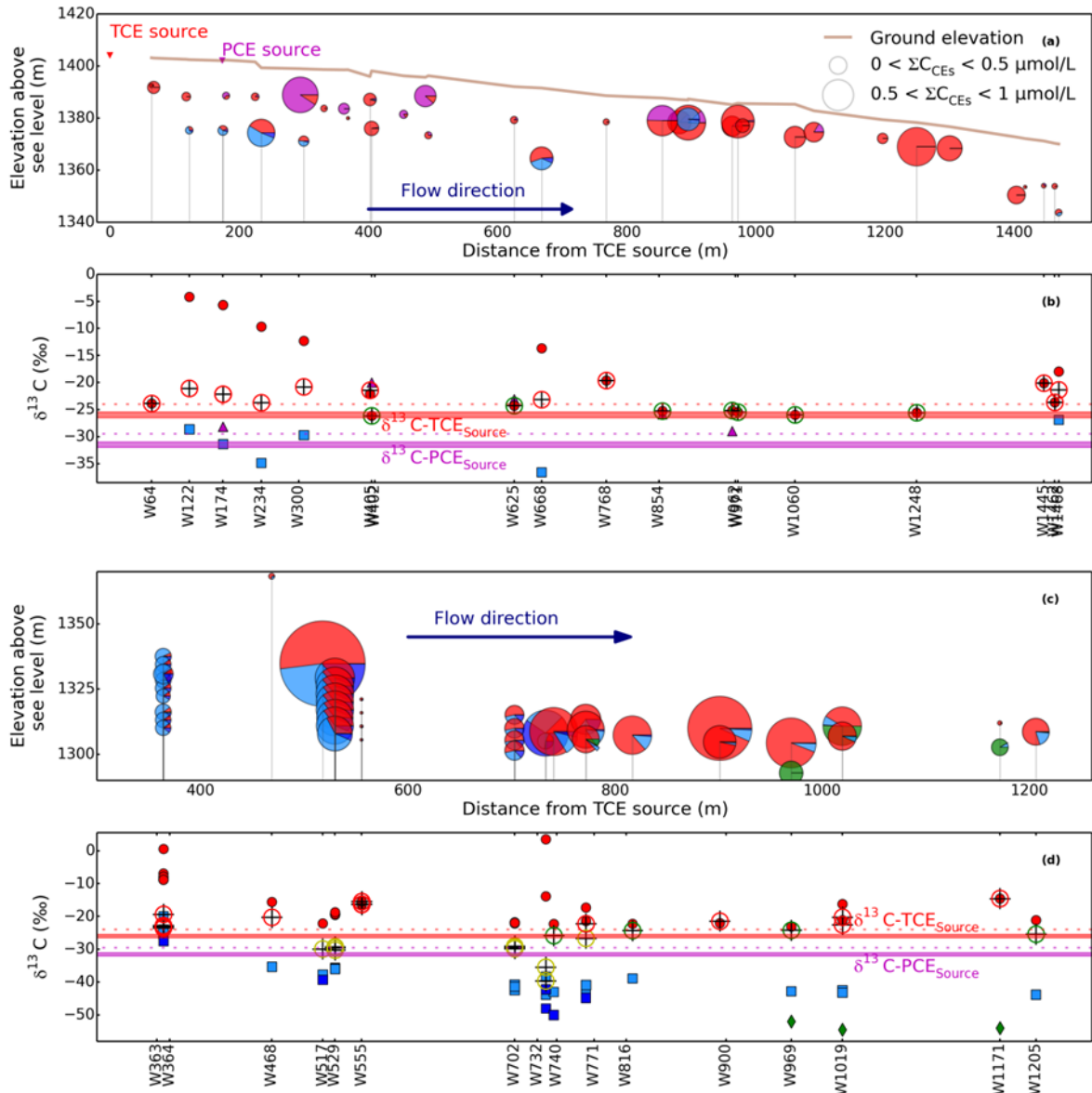


Figure A-10 a-d. Proportion of CE constituents and $\delta^{13}\text{C}$ isotope signatures at sampling locations along the plume flow gradient. Locations showing either TCE or PCE $\delta^{13}\text{C}$ enrichment are shown, together with other relevant wells. (a, c) Cross-section showing the total CEs concentrations and their relative molar proportion (PCE: purple; TCE: red; c-DCE: light blue; t-DCE: dark blue; ethene: green) for the shallow (a) and deep plume (c). (b, d) Graph of C isotope ratios (PCE: purple triangles; TCE: red circles; c-DCE: blue squares; t-DCE: dark blue squares; ethene: green diamonds) and C-IMB (black crosses) for the shallow (b) and deep plume (d); Circles indicate samples with significantly enriched (red), not significantly enriched (green), and depleted C-IMB (yellow). C-IMB excludes PCE and ethene, and does not include t-DCE when $\delta^{13}\text{C-t-DCE}$ was not known.

4.2 Assessment of PCE Degradation

The PCE plume at OU10 is migrating near the water table where the geochemical conditions are largely oxic. One goal of CSIA at the site is to evaluate the potential degradation of PCE in the

shallow aquifer. While laboratory studies found an enzyme and a fungus species capable of PCE degradation under aerobic conditions (Ryoo, Shim et al. 2000; Marco-Urrea, Gabarrell et al. 2008), PCE has generally been found to be recalcitrant to aerobic degradation, and is therefore not expected to degrade in Unit A.

The largest $\delta^{13}\text{C}$ -PCE enrichments occur in the deepest part of Unit A, close to Unit B (U9-13-013/W174, U10-011/W405), or in silty to clayish zones (U10-106/W625, U10-175/W854) (**Figure A-11**). The fifth well (U10_037/W962), screened in a sand layer, is the least enriched of those five wells ($\delta^{13}\text{C}$ -PCE = -29‰). The low-porosity sediments where enriched $\delta^{13}\text{C}$ -PCE is found is likely to present reducing conditions and not to provide adequate conditions for oxidative transformation.

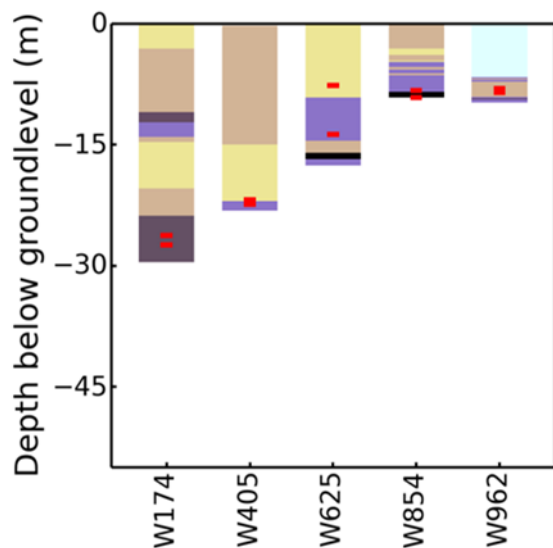


Figure A-11. Lithology of the subsurface for wells presenting a significant enrichment for PCE. The well screen top and bottom are indicated with a red symbol. The lithology classified in 5 main groups: clay (black); silty clay and clayey silt (dark brown); silt, and interbedded clay, silt and sand (purple); silt sand and fine grained sand (light brown); sand (yellow), not sampled (white), no recovery (light blue).

Dual C-C1 CSIA can shed further light on the kind of degradation process attenuating PCE. For CEs, the oxidation limiting step is expected to be the formation of an epoxide (Habets-Crutzen, Brink et al. 1984). C1 atoms are, therefore, not directly involved, reducing expectations of C1 enrichment. Conversely, RD of PCE showed clear, albeit small, C1 isotope fractionation ($\epsilon_{\text{C1}} = -2.0\text{‰}$ [Wiegert, Aeppli et al. 2012]).

Unfortunately, the most enriched wells showed PCE concentrations too low for the accurate determination of C1 isotope ratios and, therefore, no results are available. Plots in **Figure A-12** show dual isotope $\epsilon_{\text{C1}}/\epsilon_{\text{C}}$ slopes for PCE RD (1.12 and 0.42, field data, [Wiegert, Aeppli et al. 2012]) and for both DCE and VC oxidation (0.042 and 0.035, respectively, laboratory data, [Abe and Hunkeler 2006]). Although $\delta^{37}\text{Cl}$ -PCE enrichment occurs for only few samples, and the overall enrichment does not exceed Cl-CSIA uncertainty, the enriched samples tend to follow the $\epsilon_{\text{C1}}/\epsilon_{\text{C}}$ slope of PCE RD. Therefore, it is likely that PCE degrades through RD, despite the overall aerobic conditions in the shallow aquifer.

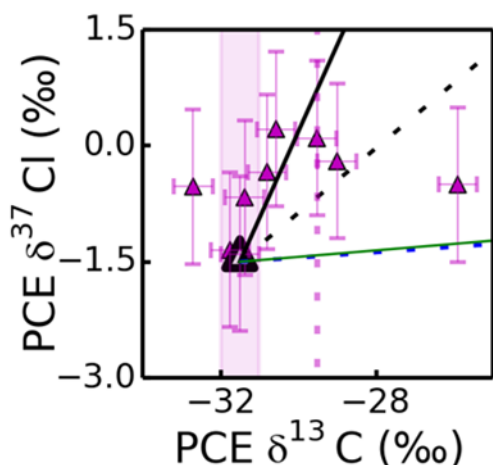


Figure A-12. Dual $\delta^{37}\text{Cl}$ vs $\delta^{13}\text{C}$ plot for PCE field samples. The black, large triangle represents the estimated source isotope ratios; small purple triangles represent values from monitoring wells. The range in $\epsilon_{\text{Cl}}/\epsilon_{\text{C}}$ slope of PCE during RD as observed at another field study is plotted for comparison (black: 0.42, dashed black: 1.12 (Wiegert, Aeppli et al. 2012)). For comparison, $\epsilon_{\text{Cl}}/\epsilon_{\text{C}}$ values for DCE and VC oxidation are also represented (dashed blue: DCE, 0.035; solid green: VC, 0.042 (Abe, Aravena et al. 2009)).

TCE produced through anaerobic metabolism of PCE is likely to have a different C, Cl, and H isotope signature than industrially produced TCE. The isotopic composition of TCE in the shallow PCE plume theoretically may, therefore, confirm occurrence of RD of PCE. However, the total mass of PCE represents only 2% of the TCE shallow plume's mass, therefore the fraction of produced TCE might be negligible compared to the fraction spilled.

For H isotope analyses, $\delta^2\text{H}$ -TCE derived from PCE is expected to be -270‰, or below. The source TCE at the current site presents a depleted $\delta^2\text{H}$ -TCE_{Source} of -255‰. The difference between industrial/source TCE and TCE from PCE dechlorination using H-CSIA is indistinguishable at this site. Therefore, H isotope ratios cannot be used for confirming PCE degradation processes.

C and Cl isotope ratios from CEs daughter products are initially depleted compared to their precursor's signature. For Cl, strong depletion arises from SKIEs for Cl isotope fractionation. Because $\delta^{13}\text{C}$ -TCE and $\delta^{37}\text{Cl}$ -TCE values for all wells are more enriched than both the PCE and TCE source signatures (**Figure A-9**), it is not possible to draw the conclusion that any of the sampled TCE derives from PCE RD. Further degradation of TCE would also impact TCE isotope ratios; therefore, investigations in support of MNA should consider TCE daughter products.

Calculation of the C isotope mass balance (C-IMB) without PCE was employed to detect the presence of PCE daughter products. Since $\delta^{13}\text{C}$ -PCE_{Source} is more depleted than the $\delta^{13}\text{C}$ -TCE_{Source}, including PCE and PCE daughter products in the C-IMB inevitably lowers the balance towards $\delta^{13}\text{C}$ -PCE_{Source}, making C-IMB implications ambiguous. However, C-IMB without PCE indicates the presence of PCE RD when depleted.

In our study, C-IMB relatively to $\delta^{13}\text{C}$ -TCE_{Source} was enriched only at the well showing both $\delta^{13}\text{C}$ -PCE enrichment and DCE concentrations. Since the total PCE mass was small compared to TCE, and since PCE degradation occurs mostly within the TCE plume, PCE daughter products are indistinguishable from the TCE plume. As argued before, PCE is likely to degrade through RD near fine grained and more reducing sediments. Since PCE mixes in the fine-grained zone with the shallow TCE plume, signals of PCE degradation other than PCE isotope composition such as depleted C-IMB or depleted $\delta^{13}\text{C}$ -TCE are not strong enough to be detected.

4.3 Assessment of TCE Transformation Pathways

With the exception of two wells, $\delta^{13}\text{C}$ -TCE enrichment in the shallow plume occurs only in the proximity of fine grained sediments such as silts as in the vicinity of Unit B or Unit C (**Figures A-13, A-7, and A-8**) while in the deep plume the most enriched values occur close to the source area (i.e., where the shallow plume flows into the deeper Unit C). Note both patterns are atypical as degradation usually leads to increasing $\delta^{13}\text{C}$ enrichment with distance and time. Those unusual patterns are likely due to the heterogeneity of the site and are discussed in the following paragraphs.

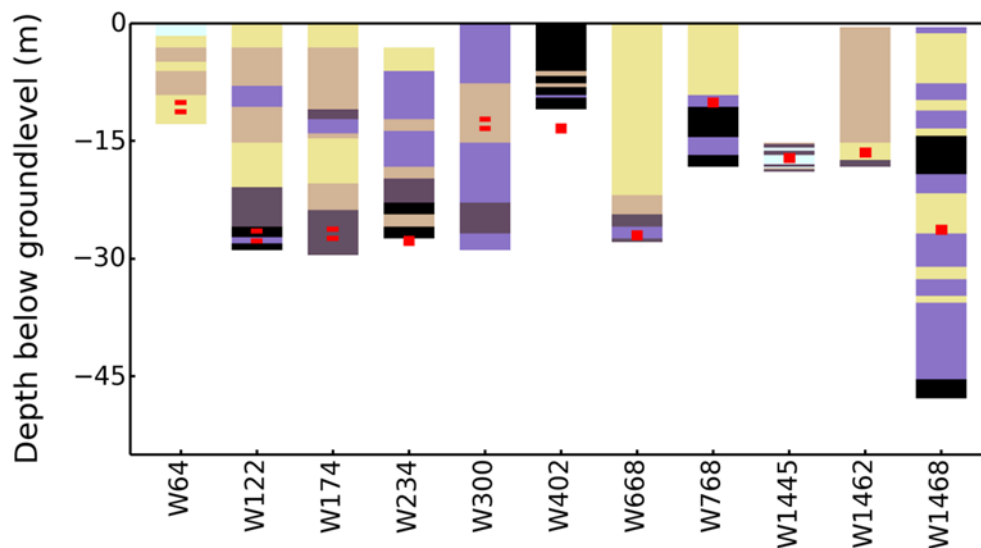


Figure A-13. Lithology of the subsurface for wells presenting a significant enrichment for TCE. The well screen top and bottom are indicated with a red symbol. The lithology classified in 5 main groups: clay (black); silty clay and clayey silt (dark brown); silt, and interbedded clay, silt and sand (purple); silt sand and fine grained sand (light brown); sand (yellow), not sampled (white), no recovery (light blue).

Microbial studies at the OU10 site suggest that aerobic cometabolism of TCE is possible in the shallow plume. Previous laboratory studies of TCE aerobic cometabolism show that ϵC are dependent on the bacterial strains, and vary within a large range (-1.1‰ to -20.7‰ (Barth, Slater et al. 2002; Chu, Mahendra et al. 2004; Pooley, Blessing et al. 2009). If at this site, ϵC is in the lower range, even important TCE degradation through cometabolism would lead to negligible final $\delta^{13}\text{C}$ -TCE enrichment, making the detection of TCE cometabolism difficult.

Out of the 4 wells where both TCE and TCE cometabolic bacteria were detected, only one well shows significant enrichment of $\delta^{13}\text{C}$ -TCE. At this well screened in Unit B, DCE molar fraction is 40% indicating that reductive dechlorination is most likely responsible for $\delta^{13}\text{C}$ -TCE enrichment. Therefore, CSIA results do not conclusively indicate TCE oxidation processes in the shallow aquifer even in the presence of active TCE cometabolic bacteria.

In addition to confirming the presence and activity of competent bacteria, the total dissolved mass of TCE was shown to be decreasing in the shallow plume (5.5.1.2 in [CH₂MHILL 2009]), based

on a Thiessen analysis (Gorder and Hobert 2010). Reduction in mass of TCE supports possible cometabolism as an attenuation pathway.

However, only six wells showed important concentration decreases, the other 7 wells used for the Thiessen analysis showing increasing concentrations (**Figure A-14**). Two of the wells with decreasing concentrations are situated in an area where reductive dechlorination was proven. The four other wells (U10-043, U10-035, U10-020 and U10-029) would, therefore, be the only locations where TCE degradation through aerobic cometabolism is expected. The isotope enrichments observed at these wells are not significantly different from the source ($\leq -25\%$). Although TCE cometabolic bacteria were detected at U10-043, the absence of $\delta^{13}\text{C}$ -TCE enrichment suggests that TCE concentration decrease is not caused by biodegradation. Since the TCE source is depleted, decreasing concentrations may be a result of dilution. However, it is also possible that CSIA was not sensitive enough to detect cometabolic degradation at this site. Further information, such as isotope data from a microcosm experiment for TCE cometabolism, might decrease the uncertainty on this crucial point.

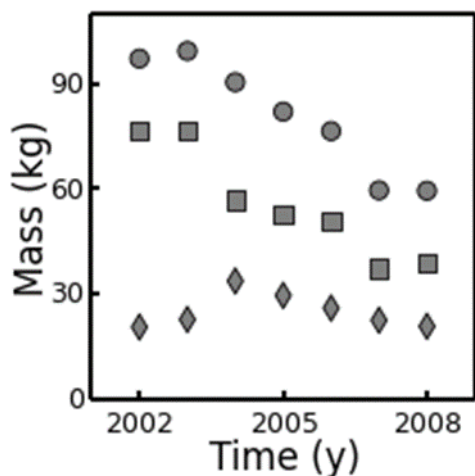


Figure A-14. Estimated mass of TCE based on the Thiessen analysis method. Three wells only (squares) represent already 60 to 80% of the total mass (circles) calculated through this method. Degradation or dilution on those specific spots impacts the estimation of the degradation. The other wells (diamonds) do not show a significant change.

The dual C-Cl CSIA plot (**Figure A-9**) shows that the ratio between δC and δCl seem to follow a similar trend for both plumes, which might indicate that TCE degrades according to similar mechanisms. The observed trend is in the range of previous $\epsilon\text{C}/\epsilon\text{Cl}$ slopes observed for TCE reductive dechlorination in the literature (Wiegert, Aeppli et al. 2012; Cretnik, Thoreson et al. 2013; Kuder, van Breukelen et al. 2013) (**Figure A-9**). Enriched $\delta^{13}\text{C}$ -TCE correlates with the presence of DCE for 60% (shallow) to 90% (deep) of wells, suggesting that reductive dechlorination is the most likely cause for TCE enrichment in both plumes. In the shallow plume, four wells present TCE C enrichment without DCE being detected, which could be a sign of TCE cometabolism (**Figure A-10 [a,b]**). Of those wells, two are situated at the extremity of the shallow plume (U10-027/W1462, and U10-045/W1445), one in an isolated clay layer (U10-088A/W768), and one is close to the spill location, in a sandy area (U9-12-016/W64) (**Figure A-13**). Cl isotopes are available for W768 only. On the bivariate $\epsilon\text{Cl} - \epsilon\text{C}$ plot for TCE values, W768 ($\delta^{13}\text{C}$ -TCE = -19.6‰, $\delta^{37}\text{Cl}$ -TCE = 2.7‰) is aligned with the wells showing TCE reductive dechlorination. Since the TCE concentration is low at that well, it is likely that TCE reduced to DCE, which further degraded, provoking the C-IMB enrichment (**Figure A-10 [b]**). Similarly, W1462 and W1445 are close to Unit C, therefore, both wells have redox conditions potentially favorable to TCE reductive dechlorination. Therefore, only one well in the shallow aquifer shows evidence of TCE aerobic cometabolism. Based on these results, reductive dechlorination appears to be the primary

biological attenuation mechanism leading to isotope enrichment in all zones, with oxidative cometabolism being a weaker influence.

4.4 Occurrence of Oxidative Transformation of TCE daughter products

Note the C-IMB would be constant if reductive dechlorination was the sole degradation pathway of CEs, in absence of further ethene degradation. Significantly enriched C-IMB values (with respect to the TCE source, i.e., $\delta^{13}\text{C-TCE} > -24\text{‰}$, see before) were observed at roughly 30% of the wells in the shallow TCE plume, scattered throughout the aquifer (**Figure 3A**). About 50% of the wells in the deep plume show significant enrichments of the C-IMB, with shifts reaching 10‰ above $\delta^{13}\text{C-TCE}_{\text{Source}}$. DCE (cis- or trans-DCE) is detected in more than half of these wells.

To explain the process leading to the C-IMB enrichment, two degradation schemes are theoretically possible: (i) partial TCE oxidation (enriching the C-IMB) followed by reductive dechlorination; and (ii) TCE reductive dechlorination followed by oxidation of daughter product(s). For both aquifers, C-IMB enrichment is always related to $\delta^{13}\text{C-TCE}$ enrichment, while TCE reductive dechlorination to DCE is the main degradation pathway for TCE (see above). Moreover, those enriched C-IMB values indicative of oxidation are unrelated to the oxygen levels (**Figure A-15**), probably due to mixing of groundwater from different layers in the long wells (3 to 6 m) while sampling (**Table 2-7** in [CH₂MHILL 2009]). Since TCE reductive dechlorination is not supposed to lead to C-IMB enrichment, the observed C-IMB enrichment likely results from further DCE degradation.

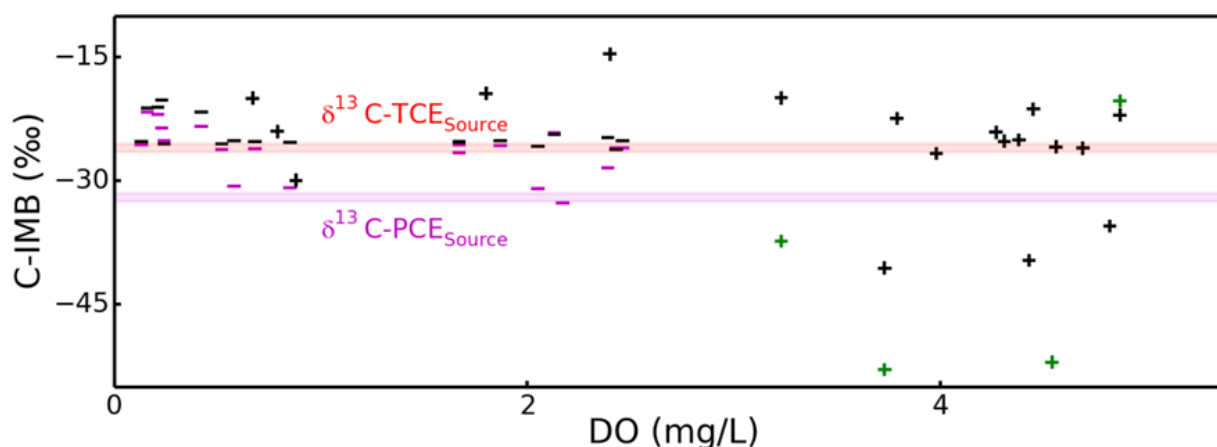


Figure A-15. Carbon isotope mass balance (C-IMB) versus dissolved oxygen concentrations. (-): shallow wells, excluding (black) or including (purple) PCE; (+): deep plume, excluding (black) or including (green) ethene. The red and purple shaded areas show the range in which the plume samples are not significantly different from the sources.

We hypothesize that DCE production from reductive dechlorination occurred before the CE plume moved through aerobic zones, causing the oxidation of DCE and of its daughter products, and, potentially TCE aerobic cometabolism. Since TCE aerobic cometabolism is slower than its daughter products' degradation, TCE oxidation, if any, is expected to be of lesser importance than DCE oxidation.

Because of the mixed redox conditions at the site, many degradation pathways are possible in addition to DCE reductive dechlorination: TCE cometabolic bacteria, are potentially capable of DCE and VC aerobic cometabolism (Alvarez-Cohen and Speitel 2001). Given the demonstrated

presence and activity throughout both the shallow and the deep plume of cometabolic bacteria, DCE and VC might degrade through cometabolism. Also traces of ethane were detected near Unit C (**Figure A-1**); therefore further degradation of ethene through anaerobic degradation into ethane may have occurred. VC and DCE mineralization to CH₄ and CO₂ under reductive conditions was suggested as a potential degradation pathway in iron reducing and methanogenic conditions (Bradley, 1996; Bradley and Chapelle, 1997). However, a recent study proved that VC degrades under hypoxic conditions, below the traditional limit of 0.5 mg DO/L employed to characterize anoxic environments (Gossett, 2010).

The importance of anaerobic oxidation for VC and DCE degradation in nominally anoxic conditions might be overestimated (Bradley and Chapelle, 2011), and is not considered as a potential degradation pathway at this site. Since hypoxic conditions can be induced by recharge events, VC and DCE direct oxidation is also likely where water from the surface infiltrates in the Unit C. The variable redox conditions suggest therefore the coexistence of different pathways for DCE and VC degradation.

4.5 TCE and PCE Plume Mixing

The shallow PCE and TCE plume partly mix in Unit A. Since $\delta^{13}\text{C-PCE}_{\text{Source}}$ is depleted compared to $\delta^{13}\text{C-TCE}_{\text{Source}}$, the mixing of both plumes will cause the complete C isotope mass balance including PCE (C-IMBPCE) to take any value between both source values. In the presence of two plumes with different source values in a reductive environment, C-IMB is then a precious indicator of mixing. In the shallow plume, only few wells might present mixing between PCE and TCE plumes, most of the wells being impacted by a dominant compound, either TCE or PCE (**Figure A-16**). The wells where PCE is the main compound are, as mentioned earlier, near the water table.

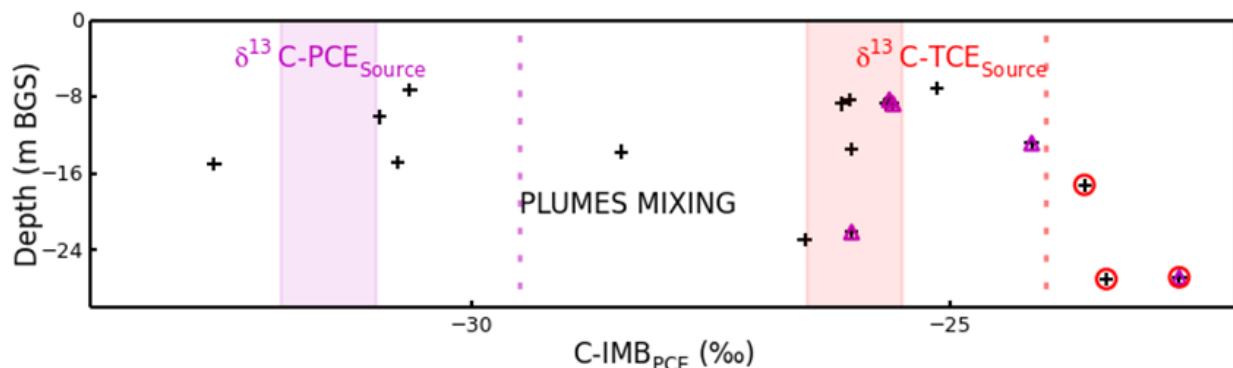


Figure A-16. Complete C-IMB (PCE values included) versus depth (meter below ground surface) for wells where PCE was detected. The source values are represented by their uncertainties range, in purple for PCE and red for TCE. The dashed lines represent the value above which C-IMB is significantly enriched compared to $\delta^{13}\text{C-TCE}_{\text{Source}}$ (red) and $\delta^{13}\text{C-PCE}_{\text{Source}}$ (magenta). Significantly enriched $\delta^{13}\text{C-TCE}$ and $\delta^{13}\text{C-PCE}$ are signaled by red circles and magenta triangle, respectively.

4.6 Relevance of Permeability Heterogeneity for Degradation

In the deep plume, TCE and DCE C isotope ratios are less enriched downgradient than near the source zone (see **Figure A-10 [b, d]**). The coexistence of a mobile and an immobile domain, or heterogeneities in porosity, is suggested in the Remediation Investigation (RI) report in paragraph

5.6.1.4 (CH₂MHILL 2009). In the immobile domain, the conditions are likely to be reductive, and CEs remain in contact with dechlorinating microorganisms for a longer time, while on the contrary, the presence of advective groundwater flow in the mobile domain flushes the CEs further away in the aquifer with little potential and time for degradation.

Back-diffusion (matrix diffusion) of CEs from low permeability zones releases degraded CEs in the mobile aquifer domain (Parker, 2008), when in contact with lesser polluted water. Moreover, low permeability layers have an important role in degradation, as they present reductive conditions and are likely to host microbial populations capable of reductive dechlorination, and methanogenic bacteria (Takeuchi, Kawabe et al. 2011; Damgaard, Bjerg et al. 2013). Therefore, the presence of clay layers embedded in a sandy aquifer supports this hypothesis (**Figures A-11** and **A-13**, cross sections A-8, A-9).

Other processes are also influenced by the presence of clay lenses. CEs aerobic cometabolic degradation through the methane monooxygenase (sMMO) enzyme, for example, requires the proximity of methane and oxygen. Groundwater flowing from Unit A to Unit C might create the necessary aerobic/anoxic interfaces at the surface of the clay lenses to enable this process.

4.7 Sorption as Explanation for Depleted C-IMB Values in the Deep TCE Plume

Throughout the deep plume, 8 wells, (including 2 wells sampled with PDBs), present a C-IMB significantly lower than the lowest $\delta^{13}\text{C}$ -TCE measured at the site (i.e., C-IMB < -26.2‰). C-IMBs of 4 of these wells are even lower than PCE source value ($\delta^{13}\text{C}$ -PCE_{Source} = -31.5‰). For 3 of those 8 wells, the C-IMB depletion related to the detection of depleted ethene (**Figure A-10 [c]**), which is a potential product of CEs reduction.

However, the extremely low C-IMB observed in the presence of ethene ($\delta^{13}\text{C}$ -ETH = -53 to -38‰; <0.03 $\mu\text{mol/L}$), as well as the general absence of VC in the aquifer, suggests that the presence of ethene is disconnected from the other CEs. This is possibly caused by different flow velocities of the CEs, induced by a decreased preference for sorption in the order TCE to ethene. Indeed, based on the retardation factors calculated for the CEs (**Table A-4**), TCE would travel 3 times slower than ethene in Unit C. Likewise, DCE, which is present in 7 of those 8 wells, is travelling twice as fast as TCE, and a surplus of depleted DCE or ethene due to disproportionate travel speed could contribute to the depletion of the C-IMB. Since groundwater velocity is higher in this part of the aquifer (**Figure A-5**), the impact of retardation is more likely to be visible even with small travel distances. Observations are in line with the effects of sorption on C isotope balances as modeled by van Breukelen et al., which presented a similar decrease of C-IMB with distance (van Breukelen et al., 2005). Sorption effects associated with depleted C-IMBs are not observed in Unit B, either because the C-IMB enrichment due to oxidation is higher than the depletion effect of sorption, or because chromatographic effects are lower in Unit B. Indeed, if the retardation factors observed in the porous fraction of Unit B are comparable with those observed in Unit A, retardation between TCE and cDCE is negligible (**Table A-4**), whereas adsorption in Unit C has a large impact on CEs' transport.

4.8 Groundwater Age and Isotope Effects of Transport Processes

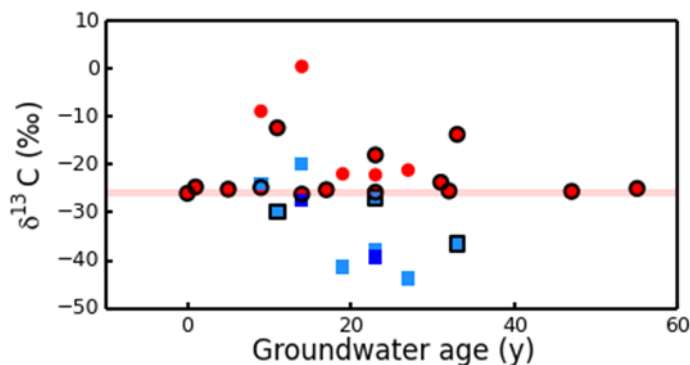


Figure A-17. C isotope ratios for TCE (red circles), cDCE (light blue squares) and tDCE (dark blue squares), along with the groundwater age. Shallow wells are identified with a black halo. The red line corresponds to the uncertainty on the source.

Groundwater age based on tritium-helium dating was determined before for 38 wells throughout the aquifer (CH₂MHILL 2007), of which 18 detected CEs. Whereas the expected trend for homogeneous first-order degradation is linear, δ¹³C enrichment with age, a trend with groundwater age is absent for both DCE and TCE (**Figure A-17**). This is in line with the previous CSIA versus distance plot (**Figure A-10 [b, c]**).

Consequently, since uniform progress of degradation with time is not applicable at this site, the model compared wells based on reaction progress and with the first-order degradation rates set relative to the one of TCE (k_{TCE}) without a specified time unit. Note this approach does not consider the effects of physical transport processes on isotope ratios. Since hydrodynamic dispersion was shown to attenuate isotope signals (Abe and Hunkeler 2006; Van Breukelen and Prommer 2008; Abe, Aravena et al. 2009), this batch model setup might lead to underestimation of the enrichment factors (ϵ) in our model. Consequently, the extent of degradation calculated through the Rayleigh equation might be underestimated. Counteracting this effect, diffusion into low permeability layers would provoke enrichment of pollutants in the mobile domain, since light isotopologues diffuse at greater rates (LaBolle, Fogg et al. 2008). Similar effects are expected for sorption at the fringes of the plume (Van Breukelen and Prommer 2008). Since, at this site, interbedded clay layers are frequent, diffusion and sorption in the clay layers is potentially enriching C and Cl isotopes with distance, leading to an overestimation of degradation.

5.0 RESULTS AND DISCUSSION: MODEL APPLICATION

Several simulations were performed with the RTM described in **Sections 5-8** in the main report, and compared with site CSIA data with the goal of identifying dominant contaminant attenuation processes. The model approach and input parameters are described below with results described in **Sections 5.2** through **5.4**.

5.1 Model Approach

Site heterogeneities in both geochemistry and hydrogeology exert a large impact on both CEs degradation extent and repartition. CEs degradation as judged from CSIA results, appears to be unevenly spread across the shallow plume, while occurring only near the former source of the deep plume (**Figure A-10 [b,d]**). A “black box” model approach describes best the observations and allows for the estimation of area-specific enrichment factors. In this batch model all reactions were assumed to occur simultaneously in time without simulation of actual transport processes. Consequently, both the potential C isotope enrichment with distance due to diffusion and sorption, and the attenuation of isotope signals due to hydrodynamic dispersion, are not taken into consideration.

Since both the deep and the shallow plumes originate from the same source, observations of both TCE plumes were combined in the batch model. PCE degradation was not included in the model for TCE, because its impact on TCE was estimated to be insignificant (see above). The model included two main steps: (i) determination of the C, Cl and H enrichment factors for TCE reductive dechlorination; and (ii) the modeling of both DCE degradation pathway hypotheses (oxidation and reductive dechlorination, see above), for comparison with the observed data.

VC was mostly not detected during Winter 2012/2013, and only present as traces since the beginning of the investigation. Since VC isotope ratios are not available at the site, the few available ethene results were not modeled. VC disappearance was modeled through fast oxidation, which is a reasonable assumption since VC oxidation rates are generally relatively high (Alvarez-Cohen and Speitel 2001). For this purpose, k_{VC} , the first-order rate for VC oxidation, was set to $10 \times k_{TCE}$.

Out of the 59 wells investigated at the site, only 6 wells present t-DCE molar fractions with respect to total CEs above 15%. When present, t-DCE stands in average for about 20% of total DCEs. In general, the highest t-DCE fractions are found in the first half of the deep TCE plume. In the shallow plume, the average t-DCE fraction is 5% when t-DCE is detected, and is even lower in the second half of the deep TCE plume with 1%. Therefore, t-DCE will be modeled only for approximately the first half of the deep plume, and neglected for the shallow plume and the second half of the deep TCE plume.

Table A-5. Calibrated Isotope Fractionation Factors (%)

Reaction	Carbon		Chlorine		Hydrogen
	ϵC (bulk)	ϵCl_{bulk}	ϵCl_{SKIE}	ϵCl_{KIE}	ϵH_{bulk} SKIEs
TCE → c-DCE	-20.2 a	-3.8d	-3.3b	-5.1c	-0 ± 10h
TCE → t-DCE	-25e	-3.8e	-3.3e	-5.1e	nm
c-DCE → VC	-26.8f	-1.7f	-1.7g	-1.7g	nm
t-DCE → VC	-26.8e	-1.7e	-1.7e	-1.7e	nm
c-DCE → CO ₂	-8.5f	-0.3f	na	nm	nm
t-DCE → CO ₂	-8.5e	-0.3e	na	nm	nm
VC → CO ₂	nm	na	na	nm	nm

a. Average of the observed difference between initial $\delta^{13}C$ -DCE and parent $\delta^{13}C$ -TCE (**Table A-9**)

b. Average of the observed difference between initial $\delta^{37}Cl$ -DCE and parent $\delta^{37}Cl$ -TCE (**Table A-9**)

c. ϵCl_{KIE} of the TCE to c-DCE step follows from $3 \times \epsilon Cl_{bulk} - 2 \times \epsilon Cl_{SKIE}$ (MEAN)

d. $\epsilon Cl = \epsilon C \times \epsilon Cl / \epsilon C$

e. Set similar to enrichments relative to c-DCE reactions – except for ϵC , set lower for t-DCE production

f. Taken from the literature (Abe et al., 2009; Kuder et al., 2013)

g. Because of the absence of VC, it is not possible to differentiate $\epsilon Cl_{SKIE}(\beta c)$ and ϵCl_{KIE} which are then equal to ϵCl_{bulk}

h. Obtained by manual fitting

na = not applicable, nm = not modeled/fitted

In the attempt to model the data measured at the site, 4 sets of simulations were performed (**Table A-6**). TCE reductive dechlorination to DCE was first simulated, with and without production of t-DCE, by using the enrichment factors determined for this field site as presented in **Table A-5**. For a better description of the data, DCEs degradation was simulated. Both reductive dechlorination and oxidation of c-DCE were compared, using enrichment factors from the literature. Other model parameter values obtained by calibration (source values and degradation rates) are presented in **Tables A-7** and **A-8**.

Table A-6. Description of the 4 Set of Simulations

Model	Set of data	Other characteristics		Figure
Model 1 Reductive dechlorination only	End of deep plume Shallow plume	Variations in source value within the range for chlorine and hydrogen		A-18
Model 2 Reductive dechlorination only	Beginning of deep plume	Variations in source value within the range for chlorine and hydrogen		A-19
Model 3 c-DCE oxidation vs c-DCE reductive dechlorination	End of deep plume Shallow plume	Variations in DCE relative degradation rate	Simultaneously with TCE reductive dechlorination	A-20
Model 4 c-DCE and t-DCE oxidation vs c-DCE and t-DCE reductive dechlorination	Beginning of deep plume	Variations in DCE relative degradation rate	Simultaneously with TCE reductive dechlorination	A-21

Table A-7. Source Values for Carbon, Chlorine and Hydrogen Isotope Ratios

	$\delta^{13}\text{C-TCE0}$	$\delta^{37}\text{Cl-TCE0}$	$\delta^2\text{H-TCE0}$
Model 1			
1.1	-26	1.5	-240
1.2	-26	3.5	-255
1.3	-26	2.5	-270
Model 2			
2.1	-26	2.5	-
2.2	-26	1.5	-
2.3	-26	3.5	-
2.4	-26	2.5	-
Model 3	-26	2.5	-
Model 4	-26	2.5	-

Table A-8. Degradation Rates

	$TCE \rightarrow t\text{-DCE}$	$TCE \rightarrow t\text{-DCE}$	$c\text{-DCE} \rightarrow VC$	$t\text{-DCE} \rightarrow VC$	$c\text{-DCE} \rightarrow CO_2$	$t\text{-DCE} \rightarrow CO_2$	$VC \rightarrow CO_2$
Model 1							
1.1-1.2-1.3	1	-	-	-	-	-	-
Model 2							
2.1	1	-	-	-	-	-	-
2.2-2.3-2.4	0.8	0.2	-	-	-	-	-
Model 3							
3.1	1	-	0.2	-	-	-	10
3.2	1	-	0.8	-	-	-	10
3.3	1	-	-	-	0.4	-	-
3.4	1	-	-	-	1.2	-	-
Model 4							
4.1	0.8	0.2	0.2	0.2	-	-	10
4.2	0.8	0.2	0.8	0.8	-	-	10
4.3	0.8	0.2	-	-	0.4	0.4	-
4.4	0.8	0.2	-	-	1.2	1.2	-

5.2 Modeling the Fate of TCE

At first, TCE reductive dechlorination was modeled using the site observations where t-DCE was negligible. The difference between $\delta^{13}\text{C-TCE}$ and $\delta^{13}\text{C-DCE}$ at the initial stage of transformation provides an estimate of the C isotope enrichment factor of TCE, $\epsilon\text{C-TCE}$ (Hunkeler, Aravena et al. 1999). We considered a DCE molar yield of less than 20% as the reaction being in initial stage (**Table A-9**). However, since simultaneous DCE reductive dechlorination enriches $\delta^{13}\text{C-DCE}$, $\epsilon\text{C-TCE}$ might be underestimated. The resulting $\epsilon\text{C-TCE}$ was approximately -20‰ (**Table A-9**), which provided a good fit of the observations (**Figure A-18**).

Table A-9. Initial values for SKIE calculation: wells with presence of DCE with low fractions, $C-IMB \approx C-IMB_0$ and $\delta^{13}C-TCE \approx \delta^{13}C-TCE_{Source}$.

	$\delta^{13}C-TCE$	$\delta^{13}C-DCE$	Initial $\delta^{13}C$ gap (TCE-DCE)	$\delta^{37}Cl-TCE$	$\delta^{37}Cl-DCE$	C-IMB	xDCE	ϵ_{ClSKIE}
Unit	‰	‰	‰	‰	‰	‰	%	‰
U10_089C	-24.2	-44.2	20.0	2.6	-0.6	-25.4	5.8	3.2
U10_150C	-23.1	-42.8	19.6	2.9	-0.1	-24.2	5.4	3.0
U10_179B	-23.7	-42.2	18.5	3	-0.6	-26.3	14.4	3.6
U10_086A	-21.1	-43.8	22.6	3.5	0.5	-25.4	18.8	3.0
Average	-	-	20.19	-	-	-	-	3.2

The calculation of the ϵ_C/ϵ_{Cl} slope of TCE was limited to wells i) fitted with $\epsilon_C-TCE = -20.2\text{‰}$, and ii) presenting no evidence of oxidation (i.e., $C-IMB < -24\text{‰}$). Such wells are likely to present TCE reductive dechlorination only. The resulting ϵ_{Cl}/ϵ_C for those wells reaches 0.19 (**Figure A-18** [g]), which is in the literature range (0.16 – 0.37, see **Figure A-9**).

The Cl bulk enrichment factor $\epsilon_{Clbulk-TCE}$ was calculated from the ϵ_C/ϵ_{Cl} slope of TCE and ϵ_C-TCE values as determined before, following the method employed in Wiegert et al. (Wiegert, Aeppli et al. 2012). The subsequent ϵ_{Clbulk} was found to be -3.8‰ . Since the reacting Cl atom is released, the difference between the observed $\delta^{37}Cl-TCE$ and $\delta^{37}Cl-DCE$ at the initial stage of degradation corresponds to a secondary KIE (SKIE; $\epsilon_{ClSKIE} = -3.2\text{‰}$, **Table A-9**) (Hunkeler, 2009). Indeed, during reductive dechlorination, the reacting Cl splits off and is not transmitted to the daughter products; therefore Cl isotope effects between parent and daughter compounds are only due to secondary effects. The primary KIE ($\epsilon_{ClKIE} = -5.1\text{‰}$) was subsequently calculated from $3 \times \epsilon_{Clbulk} - 2 \times \epsilon_{ClSKIE(MEAN)}$ as presented in (Kuder, van Breukelen et al. 2013). ϵ_{Clbulk} , ϵ_{ClKIE} and $\epsilon_{ClSKIE(MEAN)}$ are similar to the values obtained from a microcosm experiment (-3.6‰ , -4.2‰ , and -3.3‰ , respectively (Kuder, van Breukelen et al. 2013).)

Because of the good results obtained for C and Cl isotope ratios, hydrogen isotope ratios were also investigated. CEs dechlorination involves the replacing of a Cl atom through protonation. Therefore, the hydrogen atoms transferred from TCE to DCE are affected only by secondary isotope effects, yielding a small SKIE. Fitting the model is complicated since the source value is not precisely known. Reasonable fits are obtained for $\epsilon_{Hbulk SKIEs}$ in a small range around 0 (-10‰ – $+10\text{‰}$). This is slightly lower than the only previously reported value for TCE by Kuder et al. ($\epsilon_{Hbulk SKIEs}$, $+34\text{‰}$) (Kuder, van Breukelen et al. 2013.) but similar to $\epsilon_{Hbulk SKIEs}$ for DCE reported in the same study ($\epsilon_{Hbulk SKIEs} = +10\text{‰}$).

Figure A-18 shows that the wells of the deep plume (those with low t-DCE fraction) show little degradation in general: both $\delta^{13}C-TCE$ and $\delta^{13}C-DCE$ are relatively depleted. The groundwater at the extreme end of this deep plume is of up to 25-30 years old. Consequently, TCE degradation has been a very slow process in the groundwater reaching this area. Conversely, degradation is important in the shallow plume, but only at 11 wells, including one in the ERD pilot test zone. The other wells present no C isotope enrichment. In the shallow plume, CEs degradation is characterized by large TCE C isotope enrichment ($\Delta^{13}C-TCE$ up to about 20‰ ; $\Delta^{37}Cl-TCE$ up to $2-4\text{‰}$ compared to TCE source values). Since the two groups of wells present large differences concerning the degradation extent, it may not be appropriate to employ the same set of enrichment

factors for modeling both sets of observations. This method seems to provide correct results, notably concerning the ϵ_{Cl}/ϵ_C ratios (**Figure A-18 [g]**). The model shows that $\delta^{37}Cl$ -DCE take values within a narrow range, making practically indiscernible the enrichment relative to DCE further degradation from the uncertainty on the source value ($\pm 1\text{‰}$) (**Figure 18 [f]**).

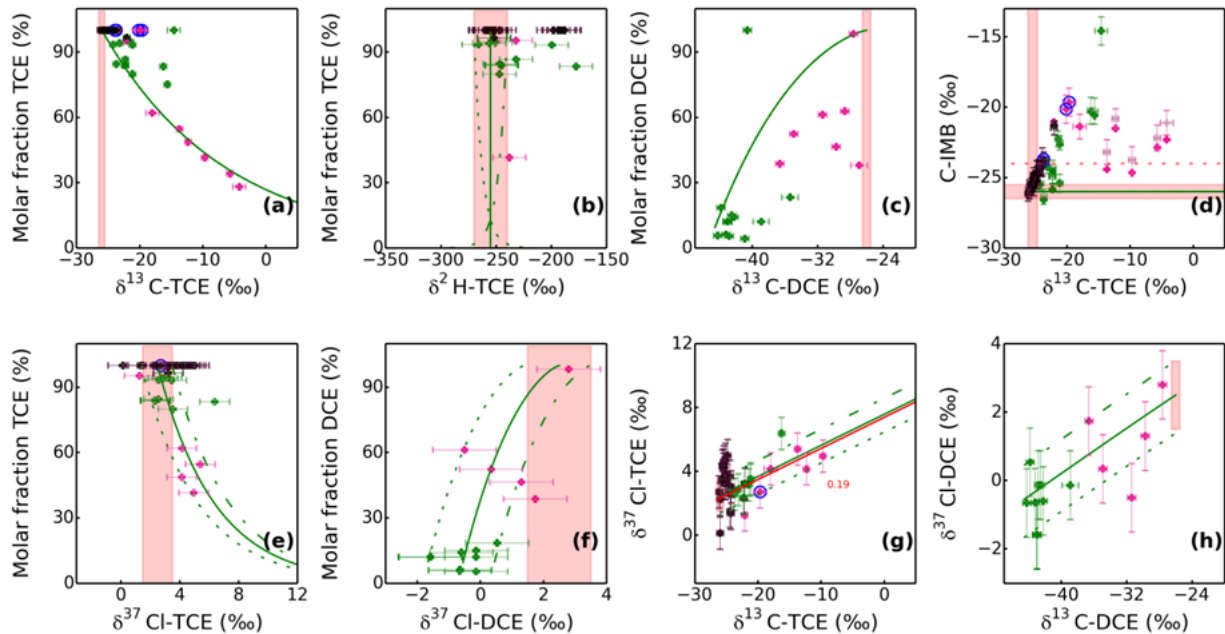


Figure A-18. Model for TCE reductive dechlorination only. Source values for Cl and H were varied within their respective uncertainty range. Different values (-10‰ , 0‰ , 10‰) were employed for $\epsilon_{H_{Bulk}} SKIEs$. The red rectangles present the C and Cl TCE source signature's uncertainty range. Symbols depict observations: shallow plume (pink), extremity of the deep plume (green), data presenting no $\delta^{13}C$ -TCE enrichment (black). Wells with significantly enriched TCE but not detecting DCE are marked with a blue circle.

For wells in the deep plume where t-DCE production is not negligible (t-DCE molar fraction $> 6\%$), trans-DCE production and degradation was added to the model. In order to respect the ratios of c-DCE to t-DCE, k_{TCE} was set to 0.8 for TCE \rightarrow c-DCE and k_{TCE} to 0.2 for TCE \rightarrow t-DCE in order to fit the observations instead of $k_{TCE} = 1$ in the previous simulations. Only C isotope ratios are available for t-DCE, showing that $\delta^{13}C$ -t-DCE reaches more depleted values than $\delta^{13}C$ -c-DCE. Therefore enrichment factors for TCE \rightarrow t-DCE were set to the same values as for TCE \rightarrow c-DCE, except of ϵ_C , which was set lower (-25‰ versus -20‰). The model modification does not strongly affect TCE and c-DCE isotope ratios, since both models, either including or excluding t-DCE, match in **Figure 19 [g, h]**.

However, TCE, c-DCE and t-DCE molar fractions are not well represented (**Figure 19 [a, b, d]**). For example, TCE molar fractions are mostly overestimated by the model. While the TCE enrichment factor seems too large compared to the observations, a smaller enrichment factor would not fit the most depleted $\delta^{13}C$ -c-DCE. Note that in this aquifer area the lithology presents large variability, therefore, site heterogeneity might strongly impact pollutant transport, further accentuated by the high groundwater flow. While no satisfying explanation could be suggested, we expect the transport processes to influence greatly the isotope ratios and the distribution of the

pollutants at this location. Moreover, the spatial well density is low, and the variability over depth, if any, is poorly represented by the long wells. The only well of this group likely to present TCE reductive dechlorination only ($C-IMB \approx \delta^{13}C-TCE_{Source}$) is fitted relatively well by the model (**Figure 19**, in green).

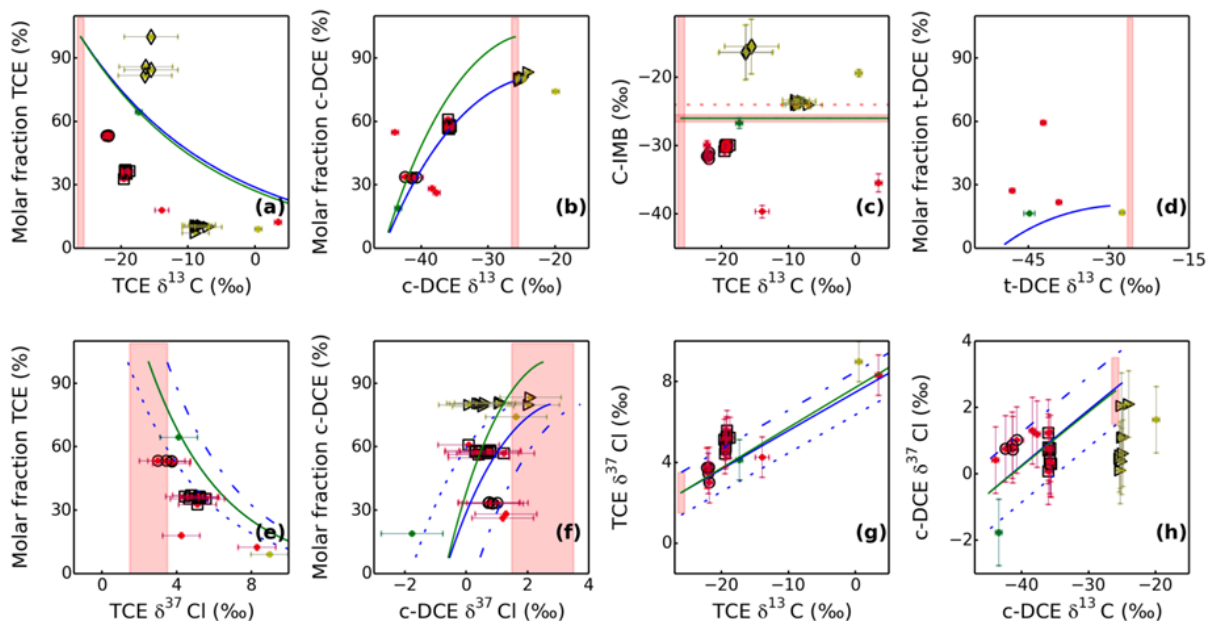


Figure A-19. Model for TCE reductive dechlorination only, with (blue) and without (green) inclusion of *t*-DCE production and degradation. Only wells presenting high *t*-DCE molar fraction (first half of the deep plume) are represented. Source values for Cl were varied within uncertainty limits. The marker colors present wells having depleted C-IMB (red), enriched C-IMB (yellow), and $C-IMB \approx \delta^{13}C-TCE_{Source}$ (green). Black symbols are for long wells sampled through PDBs: U10-042 (circle), U10-093 (diamond), U10-104 (square), U10-116 (triangle).

5.3. DCE Degradation Pathways

VC and ethene were detected in both Unit B and C, indicating that DCE likely degraded reductively. However, the current absence of VC and the relatively little ethene, present at 4 wells in relatively high concentrations, and ethane, only found as traces at the site suggest that CEs or ethene are mostly oxidized. As mention earlier, the patterns of DCE's $\delta^{13}C$ and $\delta^{37}Cl$ enrichment can help determining DCE degradation pathway.

In the shallow plume, the $\delta^{13}C$ -DCE ratios are more depleted than modeled $\delta^{13}C$ of DCE produced by TCE reductive dechlorination, which indicates further DCE degradation (**Figure A-18 [c]**). However, TCE is rarely completely degraded with the exception of one well situated in the Enhanced Reductive Dechlorination (ERD) zone, which presents complete TCE reductive dechlorination (**Figure A-18 [a]**). Therefore, at most of the wells, DCE degradation and TCE reductive dechlorination contribute to the DCE isotopes variations. Moreover, the lack of information on VC isotope ratios hinders the estimation of DCE enrichment factors in case of DCE reductive dechlorination. Consequently, the observations were compared in the following to the two possible DCE degradation pathways, reductive dechlorination and aerobic cometabolism, modeled using enrichment factors from the literature. Enrichment factors were taken from Abe et

al. (Abe, Aravena et al. 2009) for DCE oxidation and Kuder et al. for DCE reductive dechlorination (Kuder, van Breukelen et al. 2013).

The models for DCE reductive dechlorination and DCE oxidation with simultaneous TCE reductive dechlorination are presented **Figure 20**. Simultaneous reductive and oxidative degradation of CEs is not expected at a field site, but such a model might still represent the observations. Indeed, sampling is conducted through long wells (> 3 m) therefore species from different redox environment might become mixed during sampling. Since TCE molar fractions are slightly underestimated by the model (**Figure 20 [a]**), ϵ_C could be set to a smaller value than -20‰ for the shallow plume. Further fitting of the model is not done, since it would introduce more uncertainties into the results. C isotope enrichments alone do not distinguish between the two DCE degradation processes. However, some wells in Unit B which present some of the largest C1 enrichment compared to the produced DCE, might, to some extent, be better represented by DCE reductive dechlorination followed by quick VC oxidation (**Figure 20**).

As mentioned earlier, $\delta^{37}\text{Cl}$ -DCE does not present large differences between degraded and non-degraded DCE, which hinders the determination of DCE degradation pathway. The model shows that DCE degradation seems to be the cause for significant C-IMB enrichment, and therefore, is a necessary step towards CEs mineralization at the site. DCE reduced reductively in the past into VC, which probably oxidized, however, whether or not DCE is degraded through aerobic cometabolism is not clear.

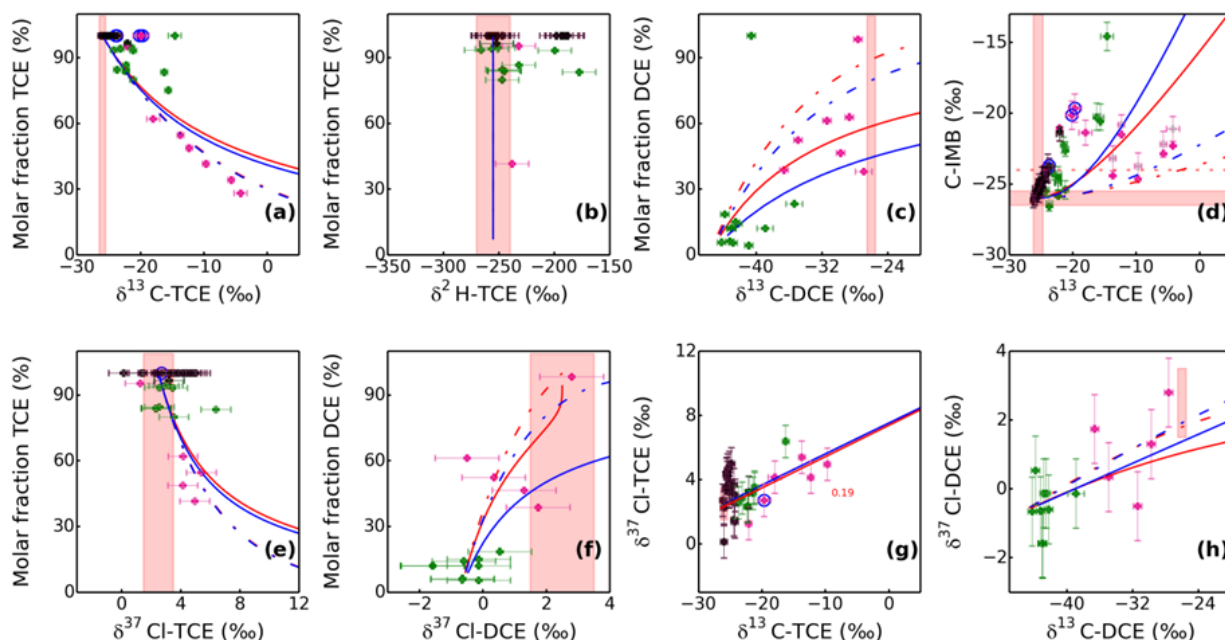


Figure A-20. DCE oxidation model (blue dashed, $k_{DCE} = 0.2 \times k_{TCE}$; blue solid, $k_{DCE} = 1 \times k_{TCE}$) versus DCE reductive dechlorination followed by quick VC oxidation model (red dashed, $k_{DCE} = 0.2 \times k_{TCE}$; red solid, $k_{DCE} = 1 \times k_{TCE}$). The red area indicates the TCE source signature with uncertainty limits. Symbols depict observations: shallow plume (pink), extremity of the deep plume (green), data presenting no $\delta^{13}\text{C}$ -TCE enrichment (black). Wells with significantly enriched TCE but not detecting DCE are marked with a blue circle.

Close to the source of the deep plume, the group of wells presenting non-negligible t-DCE concentrations is showing both enriched and depleted C-IMB (**Figure 21 [c]**). As explained earlier, physical processes are likely to impact the pollutants distribution at the site. Isotope analysis brings further information concerning the degradation processes, despite the low number of wells in this group. At this location, for two out of the three wells showing enriched C-IMB, $\delta^{13}\text{C}$ -c-DCE and $\delta^{13}\text{C}$ -TCE present the highest enrichment (in yellow, **Figure 21 [a, b]**). For TCE, both the final high isotope enrichment observed for DCE, and the 2D-CSIA plots (**Figure 21 [b, g, h]**) would suggest that TCE reductive dechlorination has been a continuous process until an advanced stage of degradation. DCE degradation would therefore here again cause the observed C-IMB enrichment. At the contrary, the wells with depleted C-IMB correspond to lesser enriched $\delta^{13}\text{C}$ for both TCE and DCE. At those wells, the model underestimates c-DCE and t-DCE molar fractions, but overestimates TCE's. Since TCE degradation would enrich the C-IMB, and not deplete it, pollutants transport is likely causing C-IMB depletion.

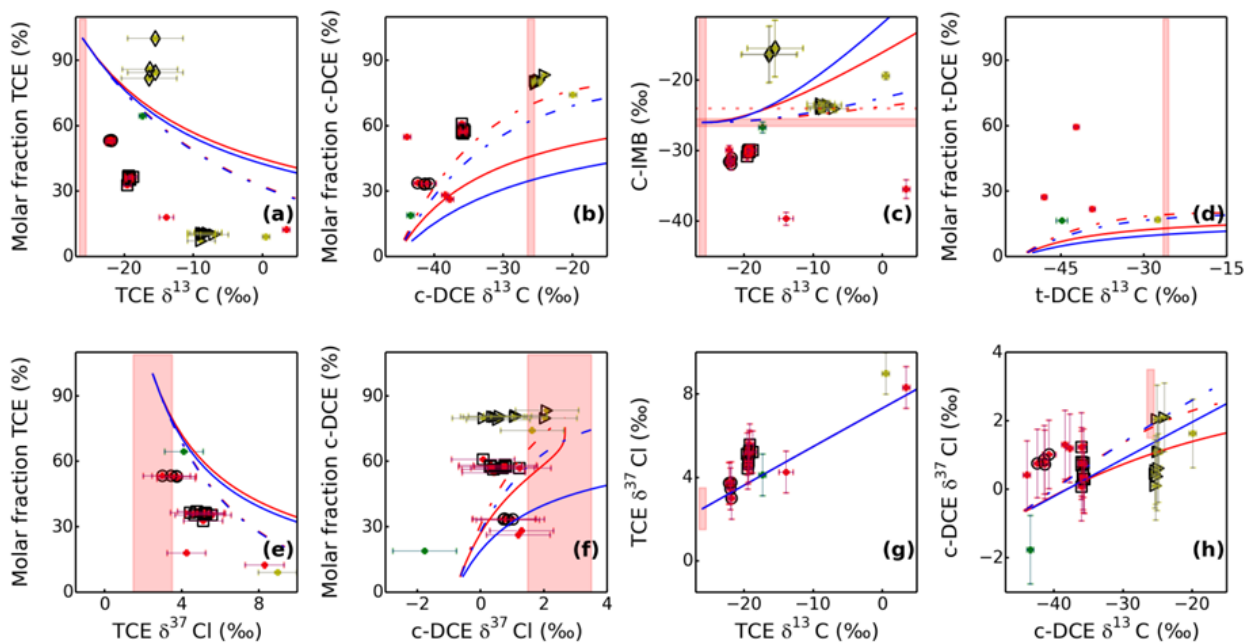


Figure A-21. DCE oxidation model (blue (dash), $k_{DCE} = 0.2 \times k_{TCE}$; blue, $k_{DCE} = 1 \times k_{TCE}$) vs. DCE reductive dechlorination model (red (dash), $k_{DCE} = 0.2 \times k_{TCE}$; red, $k_{DCE} = 1 \times k_{TCE}$). Red area indicates TCE source signature and uncertainty. Only wells presenting high t-DCE molar fraction are represented. Distinction is made between wells presenting depleted C-IMB (red), enriched C-IMB (yellow) and C-IMB $\approx \delta^{13}\text{C}$ -TCE_{Source} (green). Black symbols are for long wells sampled through PDBs: U10-042 (circle), U10-093 (diamond), U10-104 (square), U10-116 (triangle).

5.4 Degradation Extent and Spatial Repartition

The model shows that TCE reduction, and DCE degradation, either through oxidation or reductive dechlorination, are the processes governing CEs mineralization. CEs mineralization is considered achieved when all the DCE produced by TCE reduction is itself degraded. The portion of CEs mineralized (CE_{Deg}) can be estimated using the known degraded fraction of TCE and DCE, as follow:

$$CE_{deg} = (1 - f_{TCE})(1 - f_{DCE}) \quad (2)$$

Where f_{TCE} and f_{DCE} are the remaining fraction of TCE and DCE, respectively. For example, if 40% of TCE and 20% of DCE degraded (i.e., $f_{DCE} = 80\%$) then the total fraction of CE degraded will be $40\% \times 20\% = 8\%$. And if 100% of the produced DCE degraded, $CE_{deg} = 40\% \times 100\% = 40\%$. Remaining fractions f are estimated based on the C isotope ratios measured at the site, and the enrichment factors determined for each degradation process, by applying the model used in the previous sections. Through the model, $\delta^{13}C$ -TCE enrichment describes the remaining fraction of TCE and expected isotope ratios for the produced DCE. Consequently, under the hypotheses that the DCE measured at the same well is the product of TCE degradation, and that DCE degradation is not simultaneous with TCE's, the measured $\delta^{13}C$ -DCE is either equal or enriched compared to the expected $\delta^{13}C$ -DCE for TCE reductive dechlorination only. The difference $\Delta^{13}C$ between the expected value and the detected value is due to DCE degradation process. The fraction of degraded DCE can be calculated from $\Delta^{13}C$ using the Rayleigh equation, and injected in equation (2). Since the DCE degradation pathway is difficult to characterize, the extent of total CEs degradation observed at the site can only be roughly estimated. Based on the model described above, the measured data could be compared to an isomap presenting CE_{Deg} of 5%, 20%, and 50%.

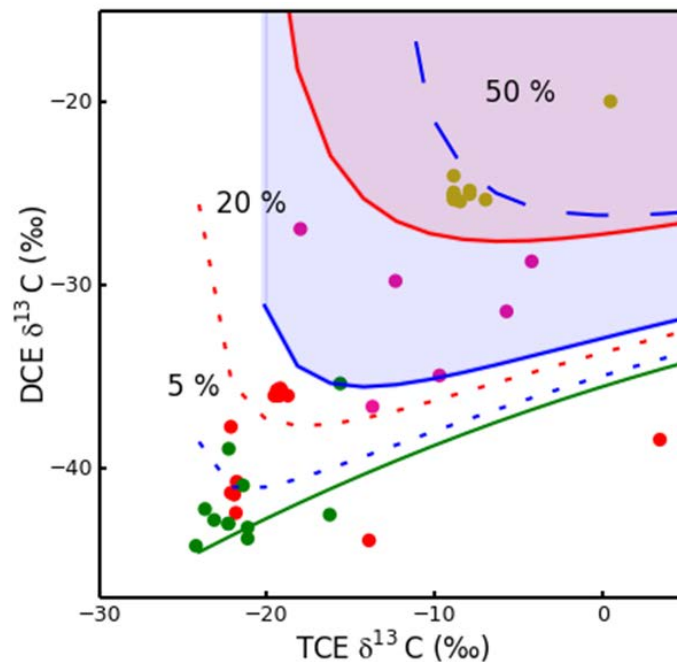


Figure A-22. Isolines characterizing the percentage of total CEs oxidation (small dashes, 5%, full line/shaded area, 20%, large dashes, 50%), for both DCE reductive dechlorination (red) and oxidation (blue), under the condition that VC from DCE reductive dechlorination is degraded instantaneously, in comparison with the model line for TCE reductive dechlorination only (green). The enrichment factors employed are listed in **Table A-5**. Difference was made between wells from the extremity of the deep plume (green); wells presenting significant *t*-DCE concentrations with depleted C-IMB (red), and with enriched C-IMB (yellow); and the shallow wells (magenta).

The results shown **Figure 22** suggest that even in case of DCE oxidation, which shows the smallest enrichment factor (-8.5‰), few wells present an overall CE_{Deg} of above 20%, almost no location reaching 50%. The model gives only an estimate but shows that degradation is limited. Moreover, the model confirms that overall degradation is not important at the extremity of the deep plume (in green, see **Figure 22** and **Figure 23**). Since the shallow plume is sinking in the Unit C, where the deep plume itself shows little degradation, both shallow and deep plumes are likely not to degrade further. **Table A-10** summarizes the results extracted for the study of the site and the model.

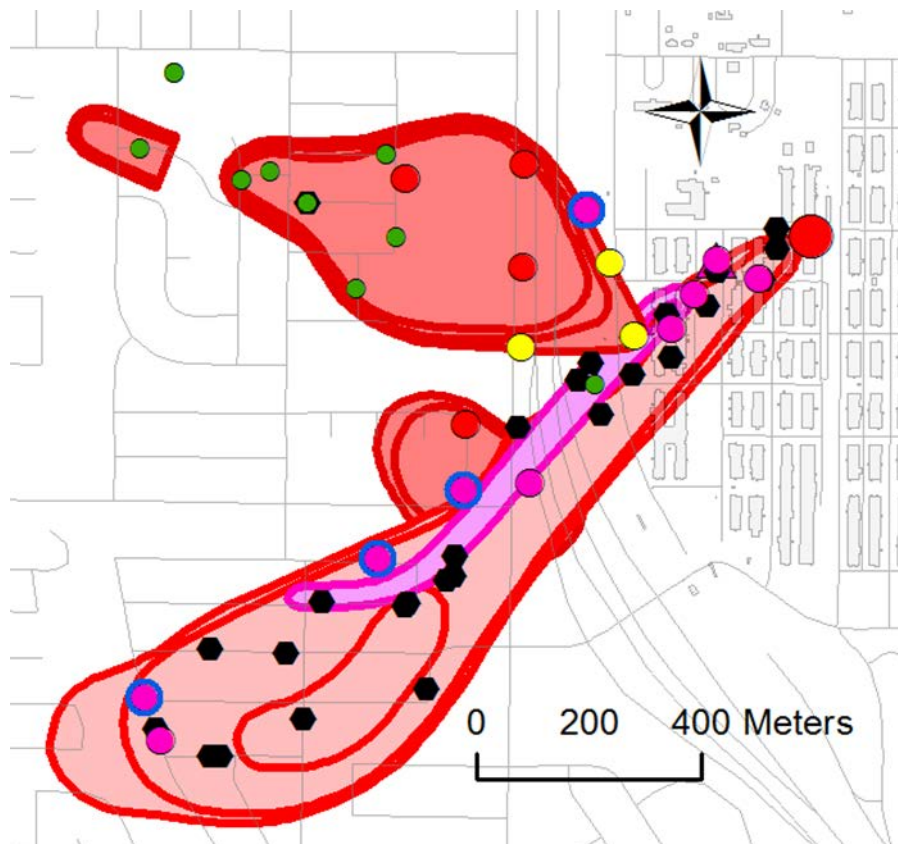


Figure A-23. Map summarizing conclusions: Shallow and deep well extent of degradation. Measured data: Shallow wells with (pink); Deep wells with little TCE reductive dechlorination (green); with *t*-DCE production and some CEs oxidation (red); and, with large extent of oxidation (yellow). The blue arrows shows the leakage from the shallow plume to the Unit C. Wells in black presented no $\delta^{13}C$ -TCE enrichment.

Table A-10. Summary Conclusions

Conclusion	Criteria	Shallow plume	(%)	Deep plume	(%)
No degradation – no measurable proof of TCE cometabolism	No $\delta^{13}\text{C}$ -TCE enrichment	24	65%	1	4%
TCE reductive dechlorination	Fits $\epsilon_{\text{Cl}}/\epsilon_{\text{C}}$ slope even when DCE is not detected	11	30%	20	87%
No TCE	Pure PCE (one well in the shallow plume), DCE (ERD zone), and DCE/Ethene (deep plume)	2	5%	2	9%
Total		37	100%	23	100%
Further DCE degradation	Align correctly with the model	4		3	
Unusual behavior potentially due to transport	Align partially with the model except for CE molar fractions	2		8	
Potential further DCE degradation until disappearance	$\delta^{13}\text{C}$ -TCE degraded through reductive dechlorination, DCE is not detected	4		1	

6.0 CONCLUSIONS

This study presents the first application of C, Cl, and H CSIA data for the investigation of CEs source apportionment and degradation pathways at a field site consisting of both mixed redox conditions and complex hydrogeology. The studied field site presented three CEs plumes: a shallow PCE and TCE plume and a deep TCE plume. The heterogeneous nature of the aquifer, consisting of interbedded layers of sand and clay greatly impacted the spatial distribution of degradation these conditions were circumvented using a batch model for CEs degradation. Wherein physical transport processes were not taken into account, i.e., the subsurface was regarded as a reaction vessel.

The utilization of C, Cl and H CSIA enabled a better grasp of the degradation pathways at the site. Despite being situated in the aerobic layer the PCE plume showed C isotope enrichment in the deepest part of the (aerobic) aquifer close to fine grained sediment likely to present reductive conditions. PCE degradation was therefore mostly attributable to reductive dechlorination. TCE from PCE reductive dechlorination was to be enriched in the heavy isotopes $\delta^{13}\text{C}$ and $\delta^{37}\text{Cl}$ compared to the primary TCE release. Unfortunately, H isotope ratios could not help distinguishing the industrial TCE from the product of PCE degradation. The product of PCE degradation was not detected, probably due to either mixing with large quantities of industrial TCE, or further TCE degradation.

Based on C and Cl CSIA data, the only pathway clearly identified for TCE degradation is reductive dechlorination, other degradation processes are expected to be insignificant, or do not impact isotope ratios. The enrichment of TCE in ^{13}C was neither linear with groundwater age nor distance. There was no noticeable relation between oxygen concentration and isotope shifts. CSIA modeling resulted in ϵC and ϵCl comparable to previous literature values. It was necessary to include Cl SKIE for properly modeling $\delta^{37}\text{Cl}$ -DCE. The resulting $\epsilon\text{Cl}_{\text{Bulk}}$, $\epsilon\text{Cl}_{\text{Bulk}}$ and ϵH for TCE reductive dechlorination were similar to a previous microcosm experiment (Kuder and Philp 2013). If TCE cometabolism is occurring in the shallow aquifer, this process had no impact on the C isotope ratios.

In the shallow plume, TCE degradation occurred mostly in the vicinity of fine grained sediments amendable to reductive dechlorination. Surprisingly, TCE reductive dechlorination was a slow process in the sandy deep aquifer albeit being mostly anaerobic up to methanogenic. In contrast, large TCE enrichment, and large DCE molar fractions, were found at the leakage area where the deep plume starts and where the heterogeneity of groundwater velocity and permeability is higher. It is likely that the reaction occurred in the interbedded clay layers, where reductive conditions might be stronger, followed by back-diffusion of the CEs in the aquifer.

C-IMB enrichments, which are likely to indicate oxidation processes, were observed mainly where preceding TCE reductive dechlorination occurred. CSIA modeling confirmed that DCE further degradation is indeed responsible for C-IMB enrichment in ^{13}C . While DCE reductive dechlorination occurred in the past, it is not clear whether DCE also oxidize or not. Since VC and ethene were detected in past measurements but are predominately absent in more recent measurements, those compounds degraded further. Whilst their degradation pathway could not be identified, it is expected to be quick compared to their production. Enriched C-IMB is here a precious tool to determine the occurrence or not of CEs mineralization, however, the complexity of the site limits the possibility to bring strong conclusions concerning which of the compounds (DCE, VC, or ethene) is the end product of reductive dechlorination, i.e., is oxidized.

Since $\delta^{13}\text{C-PCE}_{\text{Source}}$ is depleted in ^{13}C relative to $\delta^{13}\text{C-IMB}$, unaffected by reductive dechlorination, could also detect PCE and TCE plumes mixing. However, since C-IMB is also enriched by oxidation processes at this site, mixing gave a clear signal only in the absence of further degradation.

Interbedded clay layers and the aquitard likely played an important role in CEs degradation through reductive dechlorination, and transport. Physical processes, such as sorption, diffusion, and volatilization might also have impacted isotope ratios at this site. Despite the complexity of the site, the degradation processes could be characterized through the use of CSIA modeling in a batch model. Assumptions concerning the enrichment factor for DCE degradation supported development of a first estimation of the extent of CEs mineralization. As a result, CEs degradation patterns as revealed by CSIA is expected to be the most important in Unit B and close to the leakage area to Unit C.

CASE STUDY REFERENCES

- Abe, Y., R. Aravena, J. Zopfi, O. Shouakar-Stash, E. Cox, J. D. Roberts and D. Hunkeler (2009). "Carbon and Chlorine Isotope Fractionation during Aerobic Oxidation and Reductive Dechlorination of Vinyl Chloride and cis-1,2-Dichloroethene." Environmental Science & Technology 43(1): 101-107.
- Abe, Y. and D. Hunkeler (2006). "Does the Rayleigh Equation Apply to Evaluate Field Isotope Data in Contaminant Hydrogeology?" Environ. Sci. Technol. 40(5): 1588-1596.
- Alvarez-Cohen, L. and G. E. Speitel, Jr. (2001). "Kinetics of aerobic cometabolism of chlorinated solvents." Biodegradation 12(2): 105-126.
- Amos, B. K., K. M. Ritalahti, C. Cruz-Garcia, E. Padilla-Crespo and F. E. Löffler (2008). "Oxygen Effect on Dehalococcoides Viability and Biomarker Quantification." Environmental Science & Technology 42(15): 5718-5726.
- Barth, J. A., G. F. Slater, C. Schuth, M. Bill, D. C. Downey, M. Larkin and R. M. Kalin (2002). "Carbon isotope fractionation during aerobic biodegradation of trichloroethene by Burkholderia cepacia G4: a tool to map degradation mechanisms." Applied and Environmental Microbiology 68(4): 1728-1734.
- Bradley, P. M. and F. H. Chapelle (1997). "Kinetics of DCE and VC Mineralization under Methanogenic and Fe(III)-Reducing Conditions." Environmental Science & Technology 31(9): 2692-2696.
- CH₂MHILL (2007). Aquifer Age Dating and Well Screen Profiling for Shallow and Deep Groundwater Plumes, Operable Unit 10, Hill AFB, Utah. Hill AFB, Utah, CH₂M Hill for USAF.
- CH₂MHILL (2009). Groundwater Flow and Transport Model Documentation. Salt Lake City, UT, AFCEE and the Environmental Management Division (75 CEG/CEVR) Hill Air Force Base, Utah.
- CH₂MHILL (2009). Operable Unit 10 Remedial Investigation Report. Salt Lake City, UT, CH₂M Hill for Air Force Center for Engineering and the Environment and Hill Air Force Base, Utah.
- CH₂MHILL (2011). Hill AFB OU10 ERPIMS Database. C. M. f. U. A. Force.
- Chu, K.-H., S. Mahendra, D. L. Song, M. E. Conrad and L. Alvarez-Cohen (2004). "Stable carbon isotope fractionation during aerobic biodegradation of chlorinated ethenes." Environmental Science and Technology 38(11): 3126-3130.
- Cretnik, S., K. A. Thoreson, A. Bernstein, K. Ebert, D. Buchner, C. Laskov, S. Haderlein, O. Shouakar-Stash, S. Kliegman, K. McNeill and M. Elsner (2013). "Reductive Dechlorination of TCE by Chemical Model Systems in Comparison to Dehalogenating Bacteria: Insights from Dual Element Isotope Analysis (13C/12C, 37Cl/35Cl)." Environmental Science & Technology 47(13): 6855-6863.
- Damgaard, I., P. L. Bjerg, J. Bælum, C. Scheutz, D. Hunkeler, C. S. Jacobsen, N. Tuxen and M. M. Broholm (2013). "Identification of chlorinated solvents degradation zones in clay till by high resolution chemical, microbial and compound specific isotope analysis." Journal of Contaminant Hydrology 146(0): 37-50.
- Gorder, K. and C. Hobert (2010). Thiessen Area and Mass Calculator for Assessment of Plume Dynamics. Remediation of Chlorinated and Recalcitrant Compounds: Seventh International Conference on Remediation of Chlorinated and Recalcitrant Compounds, Monterey, CA, Battelle Memorial Institute.

- Habets-Crutzen, A. Q. H., L. E. S. Brink, C. G. vanGinkel, J. A. M. deBont and J. Tramper (1984). "Production of epoxide from gaseous alkenes by resting-cell suspensions and immobilized cells of alkene-utilizing bacteria." Applied Microbiology and Biotechnology 20: 245-250.
- Hunkeler, D., R. Aravena and B. J. Butler (1999). "Monitoring Microbial Dechlorination of Tetrachlorethene (PCE) in Groundwater Using Compound-Specific Stable Carbon Isotope Ratios: Microcosm and Field Studies." Environmental Science and Technology 33(16): 2733-2738.
- Hunkeler, D., N. Chollet, X. Pittet, R. Aravena, J. A. Cherry and B. L. Parker (2004). "Effect of source variability and transport processes on carbon isotope ratios of TCE and PCE in two sandy aquifers." Journal of Contaminant Hydrogeology 74(1-4): 265-282.
- Hunkeler, D., B. M. Van Breukelen and M. Elsner (2009). "Modeling Chlorine Isotope Trends during Sequential Transformation of Chlorinated Ethenes." Environmental Science & Technology 43(17): 6750-6756.
- Kuder, T., B. M. van Breukelen, M. Vanderford and P. Philp (2013a). "3D-CSIA: Carbon, Chlorine, and Hydrogen Isotope Fractionation in Transformation of TCE to Ethene by a Dehalococcoides Culture." Environmental Science & Technology 47(17): 9668-9677.
- Kuder, T. and P. Philp (2013). "Demonstration of Compound-Specific Isotope Analysis of Hydrogen Isotope Ratios in Chlorinated Ethenes." Environmental Science & Technology 47(3): 1461-1467.
- LaBolle, E. M., G. E. Fogg, J. B. Eweis, J. Gravner and D. G. Leaist (2008). "Isotopic fractionation by diffusion in groundwater." Water Resources Research 44(7): W07405.
- Marco-Urrea, E., X. Gabarrell, G. Caminal, T. Vicent and C. Reddy (2008). "Aerobic degradation by white-rot fungi of trichloroethylene (TCE) and mixtures of TCE and perchloroethylene (PCE)." Journal of Chemical Technology and Biotechnology 83: 1190-1196.
- Parkhurst, D. L. and C. A. H. Appelo (1999). Users Guide to PHREEQ (Version 2) -- A computer program for speciation, Batch-Reaction, One-Dimensional Transport and Inverse Geochemical Calculations. Denver, CO, U.S. Department of Interior, U.S. Geological Survey.
- Pooley, K. E., M. Blessing, T. C. Schmidt, S. B. Haderlein, K. T. B. Macquarrie and H. Prommer (2009). "Aerobic Biodegradation of Chlorinated Ethenes in a Fractured Bedrock Aquifer: Quantitative Assessment by Compound-Specific Isotope Analysis (CSIA) and Reactive Transport Modeling." Environmental Science & Technology 43: 7458-7464.
- Puls, R. W. and M. Barcelona (1996). Low-flow (Minimal Drawdown) Groundwater Sampling Procedures. Washington D.C., USEPA: 12.
- Ryoo, D., H. Shim, K. Canada, P. Barbieri and T. K. Wood (2000). "Aerobic degradation of tetrachloroethylene by toluene-o-xylene monooxygenase of Pseudomonas stutzeri OX1." Nature America 18: 775-778.
- Sakaguchi-Soder, K., J. Jager, H. Grund, F. Mattaus and C. Schuth (2007). "Monitoring and evaluation of dechlorination processes using compound-specific chlorine isotope analysis." Rapid Communications in Mass Spectrometry 21(18): 3077-3084.
- Stelzer, N., G. Imfeld, M. Thullner, J. Lehmann, A. Poser, H.-H. Richnow and I. Nijenhuis (2009). "Integrative approach to delineate natural attenuation of chlorinated benzenes in anoxic aquifers." Environmental Pollution 157(6): 1800-1806.
- Takeuchi, M., Y. Kawabe, E. Watanabe, T. Oiwa, M. Takahashi, K. Nanba, Y. Kamagata, S. Hanada, Y. Ohko and T. Komai (2011). "Comparative study of microbial dechlorination

- of chlorinated ethenes in an aquifer and a clayey aquitard.” Journal of Contaminant Hydrology 124(1–4): 14-24.
- Van Breukelen, B. M. and H. Prommer (2008). “Beyond the Rayleigh equation: Reactive transport modeling of isotope fractionation effects to improve quantification of biodegradation.” Environmental Science & Technology 42(7): 2457-2463.
- Wiegert, C., C. Aeppli, T. Knowles, H. Holmstrand, R. Evershed, R. D. Pancost, J. Macháčková and Ö. Gustafsson (2012). “Dual Carbon–Chlorine Stable Isotope Investigation of Sources and Fate of Chlorinated Ethenes in Contaminated Groundwater.” Environmental Science & Technology 46(20): 10918-10925.

**APPENDIX B. LITERATURE SOURCES FOR CARBON AND CHLORINE
ENRICHMENT FACTORS**

Table B-1. Literature Sources for Carbon and Chlorine Enrichment Factors

Compound	Degradation process	$\epsilon^{13}\text{C}$ (‰)	\pm (‰)	$\epsilon^{37}\text{Cl}$ (‰)	\pm (‰)	Reference	Publication Date
PCE	Biodegradation, reductive dechlorination	-19	0.9	-5	0.1	Cretnik	2014
PCE	Biodegradation, reductive dechlorination	-17	4.5			Cichocka	2008
PCE	Biodegradation, reductive dechlorination	-7.1				Liang	2007
PCE	Biodegradation, reductive dechlorination	-5.5	0.8			Slater	2001
PCE	Biodegradation, reductive dechlorination	-5.3		-3.5		Wiegert	2013
PCE	Biodegradation, reductive dechlorination	-5.2				Nijenhuis	2005
PCE	Biodegradation, reductive dechlorination	-5.2	0.3			Slater	2001
PCE	Biodegradation, reductive dechlorination	-3.3	1.2			Aeppli	2010
PCE	Biodegradation, reductive dechlorination	-2.7	0.9			Slater	2001
PCE	Biodegradation, reductive dechlorination	-2				Hunkeler	1999
PCE	Biodegradation, reductive dechlorination	-1.4				Liang	2007
PCE	Biodegradation, reductive dechlorination	-1.3				Liang	2007
PCE	Biodegradation, reductive dechlorination	-0.5				Cichocka	2007
PCE	Biodegradation, reductive dechlorination	-0.4				Nijenhuis	2005
PCE	Chemical reduction	-30	4.3			Liang	2007
PCE	Chemical reduction	-30	0.83			Liang	2007
PCE	Chemical reduction	-25				Dayan	1999
PCE	Chemical reduction	-25	1.1			Liang	2007
PCE	Chemical reduction	-13				VanStone	2004
PCE	Chemical reduction	-7.5				VanStone	2004
TCE	Biodegradation, reductive dechlorination	-19	1			Cichocka	2007
TCE	Biodegradation, reductive dechlorination	-16	0.4	-3.6	0.3	Kuder	2013
TCE	Biodegradation, reductive dechlorination	-16	1.5			Lee	2007
TCE	Biodegradation, reductive dechlorination	-16	0.6			Lee	2007
TCE	Biodegradation, reductive dechlorination	-15	0.79			Liang	2007
TCE	Biodegradation, reductive dechlorination	-14	0.7			Slater	2001
TCE	Biodegradation, reductive dechlorination	-14	1.8			Cichocka	2008
TCE	Biodegradation, reductive dechlorination	-13	1.6			Liang	2007
TCE	Biodegradation, reductive dechlorination	-12	2.3			Cichocka	2007
TCE	Biodegradation, reductive dechlorination	-12	0.5	-3.6	0.1	Cretnik	2013
TCE	Biodegradation, reductive dechlorination	-12	1	-3.6	0.2	Cretnik	2014
TCE	Biodegradation, reductive dechlorination	-9.8	2.6			Fletcher	2011
TCE	Biodegradation, reductive dechlorination	-9.6	0.4			Lee	2007
TCE	Biodegradation, reductive dechlorination	-9.1	0.6	-2.7	0.6	Cretnik	2013
TCE	Biodegradation, reductive dechlorination	-8.8		-3.5		Wiegert	2013
TCE	Biodegradation, reductive dechlorination	-8.5	0.6			Cichocka	2008
TCE	Biodegradation, reductive dechlorination	-8	0.4			Fletcher	2011
TCE	Biodegradation, reductive dechlorination	-7.1				Sherwood-Lollard	1999

Compound	Degradation process	$\epsilon^{13}\text{C}$ (‰)	\pm (‰)	$\epsilon^{37}\text{Cl}$ (‰)	\pm (‰)	Reference	Publication Date
TCE	Biodegradation, reductive dechlorination	-6.6				Bloom	2000
TCE	Biodegradation, reductive dechlorination	-6	0.7			Cichocka	2008
TCE	Biodegradation, reductive dechlorination	-4.1	0.48			Liang	2007
TCE	Biodegradation, reductive dechlorination	-4				Hunkeler	1999
TCE	Biodegradation, reductive dechlorination	-3.5	0.2			Cichocka	2008
TCE	Biodegradation, reductive dechlorination	-3.3	0.3			Lee	2007
TCE	Biodegradation, reductive dechlorination	-2.5				Bloom	2000
TCE	Biodegradation, reductive dechlorination			-5.5		Numata	2002
TCE	Biodegradation, reductive dechlorination			-5.6		Numata	2002
TCE	Biodegradation, reductive dechlorination			-5.7		Numata	2002
TCE	Biodegradation, aerobic cometabolism	-21				Barth	2002
TCE	Biodegradation, aerobic cometabolism	-18				Barth	2002
TCE	Biodegradation, aerobic cometabolism	-15				Pooley	2009
TCE	Biodegradation, aerobic metabolism	-11	0.4			Schmidt K	2014
TCE	Biodegradation, aerobic cometabolism	-1.1	0.3			Chu	2004
TCE	Chemical reduction	-33	1.5			Liang	2007
TCE	Chemical reduction	-28	1.3			Liang	2007
TCE	Chemical reduction	-25	1.9			Slater	2002
TCE	Chemical reduction	-24	2.8			Elsner	2008
TCE	Chemical reduction	-20	1.7			Slater	2002
TCE	Chemical reduction	-20				Prommer	2008
TCE	Chemical reduction	-20				Prommer	2008
TCE	Chemical reduction	-19	4.1			Slater	2002
TCE	Chemical reduction	-17	0.4			Slater	2002
TCE	Chemical reduction	-17	1.4			Slater	2002
TCE	Chemical reduction	-16	1.7			Slater	2002
TCE	Chemical reduction	-15	0.6	-2.6	0.1	Audimiro	2013
TCE	Chemical reduction	-13				VanStone	2004
TCE	Chemical reduction	-10	0.6			Schuetth	2003
TCE	Chemical reduction	-9				VanStone	2004
TCE	Chemical reduction	-8.6				Dayan	1999
TCE	Chemical reduction	-3.3	0.3			Liu	2014
cDCE	Biodegradation, reductive dechlorination	-31	1.5			Schmidt M	2014
cDCE	Biodegradation, reductive dechlorination	-30	1.6			Lee	2007
cDCE	Biodegradation, reductive dechlorination	-27		-1.7		Kuder	2013
cDCE	Biodegradation, reductive dechlorination	-25	1			Fletcher	2011
cDCE	Biodegradation, reductive dechlorination	-22				Jennings	2009
cDCE	Biodegradation, reductive dechlorination	-22	1.3			Fletcher	2011
cDCE	Biodegradation, reductive dechlorination	-21	1.8			Lee	2007
cDCE	Biodegradation, reductive dechlorination	-20	1.2			Slater	2001

Compound	Degradation process	$\epsilon^{13}\text{C}$ (‰)	\pm (‰)	$\epsilon^{37}\text{Cl}$ (‰)	\pm (‰)	Reference	Publication Date
cDCE	Biodegradation, reductive dechlorination	-20	1.5			Hunkeler	2002
cDCE	Biodegradation, reductive dechlorination	-19		-1.5		Abe	2009
cDCE	Biodegradation, reductive dechlorination	-18	2.8			Fletcher	2011
cDCE	Biodegradation, reductive dechlorination	-18	2.7			Fletcher	2011
cDCE	Biodegradation, reductive dechlorination	-17				Jennings	2009
cDCE	Biodegradation, reductive dechlorination	-17	1.4			Lee	2007
cDCE	Biodegradation, reductive dechlorination	-16				Bloom	2000
cDCE	Biodegradation, reductive dechlorination	-16	1.1			Fletcher	2011
cDCE	Biodegradation, reductive dechlorination	-15	0.5			Fletcher	2011
cDCE	Biodegradation, reductive dechlorination	-14				Bloom	2000
cDCE	Biodegradation, reductive dechlorination	-12				Hunkeler	1999
cDCE	Biodegradation, aerobic metabolism	-15	0.5			Schmidt	2010
cDCE	Biodegradation, aerobic cometabolism	-9.8	1.7			Tiehm	2008
cDCE	Biodegradation, aerobic cometabolism	-8.8	1			Tiehm	2008
cDCE	Biodegradation, aerobic metabolism	-8.5		-0.3		Abe	2009
cDCE	Biodegradation, aerobic cometabolism	-8.2	3.5			Tiehm	2008
cDCE	Biodegradation, aerobic cometabolism	-7.2				Pooley	2009
cDCE	Biodegradation, aerobic cometabolism	-7.1	0.9			Tiehm	2008
cDCE	Biodegradation, aerobic cometabolism	-0.4	0.5			Chu	2004
cDCE	Chemical reduction	-40				Prommer	2008
cDCE	Chemical reduction	-22	1.8			Elsner	2008
cDCE	Chemical reduction	-21	1.8	-6.2	0.8	Audimiro	2013
cDCE	Chemical reduction	-20				Prommer	2008
cDCE	Chemical reduction	-16				VanStone	2004
cDCE	Chemical reduction	-14				Dayan	1999
cDCE	Chemical reduction	-9.4				VanStone	2004
tDCE	Biodegradation, reductive dechlorination	-30	1.9			Hunkeler	2002
tDCE	Biodegradation, reductive dechlorination	-28	1.4			Lee	2007
tDCE	Biodegradation, reductive dechlorination	-21	0.9			Lee	2007
tDCE	Biodegradation, reductive dechlorination	-21	1.5			Fletcher	2011
tDCE	Biodegradation, reductive dechlorination	-21	2.8			Fletcher	2011
tDCE	Biodegradation, aerobic cometabolism	-6.7				Brungard	2003
tDCE	Biodegradation, aerobic cometabolism	-3.5				Brungard	2003
11DCE	Biodegradation, reductive dechlorination	-24	1.2			Lee	2007
11DCE	Biodegradation, reductive dechlorination	-12	1.1			Schmidt M	2014
11DCE	Biodegradation, reductive dechlorination	-8.4	0.3			Lee	2007
11DCE	Biodegradation, reductive dechlorination	-7.3	0.4			Hunkeler	2002
11DCE	Biodegradation, reductive dechlorination	-6.3	1.2			Fletcher	2011
11DCE	Biodegradation, reductive dechlorination	-5.8	0.5			Lee	2007
11DCE	Biodegradation, reductive dechlorination	-5.1	0.3			Fletcher	2011

Compound	Degradation process	$\epsilon^{13}\text{C}$ (‰)	\pm (‰)	$\epsilon^{37}\text{Cl}$ (‰)	\pm (‰)	Reference	Publication Date
VC	Biodegradation, reductive dechlorination	-31	0.4			Hunkeler	2002
VC	Biodegradation, reductive dechlorination	-29	1.5			Schmidt M	2014
VC	Biodegradation, reductive dechlorination	-27	1.9	-2.7	0.4	Kuder	2013
VC	Biodegradation, reductive dechlorination	-27				Bloom	2000
VC	Biodegradation, reductive dechlorination	-26				Hunkeler	1999
VC	Biodegradation, reductive dechlorination	-25		-1.8		Abe	2009
VC	Biodegradation, reductive dechlorination	-24	2			Lee	2007
VC	Biodegradation, reductive dechlorination	-24	1.1			Fletcher	2011
VC	Biodegradation, reductive dechlorination	-23	1.8			Fletcher	2011
VC	Biodegradation, reductive dechlorination	-23	1.1			Fletcher	2011
VC	Biodegradation, reductive dechlorination	-23	0.8			Lee	2007
VC	Biodegradation, reductive dechlorination	-22	1.8			Slater	2001
VC	Biodegradation, reductive dechlorination	-22	1.2			Fletcher	2011
VC	Biodegradation, reductive dechlorination	-22				Bloom	2000
VC	Biodegradation, reductive dechlorination	-20	0.6			Fletcher	2011
VC	Biodegradation, aerobic metabolism	-8.2	0.1			Chartrand	2005
VC	Biodegradation, aerobic metabolism	-7.6	0.1			Chartrand	2005
VC	Biodegradation, aerobic metabolism	-7.2		-0.3		Abe	2009
VC	Biodegradation, aerobic metabolism	-7.1	0.2			Chartrand	2005
VC	Biodegradation, aerobic metabolism	-7.1	0.4			Chartrand	2005
VC	Biodegradation, aerobic metabolism	-7	0.3			Chartrand	2005
VC	Biodegradation, aerobic metabolism	-6.5	0.4			Thiem	2008
VC	Biodegradation, aerobic metabolism	-6.3	0.3			Thiem	2008
VC	Biodegradation, aerobic metabolism	-5.7	1.1			Chu	2004
VC	Biodegradation, aerobic (mixed culture)	-5.5	0.8			Chu	2004
VC	Biodegradation, aerobic metabolism	-5.5	0.3			Thiem	2008
VC	Biodegradation, aerobic metabolism	-5.4	0.8			Thiem	2008
VC	Biodegradation, aerobic metabolism	-5.4	0.4			Thiem	2008
VC	Biodegradation, aerobic cometabolism	-4.8	0.3			Chu	2004
VC	Biodegradation, aerobic (mixed culture)	-4.5	1			Chu	2004
VC	Biodegradation, aerobic cometabolism	-3.2	0.3			Chu	2004
VC	Chemical reduction	-19	0.8			Elsner	2008
VC	Chemical reduction	-18				VanStone	2004
VC	Chemical reduction	-8.7				VanStone	2004
VC	Anerobic oxidation	-4.3				Smits	2011
ETH	Biodegradation, reductive dechlorination	-6.7	0.4			Mundle	2012
ETH	Biodegradation, reductive dechlorination	-4	0.8			Mundle	2012
ETH	Biodegradation, reductive dechlorination	-3				Bloom	2000
ETH	Biodegradation, aerobic metabolism	-3	0.3			Mundle	2012
ETH	Chemical reduction	-0.1				Prommer	2008

Notes:

1. PCE = tetrachloroethene, TCE = trichloroethene, c DCE = cis-1,2- dichloroethene, t DCE = trans-1,2- dichloroethene, 1,1DCE= 1,1- dichloroethene, VC = vinyl chloride, ETH = ethene.
2. $\epsilon^{13}\text{C}$ (‰) = enrichment factor for carbon, $\epsilon^{37}\text{Cl}$ (‰) , \pm (‰) = standard deviation or statistical variability of enrichment factor determined from the study.
3. Reference – first author, last name of the literature citation from the reference list, below.
4. Publication date – date of publication of the reference.

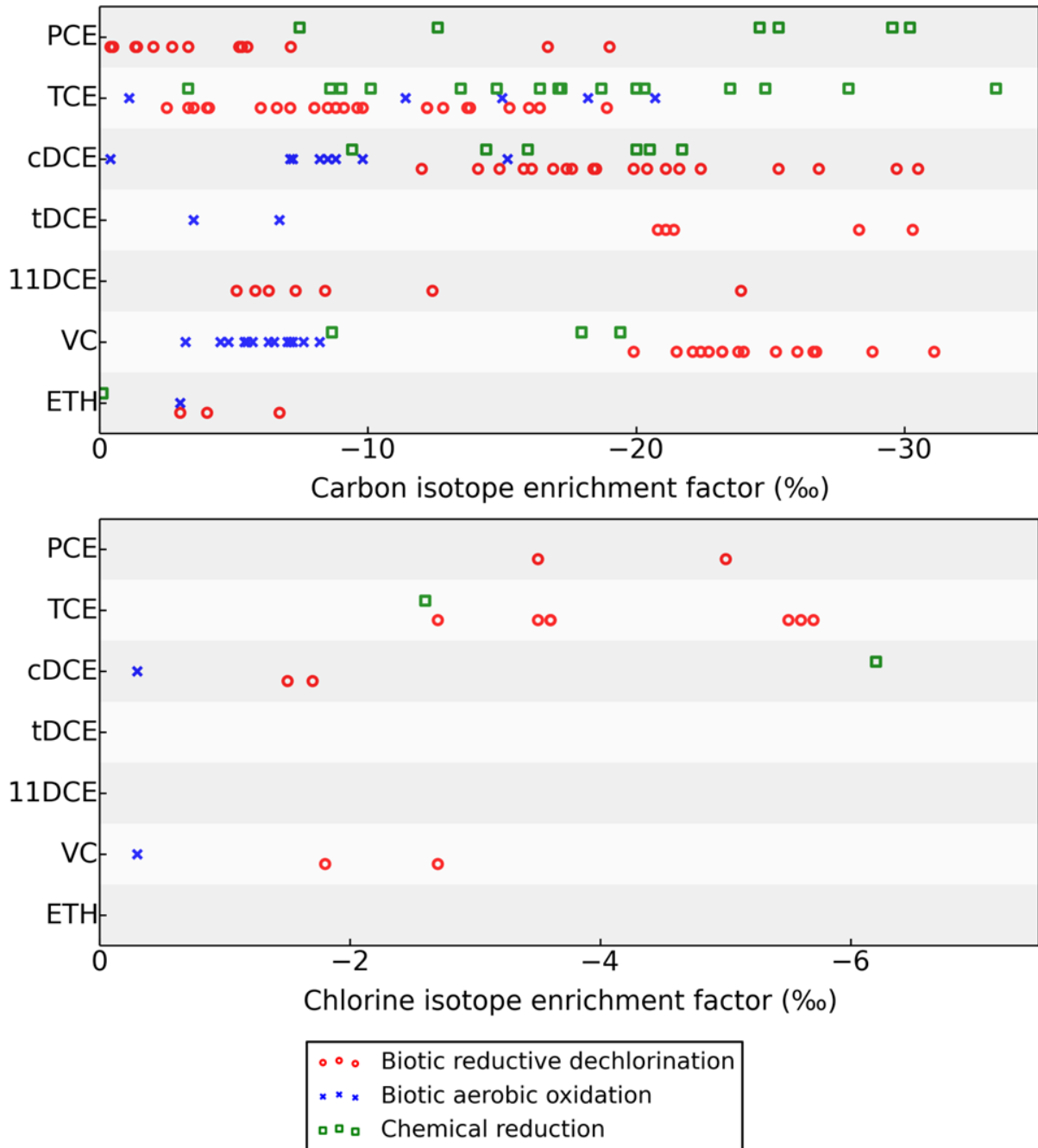


Figure B-1. Carbon and chlorine isotopic enrichment factors (ϵ) for several contaminants and degradation processes.

REFERENCES FOR TABLE B-1 AND FIGURE B-1

- Abe, Y. et al., 2009. Carbon and Chlorine Isotope Fractionation during Aerobic Oxidation and Reductive Dechlorination of Vinyl Chloride and cis-1,2-Dichloroethene. *Environmental Science & Technology*, 43(1): 101-107.
- Aeppli, C. et al., 2010. Quantifying In Situ Transformation Rates of Chlorinated Ethenes by Combining Compound-Specific Stable Isotope Analysis, Groundwater Dating, And Carbon Isotope Mass Balances. *Environmental Science & Technology*, 44(10): 3705-3711.
- Audí-Miró, C. et al., 2013. Cl and C isotope analysis to assess the effectiveness of chlorinated ethene degradation by zero-valent iron: Evidence from dual element and product isotope values. *Applied Geochemistry*, 32(0): 175-183.
- Barth, J.A.C. et al., 2002. Carbon isotope fractionation during aerobic biodegradation of trichloroethene by *Burkholderia cepacia* G4: a tool to map degradation mechanisms. *Applied and Environmental Microbiology*, 68(4): 1728-1734.
- Bloom, Y., Aravena, R., Hunkeler, D., Edwards, E. and Frappe, S.K., 2000. Carbon isotope fractionation during microbial dechlorination of trichloroethene, cis-1,2-dichloroethene, and vinyl chloride: Implications for assessment of natural attenuation. *Environ. Sci. Technol.*, 34(13): 2768-2772.
- Brungard, K.L., Munakata-Marr, J., Johnson, C.A. and Mandernack, K.W., 2003. Stable carbon isotope fractionation of trans-1,2-dichloroethylene during co-metabolic degradation by methanotrophic bacteria. *Chem. Geol.*, 195(1-4): 59-67.
- Chartrand, M.M.G. et al., 2005. Carbon isotopic fractionation during aerobic vinyl chloride degradation. *Environmental Science & Technology*, 39(4): 1064-1070.
- Chu, K.-H., Mahendra, S., Song, D.L., Conrad, M.E. and Alvarez-Cohen, L., 2004. Stable carbon isotope fractionation during aerobic biodegradation of chlorinated ethenes. *Environ. Sci. Technol.*, 38(11): 3126-3130.
- Cichocka, D., Imfeld, G., Richnow, H.H. and Nijenhuis, I., 2008. Variability in microbial carbon isotope fractionation of tetra- and trichloroethene upon reductive dechlorination. *Chemosphere*, 71(4): 639-648.
- Cichocka, D. et al., 2007. Factors controlling the carbon isotope fractionation of tetra- and trichloroethene during reductive dechlorination by *Sulfurospirillum* ssp and *Desulfitobacterium* sp strain PCE-S. *Fems Microbiology Ecology*, 62(1): 98-107.
- Cretnik, S., Bernstein, A., Shouakar-Stash, O., Loeffler, F. and Elsner, M., 2014. Chlorine Isotope Effects from Isotope Ratio Mass Spectrometry Suggest Intramolecular C-Cl Bond Competition in Trichloroethene (TCE) Reductive Dehalogenation. *Molecules*, 19(5): 6450-6473.
- Cretnik, S. et al., 2013. Reductive Dechlorination of TCE by Chemical Model Systems in Comparison to Dehalogenating Bacteria: Insights from Dual Element Isotope Analysis (C-13/C-12, Cl-37/Cl-35). *Environmental Science & Technology*, 47(13): 6855-6863.
- Dayan, H., Abrajano, T., Sturchio, N.C. and Winsor, L., 1999. Carbon isotopic fractionation during reductive dehalogenation of chlorinated ethenes by metallic iron. *Organic Geochemistry*, 30(8A): 755-763.
- Elsner, M., Chartrand, M., Vanstone, N., Couloume, G.L. and Lollar, B.S., 2008. Identifying abiotic chlorinated ethene degradation: Characteristic isotope patterns in reaction products with nanoscale zero-valent iron. *Environmental Science & Technology*, 42(16): 5963-5970.

- Fletcher, K.E., Nijenhuis, I., Richnow, H.H. and Löffler, F.E., 2011. Stable Carbon Isotope Enrichment Factors for cis-1,2-Dichloroethene and Vinyl Chloride Reductive Dechlorination by Dehalococcoides. *Environmental Science & Technology*, 45(7): 2951-2957.
- Hunkeler, D., Aravena, R. and Butler, B.J., 1999. Monitoring microbial dechlorination of tetrachloroethene (PCE) in groundwater using compound-specific stable carbon isotope ratios: Microcosm and field studies. *Environ. Sci. Technol.*, 33(16): 2733-2738.
- Hunkeler, D., Aravena, R. and Cox, E., 2002. Carbon isotopes as a tool to evaluate the origin and fate of vinyl chloride: Laboratory experiments and modeling of isotope evolution. *Environ. Sci. Technol.*, 36: 3378-3384.
- Jennings, L.K. et al., 2009. Proteomic and Transcriptomic Analyses Reveal Genes Upregulated by cis-Dichloroethene in *Polaromonas* sp Strain JS666. *Applied and Environmental Microbiology*, 75(11): 3733-3744.
- Kuder, T. and Philp, P., 2013. Demonstration of Compound-Specific Isotope Analysis of Hydrogen Isotope Ratios in Chlorinated Ethenes. *Environmental Science & Technology*, 47(3): 1461-1467.
- Lee, P.K.H., Conrad, M.E. and Alvarez-Cohen, L., 2007. Stable carbon isotope fractionation of chloroethenes by dehalorespiring isolates. *Environmental Science & Technology*, 41(12): 4277-4285.
- Liang, X. et al., 2007. Distinguishing abiotic and biotic transformation of tetrachloroethylene and trichloroethylene by stable carbon isotope fractionation. *Environmental Science & Technology*, 41(20): 7094-7100.
- Liu, Y. et al., 2014. Carbon and chlorine isotope fractionation during Fenton-like degradation of trichloroethene. *Chemosphere*, 107: 94-100.
- Lollar, B.S. et al., 1999. Contrasting carbon isotope fractionation during biodegradation of trichloroethylene and toluene: Implications for intrinsic bioremediation. *Organic Geochemistry*, 30(8A): 813-820.
- Mundle, S.O.C. et al., 2012. Monitoring Biodegradation of Ethene and Bioremediation of Chlorinated Ethenes at a Contaminated Site Using Compound-Specific Isotope Analysis (CSIA). *Environmental Science & Technology*, 46(3): 1731-1738.
- Nijenhuis, I. et al., 2005. Stable isotope fractionation of tetrachloroethene during reductive dechlorination by *Sulfurospirillum multivorans* and *Desulfitobacterium* sp strain PCE-S and abiotic reactions with cyanocobalamin. *Applied and Environmental Microbiology*, 71(7): 3413-3419.
- Numata, M., Nakamura, N., Koshikawa, H. and Terashima, Y., 2002. Chlorine isotope fractionation during reductive dechlorination of chlorinated ethenes by anaerobic bacteria. *Environ. Sci. Technol.*, 36(20): 4389-4394.
- Pooley, K.E. et al., 2009. Aerobic Biodegradation of Chlorinated Ethenes in a Fractured Bedrock Aquifer: Quantitative Assessment by Compound-Specific Isotope Analysis (CSIA) and Reactive Transport Modeling. *Environmental Science & Technology*, 43(19): 7458-7464.
- Prommer, H., Aziz, L.H., Bolano, N., Taubald, H. and Schuth, C., 2008. Modelling of geochemical and isotopic changes in a column experiment for degradation of TCE by zero-valent iron. *Journal of Contaminant Hydrology*, 97(1-2): 13-26.
- Schmidt, K.R., Augenstein, T., Heidinger, M., Ertl, S. and Tiehm, A., 2010. Aerobic biodegradation of cis-1,2-dichloroethene as sole carbon source: Stable carbon isotope fractionation and growth characteristics. *Chemosphere*, 78(5): 527-532.

- Schmidt, K.R., Gaza, S., Voropaev, A., Ertl, S. and Tiehm, A., 2014. Aerobic biodegradation of trichloroethene without auxiliary substrates. *Water Research*, 59: 112-118.
- Schmidt, M., Lege, S. and Nijenhuis, I., 2014. Comparison of 1,2-dichloroethane, dichloroethene and vinyl chloride carbon stable isotope fractionation during dechlorination by two *Dehalococcoides* strains. *Water Research*, 52: 146-154.
- Slater, G.F., Lollar, B.S., King, R.A. and O'Hannesin, S., 2002. Isotopic fractionation during reductive dechlorination of trichloroethene by zero-valent iron: influence of surface treatment. *Chemosphere*, 49(6): 587-596.
- Slater, G.F., Lollar, B.S., Sleep, B.E. and Edwards, E.A., 2001. Variability in carbon isotopic fractionation during biodegradation of chlorinated ethenes: Implications for field applications. *Environ. Sci. Technol.*, 35(5): 901-907.
- Smits, T.H.M., Assal, A., Hunkeler, D. and Holliger, C., 2011. Anaerobic Degradation of Vinyl Chloride in Aquifer Microcosms. *Journal of Environmental Quality*, 40(3): 915-922.
- Tiehm, A. and Schmidt, K.R., 2011. Sequential anaerobic/aerobic biodegradation of chloroethenes - aspects of field application. *Current Opinion in Biotechnology*, 22(3): 415-421.
- Tiehm, A., Schmidt, K.R., Pfeifer, B., Heidinger, M. and Ertl, S., 2008. Growth kinetics and stable carbon isotope fractionation during aerobic degradation of cis-1,2-dichloroethene and vinyl chloride. *Water Research*, 42(10-11): 2431-2438.
- VanStone, N.A., Focht, R.M., Mabury, S.A. and Lollar, B.S., 2004. Effect of iron type on kinetics and carbon isotopic enrichment of chlorinated ethylenes during abiotic reduction on Fe(0). *Ground Water*, 42(2): 268-276.
- Wiegert, C. et al., 2013. Carbon and Chlorine Isotope Fractionation During Microbial Degradation of Tetra- and Trichloroethene. *Environmental Science & Technology*, 47(12): 6449-6456.

APPENDIX C. RTM CSIA MNA TRAINING COURSE

**RTM-CSIA-MNA:
Interpretation of
Compound-Specific Isotope Analysis Data
with Reactive Transport Modeling
for Improved Monitored Natural Attenuation
of Chlorinated Solvent Plumes**

**Presented at the Ninth International Conference on Remediation
of Chlorinated and Recalcitrant Compounds**

Monterey, California

May 19-22, 2013

Instructors

Dr. Boris M. van Breukelen (VU University Amsterdam, NL)
Dr. Mindy Vanderford (GSI Environmental Inc., Houston, TX)

Copyright © Boris M. van Breukelen, 2014



Instructors

Dr. B.M. van Breukelen (VU University Amsterdam).

Dr. B.M. van Breukelen is assistant professor of Hydrogeochemistry at the VU University Amsterdam, the Netherlands. He received his Ph.D. from the same university in 2003. He authored and co-authored more than 35 scientific articles. Dr. Van Breukelen is international expert in reactive transport modeling and model-based interpretation of CSIA data. He has given 6 professional 3-4 day courses in reactive transport modeling as sole instructor since 2009 including a 3.5 day course on “reactive transport modeling of isotope ratios in the environment” organized as EU Marie Curie Initial Training Network Course in 2013.

Dr. Mindy Vanderford (GSI Environmental Inc.).

Dr. Vanderford is an Environmental Scientist at GSI Environmental, Inc. in Houston, TX. She received a Ph.D. in Environmental Sciences and Engineering from the University of North Carolina Chapel Hill and M.S. and undergraduate degrees from Rice University. She is principal investigator and developer for the AFCEC MAROS software for GSI and has extensive experience using statistical methods and decision matrices to analyse and optimize groundwater remediation projects. She has developed and conducted classes in Long-Term Monitoring Optimization and statistical analysis for the USEPA, DoD, and several state environmental agencies. Her project experience includes environmental site investigation, human and ecological risk assessment, monitored natural attenuation evaluation, and the application of geographic information system (GIS) tools.

Computer and Software Requirements

This course contains hands-on computer-based exercises. Students are requested to bring a laptop computer running MS Windows Vista/7/8.

Students need to install the two freeware computer programs listed below on their laptops prior to the course. Detailed installation procedures are given in Appendix 1.

Python(x,y) current release (2.7.6.0): <http://code.google.com/p/pythonxy/wiki/Downloads>
PHREEQC for Windows current release (2.18.00): <http://pfw.antipodes.nl/download.html>

ACRONYMS

CSIA	Compound-Specific Isotope Analysis
cDCE	<i>cis</i> -1,2- Dichloroethene
ETH	Ethene
IMH	Intermolecular Heterogeneity
KIE	Kinetic Isotope Effects
TCE	Trichloroethene
PCE	Tetrachloroethene
RTM	Reactive Transport Modelling
sKIE	Secondary Kinetic Isotope Effects
VC	Vinyl chloride

Contents

<i>A: Lab Batch Modelling of Sequential Reductive Dechlorination</i> _____	<i>1</i>
Exercise 1: Modeling of Carbon-CSIA data _____	1
Exercise 2: Modeling of Chlorine-CSIA data _____	3
<i>B: 1-D Flow Path Modelling</i> _____	<i>6</i>
Exercise 3: VC stall: detection of potential oxidation _____	6
<i>Appendix 1: Software Installation</i> _____	<i>8</i>
<i>Appendix 2: Short introduction to Python</i> _____	<i>9</i>

A: Lab Batch Modelling of Sequential Reductive Dechlorination

Exercise 1: Modeling of Carbon-CSIA data

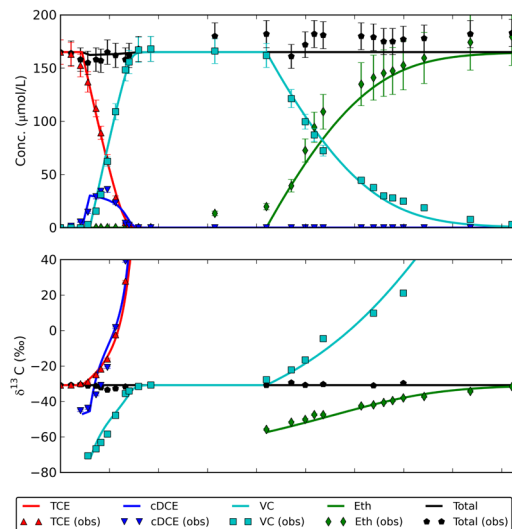


Figure 1: Simulation of Carbon CSIA during sequential reductive dechlorination of TCE

NOTE: The model used in this exercise has been funded by ESTCP and is part of a scientific publication. Sharing and dissemination of this model is prohibited prior to completion of publications and the final report to ESTCP. The model will be available to the public after the final report and papers are accepted.

In this exercise you will learn how carbon CSIA data can be simulated during sequential reductive dechlorination of TCE, via DCE, VC, and finally Ethene. You will first inspect the Phreeqc database and input file and insert values for the parameters. Subsequently, you will try to fit the model to the observations.

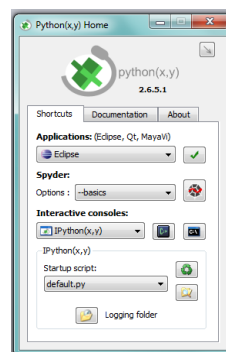
- ① Inspect the Phreeqc input file 'Microcosm-Carbon-CSIA-RTM.phrq':
- ① The input file is structured with a series of **KEYWORDS** coloured in blue in Phreeqc.
- ① At **DATABASE** path\Microcosm-C-Cl.dat, Phreeqc is instructed to use this specific database file.
- ① Open this database file and have a look. The database contains all information for the carbon and chlorine (to be explained later) isotope sub models:
 - Note the database information for the isotope submodels is added to a general hydrogeochemical database (PHAST).
 - **SOLUTION MASTER SPECIES** and **SOLUTION SPECIES** where the various isotope species are defined
 - **RATES** (at the end of the database) where the rate definitions and mathematical formulations are given (programmed in BASIC).
- ① Specify the correct path in the Phreeqc input file as on your computer.
- ① Back to the Phreeqc input file: At **SOLUTION**, replace all \$\$\$ signs (2×) with the starting concentrations of the light and heavy carbon TCE isotopes (TCE concentration = 165 µmol/l, $\delta^{13}\text{C-TCE} = -30.8 \text{ ‰}$). Hereto, use the excel spreadsheet 'Calculation of Initial Isotope or Isotopologue Concentrations.xls'.
- ① At **CALCULATE_VALUES**, the values of all the model parameters are stated and are available in the 'global memory' of the model meaning that they can be retrieved in the RATES definitions with calc_value("Parameter name"). For example, have a look at

end of the database file where for the rate of Vc_H_to_Eth_cl_RD, the Vmax of the reaction is applied with `calc_value("VC_k_max")`. Note the carbon isotope fractionation factors are set to zero (you will optimize these later on). The kinetic rate parameters are already calibrated.

- ① At [KINETICS](#), have a look at the stoichiometry of the carbon isotope reactions and compare some of these with the reaction network presented during the lecture.
- ① At [USER_PUNCH](#), have a look at BASIC line 180 how the TCE carbon isotope ratio is calculated from the concentrations of the light and heavy carbon isotope.

② Run the model and plot the results with the python script 'PlotResultsMicrocosmC-CSIA.py'. Hereto, follow these steps:

- ② Save the Phreeqc model: click 
- ② Run the Phreeqc model: click 
- ② Phreeqc runs the model. Any WARNING given is not a problem. When finished ('end of Run'), you can click the 'Done' button: 
- ② Start Python(x,y) with All Programs > Python(x,y) > Python(x,y)
- ② The screen to the right should open after 10 seconds:



- ② Now open Spyder, a graphical user interface of Python, click this button: 
- ② In Spyder, select as working directory the exercise's folder: use the browse function in

the toolbar:



- ② File > open: Browse to working directory and open the py file for the exercise
- ② Run script with green traffic light button (or: press F9; or: Interactive console > Run)
- ② Inspect the results in the figure window: if you performed the calculations of the initial isotope concentrations well you should see horizontal lines of $\delta^{13}\text{C}$ intersecting the initial $\delta^{13}\text{C}$ -TCE.
- ③ Try now to fit the carbon isotope ratios by trial-and-error:
- ③ Replace all zeros in the Phreeqc input file with reasonably chosen values for carbon isotopic enrichment factors of the 3 degradation steps from TCE to ETH. Select initially average values for isotope enrichment factors (see Table 1). Keep those of TCE to cDCE and to tDCE equal; take a value of -30.3 ‰ for the tDCE to VC step as this is the only literature value known.
- ③ Note this is done most efficiently through optimizing the isotope enrichment factors in the order TCE to VC.

Table 1 Carbon isotopic enrichment factors, ϵ_c (‰), reported in the literature			
PCE	TCE	cDCE	VC
-3.9 ^{*1}	-10.2	-20.6	-26.1
[-0.4 – -5.3] ^{*2}	[-3.3 – -16.4]	[-15.1 – -29.7]	[-23.1 – -31.1]
*1 Average value			
*2 Range reported			

- ★ Optionally, you can compare the obtained TCE and VC fractionation factors with those directly obtained from a statistical regression (data available in MicrocosmData.xls). This works out as TCE and VC are not produced during their degradation.

Exercise 2: Modeling of Chlorine-CSIA data

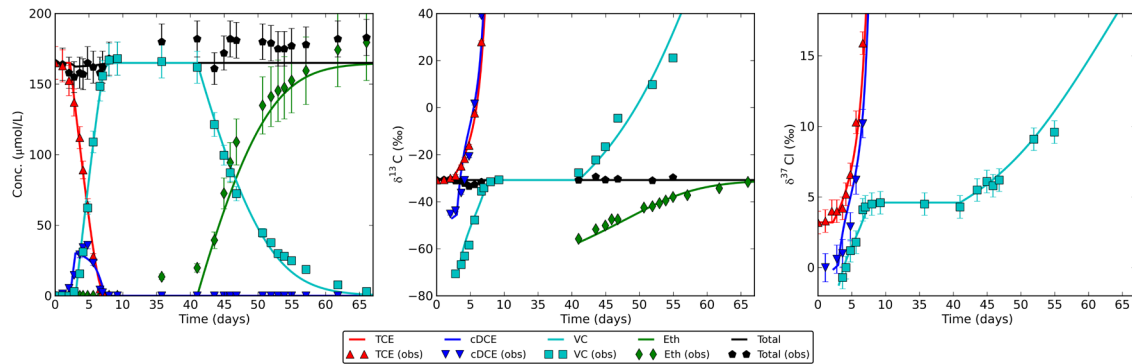


Figure 2: Simulation of carbon and chlorine isotope fractionation during reductive dechlorination of TCE to ETH in a microcosm experiment.

- ① Inspect the Phreeqc input file 'Microcosm-Carbon-Chlorine-CSIA-RTM.phrq'. This model extends the previous model with chlorine isotope fractionation:
- ① Again specify the correct path as for your computer at [DATABASE path](#)\Microcosm-C-Cl.dat. Have a look this time at the chlorine isotope sub models in the database file.
- ① Back to the Phreeqc input file: At [SOLUTION](#), insert the initial values of the 8 (!) chlorine TCE isotopologue/isomers (TCE concentration = 165 µmol/l, $\delta^{37}\text{Cl-TCE} = +3.2\text{‰}$). Use the excel spreadsheet as done before.
- ① At [CALCULATE_VALUES](#), the chlorine isotope submodel parameters are added. Note those are set to zero and you will optimize these later on.
- ① At [KINETICS](#), have a look at the stoichiometry of the chlorine isotopologue reactions and compare some of these with the reaction network presented during the lecture.
- ① At [USER_PUNCH](#), have a look at BASIC line 300 how the TCE chlorine isotope ratio is calculated from the concentrations of its 8 isotopologues/isomers.
- ② Run the model and plot the results with the python script 'PlotResultsMicrocosmC-Cl-CSIA.py': If you performed the calculations of the initial isotopologue concentrations well you should see horizontal $\delta^{37}\text{Cl}$ lines intersecting the initial $\delta^{37}\text{Cl-TCE}$.
- ③ Try to fit the chlorine isotope ratios by trial-and-error through optimizing (i.e., through manual entry of parameter values) the ϵ_{ClKIE} values and assuming you can neglect the occurrence of secondary kinetic isotope effects (sKIEs; keep those at zero). Keep those for TCE to cDCE/tDCE equal, as well as those for cDCE/tDCE to VC. Note the bulk enrichment factors (ϵ_{bulk}) for TCE and VC can also be determined with a regression on the data available in MicrocosmData.xls. Compare your model optimized ϵ_{ClKIE} values with the ϵ_{bulk} values from the statistical regression or use the latter directly. Note that for TCE: $\epsilon_{\text{ClKIE}} = 3 \times \epsilon_{\text{bulk}}$.
- ③ Do you see that you can fit $\delta^{37}\text{Cl-TCE}$ and reasonably well $\delta^{37}\text{Cl-VC}$ after 40 days but not at all $\delta^{37}\text{Cl-cDCE}$? Do you see that $\delta^{37}\text{Cl-cDCE}$ and $\delta^{37}\text{Cl-VC}$ values are always higher than initial $\delta^{37}\text{Cl-TCE}$?

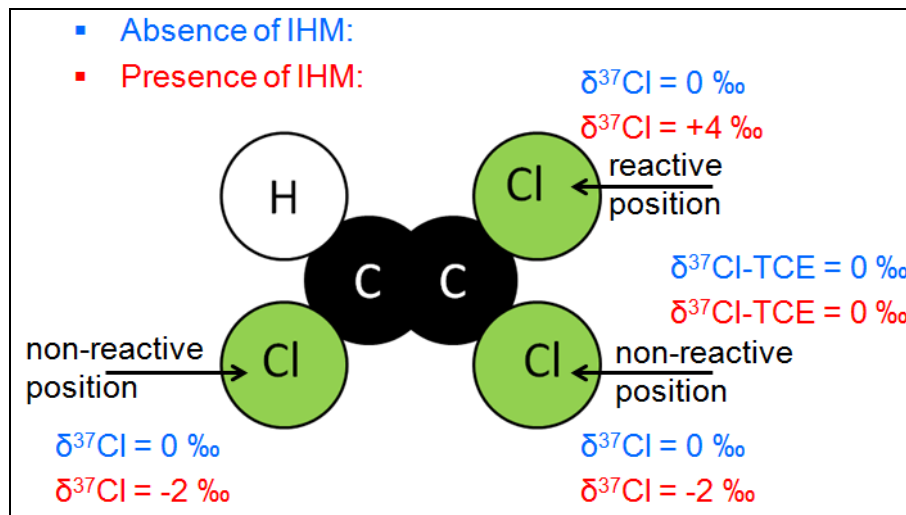


Figure 3: Illustration of possible Intramolecular Heterogeneity (IHM) in chlorine isotope ratios of individual chlorine atoms of TCE. Reactive and non-reactive positions are indicated in the transformation to cis-DCE.

- ★ A possible solution to create depleted initial $\delta^{37}\text{Cl}$ -DCE values is to assume the occurrence of Intramolecular Heterogeneity (IMH) of the initial chlorine isotope ratios of the individual chlorine atoms in TCE, meaning they are not equal but different (see Figure 3 and lecture slide).
- ★ Check the data in MicrocosmData.xls and note the spacing between $\delta^{37}\text{Cl}$ -TCE and initially produced $\delta^{37}\text{Cl}$ -cDCE is 3.3 ‰. Assuming IMH is the sole explanation for this spacing, the two non-reactive Cl TCE position (becoming cDCE) must have an isotope ratio 3.3 ‰ lighter than average $\delta^{37}\text{Cl}$ -TCE.
- ★ Use the 'IHM Calculations' worksheet of MicrocosmData.xls to calculate the $\delta^{37}\text{Cl}$ of the reactive and two non-reactive Cl positions keeping the average of all positions at +3.2 ‰ and the difference between the average and the two non-reactive positions at -3.3 ‰.
- ★ When done, replace in the Phreeqc input file at **SOLUTION** the original initial TCE chlorine isotopologue concentrations disregarding IMH with those calculated at the blue section. Run the model, plot the results, and optimise the $\epsilon_{\text{Cl}_{\text{KIE}}}$ of DCE a bit: Do you see that indeed initial $\delta^{37}\text{Cl}$ -cDCE can be fitted but the model is not able to fit initial $\delta^{37}\text{Cl}$ -VC? Note that the clear spacing between $\delta^{37}\text{Cl}$ -cDCE and initial $\delta^{37}\text{Cl}$ -VC cannot be explained by IHM as both DCE chlorine atoms occur in reactive positions and the Cl atom becoming part of VC must therefore have an average isotopic composition of the two Cl atoms of DCE.

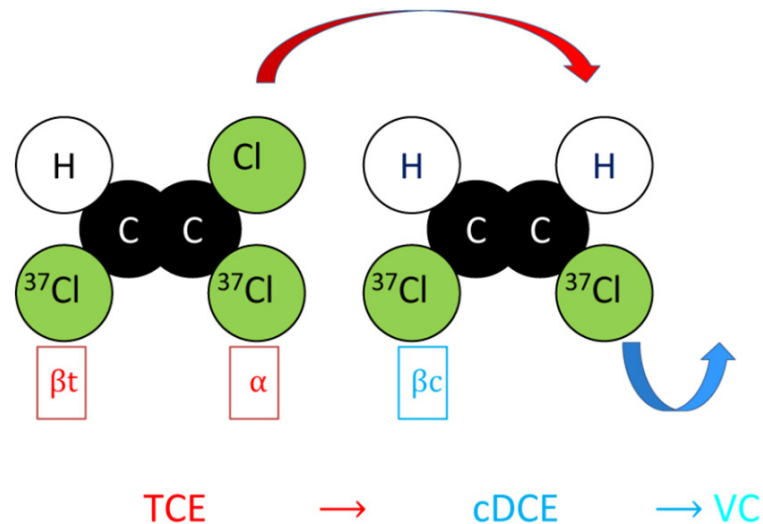


Figure 4: Illustration of potential secondary isotope effects during reductive dechlorination of TCE to VC.

- ⑤ The only way to explain the spacing between $\delta^{37}\text{Cl}$ -cDCE and $\delta^{37}\text{Cl}$ -VC is to consider secondary isotope effects (see Figure 4 and lecture slides). This scenario is also more likely for the TCE to DCE step as the obtained $\epsilon_{\text{Cl}_{\text{KIE}}}$ of TCE is outside the literature range with -10.8‰ . Assuming also secondary isotope effects will reduce the estimate of the primary isotope effect. Furthermore, the difference in $\delta^{37}\text{Cl}$ that had to be taken between the reactive and non-reactive Cl positions of TCE for the IHM model was quite large.
- ⑤ You will now try to fit the $\delta^{37}\text{Cl}$ data without IHM (put initial TCE isotopologue concentrations back to original values) but with occurrence of secondary isotope effects. All primary and secondary isotope effects can be directly obtained from the data as follows:
- ⑤ First, the mean of the SKIEs (type α and β_t ; see lecture slide) of TCE to cDCE ($\epsilon_{\text{Cl}_{\text{SKIE}}(\text{MEAN})}$, -3.3‰) was calculated from the difference between $\delta^{37}\text{Cl}$ -TCE and initial $\delta^{37}\text{Cl}$ -cDCE observed. Since only the average of these type α and β_t SKIEs can be determined they were considered as equal in the model. For the TCE to tDCE step, α and β_c SKIEs instead of α and β_t SKIEs were relevant but they were all considered of equal magnitude (-3.3‰)
- ⑤ Second, the primary KIE of TCE to DCE ($\epsilon_{\text{Cl}_{\text{KIE}}}$, -4.2‰) followed from $3 \times \epsilon_{\text{Cl}_{\text{bulk}}} - 2 \times \epsilon_{\text{Cl}_{\text{SKIE}}(\text{MEAN})}$, where $\epsilon_{\text{Cl}_{\text{bulk}}}$ ($-3.6 \pm 0.3\text{‰}$) was calculated by fitting the Rayleigh equation to the observations.
- ⑤ Third, the SKIE $_{\beta_c}$ of cDCE to VC (-1.7‰) followed from the difference between $\delta^{37}\text{Cl}$ -cDCE and initial $\delta^{37}\text{Cl}$ -VC observed. Check this in MicrocosmData.xls.
- ⑤ Fourth, the primary KIE of cDCE to VC ($\epsilon_{\text{Cl}_{\text{KIE}}}$, -4.5‰) followed from $-2 \times (\delta^{37}\text{Cl}\text{-VC}_{\text{final}} - \delta^{37}\text{Cl}\text{-TCE}_{\text{initial}}) + \epsilon_{\text{Cl}_{\text{SKIE}}(\beta_c)}$. This equation is a bit hard to explain here but you can try later to vary its value to appreciate its effect on the model outcome. The α and β SKIEs of the tDCE to VC step were assumed equal to those of the cDCE to VC step.
- ⑤ Fifth, as only a primary KIE occurred in the VC to ETH step, its value followed directly from fitting the Rayleigh equation to the observations ($\epsilon_{\text{Cl}_{\text{KIE}}} = \epsilon_{\text{Cl}_{\text{bulk}}}$, $-2.8 \pm 0.4\text{‰}$).
- ⑤ Insert all these values in the Phreeqc model, run it, and plot the results: do you see that the model describes chlorine isotope ratios quite well when considering secondary isotope effects?

B: 1-D Flow Path Modelling

Exercise 3: VC stall: detection of potential oxidation

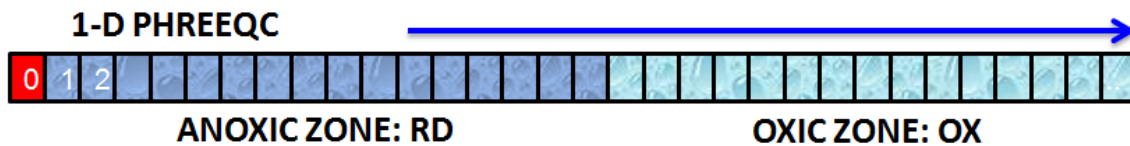


Figure 5: Model setup (1-D PHREEQC) for incomplete dechlorination under anoxic conditions resulting in a stall of VC with potential an(aerobic) oxidation further downgradient.

Reductive dechlorination of PCE or TCE often does not lead to complete conversion to ETH but rather to a 'stall' of cDCE or VC as conditions are not sufficiently anoxic and/or the relevant microorganisms are absent. However, apparently accumulating cDCE or VC may also degrade slowly further via (an)aerobic oxidation. Such processes are probable but difficult to detect and confirm as concentrations decrease also by physical processes such as dilution away from the source zone, and characteristic reaction products are not formed.

In this exercise you will find out whether such a process could be detected theoretically with 2-D carbon and chlorine CSIA. For simplicity you will consider a case where an anoxic aquifer becomes oxic downgradient (see Figure 5). We can simulate this case without including oxygen transport by assigning two different sets of kinetic reactions to the anoxic and the oxic zone, respectively.

- ① Inspect the Phreeqc input file 'FlowpathCCI-Stall.phrq'. The Phreeqc file of exercise 2 was changed as follows:
- ① As we will perform a 1-D groundwater flow path simulation. We have to define a **SOLUTION 0**, which is the water flowing into the flow path (the pollution source). An initial TCE concentration of 1000 $\mu\text{mol/l}$, a $\delta^{13}\text{C-TCE}$ of -30 ‰, and a $\delta^{37}\text{Cl-TCE}$ of +3.0 ‰ were taken to start with nice round numbers.
- ① The initially clean flow path is defined as a series of 50 cells with **SOLUTION 1-50**.
- ① With respect to the reaction network, the following further changes were made: (1) the trans-DCE pathways were taken out; (2) the rate constant and carbon and chlorine enrichment factors of VC oxidation were added to **CALCULATE_VALUES**; (3) rate formulations for carbon and chlorine isotope fractionation during oxidation of VC were included beneath at **RATES**; and (4) beneath **KINETICS**, the reaction stoichiometries of the VC oxidation reactions are stated: for each isotope and for both C and Cl, thus 4 in total. Note the reaction products Cl and CO_2 are not further considered.
- ① At **TRANSPORT**, the flow path of 50 cells is defined; with each time step (shift) the water moves from the one to its neighbouring cell; as water moves into and out of the flow path flux conditions are defined at both the inlet and outlet.
 - Can you calculate the groundwater flow velocity and the total distance travelled based on the parameter values beneath this keyword?
- ① For simplicity we like to simulate first-order kinetics but the rate formulations are available as monod kinetics in Microcosm-C-Cl.dat. Of course we could modify the whole database to simulate first-order kinetics but this will take a lot of time and error checking. A simpler approach (see lecture slides) is to use the available monod kinetics but take half-saturation constants much larger than the concentration ranges (i.e., $K_s \gg S$) and then select the k_{max} as follows: $k_1 \approx k_{\text{max}}/K_s$, where k_1 is the first-order rate constant. See **CALCULATE_VALUES**: K_s values of 1 (M) were taken and to

achieve first-order rate constants of 1 and 0.5 per year for TCE and DCE, respectively, k_{\max} values of 1 and 0.5 M per year, respectively, were adopted.

- ② Note to finish the input file you still need to assign the zones where the kinetic reactions take place with multiple **KINETICS** blocks. The model consists of 50 cells with a cell length of 10 m, thus a total flow path length of 500 m. Try to model the following situation: no reactions take place during the first 50 meters as the availability of organic matter is too low to drive reductive dechlorination, between 50-250 m reductive dechlorination takes place, between 250-300 m no reactions occur, from 300 m and further VC oxidation takes place as the aquifer turns oxic.
 - ③ When ready, run the file and plot the result with the Python script ‘FlowpathCCI-Stall.py’: Does the behaviour of the chlorinated ethenes match with their intended reactivity?
 - ③ Do you see how VC transformation via oxidation can be proved with C-CSIA and calculation of the carbon isotope mass balance (total in middle panel Figure 6)?
 - ③ How can combined C&Cl-CSIA aid in confirming the occurrence of oxidation?
 - ③ Think about how many CSIA data you should obtain along the flow path to trace the full complexity of degradation for this theoretical case.
 - ③ As shown in the lecture, a 1-D flow path cannot simulate actual concentrations as dilution of pollution is not simulated except at the plume front. However, a comparison between 1-D Phreeqc and 2-D PHAST (a 3-D Phreeqc version: Phreeqc coupled to HST3D) showed that with a 1-D model molar fractions and CSIA data are very well simulated.
- ★ Inspect the effect of the longitudinal dispersion coefficient on simulation results. For example, take a ten times larger α_L value (10 m versus 1 m). Concentrations become more dispersed: simulated concentrations peaks become lower and downgradient tails become higher and longer. Hydrodynamic dispersion attenuates isotope signals (see lecture). Predicted $\delta^{13}\text{C}$ -TCE is clearly lower than observed especially downgradient. The same effect can be observed for DCE and VC. Furthermore, $\delta^{13}\text{C}$ of these daughter products is higher near the source as a result of less enriched TCE. This second effect is particularly clear for VC. The longitudinal dispersion coefficient is thus an important fitting parameter.
- ★ Inspect the results in case of absence of sKIEs, or vary other parameter values.

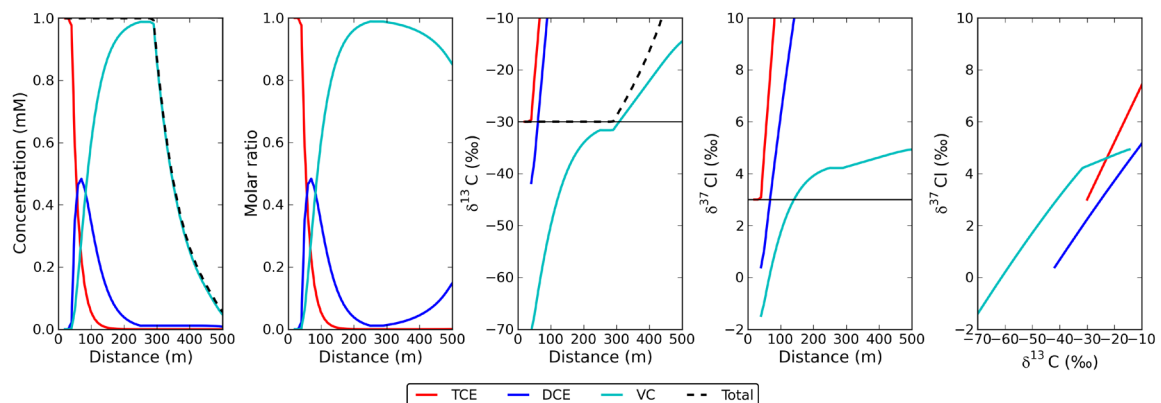


Figure 6: Model results of slow VC oxidation downgradient of a reductive dechlorination zone with a VC ‘stall’.

Appendix 1: Software Installation

1. PHREEQC

PHREEQC for Windows (current version 2.18.00, April 15, 2014) can be downloaded for free from the following web-site: <http://pfw.antipodes.nl/download.html>

Installation is easy: just run psetup21800.exe and follow the instructions. Please, set the 'tab stops' to 12 instead of 4 with edit > preferences > input > tab stops. This makes input the files prepared in this project easier to read.

PHREEQC has been developed by David Parkhurst from the USGS and Tony Appelo, author of a recommended textbook on Hydrochemistry. More information about

PHREEQC is available at the following links:

- USGS: http://wwwbrr.cr.usgs.gov/projects/GWC_coupled/phreeqc/index.html
- Tony Appelo's home page: <http://www.hydrochemistry.eu/>

For PHREEQC troubleshooting you can check: the PHREEQC get-going sheets in appendix A of the Appelo & Postma textbook on pages 599-615. There is also an extensive user's manual available distributed with the download.

2. Installing Python for Visualization of Phreeqc Results & Programming

Download: <http://code.google.com/p/pythonxy/> > Downloads > current release (2.7.6.0, April 15, 2014) > save file (~630 MB)

Installation: Install installer file > agree with license > 'Choose Components':

IMPORTANT:

1. choose 'recommended' for 'type of install'
2. install for 'all users', otherwise you are not able to use it with your regular login if you installed the program as administrator or installer.
3. 'type of install' now switches to 'custom' but that is ok.

> Continue with default steps until program is installed

Starting Python: Start > All Programs >

- A. Python(x,y) > Click on 'Spyder' button (at right side of Spyder: Options:)
- B. OR: Python(x,y) Folder > Spyder Folder > Spyder

Recommended Spyder settings:

1. View > Select: 'Run toolbar' (the green run button is now available)
2. Interactive console > Interactive console settings > Deselect: 'Dockable figures' (Figures will then pop-up as separate windows which is much more convenient than to dock them in the Spyder console)

Running Python script:

1. File > Open: Browse for file
2. Press the folder icon at right end of toolbar to select the folder where the python script is located as 'Working directory'
3. Run script with green start button OR Source > Run in interactive console OR press F9

Appendix 2: Short introduction to Python

Making plots with Python for this course

1. Start Python with Spyder: Start > All programs > Python(x,y) > Spyder (Spyder is a graphical user interface for Python)
2. Select as working directory the exercise's folder: use browse function in toolbar
3. File > open: Browse to working directory and open the py file for the exercise
4. Run script with green traffic light button (*or*: press F9; *or*: Interactive console > Run)
5. Inspect the results in the figure window

Short background on Python

Python (<http://www.python.org/>) is a programming language similar to MATLAB but is open-source and free. Python is easy to learn especially for those who have some programming experience. Matplotlib (<http://matplotlib.sourceforge.net/>) is a Python 2D plotting library which produces the same quality figures as with MATLAB. Python(x,y) (<http://www.pythonxy.com/>) is one of the several available Python distributions which has the advantage of being free, easy to install, and goes with the excellent graphical user interface called Spyder providing MATLAB-like features. Spyder enables advanced editing, interactive testing, debugging and visualization of Python scripts.

A very short introduction to the Python programming language

Like MATLAB, Python works with scripts having extension *.py*. A script contains several to many program lines to execute certain tasks, for this course, the plotting of model results and observations in figures. At the start of a script, you need to import advanced functions contained in modules to enable, for example, 2D plotting. Therefore, the first active program line reads in all python scripts for this course "from pylab import *", meaning all (*) functions from module Pylab are imported and available to use in the script. The Pylab module contains all functions needed for MATLAB type of plotting (*pyplot*) and data handling (*numpy*). If you want to make use of special mathematical functions you can import these with the module *math*, while advanced statistical functions are available in the module *scipy*. The table below summarizes some key differences between MATLAB and Python. [http://www.scipy.org/NumPy for Matlab Users](http://www.scipy.org/NumPy%20for%20Matlab%20Users) is recommended for further information.

Some important differences between MATLAB and Python		
Item	MATLAB	Python
	a = 1;	a = 1 [you do not need to place a semi colon (;) at end]
Division	1/2 = 0.5	1/2 = 0 → 1.0/2.0 = 0.5 <i>or</i> float(1)/2 = 0.5 [use decimals to indicate floats, otherwise Python takes them as integers]
Matrix	a = [1 2;3 4]	a = array([[1.,2.],[3.,4.]])
Indexing	1 (one) based indexing: a(1,2)=2	0 (zero) based indexing: a[0,1]=2: access element in first row, second column. Note brackets [] instead of parentheses ()
Element-wise multiply	a .* b	a * b [same for division and exponentiation]
	2^3=8	2**3=8
	[2:2:10]	arange(2.,12.,2.0) = array([2., 4., 6., 8., 10.])
	linspace(2,10,5)	linspace(2,10,5) = array([2., 4., 6., 8., 10.])
	zeros(3,4)	zeros((3,4))

Another major difference with MATLAB is the 'for loop' and the use of indents in Python instead of end commands in MATLAB:

MATLAB	Python
<pre>b = ones(1,10) for i is 1:10 b(i) = b(i)*i end print b</pre>	<pre>b = ones((1,10)) # array with 10 elements on one row with value 1 for i in range(0, 10): b[0,i] = b[0,i]*float(i) # note i is an integer print b b = array([[0., 1., 2., 3., 4., 5., 6., 7., 8., 9.]])</pre>

A short example

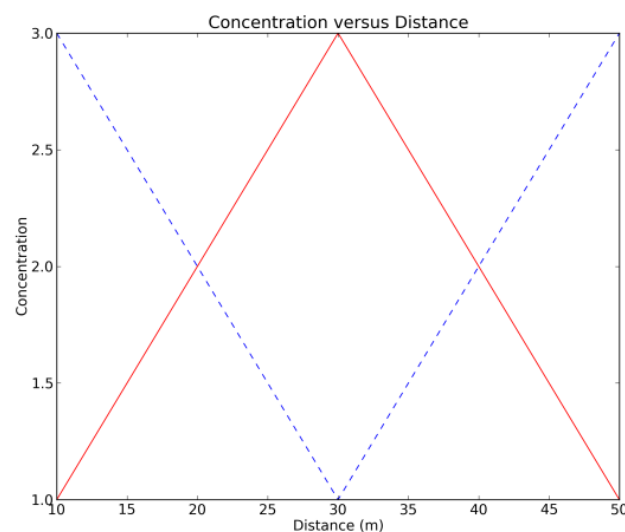
Distance	Parameter 1	Parameter 2
10	1	3
20	2	2
30	3	1
40	2	2
50	1	3

10	1	3
20	2	2
30	3	1
40	2	2
50	1	3

For example, the upper left table shows a spreadsheet with model results you want to plot. If you save the spreadsheet as a text (tab delimited) file, you can subsequently open this txt file with the command: `data = loadtxt('path and filename.txt', skiprows = 1)`. The first row of the file will be skipped (`skiprows = 1`) as it contains strings which cannot be part of a matrix (in Python a 2D array). The matrix (2D array) called `data` is shown in the upper right table.

Making a plot is now simple. The following sequence of program lines gives the plot below:

```
>>> plot(data[:,0], data[:,1], 'r') # : means all elements in this row or column
>>> plot(data[:,0], data[:,2], 'b--') # a blue dashed line, see help(plot) for all options
>>> xlabel('Distance (m)')
>>> ylabel('Concentration')
>>> title('Concentration versus Distance')
```



If you type the program lines above in a file which you save with extension `.py` (a Python script), you can simply run this script every time you modified a simulation to update the figure in a quick way.



NINTH INTERNATIONAL CONFERENCE
ON REMEDIATION OF CHLORINATED
AND RECALCITRANT COMPOUNDS

May 19-22, 2014 | Monterey, California

www.battelle.org/chlorcon

Battelle
The Business of Innovation

Short Course



**RTM-CSIA-MNA: Interpretation of CSIA data with
Reactive Transport Modeling (RTM) for improved MNA of
Chlorinated Solvent Plumes**

Date Presented: May 18, 2014

Instructor(s): dr. Boris van Breukelen (VU University Amsterdam),
dr. Mindy Vanderford (GSI Environmental Inc.)

Boris van Breukelen

- Assistant Professor at Critical Zone Hydrology Group, Department of Earth Sciences, VU University Amsterdam, the Netherlands, since 2003
- **Teaching:** Hydrochemistry (+ Phreeqc), Contaminant Hydrogeology, Transport Processes, Hydrogeology Field Courses
- **Research:** Biogeochemistry, Microbiology, Contaminant Hydrogeology, (Isotope Fractionation) - Reactive Transport Modeling (PHREEQC, PHT3D, PHAST)

3

Mindy VanderFord

- Environmental Scientist at GSI Environmental, Inc. in Houston, TX
- Ph.D. in Environmental Sciences and Engineering from the University of North Carolina Chapel Hill
- Principal investigator and developer for the AFCEC MAROS software for GSI
- She has developed and conducted classes in Long-Term Monitoring Optimization and statistical analysis for the USEPA, DoD, and several state environmental agencies
- Project experience includes environmental site investigation, human and ecological risk assessment, monitored natural attenuation evaluation, and the application of geographic information system (GIS) tools

4

ESTCP Project ER-201029

INTEGRATED STABLE ISOTOPE – REACTIVE TRANSPORT MODEL APPROACH FOR ASSESSMENT OF CHLORINATED SOLVENT DEGRADATION

Performers

Paul Philp (PI)

Tomasz Kuder

[Boris van Breukelen](#)

Heloise Thouement/Philip Stack

[Mindy Vanderford](#)



University of Oklahoma



VU University Amsterdam



GSI Environmental, Inc.



5

Course Objectives & Learning Goals

- **CSIA:** Understanding the basics of the use of Compound-Specific stable Isotope Analysis
- **RTM:** Understanding the basics of how Reactive Transport Models can be used to simulate chlorinated ethene (CE) CSIA data
 - [Carbon CSIA](#)
 - [Chlorine CSIA](#)
- **MNA:** Understanding the basics of CEs degradation and how CSIA-RTM can aid in MNA
- Basic introduction to the software (PHREEQC)
- Enthusiasm to work further with complementary exercises

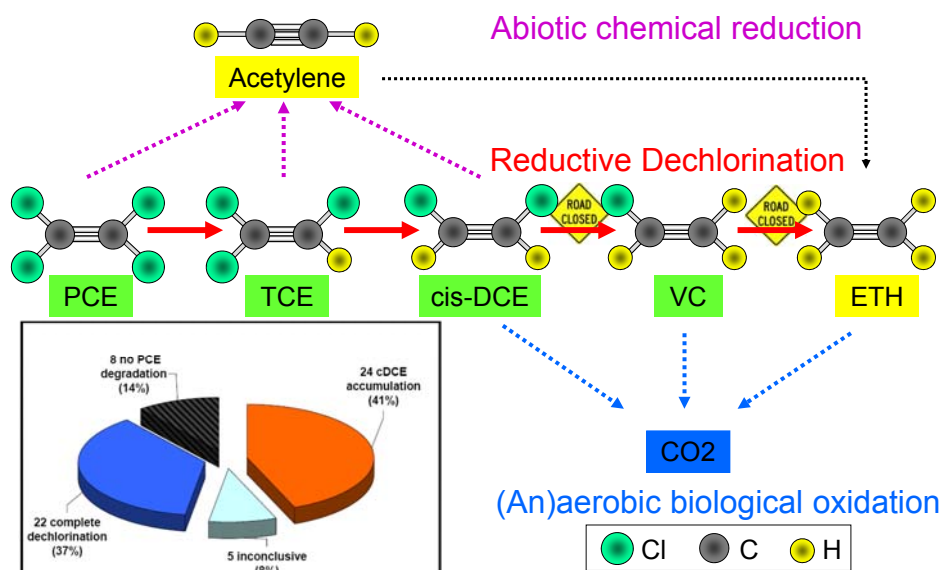
6

Schedule & Contents

RTM-CSIA-MNA: Interpretation of CSIA data with Reactive Transport Modeling (RTM) for improved MNA of Chlorinated Solvent Plumes	
08:00-08:50	- Introduction - Lecture: MNA, CSIA, RTM, Phreeqc
08:50-09:00	- <i>Coffee break</i> -
09:00-10:05	- Lecture: Introduction to Exercise 1 - Exercise 1: Modeling Carbon-CSIA during reductive dechlorination
10:05-10:15	- <i>Coffee break</i> -
10:15-11:05	- Lecture: Introduction to Exercise 2 - Exercise 2: Modeling Chlorine-CSIA during reductive dechlorination
11:05-11:15	- <i>Coffee break</i> -
11:15-12:00	- Exercise 2: Continued - Lecture: Introduction to Exercise 3 - Exercise 3: Flow path modeling of C&Cl-CSIA: RD followed by VC oxidation - Summary and further studying

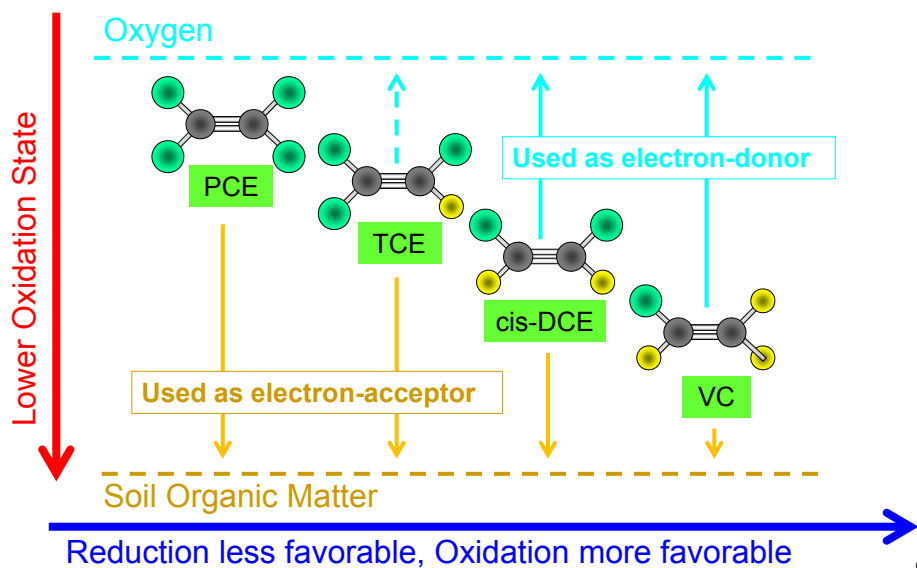
7

Chlorinated ethene (CE) degradation

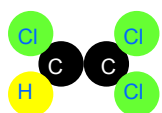


8

Chlorinated Ethene Degradation: Reductive Dechlorination vs Oxidation

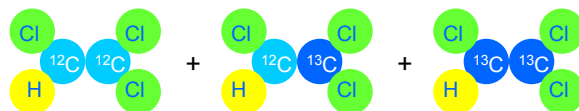


CSIA introduction: Definitions



← **Compound TCE:** C_2Cl_3H
 Consisting of 2 C, 3 Cl, and 1 H atoms

TCE occurs as 3 (stable) carbon **isotopologues**:



Isotopologues: chemically identical, isotopically varying

Isotopes: same atom (number protons the same [6]) but varying number of neutrons (thus mass (protons+neutrons))



Isotopic Abundances

Isotope ratio	Reference Standard	Ratio in standard	Abundance Heavy atom (%)	Abundance Light atom
$^2\text{H}/^1\text{H}$	Water (VSMOW)	1.5575e-4	0.015	99.985
$^{13}\text{C}/^{12}\text{C}$	Carbonate (VPDB)	1.1237e-2	1.11	98.89
$^{37}\text{Cl}/^{35}\text{Cl}$	(SMOC)	0.319766	24.23	75.77

11

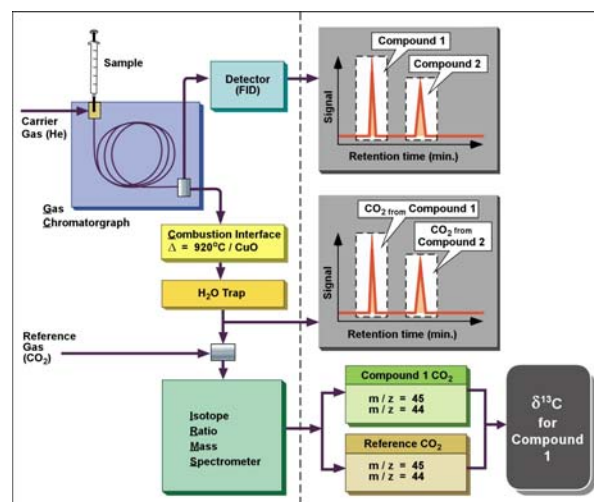
Compound-Specific Isotope Analysis (CSIA)

IRMS methods

Carbon:
CO₂ surrogate

Hydrogen:
H₂ surrogate

Chlorine:
Analyzed by GCMS



12

Isotopic Ratios & δ -notation

- Isotopic ratio in a certain molecule is defined as:

$$R = \frac{\text{abundance of rare (heavy) isotope}}{\text{abundance of abundant (light) isotope}}$$

- For the ^{13}C -isotope in carbondioxide it is expressed as:

$$^{13}\text{R}_{\text{CO}_2} = \left[\frac{^{13}\text{CO}_2}{^{12}\text{CO}_2} \right]$$

- Usually isotopic ratios are reported with reference to a certain standards

$$\delta_{A/r} = \frac{R_A - R_r}{R_r} = \frac{R_A}{R_r} - 1$$

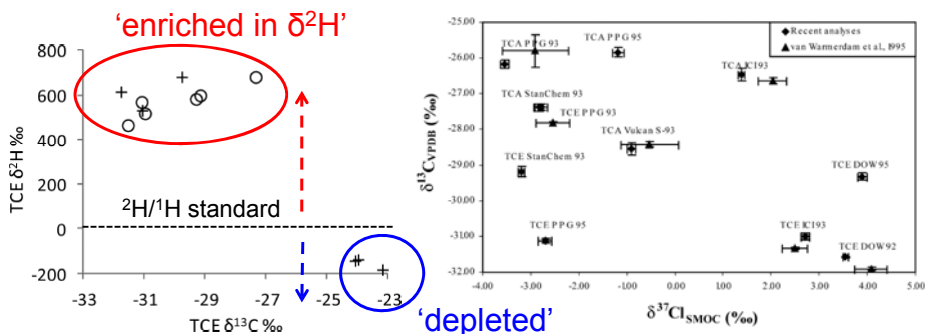
- There is international agreement on these standards, therefore

$$\delta_{A/r} \text{ is denoted as } \delta_A$$

$$\delta_A (\text{‰}) = \delta_A \times 1000$$

13

C-Cl-H CSIA TCE Source Signatures



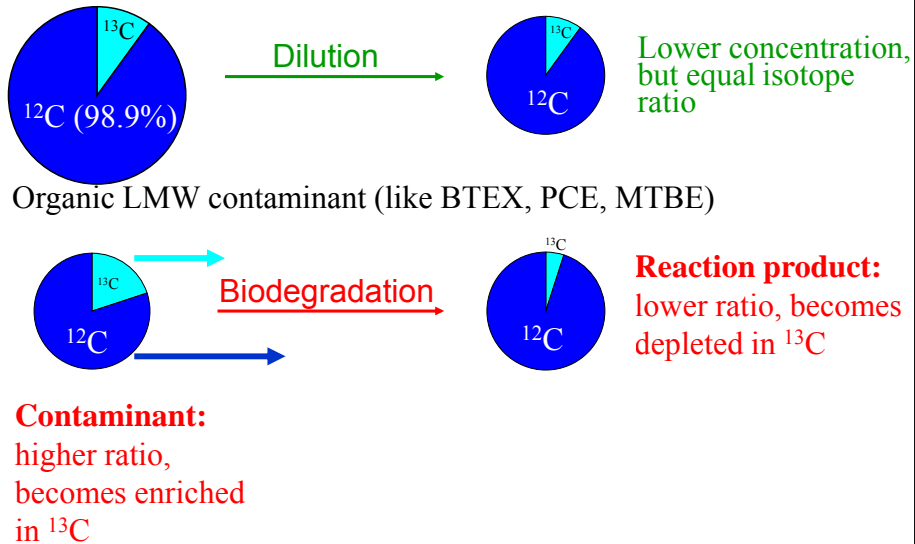
Kuder and Philp, ES&T, 2013, 47, 1461-1467

Shouakar-Stash et al, JCH, 2003, 60, 211-228

- Variations in C-Cl-H isotope signatures may vary considerably among pure products spilled at a site;
- CSIA could therefore be useful for source apportionment

14

Biodegradation & Isotope Fractionation



15

The Rayleigh equation

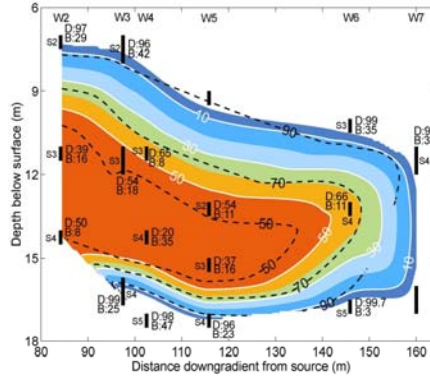
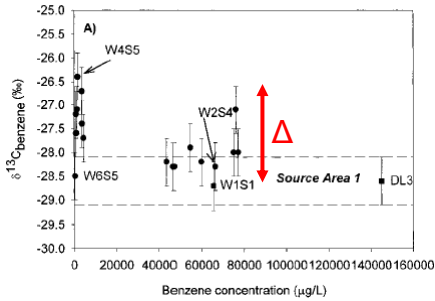
- Degradation ^{12}C -contaminant: $\frac{d^{12}\text{C}}{dt} = -k_L [^{12}\text{C}]$
- Degradation ^{13}C -contaminant: $\frac{d^{13}\text{C}}{dt} = -k_H [^{13}\text{C}]$
- Integration leads to the well known Rayleigh equation:

$$R_t = R_0 f^{(\alpha-1)}$$

- Isotope ratio: $R = \frac{^{13}\text{C}}{^{12}\text{C}}$
- Fraction remaining: $f \approx \frac{C}{C_0}$
- (Kinetic) isotopic fractionation factor: $\alpha = \frac{k_H}{k_L} \leq 1$

16

Calculating the extent of (bio)degradation in the field



$$R_t = R_0 f^{(\alpha-1)}$$

$$\ln f \cong \frac{\delta_{\text{Downgradient}} - \delta_{\text{Source}}}{\epsilon_{\text{lab}}} = \frac{\Delta}{\epsilon_{\text{lab}}}$$

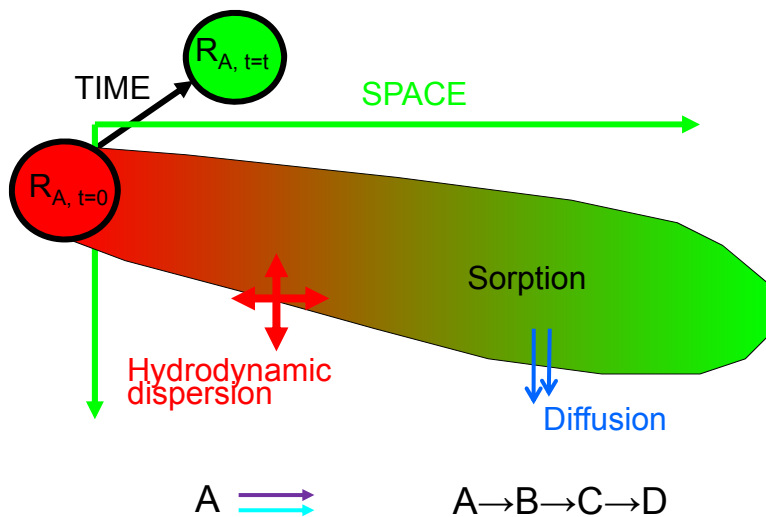
$$\text{Biodegradation} = (1 - f) \times 100(\%)$$

$$\epsilon (\text{‰}) = (\alpha - 1) \times 1000$$

Source: Van Breukelen (2007) ES&T: 41, 4980-4985; Mancini et al (2002) EST

17

Isotope fractionation in groundwater



18

Rayleigh equation: Applicability

- Validity
 - Single parent compound (BTEX, MTBE, PCE)
 - One degradation pathway, one isotopic fractionation factor
 - Closed system conditions; well-mixed reservoir: homogeneous
- Limitations
 - Does not account for hydrodynamic dispersion
 - Does not consider sorption-induced isotope fractionation effects
 - Sequential degradation of intermediates
 - Degradation via competing pathways (aerobic, anaerobic)

19

Reactive Transport Modeling (RTM)

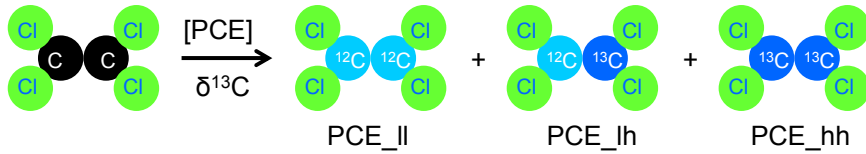
- Advection-Reaction-Dispersion (ARD) equation:

$$\frac{\partial C}{\partial t} = -v \frac{\partial C}{\partial x} + D_L \frac{\partial^2 C}{\partial x^2} - \frac{\partial q}{\partial t}$$

- Coupling of flow/transport model & biogeochemical reaction (degradation) model
 - Groundwater / vadoze zone / surface water
 - 1 to 3-D

20

Isotope Fractionation Reactive Transport Modeling (IF-RTM)



& have *slightly* different:

- degradation rate constants
- diffusion coefficients
- solid-water partitioning coefficients

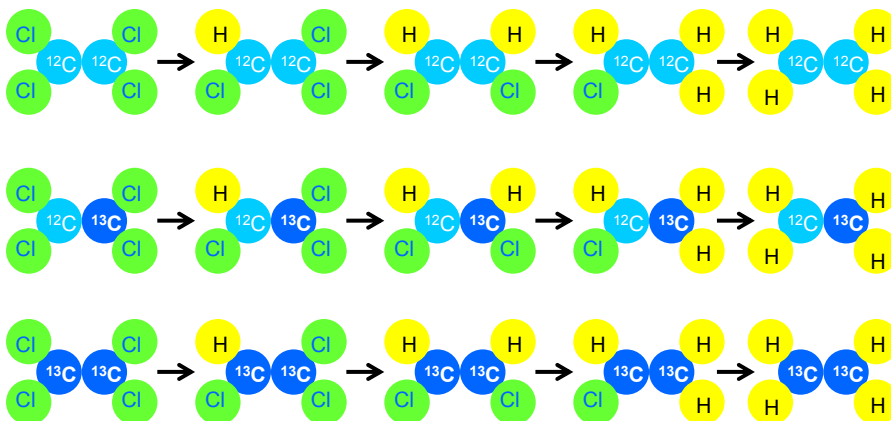
Isotope ratios are calculated from isotopologue concentrations after the model run:

$$\delta^{13}\text{C} = \frac{(2 \times \text{PCE_hh} + \text{PCE_Ih})}{(2 \times \text{PCE_II} + \text{PCE_Ih})} - 1$$

$R_{\text{reference}}$

21

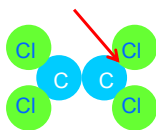
Carbon isotopologue fractionation: Reaction Network



(Negative) Degradation rate Parent = (Positive) Production rate Daughter

22

Kinetic Isotope Effect (KIE) vs. bulk isotope fractionation seen by CSIA

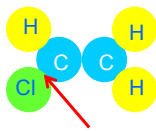


Carbon (PCE, TCE, DCE, VC, ETH):

1 C-Cl bond is broken with a KIE_{carbon}
 No isotope fractionation at other C atom
 Thus KIE is 'diluted' by 2 (carbon atoms)
 $\epsilon_{\text{C}_{\text{KIE}}} \approx \epsilon_{\text{C}_{\text{bulk}}} \times 2$

Chlorine (PCE):

1 C-Cl bond is broken with a KIE_{chlorine}
 No isotope fractionation at any other Cl atom
 Thus KIE is 'diluted' by 4 (chlorine atoms)
 $\epsilon_{\text{Cl}_{\text{KIE}}} \approx \epsilon_{\text{Cl}_{\text{bulk}}} \times 4$

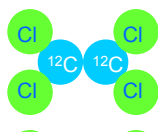


Chlorine (VC):

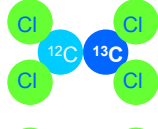
1 C-Cl bond is broken with a KIE_{chlorine}
 Other Cl atoms do not occur
 Thus KIE is therefore NOT 'diluted'
 $\epsilon_{\text{Cl}_{\text{KIE}}} \approx \epsilon_{\text{Cl}_{\text{bulk}}}$

23

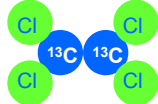
Carbon isotopologue fractionation: *First-order decay*



$$\rightarrow \text{rate}_{PCE_LL > TCE_LL} = {}^{12}k \times [PCE_LL]$$



$$\rightarrow \text{rate}_{PCE_LH > TCE_LH} = \frac{1}{2} \times {}^{12}k \times [PCE_LH] + \frac{1}{2} \times {}^{13}k \times [PCE_LH] \times \alpha_{\text{KIE}}$$



$$\rightarrow \text{rate}_{PCE_HH > TCE_HH} = {}^{13}k \times [PCE_HH] \times \alpha_{\text{KIE}}$$

$${}^{12}k \approx k \quad \alpha_{\text{KIE}} = \frac{{}^{13}k}{{}^{12}k} \quad {}^{13}k = {}^{12}k \times \alpha_{\text{KIE}} \quad \text{KIE} = \frac{{}^{12}k}{{}^{13}k}$$

24

Carbon bulk isotope fractionation

PCE → TCE → cDCE → VC → ETH

Isotopologue approach

$$\frac{\partial [^{12}\text{C}-^{12}\text{C}]}{\partial t} = [^{12}\text{C}-^{12}\text{C}] \times k_L$$

$$\frac{\partial [^{12}\text{C}-^{13}\text{C}]}{\partial t} = [^{12}\text{C}-^{13}\text{C}] \times \{k_L + k_H\} / 2$$

$$\frac{\partial [^{13}\text{C}-^{13}\text{C}]}{\partial t} = [^{13}\text{C}-^{13}\text{C}] \times k_H$$

$k_L = {}^{12}k$
 $k_H = {}^{13}k$

Bulk isotope approach

$$(1-h) \times C \times k_L = [^{12}\text{C}] \times k_L$$

$$h \times C \times k_H = [^{13}\text{C}] \times k_H$$

Mathematically equal

$$h = \frac{{}^{13}\text{C}}{[{}^{12}\text{C} + {}^{13}\text{C}]}$$

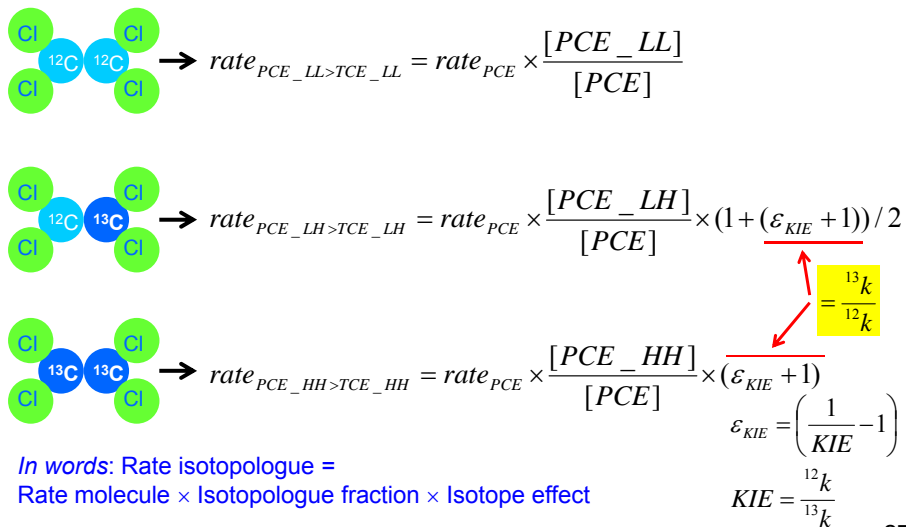
25

Definitions: Isotope Fractionation

- R: isotope ratio ($[^{13}\text{C}]/[^{12}\text{C}]$): 0.011237 (= standard)
- δ (‰): isotope ratio (signature) in ‰: 0 ‰
- Δ (‰): isotopic shift (difference sample and source)
- α : (kinetic) isotope fractionation factor: 0.9945
- ϵ (‰): (kinetic) isotope enrichment factor: $(\alpha - 1) \times 1000$: -5.5‰
- ϵ_{bulk} : ϵ as observed by CSIA for entire molecule: -5.5‰
- ϵ_{KIE} (‰): KIE expressed as ϵ at the reactive position: -11‰
 - $\epsilon_{\text{KIE}} \approx \epsilon_{\text{bulk}} \times (n/x)$
 - where n is number of atoms of the element (carbon): 2
 - (of which x are located at the reactive site: 1)
- α_{KIE} : KIE expressed as α at the reactive position: 0.9890
- KIE: kinetic isotope effect: ${}^{12}k/{}^{13}k$: $1/\alpha$: 1.011

26

Carbon isotopologue fractionation: *Any rate kinetics*

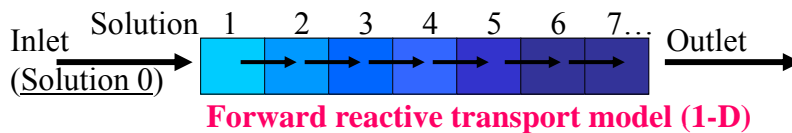


27

Software (USGS): PHREEQC

- Simulation of hydrogeochemical reactions

**Batch
(0-D)**



- Coupled to 3-D groundwater flow models:
 - PHREEQC-MODFLOW-MT3DMS: PHT3D
 - PHREEQC-HST3D: PHAST (USGS software)

28

PHREEQC for Windows (PfW): Structure

Input	via PHREEQC KEYWORDS
Database	phreeqc.dat wateq4f.dat → Equilibrium Constants minteq.dat llnl.dat
Output	Detailed Output Selected Output
Grid	Basic Spreadsheet
Chart	graphical output (USER_GRAPH)

29

Input: Keyword data blocks

KEYWORD	Function
SOLUTION_MASTER_SPECIES	Defines the main components like elements
SOLUTION_SPECIES	Defines all solution species: again elements but also their combinations: compounds
SOLUTION	Calculates composition aqueous solution
KINETICS	Kinetic parameters for rate of reactions
RATES	Rate equations defined with BASIC statements
TRANSPORT	Advective-dispersive-reactive transport
END	Demarcates end of a simulation
SELECTED_OUTPUT	Defines results output file
USER_GRAPH	To make a graph

30

First Exercise

Modeling Carbon Isotope Fractionation
During Sequential Reductive
Dechlorination from TCE to ETH

Modeling of microcosm experiment

Mixed *Dehalococcoides* (Dhc) culture fed with lactate:

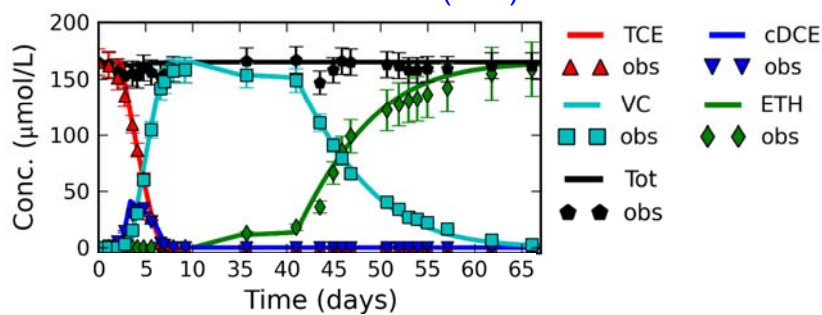


Table S1. Manually Calibrated Model Parameters Describing the Reaction Kinetics

Reaction	V_{max} ($\mu\text{M day}^{-1}$)	K_s (μM)	Lag period (days)
TCE \rightarrow cDCE	45	13	2.4
TCE \rightarrow tDCE	4.5	33	2.4
cDCE \rightarrow VC	55	8	3.4
tDCE \rightarrow VC	50	20	3.4
VC \rightarrow Ethene ^a	40	200	41.0

^a note a low V_{max} of $1 \mu\text{M day}^{-1}$ was applied between days 10-41

$$\frac{dC}{dt} = -k_{max} \frac{C}{K_s + C}$$

Experimental data from Kuder et al. ES&T 2013: 47, 9668–9677

Common degradation kinetics

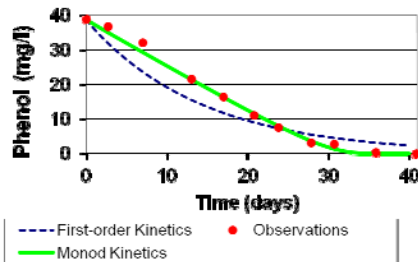
- First-order, half-life (at low concentrations)

$$S \rightarrow M \quad \frac{dS}{dt} = -k \cdot S \quad t_{1/2} = \frac{\ln(2)}{k} = \frac{0.693}{k}$$

- Zero-order (at high concentrations)

$$\frac{dS}{dt} = -k$$

- Monod kinetics (from low to high concentrations)



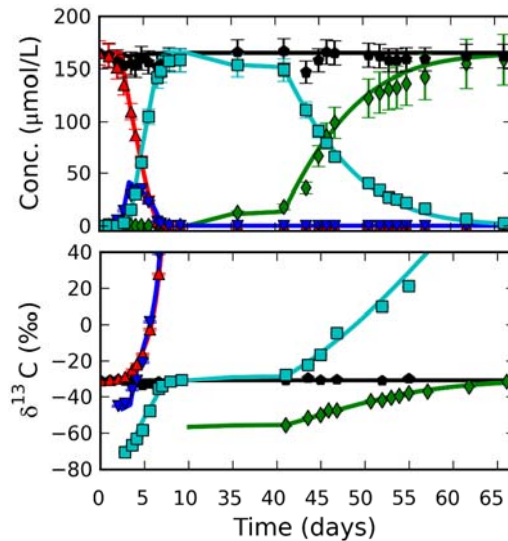
$$\frac{dS}{dt} = -k_{\max} \frac{S}{K_s + S}$$

$$\frac{dS}{dt} = -k_{\max} \quad \text{if } S \gg K_s$$

$$\frac{dS}{dt} = \frac{-k_{\max}}{K_s} S \quad \text{if } S \ll K_s$$

33

Carbon-CSIA results



Reaction	ϵ_C (bulk)
TCE → cDCE	?
cDCE → VC	?
VC → Ethene	?



34

How to Model this?

1. Define isotope species (isotopes or isotopologues)
2. Initial conditions
 - Define starting concentrations of the isotope species
3. Reaction equations (the reaction network)
 - Define how the decay of a parent isotope species produces a daughter isotope species; for all species
4. Rates formulations and parameters
 - Define the rate formulation for each reaction
 - Take starting values for model parameters like ϵ
5. Post-processing
 - Calculate delta values based on concentrations of isotope species

35

Exercise 1: Modeling Carbon-CSIA During TCE to ETH Dechlorination

1. Definition of solution species [in Database]:

SOLUTION_MASTER_SPECIES

element	species	alk	gfw_formula	element_gfw	
Tce_l	Tce_l	0.0	Tce_l	131.5	# 12C-TCE, "light" TCE
Tce_h	Tce_h	0.0	Tce_h	132.5	# 13C-TCE, "heavy" TCE
Dce_l	Dce_l	0.0	Dce_l	97	# 12C-DCE, "light" DCE
Dce_h	Dce_h	0.0	Dce_h	98	# 13C-DCE, "heavy" DCE
# etc					

SOLUTION_SPECIES

```
Tce_l = Tce_l
      log_k 0.0
# etc
```

Isotope model applied for carbon

36

Exercise 1

2. Definition of initial isotope concentrations:

SOLUTION 1 # Initial TCE concentration in cosm

units $\mu\text{mol/l}$

Tce_l ??? # Absolute ^{12}C -TCE concentration

Tce_h ??? # Absolute ^{13}C -TCE concentration

- $\delta^{13}\text{C-TCE} = -30.8 \text{ ‰}$
- $[\text{TCE}] = 165 \text{ } \mu\text{M}$
- $^{13}\text{C}/^{12}\text{C}$ abundance ratio (VPDB) = $1.1237\text{e-}2$

➤ Spreadsheet available for calculations (next slide) in exercises folder

37

Exercise 1

2. Definition of initial isotope concentrations (continued):

- $\delta^{13}\text{C-TCE} = -30.8 \text{ ‰}$
- $[\text{TCE}] = 165 \text{ } \mu\text{M}$
- VPDB = $1.1237\text{e-}2$

A: Calculate Isotope Ratio, R_A of Sample, from its δ :

$$\delta_{A/r} = \frac{R_A - R_r}{R_r} = \frac{R_A}{R_r} - 1$$

$$-30.8/1000 = \frac{R_A}{R_r} - 1$$

$$-30.8/1000 + 1 = \frac{R_A}{R_r}$$

$$R_A = (-30.8/1000 + 1) \times \text{VPDB}$$

B: Calculate Isotope Abundances

$$R_A = ^{13}\text{C}/^{12}\text{C} \quad ^{13}\text{C} + ^{12}\text{C} = 1$$

$$^{13}\text{C} = ^{12}\text{C} \times R_A$$

$$^{12}\text{C} \times R_A + ^{12}\text{C} = 1$$

$$^{12}\text{C} \times (1 + R_A) = 1$$

$$^{12}\text{C} = 1/(1 + R_A)$$

$$^{13}\text{C} = 1 - ^{12}\text{C}$$

$$[^{12}\text{C}] = ^{12}\text{C} \times \text{PCE}$$

$$[^{13}\text{C}] = ^{13}\text{C} \times \text{PCE}$$

38

Exercise 1

3. Definition of kinetic reactions: Reaction Equation

INCREMENTAL_REACTIONS true # time steps at KINETICS will be added

KINETICS 1 # here the stoichiometry and rate parameters are listed

-steps 0 700*0.1 # 700 time steps of 0.1 days

Tce_l_rd # Reductive dechlorination of "light" TCE

Tce_l is degraded, Dce_l and Chl are produced:

-formula Tce_l 1 Chl -1 Dce_l -1 # reaction stoichiometry

Tce_h_rd # Reductive dechlorination of "heavy" TCE

Tce_h is degraded, Dce_h and Chl are produced:

-formula Tce_h 1 Chl -1 Dce_h -1

Similar for RD of cDCE and VC

39

Exercise 1

4. Definition of kinetic reactions: Rate Equation

RATES # Here, the rate expressions are defined

Tce_l_rd # Degradation rate formulation of LIGHT TCE

-start

5 Tce_conc = tot("Tce_h")+tot("Tce_l")

10 if sim_time < calc_value("TCE_to_cDCE_lag") then goto 50

15 if Tce_conc < calc_value("dl_all") then goto 50

20 ratio = tot("Tce_l")/Tce_conc

30 rate = -(calc_value("TCE_to_cDCE_k_max")*Tce_conc) /
(Tce_conc + calc_value("TCE_to_cDCE_K_Sat"))

40 moles = rate * ratio * time

50 save moles

-end

$$rate_{TCE_L \rightarrow DCE_L} = \frac{k_{max} \times [TCE]}{K_{sat} + [TCE]} \times \frac{[TCE_L]}{[TCE]}$$

40

Exercise 1

4. Definition of kinetic reactions: Reaction Equation

RATES # Here, the rate expressions are defined

Tce_h_rd # Degradation rate formulation of HEAVY TCE

-start

5 Tce_conc = tot("Tce_h")+tot("Tce_l")

10 if sim_time < calc_value("TCE_to_cDCE_lag") then goto 60

15 if Tce_conc < calc_value("dl_all") then goto 60

20 ratio = tot("Tce_h")/Tce_conc

30 rate = -(calc_value("TCE_to_cDCE_k_max")*Tce_conc) /
(Tce_conc + calc_value("TCE_to_cDCE_K_Sat"))

40 alpha = ((calc_value("TCE_to_cDCE_C_e")/1000)+1)

50 moles = alpha * rate * ratio * time

60 save moles

-end

$$rate_{TCE_L>DCE_L} = \frac{k_{max} \times [TCE]}{K_{sat} + [TCE]} \times \frac{[TCE_H]}{[TCE]} \times \alpha$$

41

Exercise 1

4. Definition of kinetic reactions: Model Parameters

List of model parameter values

CALCULATE_VALUES

Rate kinetic parameters:

TCE_to_cDCE_k_max ; -start; 10 SAVE 4.100E-5 ; -end

TCE_to_cDCE_K_Sat ; -start; 10 SAVE 1.300E-5 ; -end

TCE_to_cDCE_lag ; -start; 10 SAVE 2.2 ; -end

Carbon isotopes:

TCE_to_cDCE_C_e ; -start; 10 SAVE 0 ; -end

Chlorine isotopologues:

TCE_to_cDCE_Cl_eKIE ; -start; 10 SAVE 0 ; -end

TCEtoDCE_SKIE_A ; -start; 10 SAVE 0 ; -end

TCE_to_cDCE_SKIE_Bt ; -start; 10 SAVE 0 ; -end

Note a semi-colon (;) is interpreted by Phreeqc as hard return

42

Exercise 1

5. Post-model calculation of isotope ratios:

SELECTED_OUTPUT # User specified output

-file ex1results1.txt

-reset false

USER_PUNCH

-headings TIME TCE 13C_TCE

-start

10 PUNCH TOTAL_TIME

20 PCE = tot("Tce_h")+tot("Tce_l")

110 PUNCH TCE*1e6 # convert moles to umol/l

210 VPDB = 0.011237 # Abundance ratio 13C/12C VPDB = 1.1237e-2

220 d13C_TCE = 1000*(((tot("Tce_h")/tot("Tce_l"))/VPDB)-1)

310 PUNCH d13C_TCE

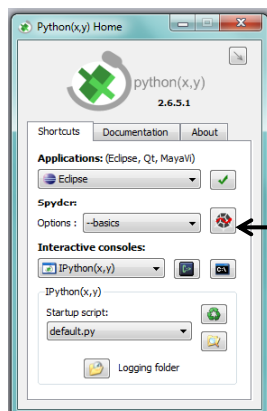
-end

END # End of model: Phreeqc will run simulation

43

Python for Visualisation

- <http://code.google.com/p/pythonxy/wiki/Downloads>
- All Programs > Python(x,y) > Python(x,y)



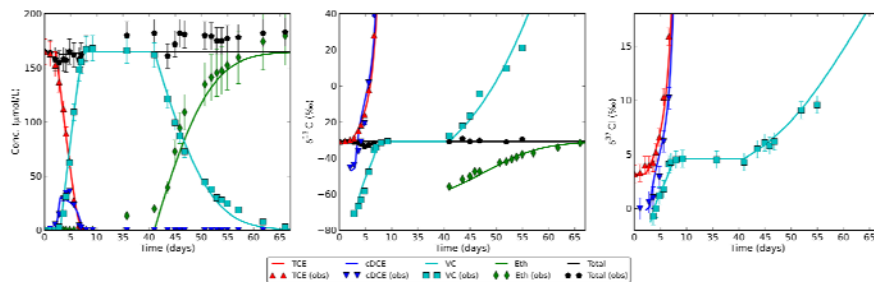
 **pythonxy**
Scientific-oriented Python Distribution based on Qt and Spyder

Click Spyder Icon

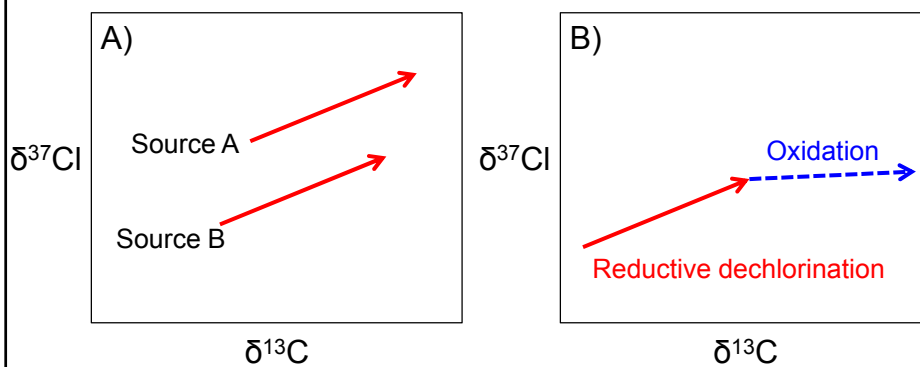
Success with Exercise 1!

44

Chlorine Isotope Fractionation

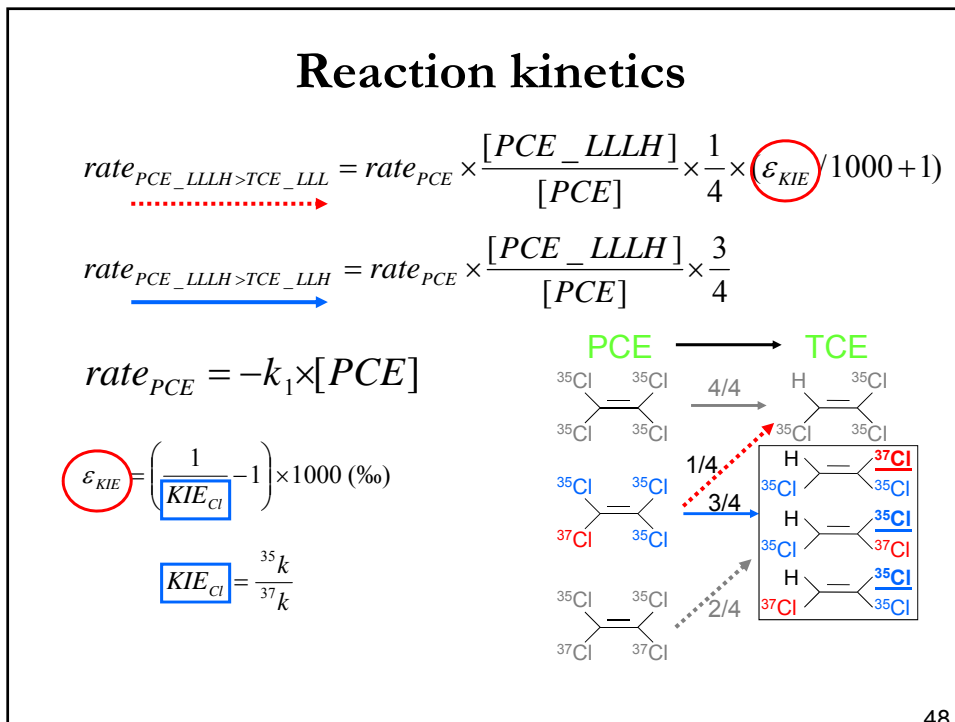
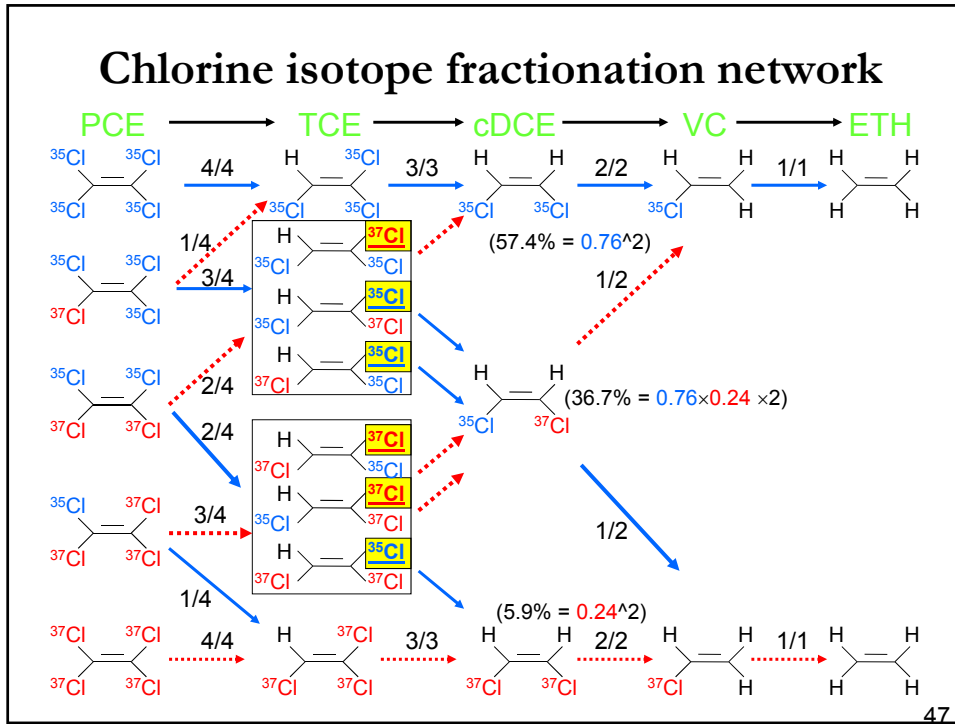


Potential Applications

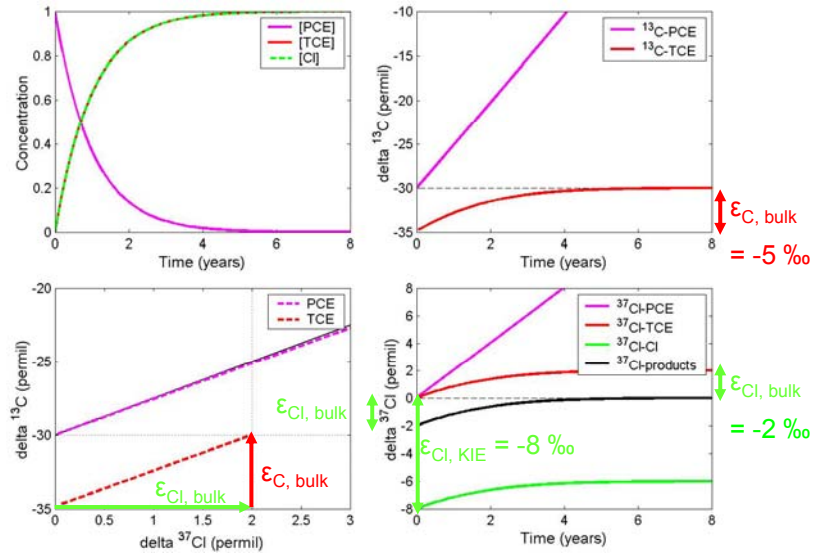


- A) Source apportionment
- B) Pathway differentiation: detection of oxidation
 - Chlorine isotope fractionation is negligible for oxidation of CEs

See also: Hunkeler, Van Breukelen, Elsner, ES&T 2009



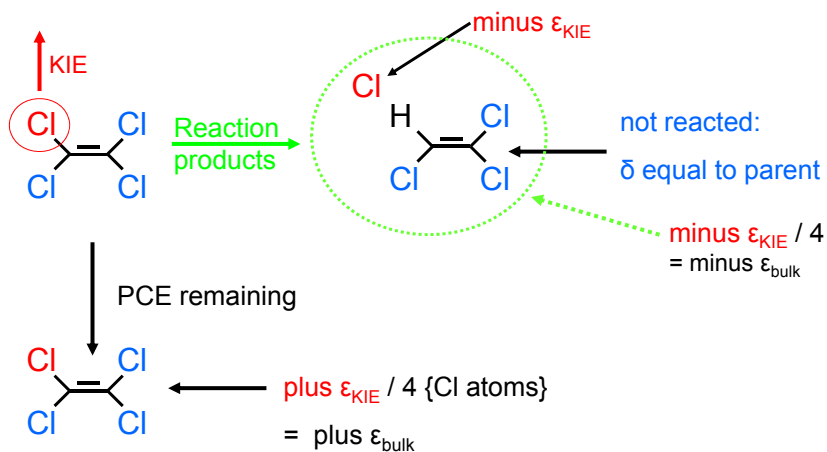
PCE to TCE degradation



Source: Hunkeler, Van Breukelen, Elsner, ES&T 2009

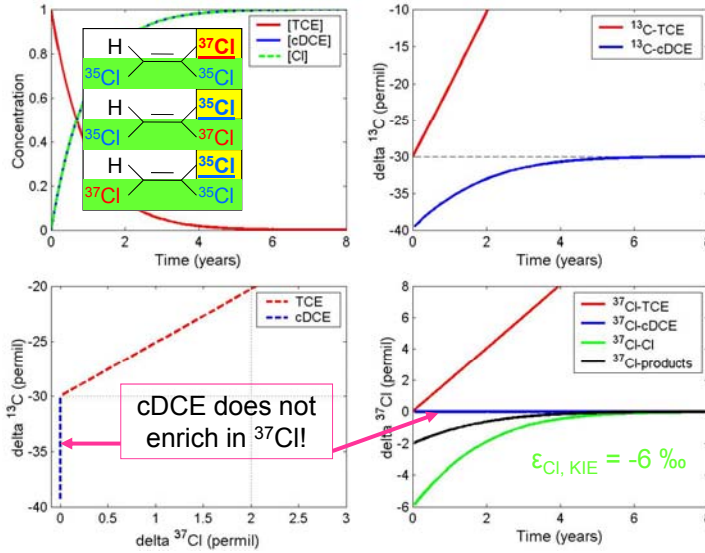
49

Conceptual model: Initial Conditions



50

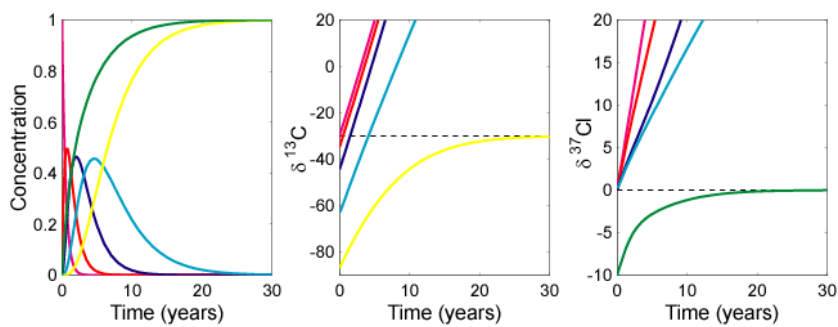
TCE to cDCE degradation



Source: Hunkeler, Van Breukelen, Elsner, ES&T 2009

51

Sequential degradation: decreasing k_1



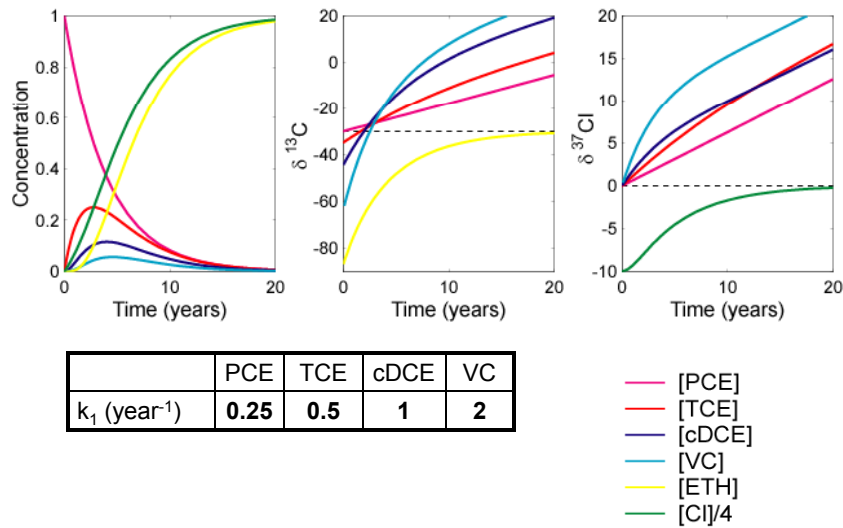
	PCE	TCE	cDCE	VC
k_1 (year ⁻¹)	2	1	0.5	0.25
ϵ_C (‰)	-5	-10	-20	-25
ϵ_{Cl} (‰)	-2.5	-3.33	-5	-5
$\Phi = \epsilon_C / \epsilon_{\text{Cl}}$	2	3	4	5

— [PCE]
 — [TCE]
 — [cDCE]
 — [VC]
 — [ETH]
 — [Cl]/4

Source: Hunkeler, Van Breukelen, Elsner, ES&T 2009

52

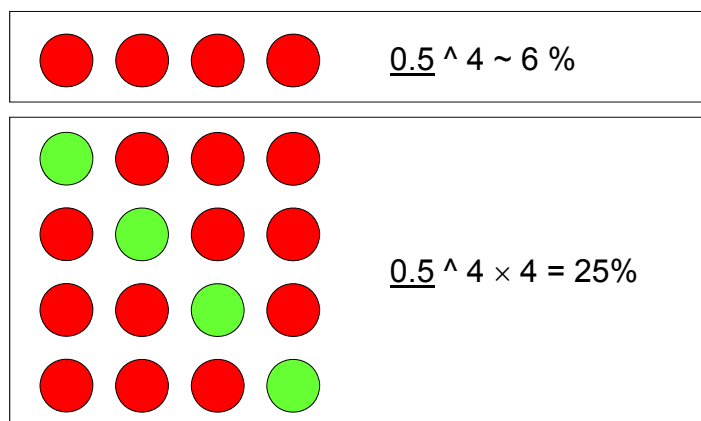
Sequential degradation: increasing k_1



Source: Hunkeler, Van Breukelen, Elsner, ES&T 2009

53

Calculation Initial Isotopologue Conc.



You have used now the probability mass function
(see next slide)

54

Calculation Initial Isotopologue Conc.

- Use the probability mass function:

$$P_i = \frac{n_i!}{H_i!(n_i - H_i)!} \cdot \pi_R^{H_i} \cdot (1 - \pi_R)^{n_i - H_i}$$

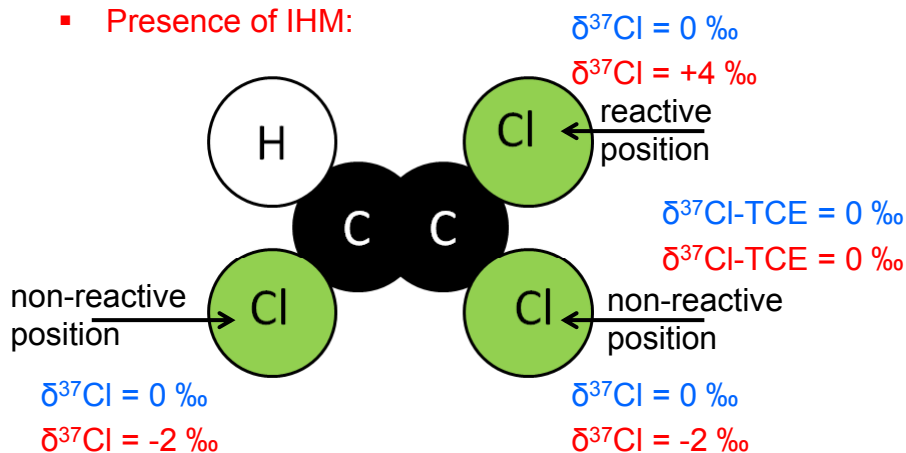
- n_i = total number of atoms of interest (C, Cl)
 - H_i = number of heavy atoms of isotopologue i . Consequently, the difference $n_i - H_i$ corresponds to the number of light atoms.
 - π_R = relative abundance of heavy isotope = $H/[H+L]$
 - ! = factorial:
- Example: assume $\pi_R = 0.01$ ($C^{13}/(C^{12}+C^{13})$); then:
 - $P(C^{12}-C^{12}) = 0.99 \times 0.99 = 0.98$
 - $P(C^{13}-C^{13}) = 0.01 \times 0.01 = 0.0001$
 - $P(C^{12}-C^{13}) = 0.99 \times 0.01 \times 2 = 0.02$
- See excel sheet
- Now you are ready for exercise 2

55

Intramolecular Heterogeneity (IHM)

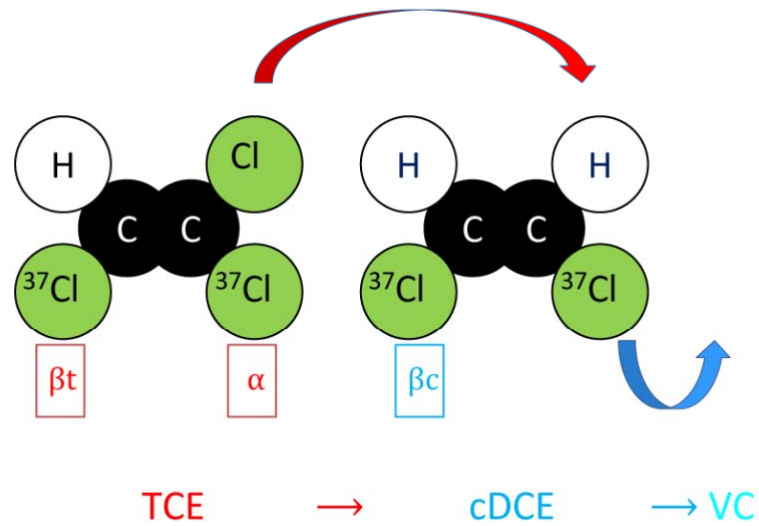
- Example: TCE to cDCE:

- Absence of IHM:
- Presence of IHM:



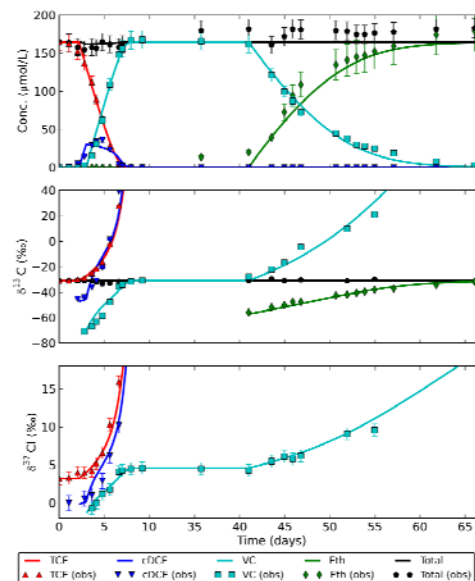
56

Chlorine Secondary Isotope Effects



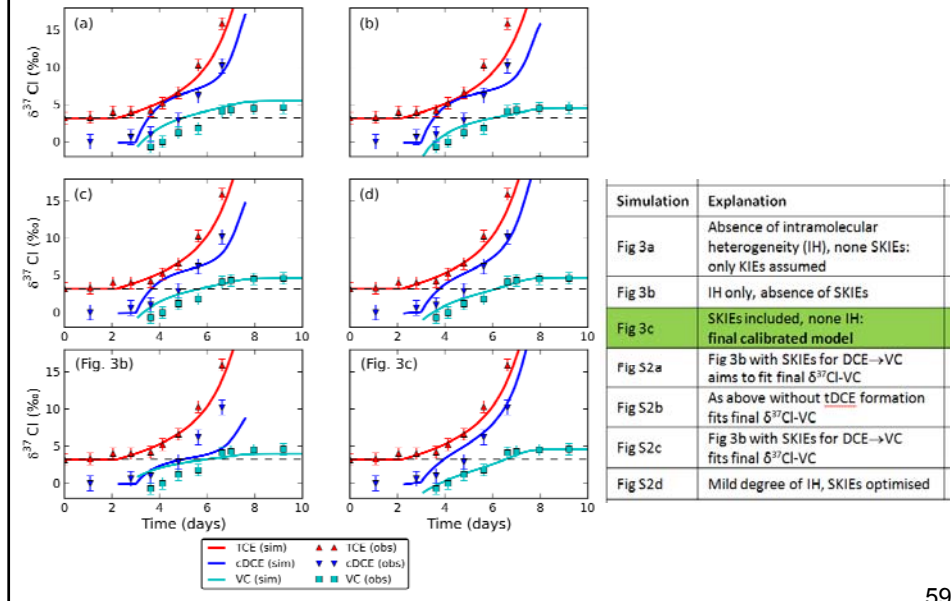
57

Final Model Results



58

Sensitivity Analysis

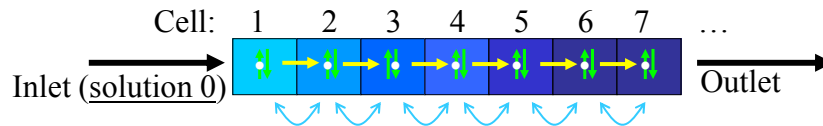


59

Exercise 3: 1-D Flow path Modeling

Virtual Case of a VC 'stall':
 How CSIA-RTM enables to detect oxidative transformation

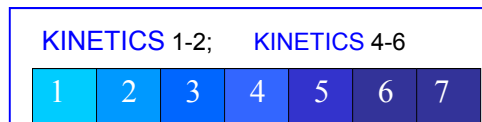
1-D Transport in Phreeqc: Basis



1-D Transport; flow direction *forward*; flux boundary conditions

Inlet solution = solution 0 if *forward*, or cells+1 (here 8) if *backward*

At each *shift* the following sequence occurs (reduces numerical dispersion):



61

1-D Transport in Phreeqc: Input

```

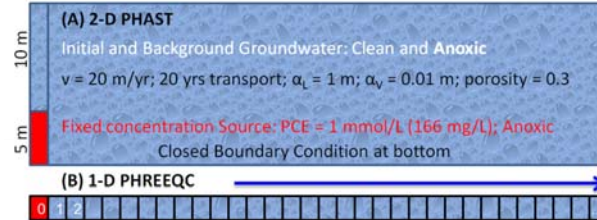
TRANSPORT # Transport including dispersion/diff. has additional options:
-cells 10 # number of cells in 1-D column / flow path
-shifts 100 # number of shifts or time steps
-time_step # time steps associated with each shift (advised) in seconds

-flow_direction # forward (default), backward, or diffusion_only
-boundary_conditions flux flux # for first and last cell: constant, closed or flux (df)
-lengths 6*5 4*2 # length of cells in m
-dispersivities 0.1 # m
-correct_disp true # only needed for modeling effluent from column exp.
-diffusion_coefficient 0.3e-9 # default in m2/s
-stagnant # only needed for simulation of dual porosity
-thermal_diffusion # optional for (simple) heat transport

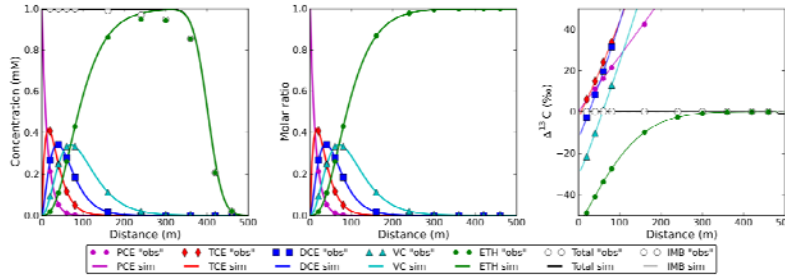
# output of model results both for ADVECTION/TRANSPORT
-print_frequency 1000 # suppress printing to output file
-punch cells 2-5 # only results for these cells to selected_output file
-punch_frequency 10 # only results for these shifts to selected_output file
    
```

62

Applicability of 1-D model for 3-D flow

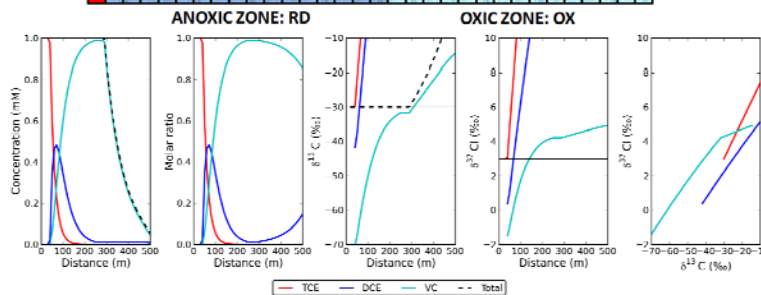
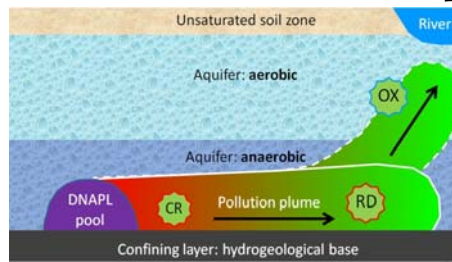


1-D PHREEQC simulates virtual observations produced by 2-D PHAST:



1-D PHREEQC simulates molar ratios and CSIA data perfectly!

Exercise 3: 1-D Transport



Summary

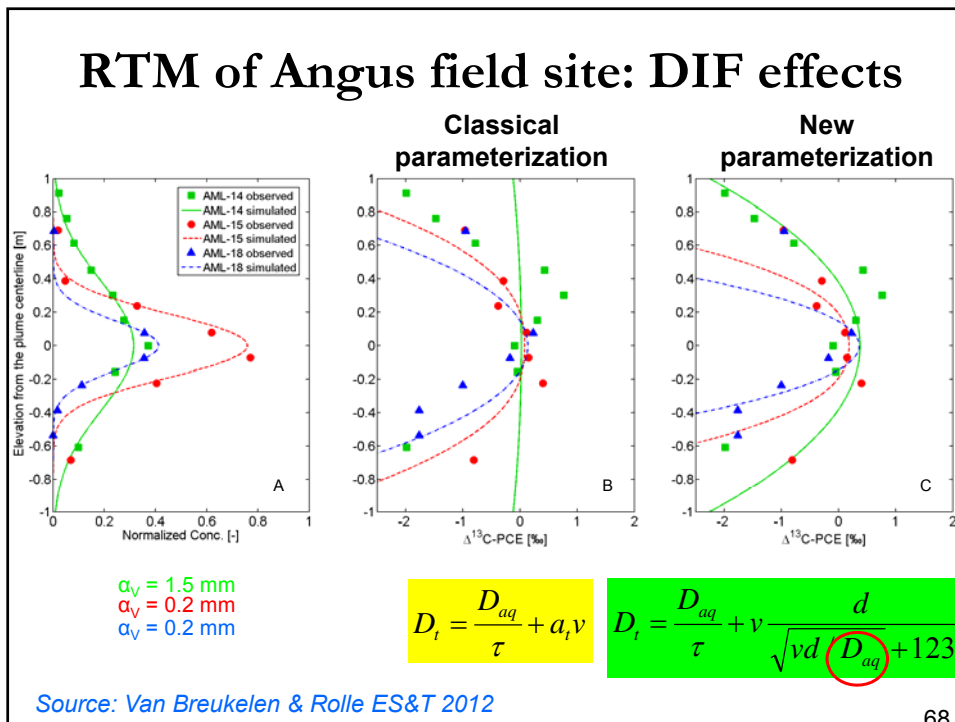
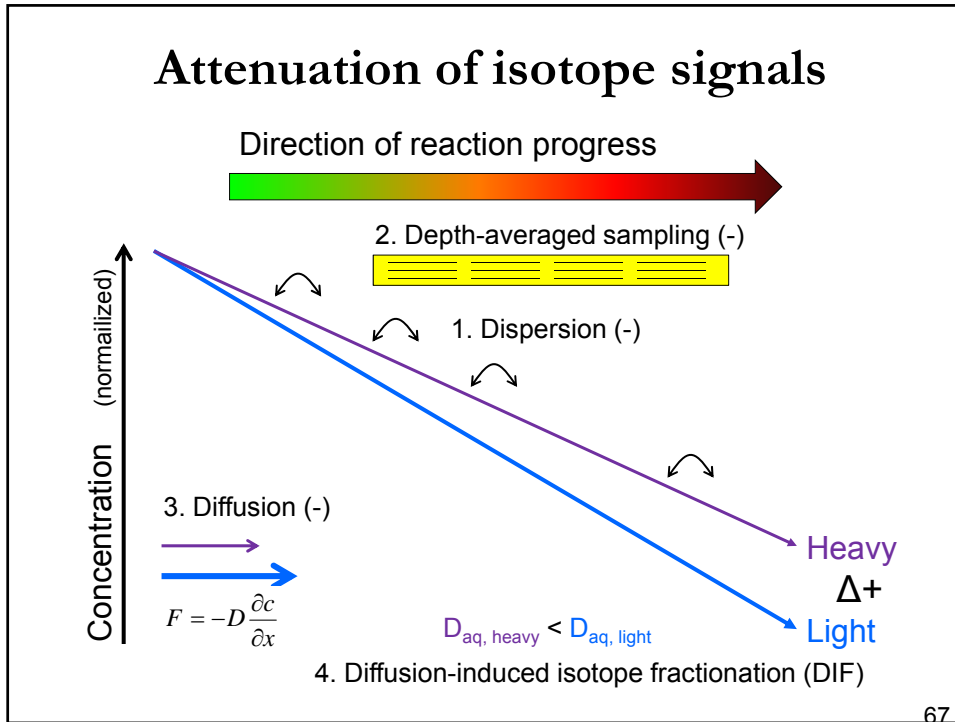
- CSIA enables detecting the occurrence of chlorinated ethene transformation other than reductive dechlorination: oxidative transformation
- Conceptual Site Models (CSMs) profit from CSIA data interpretation to identify dominant site processes
- RTM enables to verify CSIA-based CSMs and may allow for quantification of transformation and thereby improve MNA

65

Further Learning

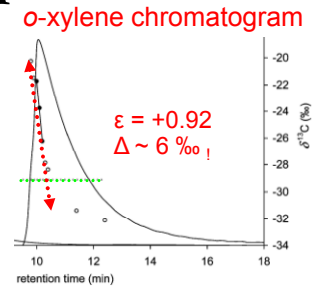
- Free digital copy of 3½ day course on “Reactive Transport Modeling of Isotope Signals in the Environment”
 - [Case studies on application of the Rayleigh equation](#)
 - [3-D plume modeling with PHAST \(3-D Phreeqc\)](#)
 - [Analytical solutions to evaluate isotope fractionation induced by sorption and transverse dispersion](#)

66



Sorption-based isotope fractionation

$$\alpha_{sorption} = \frac{K_d^{12C}}{K_d^{13C}} = \frac{K_{OC}^{12C}}{K_{OC}^{13C}} > 1$$

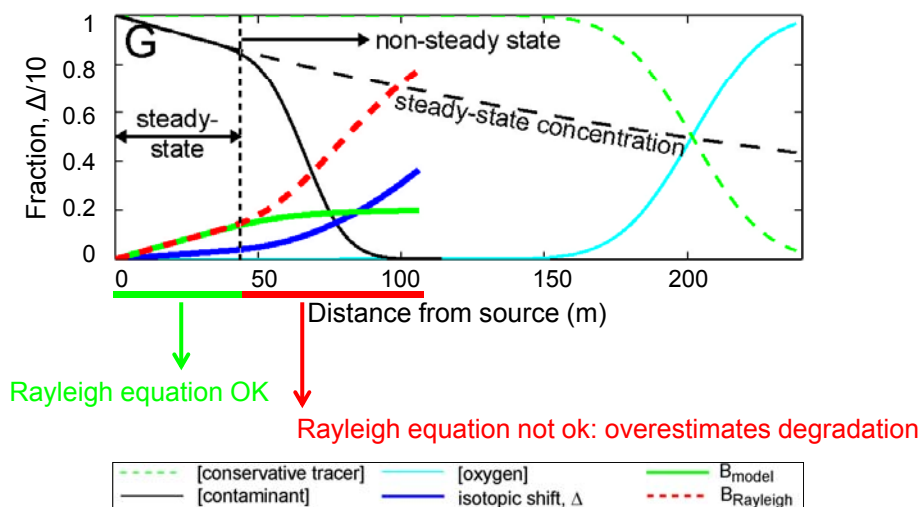


	10-step batch	Chromatographic
MTBE	~0	
Benzene	+0.44	+0.17
Toluene	+0.60	
2,4-dimethylphenol		+0.35
o-xylene		+0.92

Source: Kopinke et al. (2005) ES&T

69

Slow degradation throughout the plume



Source: Van Breukelen & Prommer ES&T 2008

APPENDIX D. CSIA SERVICE PROVIDERS

CSIA SERVICE PROVIDERS

University of Oklahoma School of Geology and Geophysics

100 E. Boyd St. SEC 810
Norman, OK 73019

P: 403.325.4469

F: 405.325.3140

Contact:

Paul Philp – pphilp@ou.edu

Tomasz Kuder – tkuder@ou.edu

Microseeps Inc.

220 William Pitt Way
Pittsburgh, PA 15238

P: 412.826.5245

www.microseeps.com

Contacts:

Rober Pirkle – rpirkle@microseeps.com

pmcl@microseeps.com

University of Waterloo

Environmental Isotopes Laboratory
200 University Avenue West
Waterloo, Ontario, Canada N2L 3G1

P: 519.888.4567 Ex 35838

<http://uweilab.ca/>

Contacts:

Richard Heemskerck

HYDROISOTOP GmbH

Woelkestraße 9
D-85301 Schweitenkirchen, Germany

P: +49 (0)8444.92890

F: +49 (0)8444.928 929

<http://www.hydroisotop.de>

Contact: info@Hydroisotop.de

University of Toronto

Department of Earth Sciences
22 Russell St.
Toronto, ON, Canada M5S 3B1

P: 416 978 3022

F: 416 978 3938

isotopes@geology.utoronto.ca

Isodetect (Germany)

Isodetect GmbH
Ingolstädter Landstr. 1
D-85764 Neuherberg, Germany

P: +49 (0)89.3187.3086

F: +49 (0)89.3187.3590

eisenmann@isodetect.de

Isotope Tracer Technologies Inc. (IT2)

695 Rupert Street, Unit B
Waterloo, ON, Canada N2V 1Z5

P: 519.886.5555

F: 519.886.5575

<http://www.it2isotopes.com/>

Contact: info@it2isotopes.com